

**DROPLET MICROFLUIDICS WITH IONIC LIQUIDS FOR  
CHEMICAL ANALYSIS AND SEPARATIONS**

**ZAHRA BARIKBIN**

SINGAPORE-MIT ALLIANCE  
NATIONAL UNIVERSITY OF SINGAPORE

2013

**DROPLET MICROFLUIDICS WITH IONIC LIQUIDS  
FOR CHEMICAL ANALYSIS AND SEPARATIONS**

**ZAHRA BARIKBIN**

(M.Eng. (Hons.) Chemical Engineering-Biotechnology, B.Sc.  
(Hons.) Chemical Engineering-Petrochemical Industries,  
Tehran Polytechnic)

A THESIS SUBMITTED FOR THE DEGREE OF DOCTOR  
OF PHILOSOPHY IN CHEMICAL AND  
PHARMACEUTICAL ENGINEERING

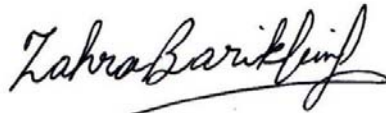
SINGAPORE-MIT ALLIANCE  
NATIONAL UNIVERSITY OF SINGAPORE

2013

## DECLARATION

I hereby declare that this thesis is my original work and it has been written by me in its entirety. I have duly acknowledged all the sources of information which have been used in the thesis.

This thesis has also not been submitted for any degree in any university previously.



---

ZAHRA BARIKBIN

06 May 2014

*To my parents*  
*Maliheh and Mohammad*  
*and*  
*my husband Hamed*  
*with love*

## **Acknowledgements**

First of all, I would like to extend my sincere gratitude to my thesis advisor, Dr. Saif A. Khan, for his guidance, wisdom, insights, and professional supports throughout my time at SMA. I truly appreciate him for the magnificent opportunity to work in his research group and for all motivating discussions and meetings. This thesis would never have come together without his continuous guidance and support from the earliest days of my PhD. Thank you Dr. Khan for all your encouraging advices and for helping me to be an independent researcher and see the world with all the wonderful different aspects. I am proud to be your student for 6 years working on my MEng and PhD projects. I have been also fortunate to have Prof. Patrick S. Doyle as my thesis advisor. My visit to MIT and work in his laboratory, though very short, has been an invaluable and unforgettable experience in my academic life. My special thanks and deep appreciation goes to Prof. Rajagopalan for the support and encouragement during the difficult time I faced in the last year. I would not be able to finish my PhD without his and Dr. Khan's sincere help and kind understanding.

I am very much grateful to my labmates for all the wonderful time, brain-storming discussions, fun, coffee breaks, playing volleyball, all outgoing events and for their continuous help and assistance. Dr. Md. Taifur Rahman, in particular, has been both a mentor and a friend. We have worked closely days and late nights in these past years, and he has taught me a tremendous amount about everything from the ancient poets to the finer points of academic thinking and writing. Thanks to my other wonderful lab friends Pravien, Suhanya, Sophia, Abhinav, Reno, Prasanna, Abu Zayed, Toldy Arpad, Swee Kun, Zita and Annalicia. The FYPs and exchange students that have worked on this project deserve mention: Peng You, Zhiyan and Gant, Josu, Dominik and Sandra.

I would like to thank Singapore-MIT Alliance and National University of Singapore (NUS) for the funding that has made this project possible. I also feel a deep appreciation for my friends, indeed my new brothers and sisters, who have made my grad school experience so sweet and unforgettable. Thanks and appreciation to Shima, Alireza R., Mona, Alireza Kh., Fatemeh, Hamed, Azadeh, Mahmood, Neda, Ehsan, Fahimeh, Asad, Ladan, Pooneh, Hossein, Fatemeh, Ahmad, Raja, Khatereh, Ehsan,

Marjan, Ramin, Dornoosh, Masoud, Zahra, Mohammad, Narjes, Sajad, and my other Iranian friends in Singapore.

Finally, I would like to thank my family for their love and support. Hamed, thank you for everything. I would not be able to write this thesis without your everyday support and understanding throughout these years. To my grandma, Zaman, grandpa, Mahdi, mum and dad, Maliheh and Mohammad, Hamed's parents, Soheila and Hassan, my brothers and their families, Behrooz, Maryam, Amirpooya, Roozbeh, Maryam, Armin and Alireza, thank you all for your love, bearing with my absence during the course of my PhD studies and for the sacrifices you have made throughout my life to give me the best. You are the true reason I am here today.

# Contents

<b>Chapter 1</b>	Introduction.....	34
1.1	Miniaturization through Microfluidics.....	34
1.2	Microfluidics .....	36
1.2.1	Design and Fabrication of Microfluidic Devices.....	39
1.2.2	Multiphase Microfluidics or Digital Microfluidics.....	43
1.3	Engineering Droplets for Chemical Processes .....	46
1.3.1	Droplet Formation or Metering.....	46
1.3.2	Mixing.....	48
1.3.3	Chemical Reaction .....	50
1.3.4	Droplet Traffic .....	53
1.3.5	Material Synthesis through Phase Change in Droplets.....	59
1.3.6	Chemical Sensing and Detection .....	63
1.4	Designer Emulsions.....	66
1.5	Designer Fluids - Ionic Liquids (ILs).....	70
1.5.1	History.....	72
1.5.2	Applications of Ionic Liquids .....	76
1.5.3	ILs and Microfluidics.....	90
1.6	Thesis Layout and Scope.....	91
1.7	References .....	93
<b>Chapter 2</b>	Microfluidic Compound Droplets: Formation and Routing .....	113
2.1	Compound Droplets Formation.....	113

2.1.1	Double Emulsion Structures .....	115
2.1.2	Partially Engulfed Structure or Compound Droplets.....	117
2.2	Compound Droplets Routing .....	121
2.3	Experimental Details .....	124
2.3.1	Materials .....	124
2.3.2	Synthesis of IL ([EMIM][NTf <sub>2</sub> ]) .....	124
	1-ethyl-3-methylimidazolium bis(trifluoromethylsulfonyl)imide .....	124
2.3.3	Physical Properties of IL [EMIM][NTf <sub>2</sub> ] .....	125
2.3.4	Microfabrication .....	126
2.3.5	Device Setup and Operation .....	131
2.4	Results and Discussion.....	133
2.4.1	Formation of Compound Droplet of Different Configurations.....	133
2.4.2	Compound Droplets Decoupling .....	140
2.4.3	Compound Droplet Splitting.....	146
2.5	Summary .....	147
2.6	References .....	148
<b>Chapter 3</b>	<b>Ionic Liquid-Aqueous Microdroplets for Biphasic Chemical Analysis and Separations .....</b>	<b>151</b>
3.1	Method Development.....	155
3.1.1	On-drop Chemical Separations .....	155
3.1.2	Dynamic pH Sensing .....	156
3.1.3	Biphasic Reactive Sensing.....	157



3.2	Experimental Details .....	160
3.2.1	Materials .....	160
3.2.2	Synthesis of IL [EMIM][NTf <sub>2</sub> ] .....	160
3.2.3	Microfabrication .....	160
3.2.4	Device Operation and Setup .....	162
3.2.5	Data Collection and Image Analysis.....	164
3.2.6	Chemical Synthesis.....	165
3.2.7	Results and Discussion .....	167
3.3	Summary .....	179
3.4	References .....	181
<b>Chapter 4</b>	<b>Microfluidic Synthesis of Polymeric Ionic Liquids with Tunable Functionalities.....</b>	<b>187</b>
4.1	Monodisperse Polymeric Ionic Liquid Microgels.....	187
4.2	Method Development.....	189
4.3	Experimental Details .....	191
4.3.1	Materials .....	191
4.3.2	Ionic Liquid Monomer Synthesis.....	192
4.3.3	Microfluidic Formation of PIL Microgels .....	193
4.3.4	Microfluidic Formation of PEGDA Microgels.....	194
4.3.5	Characterization .....	194
4.3.6	Anion-Dependent Microbead Sizes .....	195
4.3.7	Optical Microscopic Image Analysis of PIL Microgel Beads .....	196

4.3.8	Stimulus (pH)-Responsive Chemical Release .....	197
4.3.9	Chemical Separations – Heavy Metal Removal .....	197
4.3.10	Chemical Sensing – pH.....	198
4.4	Results and Discussion.....	198
4.4.1	Anion-Dependent Volume Transitions.....	198
4.4.2	Stimulus (pH)-Responsive Chemical Release .....	202
4.4.3	Chemical Separations – Heavy Metal Removal .....	203
4.4.4	Chemical Sensing – pH.....	205
4.4.5	Characterization .....	209
4.4.6	Summary.....	214
4.5	References .....	215
<b>Chapter 5</b>	<b>Conclusions and Future Directions.....</b>	<b>220</b>
5.1	Conclusions .....	221
5.2	Future Directions.....	222
5.3	References .....	227
Appendix A.....		230
Appendix B.....		234

## List of Figures

- Figure 1.1.** A typical lab-on-a-chip microfluidic device<sup>10</sup> (From [10]. Reprinted with permission from AAAS.).....35
- Figure 1.2.** Schematic illustrations of a) ‘dynamic interface’, an interface between two miscible fluids that flow next to each other and eventually mix through merely diffusion process. b) ‘pinned interface’, an stable interface that is formed between immiscible fluids. c) ‘floating interface’, an interface between two immiscible phases an acts as a semipermeable container wall. ....37
- Figure 1.3.** a) Channel based microsystems<sup>15</sup> (Reproduced with permission from [15]. Copyright 2003, John Wiley and Sons.) and b) surface based microsystems.<sup>16,17</sup>(Adapted from [16], Copyright 2010 with permission from Elsevier.; From [17]. Reprinted with permission from AAAS.).....39
- Figure 1.4.** Segmented flow microfluidics of, a) 2-phase liquid-liquid, b) 2-phase gas-liquid flows,<sup>29</sup> (Reproduced with permission from [29]. Copyright 2007, John Wiley and Sons.) c) flow regime diagram for segmented liquid-liquid microfluidic systems with transitional lines and operating conditions based on several literatures.<sup>27, 30-34</sup> (Adapted from [27] by permission of The Royal Society of Chemistry) More complex emulsion systems of d, e) 3-phase gas-liquid-liquid<sup>35-37</sup> (Panel ‘d’ reproduced with permission from [36] and [37]. Copyrights 2007 and 2005; respectively, John Wiley and Sons. Panel ‘e’ adapted from [35] by permission of The Royal Society of Chemistry) and f, g) liquid-liquid-liquid flows.<sup>38-39</sup> (Panel ‘f’ from [38]. Reprinted with permission from AAAS; Panel ‘g’ reprinted with permission from [39]. Copyright 2008, AIP Publishing LLC.).....45
- Figure 1.5.** Droplet formation or metering. Schematic views and microscopic images of main droplet generators for a-d) a T-junction geometry,<sup>43, 47</sup> and microscopic

images of droplets formation at e-h) flow-focusing geometries.<sup>41-42</sup> (© IOP Publishing. Panels ‘a-c’ and ‘e’ reproduced by permission of IOP Publishing. All rights reserved. Panels ‘f, g’ reprinted with permission from [41]. Copyright 2006, AIP Publishing LLC.; panel ‘h’ adapted from [42] by permission of The Royal Society of Chemistry.) .....47

**Figure 1.6.** Mixing and dilution in droplets. a) Formation of droplets with various chemical compositions by using a combination of opposing T-junction.<sup>55</sup> (Reproduced from [55] by permission of The Royal Society of Chemistry) b) A microfluidic system to perform a two-step reaction in which droplets are used as containers. Aqueous reagents R1 and R2 are merged in a T-junction to form a droplet which flows in oil. Mixing is accelerated by chaotic advection as droplets flow through a serpentine microchannel. After mixing section a longer channel allows the reaction in droplets to proceed. To initiate the second reaction, a third reagent, R3, is added later at the second T-junction placed in the microchannel downstream.<sup>56</sup> (Reproduced from [56] by permission of The Royal Society of Chemistry) c) Inserting a buffer solution prior to merging in a single droplet dilutes the reagents concentration.<sup>54</sup> (Adapted with permission from [54]. Copyright 2003, American Chemical Society) d-f) Mixing in liquid droplets and continuous segments through internal recirculating motions.<sup>15, 59-60, 63</sup> (Panel ‘d’ adapted from [60] by permission of The Royal Society of Chemistry; Panel ‘e’ adapted with permission from [63]. Copyright 2004, American Chemical Society; Panel ‘f’ reproduced with permission from [15]. Copyright 2003, John Wiley and Sons. and from [59], by permission of the Royal Society.).....49

**Figure 1.7.** (a-e) Merging droplets,<sup>26, 101-105</sup> (f,g) separating bubbles<sup>60</sup> and gas-liquid compound droplets<sup>35</sup> (h-k) splitting single droplets and more complex emulsions.<sup>35, 95, 106-107</sup> a) Active merging of droplets using electrocoalescence,<sup>101</sup> (Reprinted with

permission from [101]. Copyright 2006, AIP Publishing LLC.) (b) passive droplet merging by channel geometry; surface patterns induces the coalescence of droplets.<sup>102</sup> (Adapted from [102] by permission of The Royal Society of Chemistry) Schematics of c) reaction initiation by merging two droplets<sup>26</sup> d) narrowed and widening channels which affect the speed of droplets and cause their merging.<sup>26</sup> (Panels ‘c’ and ‘d’ adapted from [26]. © IOP Publishing. Reproduced by permission of IOP Publishing. All rights reserved.) e) merging droplets at a simple T junction.<sup>103</sup> (Reprinted from [103] by permission of The Royal Society of Chemistry) f) Separation of gas bubbles from liquid stream using capillary separator.<sup>60</sup> (Reprinted from [60] by permission of The Royal Society of Chemistry) g) gas-liquid compound droplets are separated using either extra oil injection or bifurcated microchannels.<sup>35</sup> h, i) bifurcating single droplets at simple T-junctions.<sup>95, 106</sup> (Panel ‘h’ reprinted with permission from [106]. Copyright 2009, AIP Publishing LLC. and panel ‘i’ reprinted with permission from [95]. Copyright 2004 by the American Physical Society.) j, k) splitting of complex emulsion at bifurcated channels.<sup>35, 107</sup> (Panels ‘g’ and ‘j’ reprinted from [35] and panel ‘k’ from [107] by permission of The Royal Society of Chemistry.) ..... 55

**Figure 1.8.** Droplets sorting using (a) bypass channels<sup>108</sup> and (b-c) dielectrophoresis<sup>110</sup>. a) Schematic (left) and snapshot (right) of two junctions in the same device fed by a single droplet generator which distributes droplets into both channels using the droplet distributor bypass. The leftmost junction with a bypass shows a perfectly alternating distribution of droplets between its two outlets. The junction on the right with no bypass shows a random alternation of droplets mainly by filtering into one arm.<sup>108</sup> b) Schematic view of the device used for dielectrophoresis sorting.<sup>110</sup> (c) In the absence of an electric field, water droplets flow into the waste channel while in the presence of an electric field, the droplets flow towards the

energized electrode and collection channel.<sup>110</sup> (Reprinted with permission from [108] and [110]. Copyright 2006, AIP Publishing LLC.) ..... 58

**Figure 1.9.** (a) Schematic diagram and optical micrographs of the extended capillary microfluidic device for generating triple emulsions that contain a controlled number of inner and middle droplets stages.<sup>123</sup> (Reproduced with permission from [123]. Copyright 2008, John Wiley and Sons.) (b) Schematic diagram and photographs of the alternating formation of aqueous droplets at the upstream junction and subsequent encapsulation at the downstream junction to form W/O/W droplets.<sup>51, 144</sup> (Reprinted from [144] by permission of The Royal Society of Chemistry.) ..... 69

**Figure 1.10.** Structures of common cations and anions of ionic liquids. .... 71

**Figure 2.1.** a) Possible equilibrium configurations corresponding to three sets of spreading parameters,  $S_i$ . Photographs of the stages of b) partial engulfing and c) complete engulfing.<sup>4</sup> (Reprinted from [4], Copyright 1970, with permission from Elsevier.) ..... 114

**Figure 2.2.** Left: sketch of the partially engulfing configuration with the phases A and B surrounded by the phase 0 and the Neumann's triangle whose sides have lengths proportional to the surface tensions. Right: the diagram representing possible morphologies formed by the phases A (green) and B (red) in the case of equal droplet volumes  $V_A = V_B$ . The dotted line corresponds to the condition  $\theta_B = \theta_A$ .<sup>5</sup> (Adapted from [5] with permission of The Royal Society of Chemistry.) ..... 116

**Figure 2.3.** Configurations of partially engulfed droplets for various  $\theta_0$  in the limiting case  $\sigma_{AB} \rightarrow \sigma_{OA}$  and  $\sigma_{OB} \sigma_{AB} \rightarrow 0$ , which corresponds to  $\theta_A = \pi$  (Solid-like phase A).<sup>5</sup> (Adapted from [5] with permission of The Royal Society of Chemistry.) ..... 118

**Figure 2.4.** Configurations of partially engulfed droplets for various  $\theta_B$  in the limiting case  $\sigma_{OB} \rightarrow \sigma_{OA}$  and  $\sigma_{OA} \sigma_{AB} \rightarrow \infty$ , which corresponds to  $\theta_0 = \pi$  (Janus-like

doublet). <sup>5</sup> (Adapted from [5] with permission of The Royal Society of Chemistry.)	119
<b>Figure 2.5.</b> Diagram represents the regions of positive and negative curvature $R^{-1}$ of the AB-interface in Janus-like droplets. The solid line corresponds to $V_B/V_A = (V_B/V_A)_{crit}$ . <sup>5</sup> (Adapted from [5] with permission from The Royal Society of Chemistry.)	120
<b>Figure 2.6.</b> Synthesis protocol of ionic liquid [EMIM][NTf <sub>2</sub> ]	125
<b>Figure 2.7.</b> A schematic illustrating formation and breakup of IL-Aq compound droplets in fluorinated oil (FO) at Brkup I droplet generator. Left inset is the AutoCAD design of the breakup point and the right inset shows schematics of some configurations of compound droplets generated in this work.	128
<b>Figure 2.8.</b> (a) Stereomicroscopic image, and (b) schematic of compound droplets generation at the Brkup II drop dispensing junction of a PDMS microfluidic device, respectively: merger of preformed aqueous droplet (Aq) with a thin stream of ionic liquid (IL), producing ionic liquid-aqueous (IL-Aq) bi-compartmental compound droplets flowing in continuous phase (fluorinated oil, FO).	128
<b>Figure 2.9.</b> A schematic of a typical bifurcated junction used in this thesis. Characteristic lengths for both microchannel and compound droplets are also highlighted.	129
<b>Figure 2.10.</b> AutoCAD design of the device containing Brkup I design for compound droplet generation and BIF I bifurcation in downstream of the microdevice. This design was used to study the decoupling of the two compartments of compound droplets versus non-decoupling behavior. Different devices with two different dimensions of bifurcated channels (BIF I and BIF II) were using Brkup I droplet generator.	129

<b>Figure 2.11.</b> AutoCAD design of the Brkup II - BIF II device used to study the splitting of IL-aqueous biphasic droplets.....	130
<b>Figure 2.12.</b> Constriction geometry at $l=17.34$ cm of the Brkup II microfluidic device to study the decoupling of IL-Aq compound droplets.....	130
<b>Figure 2.13.</b> Stereomicroscope images of compound droplet structures: (a) fully engulfed aqueous-in-ionic liquid compound droplets, formed in a continuous phase of silicone oil, and (b)–(d) partially engulfed aqueous-ionic liquid droplets formed in a fluorinated oil continuous phase. Abbreviations: Aq: aqueous (containing Methyl Blue), IL: ionic liquid (containing Orange II), SO: silicone oil, and FO: fluorinated oil (perfluorodecalin: perfluorooctanol, 10:1 (v/v)).....	134
<b>Figure 2.14.</b> (a) Schematic illustrating the our method and other droplet morphologies obtained with silicone oil as continuous phase (b) - (c) Stereomicroscopic images of different morphologies of the compound droplets obtained with $Q_{IL}$ (b) $2 \mu\text{L}\cdot\text{min}^{-1}$ (c) $5 \mu\text{L}\cdot\text{min}^{-1}$ at constant $Q_{Aq}$ ( $5 \mu\text{L}\cdot\text{min}^{-1}$ ) and $Q_{SO}$ ( $15 \mu\text{L}\cdot\text{min}^{-1}$ ). Scale bars represent $300 \mu\text{m}$ .....	134
<b>Figure 2.15.</b> (a) Aqueous- $[\text{MMIM}][\text{NTf}_2]$ (structure provided in Fig. S2) compound droplet generation in fluorinated oil (b, c) Three-phase flow with phosphonium ionic liquid $[\text{C}_{12}(\text{C}_4)_3\text{P}][\text{NTf}_2]$ . Compound droplets are not formed in this case as the ionic liquid does not satisfy a key criterion for compound droplet formation; it competes with the fluorinated oil in wetting the PDMS microchannel surface. Scale bars are $300\mu\text{m}$ .....	135
<b>Figure 2.16.</b> Stereomicroscopic images of IL-Aq compound droplet break up at Brkup I junction which is operated based on a hybrid of cross-flow and co-axial schemes.....	137



**Figure 2.17.** Stereomicroscopic images of different compound droplet structures obtained with increasing values of  $Q_{FO}$  (a)  $9 \mu\text{L}\cdot\text{min}^{-1}$  (b)  $15 \mu\text{L}\cdot\text{min}^{-1}$  (c)  $21 \mu\text{L}\cdot\text{min}^{-1}$  and (d)  $30 \mu\text{L}\cdot\text{min}^{-1}$  at constant  $Q_{IL}$  and  $Q_{Aq}$  of  $3 \mu\text{L}\cdot\text{min}^{-1}$ . ..... 138

**Figure 2.18.** Flow map of compound droplet configurations when  $Q_{FO}$  remained constant at  $9 \mu\text{L}\cdot\text{min}^{-1}$  and  $Q_{Aq}$  at either of 1, 2, 3 and  $5 \mu\text{L}\cdot\text{min}^{-1}$  while IL flow rate,  $Q_{IL}$ , was varied from 0.5 to  $15 \mu\text{L}\cdot\text{min}^{-1}$ . Scale bars are  $300\mu\text{m}$ . ..... 139

**Figure 2.19.** Flow map of compound droplet configurations when IL phase flow rate,  $Q_{IL}$ , was remained constant at either of 0.5, 1, 2, and  $3 \mu\text{L}\cdot\text{min}^{-1}$  while aqueous flow rate,  $Q_{Aq}$ , is varied from 1 to  $30 \mu\text{L}\cdot\text{min}^{-1}$  ( $Q_{FO}$  was invariable at  $9 \mu\text{L}\cdot\text{min}^{-1}$ ). Scale bars are  $300\mu\text{m}$ . ..... 140

**Figure 2.20.** Stereomicroscope images of: a) compound droplet decoupling at an obstacle in the flow path ( $U = 4.5 \text{ mm/s}$ ), b) compound droplet passing by the obstacle at lower flow speed ( $U = 1.3 \text{ mm/s}$ ), where no decoupling occurs. .... 142

**Figure 2.21.** (a) Morphology of a compound droplet (i) before, and (ii) after the decoupling process. b) Plot of occurrence of decoupling vs the flow speed (for fixed size of compound droplet compartments), i.e., ‘1’ and ‘0’ indicate successful and no decoupling respectively. A critical flow speed ( $\sim 2 \text{ mm/s}$ ) for the decoupling phenomenon is observed. .... 142

**Figure 2.22.** Time-stamped stereomicroscope images of compound droplet decoupling at two different bifurcations geometries; a) BIF I and b) BIF II. Compound droplets are formed using Brkup I droplet formation scheme. All scale bars are  $300 \mu\text{m}$ . ..... 144

**Figure 2.23.** Graphs of  $Ca$  vs non-dimensional characteristic length scales; a)  $\text{Log } Ca$  vs  $(L_{aq}/L_t)(W_C/W_B)$  b)  $\text{Log } Ca$  vs  $(L_{aq}/L_t)$ . Filled markers are related to complete

decoupling marked as D and unfilled markers show non-decoupling designated as ND.....	146
<b>Figure 2.24.</b> Time-stamped images of a compound droplet splitting into to equal-sized daughter drops at bifurcated intersection. All scale bars are 300 $\mu\text{m}$ .....	146
<b>Figure 2.25.</b> A graph of $L_{aq}/L_t$ vs $U_t$ , illustrating splitting ( $\square$ ), decoupling ( $\bullet$ ) and non-decoupling ( $\circ$ ) domains. ....	147
<b>Figure 3.1.</b> Selective and rapid extraction of OrII (orange II) into IL compartment from a mixture with MeB (Methyl Blue) as compound droplet translates along the microchannel.....	156
<b>Figure 3.2.</b> <i>On-drop dynamic pH sensing:</i> pH indicator (thymol blue)-doped IL compartment of the compound droplet changes color from neutral color to acidic/basic color as the IL becomes progressively acidic/basic by mass transfer of acid/base from the aqueous phase.....	157
<b>Figure 3.3.</b> (a) A schematic of the general concept of ‘on-drop’ biphasic chemical analysis: Interfacial analyte transport within the ionic liquid compartment of a microfluidic ‘firefly’. (b) Metal (analyte)-catalyzed fluorescence generating reaction scheme: gold ions are transferred from the aqueous to ionic liquid compartment, and catalyze the conversion of a substrate into a strongly fluorescing product, triggering bright fluorescence in the IL compartment (excitation: 365nm, emission: 496nm). (c) ‘Fireflies-on-a-chip’ visualized by mono-chrome camera under UV irradiation, Inset: bright field image of a compound droplet. (d) Stereomicroscope image of a ‘firefly-on-a-chip’ visualized using color camera under UV irradiation. Scale bars= 300 $\mu\text{m}$ . ....	159
<b>Figure 3.4.</b> AutoCAD drawing of the microchannel used for ‘on drop’ separation and pH sensing.....	161

<b>Figure 3.5.</b> AutoCAD drawing of the microchannel used for biphasic reactive sensing	162
<b>Figure 3.6.</b> Schematic view of the experimental set-up	163
<b>Figure 3.7.</b> Microfluidic experimental setup for ‘compound’ droplet generation and fluorescence imaging	164
<b>Figure 3.8.</b> Fluorescence spectra of ionic liquid, [EMIM][NTf <sub>2</sub> ], 1/ IL solution, and 2/IL solution ( $\lambda_{\text{ex}}$ 365 nm, $\lambda_{\text{emm}}$ 496nm)	167
<b>Figure 3.9.</b> (a-c) Stereomicroscopic images of selective liquid-liquid extraction of orange II out of an aqueous binary mixture with methyl blue into the ionic liquid compartment along the microchannel. All scale bars represent 300 $\mu\text{m}$ . d, e) Chemical structures of Orange II (OrII) and Methyl blue (MeB), respectively.	168
<b>Figure 3.10.</b> (a) A plot of the average color intensity (normalized) in the ionic liquid versus time ( $L/v$ , where $L$ is the distance along the microchannel and $v$ is the velocity of the compound drops; $v=0.005 \text{ ms}^{-1}$ obtained using image analysis). Inset stereomicrographs show the compound drops at the initial and final points along the microchannel. (b) Schematic illustration of compound droplets formation in a microchannel and <i>on-drop</i> liquid-liquid extraction (c) The plot shows the linear variation of average orange II color intensity (normalized) versus its concentration in ionic liquid. All scale bars represent 300 $\mu\text{m}$ .	169
<b>Figure 3.11.</b> (a) Calculated streamlines in both aqueous and IL compartments, (b) snapshots of concentration in both compartments at two different times, and (c) normalized area averaged concentration ( $\langle C \rangle^*$ ) in ionic liquid compartment as a function of time (normalized with respect to diffusive time $t_D = w^2/D$ ). The area-averaged concentration is observed to start leveling at normalized times of $\sim 2 \times 10^{-3}$ , indicating dramatic acceleration of mass transport by convection.	170

**Figure 3.12.** Molecular structures of thymol blue at neutral and acidic pHs ..... 171

**Figure 3.13.** (a) Stereomicroscopic images illustrating on-drop pH-sensing showing the ionic liquid compartment gradually changing color (from yellow to deep pink) as it translates along the length of the microchannel (b) A plot of average green intensity (normalized) of the ionic liquid droplet against time ( $L/v$ , where  $L$  is the distance along the microchannel and  $v$  is the velocity of the compound drops;  $v=0.005 \text{ ms}^{-1}$  obtained using image analysis) for two different pH values. The inset shows end-point measurements, i.e. the measured time for the saturation of color in the ionic liquid compartment at four different pH values. All scale bars represent  $300 \mu\text{m}$ . ..... 173

**Figure 3.14.** (a) Stereomicroscopic image of compound droplets generation at the drop dispensing junction of a PDMS microfluidic device: merger of preformed aqueous droplet (Aq) with a thin stream of ionic liquid (IL), producing ionic liquid-aqueous (IL-Aq) bi-compartmental compound droplets flowing in continuous phase (fluorinated oil, FO). (b) A schematic illustrating increase in fluorescence intensity within the ionic liquid compartment of a compound droplet with time as it travels along the microchannel. (c, d) Bright-field and dark-field stereomicroscopic images of an IL-Aq compound droplet flowing in microchannel, respectively. e) a schematic graph indicating increase in fluorescence intensity of IL compartment with time. Scale bars=  $300 \mu\text{m}$ . ..... 175

**Figure 3.15.** (a) Stereomicroscope images showing increase in fluorescence intensity within the ionic liquid compartment of a compound droplet with time as it travels along the microchannel. Scale bar= $300 \mu\text{m}$ . (b) Plots of normalized fluorescence intensity of IL compartments flowing at different speeds. (constant concentration of gold in aqueous compartment for all cases,  $8.8\text{mM}$ ). (c) Plots of normalized

fluorescence intensity of IL compartments versus time for two different gold concentrations in the aqueous compartment, flowing at 4.5 mm/s..... 175

**Figure 3.16.** Plot of normalized fluorescence intensity of IL compartments flowing at different speeds against the distance (location) along the microchannel (constant concentration of gold in aqueous compartment for all cases, 8.8mM)..... 178

**Figure 4.1.** a) Schematics illustrating capillary-based microfluidic method to generate poly (ionic liquid) microgels; inset shows a stereomicroscope image of a pre-polymer droplet flowing in the transparent capillary tube. (b) Chemical structures of IL monomer and PEGDA crosslinker. (c-e) Stereomicroscope images of PIL microgels showing their monodispersity and transparency (average diameters of 1000 $\mu$ m, 515 $\mu$ m, 300 $\mu$ m, respectively). All scale bars are 300 $\mu$ m. (f) FESEM image of synthesized PIL[Br]. Scale bar is 1mm..... 190

**Figure 4.2.** (a) Stereomicroscope images of samples of PIL[Br], PIL[ClO<sub>4</sub>] and PIL[NTf<sub>2</sub>] microgels with visibly similar sizes in the dried state and with distinct sizes in the hydrated state. All scale bars are 200 $\mu$ m. (b) Plot of percentage size change (shrinkage/swelling) of hydrated PIL[Br] microgels after anion exchange with Cl<sup>-</sup>, I<sup>-</sup>, MO<sup>-</sup>, TfO<sup>-</sup>, (NH<sub>4</sub>)S<sub>2</sub>O<sub>8</sub><sup>-</sup>, ClO<sub>4</sub><sup>-</sup>, PF<sub>6</sub><sup>-</sup>, NTf<sub>2</sub><sup>-</sup>. c) Plot of percentage size change of PIL[Cl], PIL[NTf<sub>2</sub>] and PEGDA microgels (compared to the dried state) in various solvents. 50 microbeads were used for each measurement..... 200

**Figure 4.3.** Histograms showing the monodispersity in the size of anion exchanged PIL microgels for the smallest PIL[NTf<sub>2</sub>], mid-size PIL[ClO<sub>4</sub>] and largest PIL[Cl] along with the parent PIL microgels PIL[Br]. ..... 201

**Figure 4.4.** (a) Stereomicroscope images of PIL[MO] microbead at pH 7 and during controlled release of methyl orange from microbead to the surrounding medium at pH

0.5 (b) Measured diffusion profiles of MO from the PIL[MO] microbead to the surrounding environment. All scale bars are 200 $\mu\text{m}$ . .....203

**Figure 4.5.** (a) Plot of chromium (VI) adsorption capacity ( $Q_e$ , Weight of adsorbed component, mg/ weight of adsorbent, g) versus  $C_e$ , concentration of potassium dichromate solution for both experimental data and Langmuir fitted curve, (b) Plot of  $C_e/Q_e$  at different concentrations of potassium dichromate solution. ....204

**Figure 4.6.** Adsorption of Cr(VI): (a) Colorless PIL[Br] microgels before any adsorption, (b) yellow color solution of 80 ppm Cr(VI) before the adsorption. (c) disappearance of yellow color of original Cr(IV) solution due to adsorption (d) dark yellow colored PIL microgels after adsorption of Cr(VI). (e) Br 3d peak is suppressed and Cr 2P peak is appeared in XPS spectra of PIL microgels after Cr(VI) adsorption. ....204

**Figure 4.7.** Six different sets of PIL[Br] microgels doped with their individual pH indicators, exposed to successive increments in pH. All scale bars are 300  $\mu\text{m}$ . .....205

**Figure 4.8.** Reversible and recyclable pH-Strip with PIL microgels. (a) *3D pH Strip*: an assortment of six pairs of different pH indicator-doped PIL microgels (two beads each contain the same pH indicator) are exposed to different pH solutions iteratively. (b) *Reversible pH sensing*: pH indicator (Thymol blue)-doped PIL microgels colorimetrically respond to the pH of the surrounding medium in a reversible fashion. The reversibility has been successfully tested for at least 10 cycles without any performance lost. All scale bars are 300 $\mu\text{m}$ . ....206

**Figure 4.9.** Capillary-based reversible pH sensing using 3D-structured PIL microgels. (a) Stereomicroscope images of 6 microgel beads containing individual pH indicators, embedded in a glass capillary with square cross-section, which is successively

exposed to flowing solutions of different pH. (b) Concept of a capillary-based 3D pH-strip for reversible pH analysis. All scale bars are 1mm. ....	208
<b>Figure 4.10.</b> FTIR spectra of PEGDA monomer, PEGDA polymer, IL monomer and poly(ionic liquid) PIL[Br]. ....	210
<b>Figure 4.11.</b> a) TGA curves for both PIL[Br] and IL monomer show similar primary decomposition temperatures (~230°C). The secondary decomposition temperature of PIL[Br] at ~330 °C indicates improvement of thermal stability presumably due to crosslinking. b) XPS spectra show the presence of C-C, C-O, C-N bonds; thereby, integration of imidazolium group into the polymeric material, and the presence of counter anion, bromide, in the synthesized polymer PIL[Br]. ....	211
<b>Figure 4.12.</b> FTIR spectra and the corresponding signature peaks for PIL[NTf <sub>2</sub> ], PIL[I], PIL[PF <sub>6</sub> ], PIL[S <sub>2</sub> O <sub>8</sub> ], PIL[ClO <sub>4</sub> ], PIL[TfO], PIL[MO] and PIL[Cl]. ....	211
<b>Figure 4.13.</b> EDX analysis confirm the exchange of parent anion, [Br], with anions such as [MO] <sup>-</sup> , [NTf <sub>2</sub> ] <sup>-</sup> and [PF <sub>6</sub> ] <sup>-</sup> , The EDX spectra show the presence of characteristic element(s) on the respective beads (a) Bromide 'Br' on the surface of PIL[Br] (b) Sulfur 'S' on PIL[MO] (inset: EDX spectra of PIL microbead after HCl induced slow release of MO; absence of the sulfur peak and prominent 'Cl' peaks indicate the ion exchange of MO with Cl) (c) Sulfur 'S' and Fluorine 'F' for PIL[NTf <sub>2</sub> ] (d) Fluorine 'F' and Phosphorus 'P' on the surface of PIL[PF <sub>6</sub> ]. ....	214
<b>Figure B 1.</b> <sup>1</sup> H-NMR of synthesized ionic liquid [EMIM][NTf <sub>2</sub> ]. ....	234
<b>Figure B 2.</b> <sup>1</sup> H NMR of synthesized substrate <b>1</b> . ....	234
<b>Figure B 3.</b> <sup>1</sup> H NMR of synthesized product <b>2</b> . ....	235
<b>Figure B 4.</b> <sup>1</sup> H NMR of synthesized ionic liquid monomer. ....	235
<b>Figure B 5.</b> <sup>13</sup> C-NMR of synthesized ionic liquid monomer. ....	236

## List of Tables

<b>Table 2.1.</b> Density, viscosity and interfacial tension of [EMIM][NTf <sub>2</sub> ] (* denotes aqueous solution containing Rhodamine B) .....	126
<b>Table 3.1.</b> Comparison between pH of the aqueous phase (after the partitioning with the IL phase) and pH of the original aqueous acid solution. (* Measurement uncertainty $\pm 0.01$ ) .....	174
<b>Table 4.1.</b> Comparison between the monomers and the polymerized product. ....	212
<b>Table 4.2.</b> Characteristic peaks for the corresponding anions in ion-exchanged PIL microbeads. ....	213



## List of Publications

### JOURNAL ARTICLES

- **Md. Taifur Rahman, Zahra Barikbin**, Abu Zayed M. Badruddoza, Patrick S. Doyle, and Saif A. Khan, " Monodisperse Polymeric Ionic Liquid Microgel Beads with Multiple Chemically Switchable Functionalities “, accepted for publication in *Langmuir*, 2013. (ZB and MTR are equal authors)
- **Zahra Barikbin, Md. Taifur Rahman**, and Saif A. Khan, " Fireflies-On-A-Chip: Ionic Liquid-Aqueous Microdroplets for Biphasic Chemical Analysis", *Small*, 2012. (ZB and MTR are equal authors)
- **Zahra Barikbin**, Md. Taifur Rahman, Pravien Parthiban, Anandkumar S. Rane, Vaibhav Jain, Suhanya Duraiswamy, S. H. Sophia Lee, and Saif A. Khan, "Ionic Liquid-Based Compound Droplet Microfluidics for ‘On-Drop’ Separations and Sensing", Emerging Investigators Issue, *Lab on a Chip*, 2010, *10*, 2458-2463.

### PUBLICATIONS IN PROGRESS

- Zahra Barikbin, and Saif A. Khan, "Compound Droplets Behavior at Microchannel Networks“, Manuscript under preparation, 2012/2013.

### CONFERENCES

- Zahra Barikbin, Md. Taifur Rahman, Dominik Jarde, Abu Zayed M. Badruddoza, Patrick S. Doyle, and Saif A. Khan, " Microfluidic Fabrication of Polymerized Ionic Liquid Microgels “, Proceedings of the 16th International Conference on Miniaturized Systems for Chemistry and Life Sciences (*MicroTAS*), 2012, Okinawa, Japan, W.4.120.
- Zahra Barikbin, Md. Taifur Rahman, and Saif A. Khan, " Fireflies-On-A-Chip“, Proceedings of the 12th International Conference on Microreaction Technology (*IMRET*), 2012, Lyon, France, T-O-09, pp. 71-72.
- Zahra Barikbin, Md. Taifur Rahman, Saif A. Khan. “Microfluidics-Based Compound Droplets: New Platform for Analytical Applications”, Proceedings of the

International Conference on Materials for Advanced Technology (*ICMAT*), 2011, Singapore, NEMS/MEMS AND MICROTAS G, G9-3, P. 52.

- Zahra Barikbin, Md. Taifur Rahman, Peng You, Josu Berasategi, Saif A. Khan,” FIREFLIES-ON-A-CHIP”, Proceedings of the 15th International Conference on Miniaturized Systems for Chemistry and Life Sciences (*MicroTAS*), 2011, Seattle-Washington, US, T17C, pp. 951-953.

- Zahra Barikbin, Md. Taifur Rahman and Saif A. Khan, “Fireflies-on-a-Chip: On-Drop Chemical Detection with Compound Droplet Microfluidics”, *AICHE* 2011 Annual Meeting, Minneapolis, US, 474b.

- Zahra Barikbin, Md. Taifur Rahman, Pravien Parthiban, Anandkumar S. Rane, Vaibhav Jain, Saif A. Khan,”On-Drop Separation and Sensing with Compound Droplet Microfluidics”, Proceedings of the 14th International Conference on Miniaturized Systems for Chemistry and Life Sciences (*MicroTAS*), 2010, Groningen, the Netherlands, W24D, pp. 1823-1825.

- Zahra Barikbin, Md Taifur Rahman, Pravien Parthiban, Anandkumar S. Rane, Vaibhave Jain and Saif A. Khan, “Compound Droplet Microfluidics for On-Drop Separations and Sensing”, *AICHE* 2010 Annual meeting, Salt Lake City, US, 168b.

- Zahra Barikbin, Md. Taifur Rahman, Saif A. Khan, “Microfluidic Emulsions for Pharmaceutical Separations”, Proceedings of the International Conference on Chemical & Biomolecular Engineering (*ChemBiotech09-10*), 2010, Singapore, P. 84.

- Zahra Barikbin, Md. Taifur Rahman, Saif A. Khan, “On-Drop Separation and Sensing with Compound Droplet Microfluidics”, SMA Annual Symposium, 2011, Singapore.

- Zahra Barikbin, M. Taifur Rahman and Saif A. Khan, “Microfluidic fireflies”, 63rd Annual DFD meeting, American Physical Society (APS) 2010, Gallery of Fluid Motion, Long Beach, CA, US.

- Zahra Barikbin and Saif A. Khan, “Microfluidic Emulsions for Pharmaceutical Separations”, SMA Annual Symposium, 2010, Singapore.

- Zahra Barikbin and Saif A. Khan, “Online Transmittance Measurement in microfluidic reactors”, 10th Anniversary of SMA Symposium, 2009, Singapore.
- Zahra Barikbin, Abhinav Jain, Daniel Wang, Saif A. Khan, “Online Transmittance Measurement in Microfluidic Devices”, ChemBiotech08-09 Conference, Regional Conference on Chemical & Biomolecular Engineering, December 2008, Singapore.

## List of Symbols

$\mu$	-	Viscosity (Pa.s)
$\rho$	-	Density (Kg.m <sup>-3</sup> )
$\sigma$	-	Surface tension (mN.m <sup>-1</sup> )
$\theta$	-	Contact angle
$Re$	-	Reynolds number
$Pe$	-	Peclet number
$We$	-	Weber number
$Ca$	-	Capillary number
$V$	-	Volume (m <sup>3</sup> )
$Q$	-	Volumetric flow rate ( $\mu\text{L}\cdot\text{min}^{-1}$ )
$U$	-	Flow speed (m.s <sup>-1</sup> )
$l$	-	Length (m)
$R$	-	Radius (m)
$v$	-	Velocity (m.s <sup>-1</sup> )
$t$	-	Time (s)
$W$	-	Width (m)

## Nomenclature

### Abbreviations

IL	-	Ionic liquid
Aq.	-	Aqueous
FO	-	Fluorinated oil
MeB	-	Methyl blue
OrII	-	Orange II
Th.B	-	Thymol blue
B.Th.B	-	Bromothymol blue
B.Ph.B	-	Bromophenol blue
B.Cr.G	-	Bromocresol green
B.Cr.B	-	Bromocresol blue
Ph.	-	Phenolphthalein
BIF	-	Bifurcation
Brkup	-	Break up
D	-	Decoupling
ND	-	Non-decoupling
1	-	Substrate
2	-	Product
<i>p</i> -TSA	-	<i>p</i> -Toluene sulphonic acid
[NTf <sub>2</sub> ]	-	bis(trifluoromethylsulfonyl)imide
[EMIM]	-	1-ethyl-3-methylimidazolium
PIL	-	Poly(ionic liquid)
PEGDA	-	Poly(ethyleneglycol) diacrylate

[PF <sub>6</sub> ]	-	Hexafluorophosphate
[TfO]	-	Trifluoromethane sulfonate
[ClO <sub>4</sub> ]	-	Perchlorate
[S <sub>2</sub> O <sub>8</sub> ]	-	Persulfate
I	-	Iodide
Cl	-	Chloride
Br	-	Bromide
MO	-	Methyl Orange

## Summary

Ionic Liquids (ILs) are liquid salts composed of organic cations and organic or inorganic anions. They possess a range of remarkable properties including high electrical conductivity, excellent thermal stability, very low volatility as well as high solvation capability for a broad range of organic, inorganic and biological molecules. Furthermore, physical properties of ILs such as viscosity, density, hydrophobicity etc. can be altered by the judicious choice of cation or anion. Due to these intriguing features, ILs are considered as new class of ‘designer’ solvents whose application in chemical separations and analysis, a crucial constituent of downstream chemical and biochemical processes, is merited. Digital or droplet-based microfluidics involves high-throughput generation and manipulation of discrete droplets/bubbles flowing in an immiscible liquid inside a microchannel. It offers precise control over the size, shape, throughput and scalability of droplets and has attracted significant interest in the areas of high-throughput chemical and biological experimentation and analysis. This thesis exploits salient features of ionic liquids as designer liquids and develops droplet-based microfluidic methods for biphasic chemical separations and analysis by controlled formation of complex emulsions. To modulate the unique features of ILs, there has been also enormous interest in material science to incorporate ionic liquids into macromolecular structures. This thesis also explores the applications of polymerized ionic liquids as matrices for advanced, stimulus-responsive chemical separations and sensing. Along this second related direction, a simple microfluidic method is also developed for fabrication of highly monodisperse poly(ionic liquid) microgel beads with a multitude of functionalities that can be chemically switched in a facile fashion by anion exchange and further enriched by molecular inclusion.

As a first demonstration, ionic liquid-aqueous biphasic droplets or compound droplets were formed and employed for chemical analysis and separation in microfluidic devices. To understand the hydrodynamics of IL-water compound droplets in more detail, the formation of these droplets in microchannels and their routing in simple microfluidic networks were studied. The flow conditions to form compound droplets or more complex emulsions and also to passively decouple or double the compound droplets at various microchannel geometries were further explored. The IL-aqueous compound droplets were later employed for selective separation of a binary mixture of molecules. These complex microfluidic emulsions with chemically functional fluids were used to perform rapid and non-invasive chemical analyses that are inaccessible at the macroscale. The chemical tunability of ionic liquids was leveraged in directing analyte (metal ion or proton  $[H^+]$ ) transport from the aqueous compartment of a biphasic droplet into an indicator-doped ionic liquid ‘reporter’ compartment and, crucially, in confining an analyte-indicator reaction within the reporter, thus enabling detection of the analyte without the addition of an indicator to the aqueous compartment. Therefore, dynamic pH-sensing of the aqueous compartment and chemical analysis (metal ion) were successfully performed.

Finally, a simple microfluidics-based method was established for fabrication of highly monodisperse PIL microgel beads with a multitude of functionalities that could be chemically switched in a facile fashion by anion exchange and further enhanced by molecular inclusion. Specifically, exquisite control over bead size and shape enabled extremely precise, quantitative measurements of anion- and solvent-induced volume transitions in these materials. In addition, by exchanging diverse anions into the synthesized microgel beads, stimuli responsiveness and various functionalities were



demonstrated including controlled release of chemical payloads, toxic metal removal from water and robust, reversible pH sensing.

# Chapter 1

## Introduction

### 1.1 Miniaturization through Microfluidics

Fredrick Balagadde, in his 2010 TED talk said “With one microfluidic chip, which is the size of an iPhone, you can diagnose 100 [HIV] patients at the same time.”<sup>1</sup> Enormous recent research has focused on how to multiply the power and availability of an unwieldy and expensive diagnostic lab by miniaturizing it to the size of a chip (Figure 1.1). Lab-on-a-Chip overlaps with microfluidics which is the science and technology of systems that precisely manipulate small amounts of fluids (nano to pico litres), using channels with cross-sectional dimensions of tens to hundreds of micrometers.<sup>2</sup>

Microfluidic devices for manipulating fluids are widespread and finding applications in numerous scientific and industrial contexts due to several advantages over their macroscale counterparts, including (i) the availability of methods for fabricating individual and integrated flow configurations with length scales on the order of tens microns and smaller<sup>3-4</sup> (ii) rapid developments in biotechnology for manipulations on sub-cellular length scale and the ability to detect small quantities and control very small volumes (less than 1 microliter),<sup>5-6</sup> (iii) the possibility of cheap portable devices able to perform simple analytical and diagnostic tasks, and (iv) the power to perform fundamental studies of physical, chemical, and biological processes.

The invention of microtechnology - a technology with features near one micron- in about 1954, led to the photolithography-based fabrication of integrated semiconductor chips. With dramatic improvement in the performance of microelectronic circuits, later in 1966, scientists applied these lithography-based techniques in miniaturization of mechanical devices like pressure sensors. In the 1980s, the term MEMS, for Micro Electro Mechanical Systems, was coined to illustrate new and sophisticated mechanical systems on a chip while fluid handling devices were also developed. The year 1979 was a milestone in the history of microfluidics when a miniaturized gas chromatograph (GC) was developed at Stanford university.<sup>7</sup> The first high-pressure liquid chromatography (HPLC) column device, fabricated by microelectronics-based technology (photolithography and etching in silicon and glass) was introduced in the early 1990s by Manz *et al.* to analyze aqueous solutions. It was then that the concept of Miniaturized Total Chemical Analysis Systems (MicroTAS) or Lab-On-A-Chip (LOC) was introduced and led to the development of micropumps, micromixers, flowsensors and microvalves.<sup>8-9</sup> Today, the MicroTAS aims to integrate all laboratory-scale activities on a single chip.

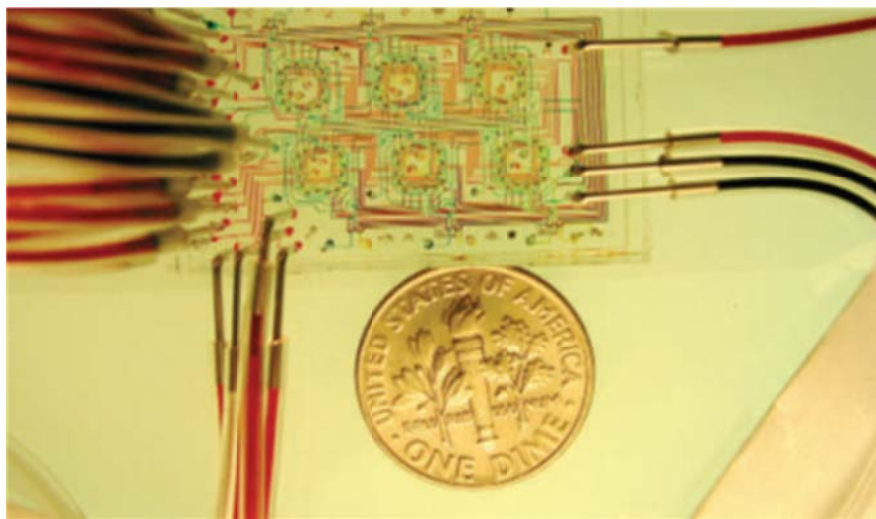


**Figure 1.1** A typical lab-on-a-chip microfluidic device<sup>10</sup> (From [10]. Reprinted with permission from AAAS.)

## 1.2 Microfluidics

An elegant effect of system size reduction from macro to micrometer scale is the vast increase in surface area to volume ratio. This allows for more efficient mass and heat transfer in microsystems as relatively more interface is available for both heat and mass transports. As the system size is shrunk, both the formation and homogenization of solute or temperature gradients are faster.

The flow behavior at microscales depends on the values of some important dimensionless numbers that compare different physical ingredients. In microfluidic system, due to the reduced size, fluid behavior is significantly influenced by viscosity rather than inertia which results in laminar flow or low Reynolds number. This offers fundamentally new abilities in the control of concentrations of molecules in space and time. Reynolds number or  $Re$  is the ratio of viscous to inertial forces. In laminar flow, transport and mixing of the molecules in micrometer length scales is mainly due to diffusion. Peclet number or  $Pe$  compares the relative importance of diffusion and convective bulk flow for molecular transport and can be easily engineered through the selection of flow velocity and the dimensions of the system. Surface tension greatly affects the flow behavior in multiphase scenarios, as there is a large surface to volume ratio in typical microfluidic systems. The competition between surface and capillary forces is recognized by Capillary number or  $Ca$ , which affects the generation, breakup and coalescence of droplets and can be adjusted by the choice of surface properties.<sup>11</sup>

Immiscible fluids can be manipulated in microsystems in a way that two phases can flow in parallel next to each other or one phase can be dispersed in another phase by forming droplets in a microchannel. In the earlier case moving or ‘dynamic interface’

is the interface between two miscible fluids that flow next to each other, under laminar flow condition, and eventually mix via diffusion (Figure 1.2a). Immiscible fluids form a stable interface or ‘pinned interface’, as a result of capillary forces, which can function as membranes (Figure 1.2b). In the latter case the interface between two phases is a ‘floating interface’ that acts as a semipermeable container wall (Figure 1.2c).<sup>12</sup>

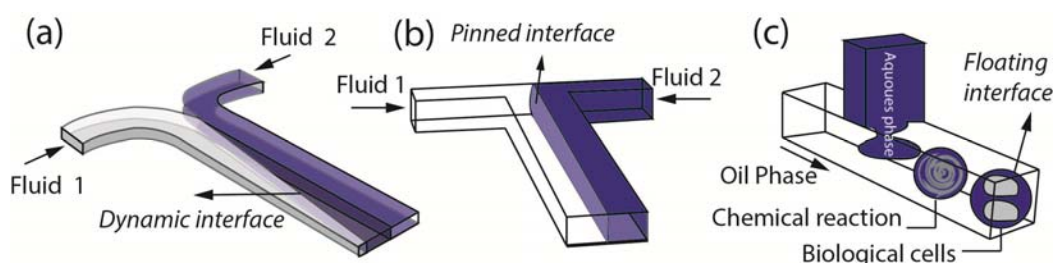


**Figure 1.2** Schematic illustrations of a) ‘dynamic interface’, an interface between two miscible fluids that flow next to each other and eventually mix through merely diffusion process. b) ‘pinned interface’, an stable interface that is formed between immiscible fluids. c) ‘floating interface’, an interface between two immiscible phases that acts as a semipermeable container wall.

Emulsions or droplets of one liquid dispersed in another, have attracted much scientific interest ever since Rayleigh studied the breakup of fluid jets in another fluid in 1879.<sup>13</sup> Taylor later in 1934 reported on factors controlling the formation and stability of such droplets.<sup>14</sup> All the early investigations of emulsions used bulk mixtures of immiscible phases to produce large quantities of droplets with a wide distribution of sizes in applications where their bulk properties would matter. However, individual droplets can now be easily manipulated and their properties can be precisely controlled with the invention of microfluidics.<sup>12</sup>

The basic idea behind multiphase microfluidic systems and in particular droplet-based or digital microfluidic systems is the use of droplets or plugs as reaction confinements

for chemical and biological processes. A multitude of parallel fabrication and screening operations, each consuming a minute amount of reagent, is enabled inside several small droplets on the platform. Digital or droplet-based microfluidics is divided into two fundamentally different setups; the channel-based and planar surface approach (Figure 1.3). The channel-based microfluidic systems are mostly the continuous generation and manipulation of droplets on the basis of pressure driven liquid flows within closed microchannels (Figure 1.3a).<sup>15</sup> On the planar surface-based microfluidic systems, discrete droplets are arbitrary actuated in two dimensions, by electrowetting (EWOD) or surface acoustic waves (SAW), representing planar programmable laboratories on-a-chip (Figure 1.3b).<sup>16-17</sup>

The pressure driven, droplet based platform relies on pumping two phase fluid through the microchannels by an externally applied pressure. The two immiscible phases are dispersed into each other in a way that a sample fluid (e.g. aqueous solution) forms droplets of a certain length, separated by the carrier fluid (e.g. oil) along the channel. This flow scheme is called segmented flow. If the size of droplets exceeds the cross sectional dimensions of the channel, it leads to formation of squeezed fluid plugs.

Since high-throughput chemical sensing and separation is the main focus of this thesis, we mainly focus on pressure-driven droplet-based microfluidics techniques in the following sections starting with brief introduction in design and fabrication of microfluidic devices.

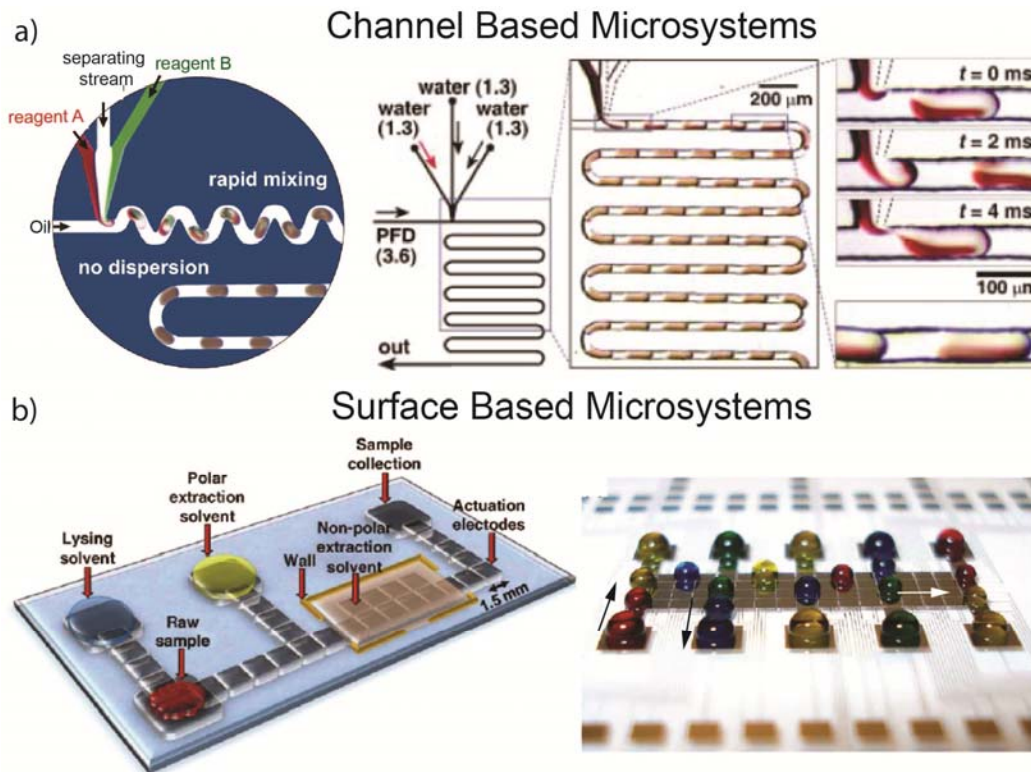


**Figure 1.3** a) Channel based microsystems<sup>15</sup> (Reproduced with permission from [15]. Copyright 2003, John Wiley and Sons.) and b) surface based microsystems.<sup>16-17</sup> (Adapted from [16], Copyright 2010 with permission from Elsevier.; From [17]. Reprinted with permission from AAAS.)

### 1.2.1 Design and Fabrication of Microfluidic Devices

Microfabrication leads to miniaturized structures of micrometer scales. Device fabrication are performed using several techniques such as electron beam lithography, isotropic and anisotropic etching, glass or silicon/glass anodic bonding devices, direct micro-machining of polymeric and metallic materials.<sup>18</sup> While most of these device materials offer great features with respect to chemical stability and durability, they are expensive and time consuming to fabricate. Most of the early microfluidic systems were fabricated by microelectronics technology, primarily lithography and etching in glass and silicon. Although traditional micromachining methods and materials such as

glass and silicon were the first choice for electronic and mechanical devices at the micrometer and millimeter scales, other materials and fabrication techniques are required for fluid applications and for higher geometric precision. Their intrinsic stiffness poses challenges in making devices with moving parts. Soft materials like polymers overcome many of the limitations of silicon. Fluidic devices inherently require more surface area than electronic circuits, the components are larger, and the interface with the surroundings is more complicated. Polymers, in contrast to silicon and glass, are inexpensive, channels can be formed easier by molding and embossing rather than etching, and devices can be sealed thermally or by using adhesives. For scientific research, it is often important to minimize the technological effort for device fabrication to quickly adopt microfluidic devices to new developments. The popular silicone elastomer polydimethylsiloxane (PDMS) is 50 times cheaper than silicon on a per volume basis. Elastomers also have a distinct mechanical property. The Young's modulus can be varied two orders of magnitude by controlling the amount of cross linking between polymer chains.<sup>19</sup> Therefore fabrication techniques broadly called "soft lithography", such as replica molding or embossing using masters fabricated by photolithographic methods or mold-machining, are the first choice for fabrication of microfluidic devices.<sup>18</sup>

Due to its simplicity in fabrication, elasticity, low background fluorescence, nontoxicity and biocompatibility, good thermal and chemical stability, optical transparency, low permeability to water, gas permeability as membrane, reversible deformability and controllable surface chemistry, the standard microfluidic device used in scientific research both for single phase flow and droplet based microfluidics is produced by replica molding using poly(dimethylsiloxane) (PDMS) silicon



rubber.<sup>20-21</sup> To fabricate PDMS devices, typically a master is produced by standard photolithography technique and a replica is molded from this master by pouring the premixed commercially available PDMS elastomer and curing agent onto these masters, degassing, and heat curing. The most frequently used photoresist for the lithographic procedure is the negative resist SU-8 which is available in different viscosities to produce a wide range of structures.<sup>22</sup> After removing the cured PDMS replica from the master the PDMS mold is typically bonded to a glass or PDMS coated glass and equipped with inlet and outlet tubing which can be simply pushed through the PDMS rubber. If oily liquids are used a more rigorous bonding of the device and sealing of the tubing are required to prevent the liquid leakage whereas this is not required for aqueous liquids. The PDMS replica and the glass cover treated shortly by oxygen plasma are  $\text{OH}^-$  terminated, resulting in formation of a covalent bond of the PDMS device and the cover after getting in contact. PDMS device fabrication techniques were also developed without the need for a lithographically fabricated master, where wires or tubing embedded into the PDMS act as a three-dimensional positive mask and finally removed after curing resulting in cylindrical microfluidic channels.<sup>23</sup> This technique, nevertheless, is limited to the fabrication of simple channels structures only.

For stable droplet formation in a microfluidic device the wetting properties of the channel walls are crucial. Unmodified PDMS presents a hydrophobic surface. Hydrophobic channel walls are required, for instance, to generate water droplets in a carrier oily phase, and vice versa for a hydrophilic channel walls. Thus, further modification of the channel wettability is required with respect to the liquids used. Sometimes simple tricks such as soaking the PDMS device prior to usage with the

continuous phase containing a high concentration of the surfactant or using certain fluids as continuous phases helps to achieve the desired wetting properties. Various coating techniques have also been developed to tailor the wettability and the chemical compatibility of PDMS.<sup>24</sup> To maintain the dimensions of a microfluidic channel during long device operation the chemical compatibility of the channel material with the liquids is also very critical since possible swelling, dissolving of the device material, and diffusion of liquids through the matrix material have to be avoided. As such, the usage of PDMS might seem quite peculiar as PDMS is fully chemically compatible to polar liquids such as water and fluorinated oils and could yet be very permeable for nonpolar liquids.<sup>25</sup> However, the desirable properties and ease of handling are still dominant considerations for most applications. If the permeability of water vapor and swelling by organic solvents prevent the usage of PDMS in fabrication of microfluidic systems, other materials such as photo-curable polymers (NOA81, NOA83H) and thermoplastic materials (poly(methylmetacrylate) (PMMA), SU-8, poly(etheretherketone) (PEEK), poly(vinyl chloride) (PVC), polycarbonate (PC), cyclic olefin copolymer (COC), polystyrene (PS)) can alternatively be used depending on wettability and feature resolution. Soft lithographic techniques including micromolding or embossing can be applied for these alternative materials.<sup>18,26</sup>

In the experiments involved in this thesis PDMS is the material of choice. Step-by-step protocols of photolithography, soft lithography for rapid prototyping, bonding and packaging are provided in Appendix A.

### **1.2.2 Multiphase Microfluidics or Digital Microfluidics**

Multiphase flows in microfluidics are created by the transport of two or more immiscible or partially miscible fluids in microchannel networks with dimensions from tens of nanometers to hundreds of micrometers wide. Multiphase microfluidics have increased conventional bench scale multiphase systems by exploiting the large interfacial area, fast mixing and reduced mass transfer limitations. Multiphase flows, also, offer several mechanisms for improving the performance of single-phase microfluidic systems by adding a second, immiscible, fluid stream that can trim down the long diffusion times and Taylor dispersion limitations associated with single-phase flows. Multiphase flows can also prevent a liquid from direct contact with the microchannel walls; thereby eliminates any possible clogging or material deposition on the wall.<sup>27</sup>

Multiphase flows are formed when two or more partially or immiscible fluids are brought in contact. Depending on the interaction between gravitational, interfacial, inertia and viscous forces, these types of flows can demonstrate different forms such as dispersed droplets, slugs and wall-wetting films (Figure 1.4c). Segmented flows, a specific form of multiphase flows with successive immiscible fluid segments, enhance mixing, reduce dispersion, and increase mass transfer across phase boundaries.<sup>27</sup> The main change that droplets bring to single phase microfluidic flows is the introduction of interfacial tension. Since the Reynolds number (1.1) is considered to be small, we deal with inertia-less fluid mechanics in microsystems. The Weber number (1.2), which compares inertia to interfacial tension, is also generally small in microfluidics. However, inertial effects can come into the picture in high speed flows or droplet breakup situations. Finally, the effect of gravity can be ignored as the Bond number

(1.3), which compares gravity to interfacial tension, is also very small. This leaves interfacial tension and viscosity in competition with each other, as both become important at small scales. The relative strength of the two is expressed by the Capillary number (1.4). Low Capillary number indicates that the stresses due to interfacial tension are strong compared to viscous stresses. Drops flowing under such a condition nearly minimize their surface area by forming spherical ends. In the opposite situation of high Capillary number, viscous effects dominate and large deformations of the drops and asymmetric shapes can be observed.<sup>28</sup> For illustrative purpose if we consider a flow of water droplets with typical speed of 1 mm/sec in fluorinated oil (viscosity = 5.1 mPa.sec, density = 1.9 gr.ml<sup>-1</sup> and interfacial tension in contact with water = 5.4 mN.m<sup>-1</sup>) in a microchannel with characteristic length of 100 μm, the dimensionless numbers are estimated as follows:

$$Re = \frac{\textit{inertial}}{\textit{viscous}} = \frac{dUp}{\mu} \sim 10^{-2} \quad (1.1)$$

$$We = \frac{\textit{inertial}}{\textit{interfacial}} = \frac{\rho U^2 d}{\sigma} \sim 10^{-5} \quad (1.2)$$

$$Bo = \frac{\textit{gravity}}{\textit{interfacial}} = \frac{pgd^2}{\sigma} \sim 10^{-2} \quad (1.3)$$

$$Ca = \frac{\textit{viscous}}{\textit{interfacial}} = \frac{\mu U}{\sigma} \sim 10^{-3} \quad (1.4)$$

Where  $d$  is the characteristic distance of the system (it would often be the characteristic length of the microchannel),  $U$  is the velocity scale of the fluid,  $\mu$  is the larger dynamic viscosity of the fluid acting in the system and  $\rho$  is the density of the of the same fluid,  $\sigma$  is the interfacial tension between the two fluid phases. Based on the

estimated dimensionless values, it can be seen that surface and viscous forces dominate in microscale multiphase flows.

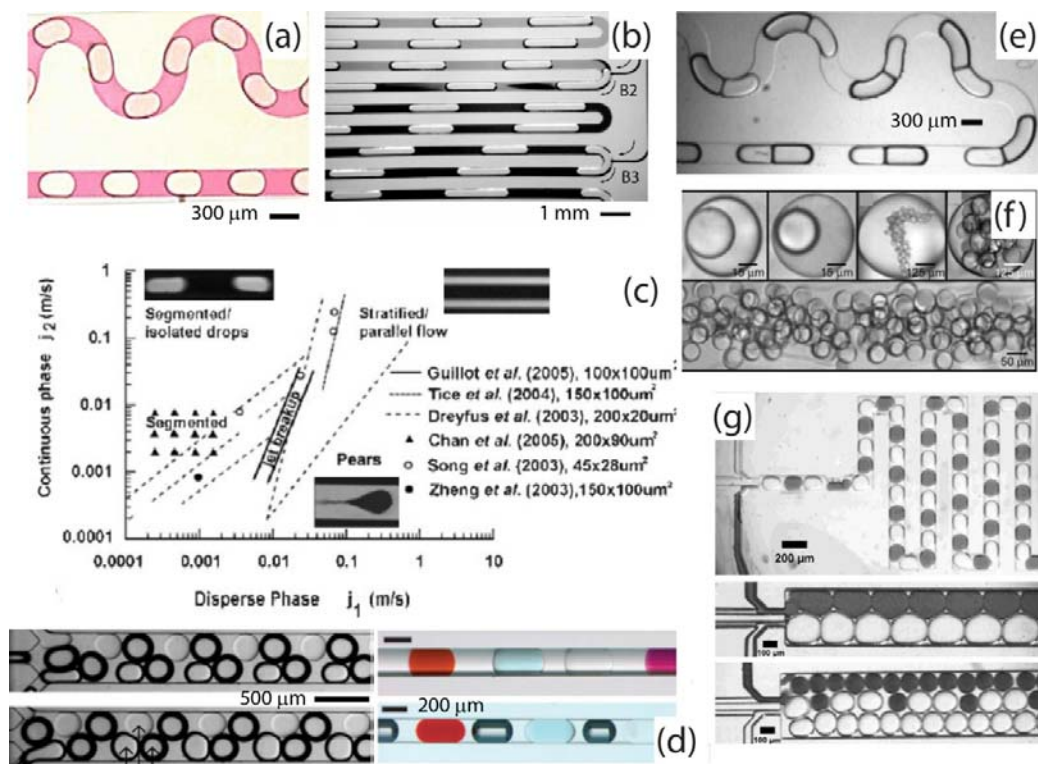


**Figure 1.4** Segmented flow microfluidics of, a) 2-phase liquid-liquid, b) 2-phase gas-liquid flows,<sup>29</sup> (Reproduced with permission from [29]. Copyright 2007, John Wiley and Sons.) c) flow regime diagram for segmented liquid-liquid microfluidic systems with transitional lines and operating conditions based on several literatures.<sup>27, 30-34</sup> (Adapted from [27] by permission of The Royal Society of Chemistry) More complex emulsion systems of d, e) 3-phase gas-liquid-liquid<sup>35-37</sup> (Panel 'd' reproduced with permission from [36] and [37]. Copyrights 2007 and 2005; respectively, John Wiley and Sons. Panel 'e' adapted from [35] by permission of The Royal Society of Chemistry) and f, g) liquid-liquid-liquid flows.<sup>38-39</sup> (Panel 'f' from [38]. Reprinted with permission from AAAS; Panel 'g' reprinted with permission from [39]. Copyright 2008, AIP Publishing LLC.)

Segmented flow microfluidics employ small plugs or droplets (liquid or gas) as microconfined reaction flasks, immersed in a second immiscible continuous phase within closed microfluidic channels. These microconfined reaction flasks (liquid or gas slugs, droplets or bubbles), are in pico- to micro-liter volume range, can be

transported by pressure gradient and can be merged, split, sorted in microfluidic channels. In principle, droplets of a dispersed liquid or gas phase are immersed in a second continuous liquid phase within a microchannel to form 2-phase liquid-liquid (Figure 1.4a) or 2-phase gas-liquid flows (Figure 1.4 b)<sup>29</sup>. If the size of inner droplets exceed the cross sectional dimensions of the channel, the droplets are squeezed accordingly to form non-spherical segments or ‘plugs’. The stability of the phase-arrangement can be enhanced, in some cases, by addition of surfactants in at least one of the phases to form 3-phase gas-liquid-liquid (Figure 1.4d,e)<sup>35-37</sup> or 3-phase liquid-liquid-liquid (Figure 1.4f,g)<sup>38-39</sup> plug interfaces. Similarly, the number of stable phases can be increase further by adjusting the interfacial tension of fluid combinations.<sup>40</sup>

### **1.3 Engineering Droplets for Chemical Processes**

In this section we aim to elaborate unit operations of chemical processes involved in droplet or digital microfluidics.

#### **1.3.1 Droplet Formation or Metering**

The most basic unit operation on droplet microfluidic platform is the generation of the plugs or droplets/bubbles. In general, there are two main microfluidic geometries to controllably generate a continuous stream of droplets; the flow focusing<sup>41-42</sup> and T-junction structures<sup>43-46</sup> (Figure 1.5).<sup>47</sup> The size of the droplets is affected by the shear forces at the channel junction where droplets are formed. Higher the shear force leads to formation of smaller droplets. In other words, the droplet size is determined by the

flow rates of both continuous and dispersed phases,<sup>48</sup> in addition to the channel geometries<sup>49</sup> and the viscosities of the two phases.<sup>50</sup>

A simple microfluidic device for producing droplets is the T-shaped channel geometry which forces two flows of immiscible liquids in a way that one liquid gets dispersed in the other.<sup>44</sup> According to the hydrophobicity of the microchannels wall at the junction and the relative flow rates of the liquids, the dispersed and continuous liquids can be selected.<sup>51</sup> Despite its simple design, the T-junction provides precise control over droplet formation and manipulation (Figure 1.5a-d), making it the ideal selection for many applications that require parallel, high-throughput predictable droplet creation.

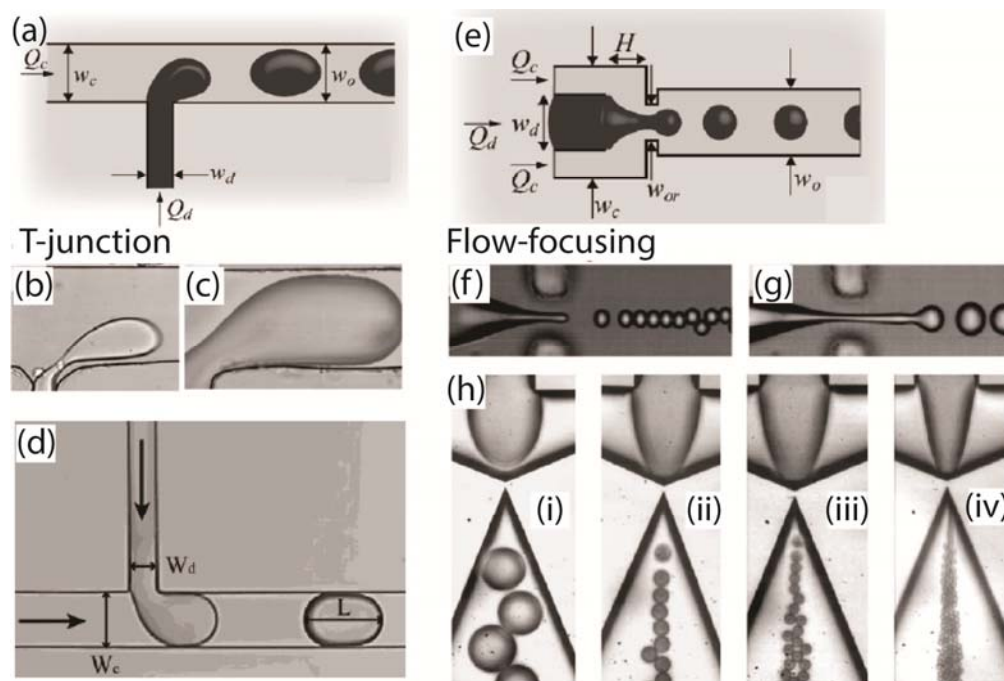


**Figure 1.5.** Droplet formation or metering. Schematic views and microscopic images of main droplet generators for a-d) a T-junction geometry,<sup>43, 47</sup> and microscopic images of droplets formation at e-h) flow-focusing geometries.<sup>41-42</sup> (© IOP Publishing. Panels ‘a-c’ and ‘e’ reproduced by permission of IOP Publishing. All rights reserved. Panels ‘f, g’ reprinted with permission from [41]. Copyright 2006, AIP Publishing LLC.; panel ‘h’ adapted from [42] by permission of The Royal Society of Chemistry.)

Dispersed droplets are also created using flow-focusing geometry, a microfluidic extension of Rayleigh's approach, in which two streams of one liquid squeeze a stream of a second immiscible liquid followed by forcing the combined two-phase flow through a small orifice. The viscous forces exerted by the outer fluid ultimately break the inner fluid into droplets, either in or just downstream of the orifice. The method is easily adjusted to produce droplets of various compositions (Figure 1.5e-h), as reported by successful synthesis of monodisperse microparticles from solutions that allow *in-situ* solidification of droplets (e.g. photopolymerization).<sup>52</sup>

### 1.3.2 Mixing

As mentioned earlier, droplets are considered as reaction confinements. In order to implement reactions inside droplets, different reactants have to be introduced into the droplet. A method to combine different reactants is to flow them as laminar flow streams with subsequent droplet formation through the injection of an immiscible fluid (Figure 1.6).<sup>15</sup> Mixing within the droplets can be accelerated by internal recirculating flow due to shear forces induced by the motion along the stationary channel wall.<sup>31</sup> When two liquids of different viscosities are mixed in a droplet the internal recirculating motions are increased further (Figure 1.6d-f).<sup>53</sup> An inert liquid can be inserted within reactant streams prior to merging in a single droplet to perform the *dilution* (Figure 1.6c). The concentration of the reactants within a droplet can be manipulated by mixing ratios through varying the volume flow rates of the reactant streams.<sup>54</sup> A combination of two opposing T-junctions connected to the main channel is used for generation of droplets of alternating composition (Figure 1.6a).<sup>55</sup> A similar technique is employed to inject an additional reactant into a liquid plug flowing



through the microchannel at an extra downstream T-junction.<sup>56</sup> In addition to liquid chemical reagents, other components like cells can also be loaded into droplets.<sup>57</sup>

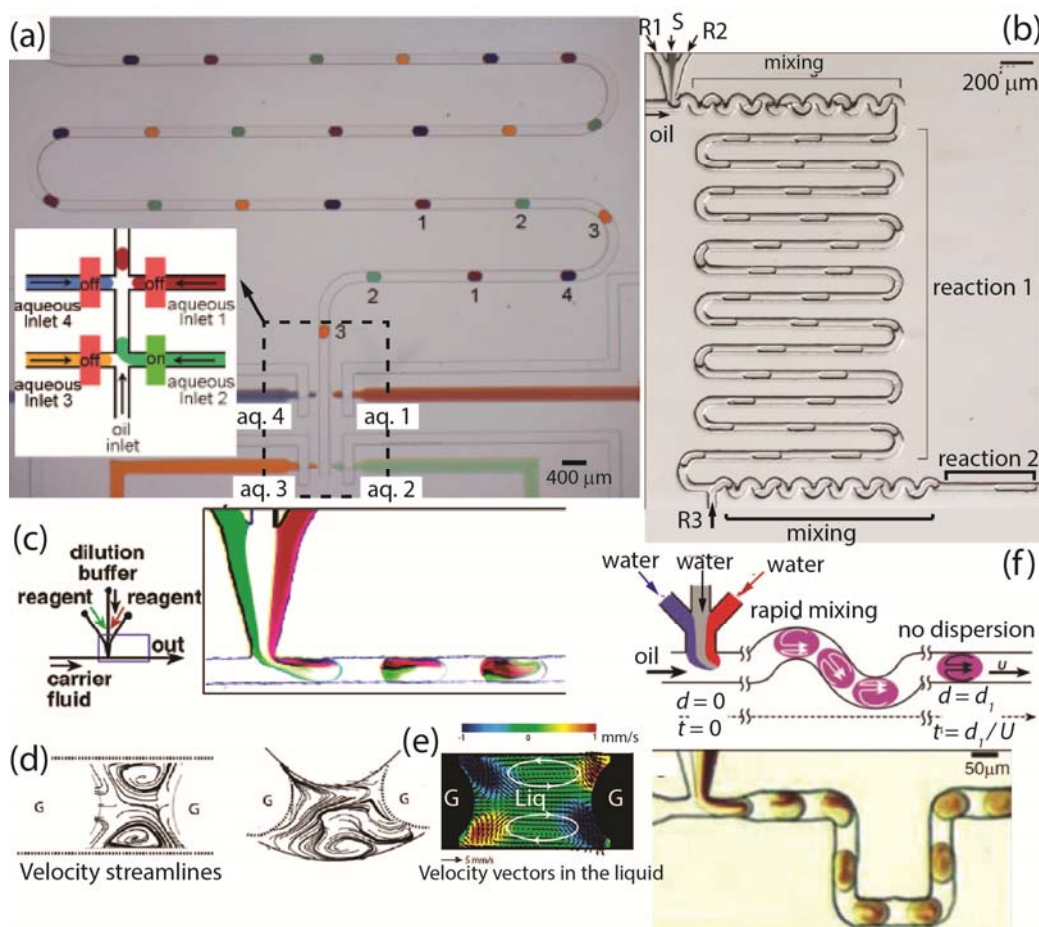


**Figure 1.6.** Mixing and dilution in droplets. a) Formation of droplets with various chemical compositions by using a combination of opposing T-junction.<sup>55</sup> (Reproduced from [55] by permission of The Royal Society of Chemistry) b) A microfluidic system to perform a two-step reaction in which droplets are used as containers. Aqueous reagents R1 and R2 are merged in a T-junction to form a droplet which flows in oil. Mixing is accelerated by chaotic advection as droplets flow through a serpentine microchannel. After mixing section a longer channel allows the reaction in droplets to proceed. To initiate the second reaction, a third reagent, R3, is added later at the second T-junction placed in the microchannel downstream.<sup>56</sup> (Reproduced from [56] by permission of The Royal Society of Chemistry) c) Inserting a buffer solution prior to merging in a single droplet dilutes the reagents concentration.<sup>54</sup> (Adapted with permission from [54]. Copyright 2003, American Chemical Society) d-f) Mixing in liquid droplets and continuous segments through internal recirculating motions.<sup>15, 59-60, 63</sup> (Panel ‘d’ adapted from [60] by permission of The Royal Society of Chemistry; Panel ‘e’ adapted with permission from [63]. Copyright 2004, American Chemical Society; Panel ‘f’ reproduced with permission from [15]. Copyright 2003, John Wiley and Sons. and from [59], by permission of the Royal Society.)

Based on this effect, a mixing scheme with serpentine microchannels<sup>58</sup> is proposed in which inner recirculation leads to stretching and folding the phases due to the changes of the orientation between the phase pattern in the droplet and the direction of motion. Consequently, sub-millisecond mixing can be achieved for multi-step chemical reactions.<sup>56, 59</sup> The internal recirculating motions can accelerate the mixing not only in dispersed fluid but also in the carrier fluid segments. Based on this effect, gas bubbles are introduced in the liquid flow and initiated internal recirculating motions within the liquid segments.<sup>60-62</sup> By implementing the gas-liquid segmented flow with enhanced mixing in the liquid segments in addition to a capillary-based technology to separate gas bubbles, Khan *et al.* have demonstrated the synthesis of highly monodisperse colloidal silica particles.<sup>63</sup>

### 1.3.3 Chemical Reaction

Owing to the power of controlled production and manipulation of droplets, individual droplets in microdevices serve as floating containers or reaction flasks that capable of accommodating different reagents for kinetic measurements.<sup>59</sup> Using microfluidic techniques, it is possible to control when a reaction begins, for how long each reaction proceeds before it is separated or combined with other reactions. The incubation or reaction time of the reagent mixed in a droplet at the junction can be easily determined by linear transformation of space (distance travelled by the droplet) into time (reaction time). As the reaction mixture is transported by the fluid stream at a constant velocity  $U$ , every spatial point  $d$  corresponds to a time point  $t$  in which  $t=d/U$ .<sup>15</sup> Hence, the incubation time can be temporally monitored by screening along the microchannel from the injection point to positions farther downstream. This is enabled in microfluidic platforms, and investigation of reaction kinetics on the order

of few milliseconds can be achieved.<sup>54</sup> Stable incubation times on the order of a week have also been demonstrated.<sup>64</sup> This is obtained by separating the droplet compartments with a carrier fluid that prevents evaporation and diffusion.

The extended microfluidic system for controlled multi-step reactions by injecting new reagents at designated downstream locations is demonstrated in Figure 1.6b. It shows a microfluidic system to perform a two-step reaction in which droplets are reaction containers. Aqueous reagents R1 and R2 are merged in a first T-junction to form a droplet flowing in oil. In this device design, mixing is accelerated by chaotic advection generated by shear stresses on droplets interface as they flow through a serpentine microchannel. After the mixing section, a longer channel gives the droplets enough residence time and the reaction proceeds further. To initiate the second reaction, a third reagent, R3, is added later at the second T-junction placed microchannel downstream.<sup>56</sup>

There are several applications that rely on reactions occurring within droplets, from protein expression to organic compound synthesis. Microscale reactions preserves expensive and valuable reagents, allows performing multiple reactions to be carried out in parallel manner, reduces the exposure to hazardous chemicals.<sup>65</sup> Scaling down the reaction in microscale reactors minimizes the risk involved with exothermic reactions and increases the reaction rates due to shorter diffusion, heat and mass transfer distances. Although chemical reactions in microfluidic systems are mostly performed in single phase flow,<sup>66</sup> there has been expanding research and industrial interest in compartmentalizing the reactions by multiphase microfluidics. Droplet microfluidics offers great control over reactions within droplets for crystal growth,<sup>67-</sup>

<sup>69</sup> particle synthesis of cobalt<sup>70</sup> and titania,<sup>71</sup> nanomaterial synthesis<sup>72</sup> such as anisotropic gold nanoparticles<sup>73</sup> and core-shell structured nanoparticles.<sup>74</sup> Semiconductor CdSe quantum dots have been synthesized in microfluidic segmented flow under high-temperature condition.<sup>75</sup> CdS/CdSe core-shell nanoparticles were also produced by droplet generation, mixing, and merging in a multi-step synthesis process.<sup>56</sup>

Using a simple biphasic hydrolysis reaction, Ahmed *et al.* showed significant increase in reaction rate and efficiency by segmentation in microreactors compare to conventional flasks. They also reported a dramatic increase in the reaction rate of a homogenous reaction (Heck reaction) using segmented flow in comparison with homogeneous single phase flow in microreactors.<sup>76</sup> Burns and Ramshaw<sup>77</sup> have also demonstrated a large enhancement in interfacial mass transfer and reaction rate in segmented multiphase microreactors by monitoring the extraction of acetic acid from kerosene and two simple acid-base titration reactions in droplets. Due to higher surface area to volume ratio, smaller droplets are expected to enhance the reaction rate even more.<sup>77</sup>

Droplet microfluidics is also used for organic phase reactions, although some organic solvents can deform the channels and cause the chemical leakage and cross contamination. In this regard, thiolene microdevices are surface treatable and reported to have higher chemical stability compare to PDMS devices to form water-in-oil and oil-in-water emulsions.<sup>78</sup> Generally, droplet-based microfluidics can offer high reproducibility of compounds while reactions are performed under chemically safe conditions, however still methods to perform biphasic reactions with an inert

continuous phase and strategies to eliminate chemical clogging and precipitation and to collect products by separating droplets and continuous phase should be developed.

### **1.3.4 Droplet Traffic**

Controlled droplet generation and navigation in complex networks, is essential for performing all these applications and tasks. Multiphase flow in network of capillaries is ubiquitous in nature and complex microchannel networks exist in blood flow,<sup>79</sup> crude oil and water flow within porous media and rock cracks,<sup>80</sup> and flow in membranes.<sup>81</sup> However, man-made microfluidic devices consist of simple units. The design of lab-on-a-chip devices implementing multiple tasks and activities in parallel<sup>82-84</sup> requires detailed insight in routing of droplet flows within networks of microchannel. This is not a trivial subject as many factors can influence the droplet trajectories as they are always associated with the passive response of the system. Puzzles often develop even in simple geometries with complex dynamics.<sup>85-86</sup> For instance, usually the viscous dissipation caused by droplets changes the distribution of pressure in the network of microchannels, and thereby position of every single droplet is affected by the path taken by the others.

To steer the droplets at microfluidic networks, both passive methods which rely on merely hydrodynamics and capillarity,<sup>15, 44, 87-91</sup> and active means (electro/dielectrophoresis, surface-acoustic waves, electrowetting, pneumatic and electric valves, etc) have been implemented<sup>85, 87, 91-92, 93-94</sup>. A significant feature of microfluidics is the possibility of creating large fluidic network<sup>82</sup> for plugs merging and splitting. Simple and basic microfluidic methods are demonstrated by the Ismagilov group to combine two streams of plugs into a single stream in a main

channel (merging). They also showed division of one stream of plugs into two streams (splitting) at a channel branching point.<sup>15</sup> The same technique was later employed by Link *et al.* to form microfluidic emulsions with controlled volume fractions and sizes.<sup>95</sup>

In general, inclusion of bifurcations and loops in a network of microchannels, significantly alter the behavior of multiphase flows.<sup>95-97</sup> A droplet reaching a bifurcation or a simple T-junction, might break into two daughter droplets or simply flows into either of the branches with lower resistance to flow.<sup>95</sup> There are flow regimes in which the presence of droplets in a bifurcated arm increases the flow resistance in that arm; thereby, affects the choice of the successive droplets.<sup>98-100</sup> This feedback is amplified by slight inherent differences in the resistance of the bifurcation arms due to the fabrication and makes the flow dynamics complicated for selection of right/left pathways.

#### **1.3.4.1 Droplet fusion (merging) and fission (splitting)**

Controlled droplet coalescence is an important unit operation for performing reactions within droplets. Microfluidics provides a means to controllably fuse droplets so that reactions can be initiated in a highly precise manner, as premature merging of droplets will still cause defective products. Active and passive merging of droplets are reported using electrodes and channel geometry, respectively. Figure 1.7a, shows an example of active methods for merging droplets using electrocoalescence. Figure 1.7b-e demonstrates passive droplet merging by channel geometry using surface patterns, narrowed and widening channels that affect the speed of droplets and cause their merging, and a simple T-junction geometry.

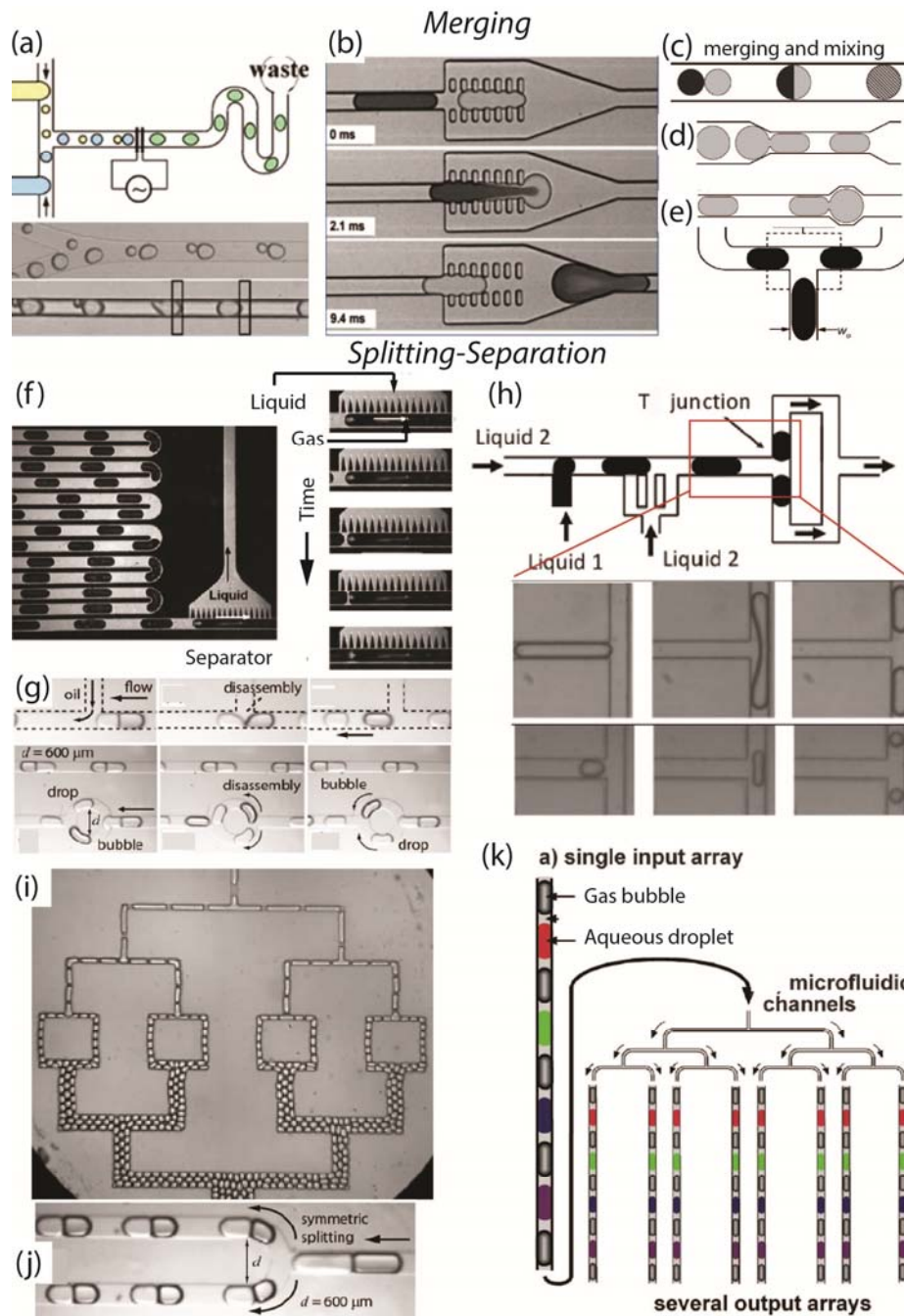


**Figure 1.7.** (a-e) Merging droplets,<sup>26, 101-105</sup> (f,g) separating bubbles<sup>60</sup> and gas-liquid compound droplets<sup>35</sup> (h-k) splitting single droplets and more complex emulsions.<sup>35, 95, 106-107</sup> a) Active merging of droplets using electrocoalescence,<sup>101</sup> (Reprinted with permission from [101]. Copyright 2006, AIP Publishing LLC.) (b) passive droplet merging by channel geometry; surface patterns induces the coalescence of droplets.<sup>102</sup> (Adapted from [102] by permission of The Royal Society of Chemistry) Schematics of c) reaction initiation by merging two droplets<sup>26</sup> d) narrowed and widening channels which affect the speed of droplets and cause their merging.<sup>26</sup> (Panels 'c' and 'd' adapted from [26]. © IOP Publishing. Reproduced by permission of IOP Publishing. All rights reserved.) e) merging droplets at a simple T junction.<sup>103</sup> (Reprinted from

[103] by permission of The Royal Society of Chemistry) f) Separation of gas bubbles from liquid stream using capillary separator.<sup>60</sup> (Reprinted from [60] by permission of The Royal Society of Chemistry) g) gas-liquid compound droplets are separated using either extra oil injection or bifurcated microchannels.<sup>35</sup> h, i) bifurcating single droplets at simple T-junctions.<sup>95, 106</sup> (Panel ‘h’ reprinted with permission from [106]. Copyright 2009, AIP Publishing LLC. and panel ‘i’ reprinted with permission from [95]. Copyright 2004 by the American Physical Society.) j, k) splitting of complex emulsion at bifurcated channels.<sup>35, 107</sup> (Panels ‘g’ and ‘j’ reprinted from [35] and panel ‘k’ from [107] by permission of The Royal Society of Chemistry.)

Droplet fission or splitting is a critical operation in droplet microfluidics since splitting a single droplet into two or more droplets can increase the experimental capacity. Droplet splitting is also a method to control the concentration of droplet content, in addition to increasing the throughput. Splitting droplets by passive methods depends on the shear forces created by channel design to divide the droplets at precise locations into controlled volumes. Several hydrodynamic designs have been used for droplet fission such as T-junctions,<sup>95, 106-107</sup> branching channels<sup>35</sup> (Figure 1.7h-k) and channel obstructions. Passive droplet splitting can be controlled by manipulation of the flow rate and the channel resistance. At symmetrical bifurcating junction the flow applied to either half of the droplet is equal and causes the splitting of droplets into two identical daughter droplets. Embedding an obstacle in the vertical axis of the channel is also used to control the sizes of the resulting droplets after break up.

#### **1.3.4.2 Droplet sorting**

A unique power of droplet microfluidics is to generate, transport and analyze droplets individually. As such, an additional unit operation of segmented microfluidics is *sorting* the stream of plugs. Sorting enables distinct control of a single droplet out of a population of droplets and facilitates a range of functions including isolation of



droplet of interest, purification of synthesized products encapsulated in a group of droplets and segregation of heterogeneous combination of droplets.

Like previously discussed operations, sorting can be performed in both passive and active ways. While in passive sorting systems a bias is applied to distinguish the species to be sorted, an active sorting system employs an increased level of complexity with dynamic control over the bias and shows more flexibility over the sorting parameters. It is noteworthy that in passive sorting the bias and the sorting parameter are coupled; whereas in active systems they need not be. This allows active systems to sort droplets using a wider range of characteristics such as particle content or functionality utilizing a mechanism to manipulate the flow of droplets and a method to detect the sorting criteria.

Gravity and channel geometry are employed to sort droplets passively whereas electrical control is used for active sorting. Cristobal *et al.* have shown a passive and regular distribution of droplets between the two arms of a simple T-junction using the ‘bypass’ (Figure 1.8a).<sup>108</sup> Figure 1.8a illustrates schematic and snapshot of two junctions in the same device fed by a single droplet generator which distributes droplets into both channels using the droplet distributor bypass. The leftmost junction with a bypass shows a perfectly alternating distribution of droplets between its two outlets. The junction on the right with no bypass shows a random alternation of droplets mainly by filtering into one arm. The Weitz group has sorted individual droplets based on the drops charges and electric fields.<sup>109</sup> They have also used active

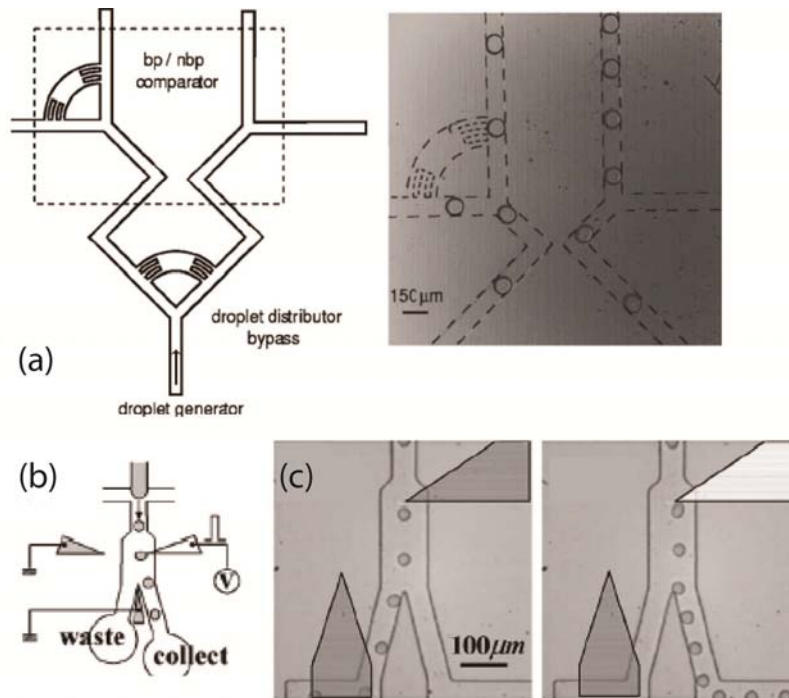


**Figure 1.8.** Droplets sorting using (a) bypass channels<sup>108</sup> and (b-c) dielectrophoresis<sup>110</sup>. a) Schematic (left) and snapshot (right) of two junctions in the same device fed by a single droplet generator which distributes droplets into both channels using the droplet distributor bypass. The leftmost junction with a bypass shows a perfectly alternating distribution of droplets between its two outlets. The junction on the right with no bypass shows a random alternation of droplets mainly by filtering into one arm.<sup>108</sup> b) Schematic view of the device used for dielectrophoresis sorting.<sup>110</sup> (c) In the absence of an electric field, water droplets flow into the waste channel while in the presence of an electric field, the droplets flow towards the energized electrode and collection channel.<sup>110</sup> (Reprinted with permission from [108] and [110]. Copyright 2006, AIP Publishing LLC.)

method of dielectrophoresis for sorting single droplets out of a droplet train (switching) at rates up to 4 kHz (Figure 1.8b).<sup>110</sup> Figure 1.8b shows the schematic view of the device that has been used for dielectrophoresis sorting. In the absence of an electric field, water droplets flow into the waste channel while in the presence of an electric field, the droplets flow towards the energized electrode and collection channel.

### **1.3.5 Material Synthesis through Phase Change in Droplets**

Many chemical and biomedical applications require materials that are in the solid or gel state rather than liquid form. Solid particles and hydrogels are used in drug delivery and encapsulation of cells for implantation and drug studies. Thereby, droplet-based systems have been created to form solid particles and hydrogel beads through different means. Two approaches are mainly utilized to change the phase of droplets from liquid to either solid or gels in microfluidic systems. In the first method either of ultra-violet (UV) light or chemical agents to initiate polymerization is used. UV light activates photo-initiators in the droplet which makes monomers to link to each other and solidifies the droplets. Chemical agents have also been employed to induce polymerization where fluidic channel design becomes an important factor in introducing these chemicals to droplets. In the second method, solvent extraction or evaporation is used in combination with droplet microfluidics to form monodisperse polymer particles. Choi *et al.* showed a simple capillary-based microfluidic method consisting of flexible tubing and a narrow gauge needle for solvent evaporation to form monodisperse microspheres.<sup>111</sup> The Weitz group demonstrated the generation of polymersomes by forming water/oil/water emulsions with diblock polymers dissolved in the oil phase followed by removing the solvents through evaporation.<sup>112</sup>

#### **1.3.5.1 Photopolymerization**

Photopolymerization uses UV light to activate photo-initiators that could then become reactive radicals. Radical polymerization then links the monomers and solidifies the droplet. Since many microfluidic devices are made of optically transparent polymers or glass, they are capable of incorporation of light source into the set up to perform photo-initiated polymerization process. More interestingly, novel particle shapes have

been created using microfluidic platforms that simply cannot be made using conventional batch techniques. Due to the simplicity of photopolymerization over other methods of solidification, a wide range of different designs have been established utilizing this method. Some research groups have shown off-chip photopolymerization process to generate gel beads. For instance, De Geest *et al.* used a flow focusing design to emulsify an aqueous dextran-hydroxyethyl methacrylate (dex-HEMA) phase within an oil phase at the junction of PDMS microfluidic channels. The droplets are collected along with the oil in a vial and immediately irradiated and polymerized by UV illumination. The resultant monodisperse microgels are biodegradable and capable of controlled delivery of proteins.<sup>113</sup> Similarly Ikkai *et al.* designed an array of microchannels in combination with off-chip UV irradiation to create N-isopropyl acrylamide gel beads.<sup>114</sup>

UV illumination can also be integrated in microfluidic devices for on-chip photopolymerization of droplets. The primary challenge of on-chip photopolymerization is to provide sufficient residence time to droplets for being exposed to the UV irradiation. Different schemes are developed to overcome this issue. For example, the photosensitive reagents accommodated in droplets were protected from the UV exposure by covering the whole PDMS-glass capillary hybrid device except a small window for polymerization of passing droplets.<sup>115</sup> It is noteworthy to highlight a novel photopolymerization technique called “continuous-flow lithography” which uses photomasks of different shapes for creation of different irregularly-shaped microparticles. Since microfluidics is the only platform for generation of such irregular microparticles in an extremely controlled manner, in the next section we elaborate the formation of such particles in more details.

### **1.3.5.2 Microfluidics for irregular particles**

Some of the polymerization mechanisms can also be performed in traditional macroscale batch processes. However, there are droplet-microfluidic techniques for formation of microparticles that are nearly impossible to be performed in macroscale batch systems.<sup>116</sup> Such novel techniques exploit the unique properties of microfluidic platforms such as laminar flow and distinct control of local flow conditions to create irregular objects including non-spherical particles, Janus droplets for synthesis of Janus microparticles, and double emulsions to form core-shell structures.

Macroscopic formation of monodisperse nonspherical particles is very difficult to be achieved due to the fact that surface forces cause droplets to hold spherical conformations in their suspending medium. On the other hand, in microfluidic systems, droplets can be physically confined in microchannels, hence the particles shape can be dictated by the channel geometry. Both Doyle and Kumacheva groups, created spherical and nonspherical particles using droplet microfluidics.<sup>89, 117</sup> After the generation of droplets, they flow towards the shape-defining region where rod-shaped or disk-shaped particles can be formed. Rod-shaped particles are created by microchannels with width and height smaller than droplet diameter while disk-shaped particles are created by microchannels with height smaller than droplet diameter and width larger than that. In such circumstances, droplets are dictated to be flattened and reshaped according to the channel geometry and after UV irradiation they retain their irregular shapes.

Besides photopolymerization, shape-controlled hydrogel microstructures (e.g. spherical, disklike, rodlike, pluglike, threadlike microparticles) were formed by a

chemical reaction of sodium alginate and  $\text{CaCl}_2$  where the size and shape of the particles were controlled by adjusting the flow parameters in microchannel.<sup>118</sup>

Another approach to create irregular particle shape is through self-assembly at liquid-liquid or gas-liquid interfaces.<sup>119-120</sup>

Recently droplet microfluidics has been used to form Janus particles with not only two distinct surface regions, but also with two types of internal compositions. Nisisako *et al.* demonstrated the formation of Janus black and white particles using microfluidic platform. The two parallel flows of black and white monomers with matching viscosities were introduced in the middle channel of a flow focusing junction to form Janus droplets. These droplets were collected and thermally polymerized to form Janus particles.<sup>90</sup> Due to the difference in electrical properties of carbon black and titanium oxide (white), the resultant Janus particles were able to be rotated in electric field which could find their potential application in display technologies. Similarly this microfluidic system can be developed further to form ternary particles instead of Janus particles. This is accessible by replacing three parallel monomer streams in the middle channel of a flow-focusing geometry. The streams can be sheared by a continuous phase to form ternary droplets prior to the UV-exposure. The final Janus particles can be chemically functionalized later. This method enables the explicit control over the coverage of the surface modification on the particle through the precise control on the material compositions of the Janus particles.

Controlled formation of monodisperse double emulsions is another type of emulsion systems with more complexity. Although conventional batch techniques are able to

form double emulsions,<sup>121</sup> polydispersity is the main hurdle for controlled production of double emulsions. Recently many groups have successfully demonstrated droplet-based microfluidic systems for controlled generation of double emulsions.<sup>38, 122-123</sup> The ability to produce monodisperse yet complex multilayer emulsions and hydrogel capsules suggests that droplet microfluidics has the potential to create novel delivery vehicles for therapeutic agents.

### **1.3.6 Chemical Sensing and Detection**

Droplet microfluidics shows great promise as a new high-throughput technology in chemical, biochemical processes, and molecular biology with droplet generation rate of up to few thousands per second.<sup>124</sup> With the technologies that have been already developed for creating, merging, dividing and sorting microdroplets, one of the main challenges to be remained is how to access their content. Droplets are self-contained microreactors that prevent sample loss and cross-contamination, general issues that are involved with continuous laminar flow microfluidics. However, the isolated nature of droplets prevents easy physical access of their contents on-chip. As such, a very crucial step in droplet microfluidic unit-operations is the sensing and detection of droplets for which it is required to track the position of individual droplets. Droplet sensing and specifically analyzing the content of droplets is one of the most important steps that is required to be optimized to achieve a fully automated droplet-based lab-on-a-chip operation.

Compared with the macroscale, manipulation and processing extremely small sample volumes in microscale systems (picolitres to hundreds of nanolitres) makes the analyte detection and identification a significant challenge of lab-on-a-chip

chemical/biochemical processes. Moreover, effective detection within microfluidic systems is affected by interconnected factors such as detector sensitivity, response time, detection limits and information content. Although microfluidics is a powerful tool to generate highly controlled chemical information like reagent concentration, temperature and pH, extraction of all available information is normally non-ideal.<sup>125</sup> For instance, thousands of chemical reactions can be processed in very short times by segmented flow microfluidics that is able to generate picolitre-sized droplets of varying chemical composition at very high frequencies (>100 Hz). However, very limited studies have exploited this feature in developing detection systems with analytical throughput as high as generation speed.

Despite the challenges involved in extracting information in microsystems, some reports have demonstrated the developments of high-throughput chemical screening. Analytical techniques such as mass spectrometry, capillary electrophoresis, and liquid chromatography have been successfully integrated with continuous-flow microfluidic devices, but their application for droplet microfluidics is still challenging.<sup>126</sup> However, by discarding the carrier fluid and converting droplet phase into continuous stream, the advantage of microdroplet systems could be combined with these analytical techniques.<sup>127-128</sup>

Droplet contents are often detected through techniques such as optical and electrical methods. The majority of systems for droplet monitoring is based on optical measurement. A high speed camera attached to optical or fluorescence microscope can simply be used to track the individual droplets in most cases. The fluorescence intensity emitted from a fluorescent dye can be intensified or diminished depends on



the chemical surroundings. The obtained fluorescence signal can be analyzed *in situ* and employed to trigger, for instance, a sorting process for high-throughput screening.<sup>129-130</sup> Adding certain types of quantum dots with a characteristic emission spectra into droplets, make the detection and sorting different types of droplets possible.<sup>131-132</sup> Measurement of size and speed of droplets are also achievable without the use of large microscope setup. Small light-sensitive diodes can be embedded on a distinct spot of the microchannel to do such automotive measurements.<sup>133-134</sup>

Many alternative droplet detection techniques rely on electrical methods. For example, the position of densely packed bubbles and droplets can be determined by capacity measurements using ferromagnetic and electrorheological fluids as the continuous phase, respectively.<sup>135-136</sup> Droplets can alternatively be sensed by their impedance signal using thin electrodes embedded in the microfluidic channel. This method allows the concentration measurements of ionic solutes in water droplets surrounded by any oily phase.<sup>137</sup> Droplets can also be detected by an electrochemical response using a single electrode in contact with a passing droplet<sup>138</sup> or, alternatively, by measuring the heat loss of an area that is kept at elevated temperature.<sup>139</sup> By defining the area fraction of an electrode covered by the droplet the *in situ* measurement of droplets size can be achieved.

Mass spectrometry (MS) is a sensitive and label-free detection method that is able to read out of low-concentration contents within droplet. Both matrix-assisted laser desorption ionization (MALDI-MS) and electrospray ionization-mass spectrometry (ESI-MS) have been applied to studying droplet contents in segmented flow.<sup>140</sup> The Ismagilov group illustrated a rapid screening method within a capillary-based

microsystem that consumed submicrogram substrate per reaction. Organic reactions were performed in discrete droplets/plugs separated and transported in fluorinated carrier fluid. The reagent droplets were merged with the substrate flow and formed the final plugs of microreactors which flew into the receiving tube. Following this, the flow of plugs was stopped and the receiving tube was isolated by sealing.<sup>141</sup> After incubation, sample was then deposited onto a matrix-assisted laser desorption/ionization (MALDI) plate and analyzed by MALDI-mass spectrometry (MALDI-MS) to assess reaction progress. Reaction optimization was achieved by screening more than 40 reagents to evaluate reactivity, and repeating the screen with a more focused reagent set while varying reaction conditions (e.g. reaction time, solvent and concentration). Although the optimization timescale is limited by the speed of MALDI-MS, the system is simple to implement and able to process reactions on submicrogram level.

## **1.4 Designer Emulsions**

Multiple emulsions or ‘emulsions of emulsions’ are microdroplets that completely engulf smaller droplets as they are surrounded by a continuous liquid phase. The two main types of multiple emulsions or double emulsions are water-in-oil-in-water (W/O/W) and oil-in-water-in-oil (O/W/O) emulsions. In the former type of emulsion, water-in-oil (W/O) emulsion is dispersed in an aqueous phase and in the latter case oil-in-water (O/W) emulsion is dispersed in an oil phase. The number and size of the inner droplets can be varied from one to multiple fine microdroplets. To form stable multiple emulsions, both hydrophilic and lipophilic surfactants are normally incorporated in the intermediate and external phase.

Multiple emulsions have attracted considerable interest due to their high potential applications in food science and technology, cosmetics, and pharmaceuticals. For instance studies on pharmaceutical applications of W/O/W have reported the encapsulation of water soluble drugs by internal aqueous droplets for controlled release and delivery. As briefly mentioned in 1.3.5.2, there are many applications of such multiple emulsions in material synthesis. Solid microcapsules of bioactive polymers were prepared by solvent extraction in W/O/W emulsions. The other reported attractive applications include the formation of composite microspheres and the use of an intermediate phase of double emulsions as permeable membrane in separation technology.<sup>142</sup>

The formation of double emulsions in conventional methods is through two-step bulk emulsification. In the first step, a primary single emulsion is prepared which is followed by the second step of gentle emulsification in the third immiscible liquid. The second step of emulsification is performed under low-shear conditions to prevent the disruption of initial single emulsions. This method, though easy to implement, still faces challenges in generating monodisperse multiple emulsions. This is attributed to the lack of control over the droplet size distribution in both emulsification steps.

On the other hand, recently developed microfabricated structures are able to prepare highly monodisperse multiple emulsions. More interestingly, some of these methods have precise control over the size, composition and structure of the final multiple emulsions. Some of these microfabricated devices include porous emulsification membranes, silicon chips with microfabricated comb-like structure, two-dimensional

(2D) microfluidic devices, and three-dimensional (3D) coaxial microcapillary devices.<sup>142</sup>

Production of precisely controlled multiple emulsions could be useful to researchers as models for investigation on the stability of dispersions and controlled release of the inner substances to the surrounding. Highly monodisperse multiple emulsions with controlled sizes and structures have a wide range of potential applications. The Weitz group has been a pioneer in high-throughput formation of highly controlled multiple emulsions and core-shell hydrogel structures using microcapillary devices.<sup>38</sup> They were able to achieve a precise control over the size, location and number of engulfed droplets at each level of emulsification (Figure 1.9a). Such multiple emulsions are flexible to be formed in either hydrophilic or hydrophobic continuous fluids. For example, the Weitz group reported the application of monodisperse multiple emulsions prepared by 3D coaxial microcapillary devices in different types of material synthesis such as polymeric shell cured by UV exposure,<sup>38</sup> and polymersomes made from diblock copolymers,<sup>38</sup> thermosensitive microcapsules from W/O/W/O emulsions being able to release the innermost aqueous droplets by increasing the temperature of the environment.<sup>123</sup> The Kumacheva group also demonstrated the production of core-shell droplets and polymer capsules with predetermined diameter of cores and thickness of shells in scalable microfluidic devices fabricated in polyurethane.<sup>143</sup> Nisisako *et al.* applied a combination of three consecutive surface modified T junctions with alternating surface wettabilities to create double emulsions in which two discrete inner aqueous droplets are encapsulated by an oil droplet suspend in an outer aqueous phase.<sup>144</sup> By using this surface modified microfluidic device, they could also report highly control over the

number of entrapped droplets (Figure 1.9b). The generated double emulsions were useful for encapsulation purposes and extractions across the thin layer that separates internal droplets and the continuous phase.<sup>144</sup>

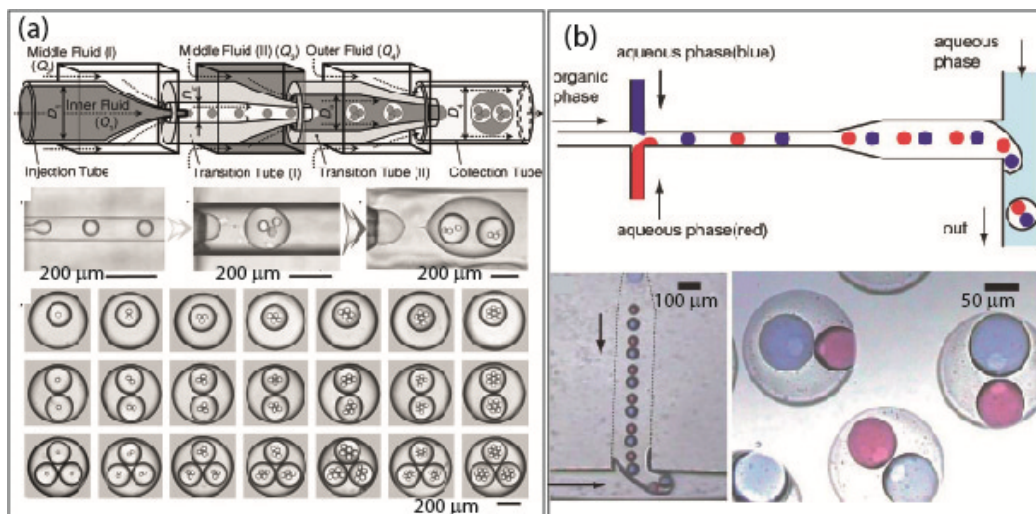


**Figure 1.9.** (a) Schematic diagram and optical micrographs of the extended capillary microfluidic device for generating triple emulsions that contain a controlled number of inner and middle droplets stages.<sup>123</sup> (Reproduced with permission from [123]. Copyright 2008, John Wiley and Sons.) (b) Schematic diagram and photographs of the alternating formation of aqueous droplets at the upstream junction and subsequent encapsulation at the downstream junction to form W/O/W droplets.<sup>51, 144</sup> (Reprinted from [144] by permission of The Royal Society of Chemistry.)

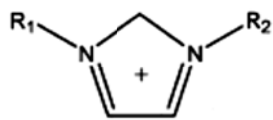
Polymeric materials with tunable morphologies from O1/O2/W emulsions are also prepared in the 2D coaxial flow-focusing microfluidic device.<sup>143</sup> It is noteworthy that for industrial applications drastic scale-up of productivity would be required. As such 2D microfluidic systems are suitable candidate due to the easy fabrication of multiple 2D drop generators in parallel on a chip using lithographic techniques.<sup>145</sup>

## 1.5 Designer Fluids - Ionic Liquids (ILs)

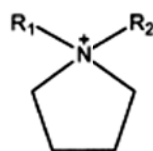
Ionic Liquids (ILs) are liquid salts composed entirely of ions. Ionic liquids, in general, melt at or below 100 °C. The ILs that are liquid at room temperature (25 °C) are called room-temperature ionic liquids (RTILs). Ionic liquids contain an organic cation (based on the imidazolium, pyridinium, ammonium, or phosphonium groups) and an inorganic (such as halides, BF<sub>4</sub>, PF<sub>6</sub>) or organic (trifluoromethanesulfonate (triflate) counter anion. The desired anions of a particular IL are achieved by metathesis reactions.<sup>146</sup> Ionic liquids differ from the molten salts studied in the mid- to late-twentieth century. Molten salts are generally mixtures of alkali metal salts, which often have limited liquid ranges, thermal and chemical stabilities.<sup>147</sup> In contrast, ILs usually contain only one type of cation-anion combination and have exceptional stability over a wide range of temperatures.

ILs have remarkable properties including wide liquid range, high electrical conductivity, excellent thermal stability, very low volatility (negligible vapor pressure) and therefore nonflammability, wide range of viscosities, reusability, adjustable miscibility and good solvation capability for a broad range of organic, inorganic and biological molecules and metal ions. Such fascinating properties make ILs 'green' solvents and motivate their use as alternative 'green' reaction media for organic and enzymatic reactions.<sup>148-150</sup> The unique features of ionic liquids are the result of the fact that ILs are composed entirely of ions. Consequently, ILs may behave differently from common molecular liquids when used as solvents. Figure 1.10 shows the structures of common cations and anions used in ILs. The relatively large size of one or both ions and low symmetry in ILs, cause the low melting points of these materials.

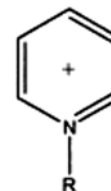
### Common cations



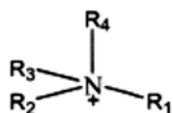
imidazolium



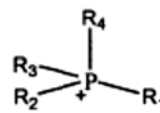
pyrrolidinium



pyridinium



tetraalkylammonium



tetraalkylphosphonium

### Common anions

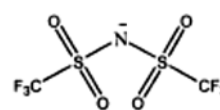
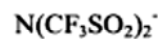
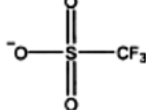
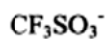
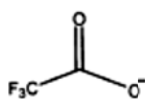


**Figure 1.10.** Structures of common cations and anions of ionic liquids.

A key feature of ionic liquids is that judicious selection of the anion and/or cation enables facile and predictive tailoring of their chemical and physical properties such as viscosity, density, hydrophilicity/hydrophobicity, ionic conductivity and chemical reactivity.<sup>151-153</sup> Combinations of various cations and anions result in formation of tremendous numbers of ILs and make custom-made ILs feasible. Therefore, ILs have been touted as ‘designer’ compounds.<sup>154</sup> This provides a large pool, from which task-specific ILs can be made. The number of available ILs is estimated to be up to  $10^{18}$ .<sup>155</sup> These intrinsic features of ILs, together with the ease of synthesis, have progressively attracted much interest in employing them in the last decades in both academia and

industry. The design of ILs with targeted properties has been possible by introduction of structural functionalities on the cationic or anionic compartments. more recently, there has been growing research interest on fundamental understanding of these solvents, predicting their physicochemical properties and their increasing use in diverse applications such as sensors, fuel cell, batteries, capacitors, thermal fluids, plasticizers, lubricants, ionogels, extractants and solvents in analysis, synthesis, catalysis and separation.<sup>156</sup> In analytical chemistry, ILs were employed as stationary phases in gas chromatography,<sup>157-158</sup> additives for capillary electrophoresis,<sup>159-161</sup> matrices for MALDI.<sup>162-163</sup> These tunable multi-purpose liquids can be used as more than just alternative green solvents.

### 1.5.1 History

Ionic liquids (ILs) are a group of organic salts with reported melting points range from  $-81^{\circ}\text{C}$  to  $100^{\circ}\text{C}$ ,<sup>164-165</sup> which are much lower than other salts. A more acceptable form of ILs is room-temperature ionic liquids (ILs) which are salts with melting point lower than ambient temperatures.<sup>166</sup>

ILs have a long history and the discovery data of the 'first' IL is disputed. Gabriel and Weiner reported the synthesis of ethanolanmonium nitrate (m.p.  $52-55^{\circ}\text{C}$ ) in 1888.<sup>167</sup> The first report of a truly room-temperature ionic liquid was the synthesis of ethylammonium nitrate  $[\text{EtNH}_3][\text{NO}_3]$ , m.p.  $12^{\circ}\text{C}$ ) in 1914, attributed to Paul Walden.<sup>168</sup> Later, in the 1970s molten salts based on pyridinium cation with halide, was developed for use as electrolytes in battery applications.<sup>169</sup> For the same purpose, a new class of RTILs consisting of dialkylimidazolium chloroaluminate, were



reported by Wilkes *et al.* in 1982.<sup>170</sup> However, little attention was paid to these ILs due to their reactivity to moisture and many chemicals.

Although the first ILs were synthesized as early as the nineteenth century, it was over 100 years later that ILs started to attract the attention of scientists, specifically with the first development of air- and moisture-stable imidazolium salts in 1992. Wilkes and Zaworotko synthesized stable 1-ethyl-3-methylimidazolium-based RTILs containing weakly complexing anions, such as  $\text{BF}_4^-$ .<sup>147</sup> Since then numerous ILs have been synthesized and reported. Lacking the stability and potential toxicity of ILs with halogen anions, result in the formation of more ILs with low halogen content or halogen-free anions, such as bis(2-ethylhexyl)sulfosuccinate [BEHSS]<sup>-</sup>, trifluoroethanoate [ $\text{CF}_3\text{CO}_2^-$ ], acetate [ $\text{CH}_3\text{CO}_2^-$ ], bis((trifluoromethyl)sulfonyl)imide [ $\text{NTf}_2^-$ ], and trifluoromethanesulfonate [ $\text{TfO}^-$ ] have been synthesized.

As mentioned earlier, though ILs with alkylimidazolium cations and chloroaluminate anions were of interest in electrochemical research in the 1980s, due to instability of these ILs in water there was a need to find alternatives. Fuller and coworkers<sup>171-172</sup> incorporated 1-ethyl-3-methylimidazolium [ $\text{BF}_4^-$ ], [triflate], and [ $\text{PF}_6^-$ ] into a poly(vinylidene fluoride)-hexafluoropropylene copolymer to make a gel electrolyte. These ILs retained the same remarkable features of earlier chloroaluminate salts, such as high ionic conductivities and wide electrochemical window yet with more water stability.

New air- and water-stable ILs, in their early applications, were also used as solvents for organic synthesis and liquid-liquid extraction. In 1995, Suarez and coworkers<sup>173</sup>

reported the synthesis of 1-n-butyl-3-methylimidazolium [BMIM] [BF<sub>4</sub>] and [PF<sub>6</sub>] served as a solvent for a two-phase catalysis reaction involving rhodium complexes for the hydrogenation of cyclohexene. BMIM [BF<sub>4</sub>], [PF<sub>6</sub>], and [TfO] (trifluoromethanesulfonate) ILs were, later, used in the hydrodimerization of 1,3-butadiene via palladium catalysts in a two-phase system.<sup>174-175</sup> The Welton group<sup>176</sup> showed that [BMIM][BF<sub>4</sub>] was an even better solvent than dichloromethane for the hydrogenation of aryl hydrocarbon using ruthenium catalysts.<sup>177</sup> Seddon research team also performed biphasic enzyme-catalyzed reactions employing [BMIM][PF<sub>6</sub>].<sup>178</sup> By 1999, ILs not based on imidazolium or pyridinium cations began emerging for specific synthesis tasks.<sup>179</sup> These studies demonstrate how ILs have become attractive replacements for traditional organic solvents.

ILs were also used as solvents in liquid-liquid extractions. The Rogers group,<sup>180</sup> in 1998, applied ILs as solvents for the extraction of simple, substituted-benzene derivatives from water. [BMIM][BF<sub>4</sub>] and [PF<sub>6</sub>] showed similar partitioning behavior to that of the traditional octan-1-ol/water system. Although distribution coefficients were higher in the traditional system, the IL possessed an acceptable extraction power for practical extractions. It is noteworthy that the interest in using ILs as replacements for organic solvents arises from their negligible vapor pressure. Next, Dai and coworkers<sup>181</sup> added crown ethers to imidazolium-based ILs with either [PF<sub>6</sub>] or [NTf<sub>2</sub>] (bis((trifluoromethyl)sulfonyl)imide) anions for the extraction of strontium nitrate from water. Alkyl chains on the imidazolium cation and the chemical nature of the anion affected the distribution coefficient of the Sr<sup>2+</sup>, with the most efficient IL having a distribution coefficient four times higher than that of traditional organic solvents.<sup>182</sup> also used alkyl-3-methyl imidazolium [PF<sub>6</sub>] ILs along with organic (1-

(pyridylazo)-2-naphthol, 1-(thiazoylazo)-2-naphthol) and inorganic (cyanide, cyanate, thiocyanate, and halides) anions to extract metal cations such as  $\text{Cd}^{2+}$ ,  $\text{Co}^{2+}$ ,  $\text{Ni}^{2+}$ ,  $\text{Fe}^{2+}$ , and  $\text{Hg}^{2+}$ . These early studies led to significant increase in the research on the use of ILs as extractants.

Ionic liquids have been also used in other separation techniques such as gas chromatography (GC). In 1999, the Armstrong group reported on separation performance of GC capillaries coated with BMIM  $[\text{PF}_6]$  or BMIM  $[\text{Cl}]$ .<sup>157</sup> Compared to a relatively nonpolar commercial column employed under the same conditions, the IL columns could separate polar compounds such as acids, bases and compounds capable of making hydrogen-bonds with much different retention behavior whereas nonpolar compounds with similar retention times.<sup>157</sup> They also showed ILs capable of dissolving large compounds, like cyclodextrins, that used as chiral GC stationary phases. This work was further investigated by a more in-depth characterization of 17 RTILs.<sup>183</sup> The nonvolatility of ILs as one of the unique features of ILs led Armstrong<sup>162</sup> to study application of ILs as potential liquid matrices in matrix-assisted laser desorption/ionization mass spectrometry (MALDIMS). The low vapor pressure of the ILs allowed them to stay as liquid in a vacuum. The hot spot issues encountered with traditional solid matrices were eliminated by homogenous dissolution of analytes in IL. In 2001, the same group tested 18 different IL matrices to be used in MALDI. They found that ILs needed to have high absorptivity at the correct wavelength as well as the ability to donate protons to the analytes, to be more effective.<sup>162</sup>

The initial success of these applications, along with the versatility and unique properties of ILs such as low volatility, low melting points, viscosity, etc., has led to

the use of ILs in applications much broader than these initial works. These unique chemical and physical properties are controlled by the structure of the cations and anions and the combination of the pairs. Changing from inorganic to organic anions can also vary these properties. By changing the architecture of the counterions, ILs can be tuned to the desired properties for use in various analytical applications.

## **1.5.2 Applications of Ionic Liquids**

### **1.5.2.1 ILs in sensing**

Applications of RTILs in chemical sensing and sensor construction are being explored by many researchers. Incorporation of ILs into the sensor films of quartz crystal microbalances (QCM) has been widely utilized for creating sensors (113-115). In one of the early reports, Dai and coworkers developed and assessed the performance of a quartz crystal microbalance device employing RTILs as the sensor for organic vapor sensors.<sup>184</sup> They showed the instant decrease in the viscosity of RTIL membrane due to analyte dissolution in RTILs which made the basics for their sensing mechanism. The change in viscosity was shown to be exclusively for gaseous chemical species and depended on RTIL type. This sensor had a rapid response of (<2 s) with excellent reversibility attributed to the fast diffusion of these analytes in RTILs. Goubaidouline *et al.* opted to synthesize a sensing film by entrapping imidazolium- or ammonium-based [NTf<sub>2</sub>] ILs in the nanoporous alumina deposited on the surface of the QCM. This method prevented issue associated with dewetting of QCM and soft IL surface.<sup>185</sup> Six organic solvents (THF, cyclohexane, i-octane, methanol, toluene, and acetonitrile) were used as test analytes and the sensor response times reported to be in the order of minutes. In a separate investigation, a gas sensor array was prepared by adding 1-ethyl-3-methyl imidazolium BF<sub>4</sub> in varying concentrations to a plasma-

polymerized film.<sup>186</sup> The specificity of the sensor array was tested with methanol, ethanol, *n*-propanol, and *n*-butanol. Introducing IL modified the discrimination ability between the alcohols by changing the interactions between the polymer film and the alcohols (lipophilicity, polarizability, and hydrogen bonding).

Another gas sensor array was developed using ILs as the thin films on quartz crystal microbalances.<sup>187</sup> A diverse sensor array was created by selection of seven ILs with imidazolium, phosphonium, and ammonium cations and various anions to maximize the solvent-analyte interactions. Ethanol, heptane, benzene, and dichloromethane were the test analytes. Great linearity of concentration curves was achieved for ethanol, heptanes, and benzene, except for the high volatile dichloromethane.<sup>187</sup> There was only one failure in detection of 28 unknown concentrations of samples.

Electrochemistry-based sensors have attracted significant attention for a long time, due to their good sensitivity and selectivity. Therefore, early sensors involving ILs tended to be electrochemically-based. Early applications of RTILs in electrochemical gas sensors were reported by Compton and coworkers.<sup>188</sup> They reported a membrane-free sensor based on a two-electrode cell design. The RTIL functioned as a nonvolatile electrolyte in the gas sensor and eliminated the need for membranes that tended to be necessary to separate the sample from the electrolyte. In this respect, several ILs were examined to create a film over the working electrode. Due to the high viscosity of ILs, oxygen diffusion through ILs was equivalent to its diffusion in similarly constructed sensors with gas-permeable membranes. However, the response time of the IL-based sensor was slower than that of the membrane electrodes.<sup>188</sup> It was proposed that these types of RTIL-based sensors may operate better in extreme

operating conditions (e.g., high temperature, pressure and volatile electrolyte solution) due to thermal stability and extreme low volatility of RTILs. [EMIM][NTf<sub>2</sub>] was also used to develop an ammonia sensor, based on the electro-oxidation of hydroquinone<sup>189</sup> The sensor performance was less affected by humidity as ILs minimized the water absorption. However, the high viscosity of ILs was associated with some problems, such as slow response times and irreversible redox reactions<sup>189</sup>

Towards the formation of more specific gas sensors, hydrophobic [bmim][PF<sub>6</sub>] was used to fill porous polyethylene membrane and make a solid-state electrolyte as a solid-state amperometric O<sub>2</sub> sensor.<sup>190</sup> This RTIL-based oxygen sensor showed a wide detection range with high stability. Similarly, the same group utilized a hydrophilic RTIL, 1 ethyl-3-methylimidazolium [BF<sub>4</sub>] (tetrafluoroborate), to fabricate a solid-state amperometric sensor for O<sub>2</sub> detection.<sup>191</sup>

Ionic liquids have also been explored to develop the optical sensors. Oter and coworkers<sup>192</sup> reported the first RTIL-based optical CO<sub>2</sub> sensor employing [MBIM][BF<sub>4</sub>] or [MBIM][Br] as the matrix with 8- hydroxypyrene-1,3,6-trisulfonic acid trisodium salt (HPTS). The CO<sub>2</sub> detection was based on the change in fluorescence signal of ion pair form of HPTS with gaseous CO<sub>2</sub>. Later, the same team improved this optical sensor by utilization of [EMIM][BF<sub>4</sub>] in ethyl cellulose matrix and could extend the detection range from 0 to 100% ρ CO<sub>2</sub>.<sup>193</sup> An IL-based optical sensor based on the formation of a hybrid electrochemical-colorimetric sensing platform was developed for detection of explosives<sup>194</sup> A thin layer of [BMIM][PF<sub>6</sub>] selectively preconcentrated and rapidly transported the explosives to the electrodes;

thereby, facilitated the formation of reduction products. The product of the electrochemical reaction was detected colorimetrically.

Since BMIM Cl dissolves both cellulose and the metal complexant 1-(2-pyridylazo)-2-naphthol, these two compounds were homogeneously mixed to prepare a mercury (II) sensor<sup>195</sup>. The IL-1-(2-pyridylazo)-2-naphthol-cellulose mixture was spread to create a thin film followed by rinsing away the IL. This film was used in determining the presence of mercury (II), in the absence of other metals such as zinc and copper. More selective complexing agents with enhanced chemical bonding of the agent to the cellulose should be applied to improve the performance of this sensor.<sup>195</sup> A fluorescence-based oxygen-sensitive solution was developed by means of complexed ruthenium-doped [BMIM][BF<sub>4</sub>] or [Br] for potential application as an optical oxygen sensor<sup>196</sup>. Also, Nonadecafluorodecanoic acid was added to the solution to enhance the amount of dissolved oxygen in the IL. As a result of perfluorochemical additive, the authors could obtain high oxygen sensitivity, complete linearity from 0% to 100% oxygen, and high stability for the sensing solution.

#### **1.5.2.2 ILs in extractions**

Purification plays a critical role in chemical analysis and it includes removal of the undesired materials and concentration of the favored chemicals. Extraction is one of the most popular methods of purification. As the first and most essential step in the process of analysis, sample preparation usually involves removal of the interfering chemicals and preconcentration of target analytes from complex matrices, such as environmental and biological samples. Most sample preparation methods used in the laboratory are based on extraction, such as supercritical fluid extraction (SFE),

subcritical water extraction (SWE), pressurized liquid extraction (PLE), microwave/sonication-assisted extraction (M/SAE), liquid–liquid extraction (LLE), liquid-phase microextraction (LPME), membrane-separated liquid extraction (MSLE), solid-phase extraction (SPE), single-drop microextraction (SDME), solid-phase microextraction (SPME), stir bar sorptive extraction (SBSE), and membrane extraction with a sorbent interface (MESI).<sup>197</sup> Most sample preparation procedures are based on solvent extraction except solvent-free methods such as SPE, SPME and SBSE. Organic solvents, besides supercritical fluids and subcritical water, have been the only choice of solvents. However, organic solvents are usually volatile at room temperature, combustible, and toxic to some extent. Since ILs can overcome these drawbacks and are able to dissolve a large range of compounds, more applications of ILs in extraction have been reported. ILs have also been introduced as solvents or matrices for headspace gas chromatography, MALDI-MS analysis, NMR analysis, and other spectral analyses.

Liquid-liquid extraction, as one of the most frequent methods for chemical purifications and sample preparation, is based on the partitioning of the target compound between two immiscible phases. ILs have been extensively applied in liquid–liquid extraction of various compounds, such as metal ions, small organic molecules and biological compounds.

**Extraction of metal ions.** In this respect, to employ ILs for extraction of metal ions from aqueous solutions, often a complexation reagent (such as crown ethers and calixarenes) was used. This method is still in use today.<sup>182</sup> Dai *et al.* reported the extraction of  $\text{Sr}^{2+}$  using dicyclohexyl-18-crown-6 ether dissolved in imidazolium



ILs.<sup>181</sup> 1-butyl-3-trimethylsilylimidazolium hexafluorophosphate [ $C_4tmsim$ ][ $PF_6$ ] was used to extract lead (Pb(II)) from aqueous solutions using dithizone as a chelator.<sup>198</sup> The lead was then back-extracted with nitric acid solution into the aqueous phase for the determination of pb. The extraction of  $La^{3+}$  and divalent metal ions ( $Cu^{2+}$ ,  $Mn^{2+}$ ,  $Co^{2+}$ ) was reported using 1-alkyl-3-methylimidazolium [ $NTf_2$ ] and thenoyltrifluoroacetone.<sup>199-200</sup> In another study, in the Li group, a mixture of branched alkyl phosphine oxides in 1-octyl-3-methylimidazolium hexafluorophosphate [ $C_8MIM$ ][ $PF_6$ ] was used to extract scandium (III) from other lanthanides (III).<sup>201</sup> Later studies showed that ILs, in their pure form, are also able to extract metals from. The same group, reported the selective extraction of cerium (IV) from nitric acid solutions containing thorium (IV) and other trivalent lanthanides using pure [ $C_8MIM$ ][ $PF_6$ ].<sup>202</sup> Task-specific ILs, have also been developed with special functional groups to aid in the extraction process. Such task-specific ILs, were created for the extraction of Wilkinson's and Jacobsen's catalysts from a homogeneous organic phase.<sup>203</sup> The functional groups included amino, hydroxyl, thioether, carboxylic, and olefin groups. Also, ILs with longer carbon chains containing amino or thioether functional groups performed the best for extracting the catalysts<sup>203</sup>

**Extraction of nanomaterials.** The introduction of nanomaterials into the environment due to the wide applications of such engineered materials, in unavoidable and the environmental risk associated with this needs to be assessed accurately. Current available methods for nanomaterials quantification are based on elemental analysis technologies such as ICP-MS<sup>204-205</sup>, and ICP-OES<sup>206</sup> and LC. These methods do not offer conclusive enough information for biologically abundant elements such as iron, carbon and selenium. Nanomaterials should be extracted from

biological samples and other environmental matrices for further analysis. Wei and others, reported that gold nanoparticles and nanorods were efficiently transferred from an aqueous phase to a [BMIM][PF<sub>6</sub>] RTIL (1-butyl-3-methylimidazolium PF<sub>6</sub>) phase without using capping reagents like thiols or amines. It is reported that the extraction capabilities of RTILs are attributed to their alcohol-like polarity and salt-like compositions<sup>207</sup> Huang *et al.* also reported the extraction of 80-95% nanosize CuO and other forms of copper (such as Cu, Cu<sup>2+</sup>,...) into RTIL [C<sub>4</sub>MIM][PF<sub>6</sub>].<sup>208</sup> [C<sub>4</sub>MIM] RTIL with [NTf<sub>2</sub>] anion was employed, in another study, to extract CdTe nanocrystals.<sup>209</sup> Nakashima and Kawai attributed this extraction to a cation-exchange process at the IL-water interface. Thus, ILs may illuminate a path for analysis of nanomaterials in complicated matrices.

**Extraction of organic molecules.** ILs have been popularly used as solvents for the extraction of a variety of small organic compounds such as, aromatic and aliphatic hydrocarbons,<sup>210-211</sup> acids,<sup>212</sup> phenols and amines.<sup>213</sup> Three imidazolium-based IL-aggregates were used to extract polycyclic aromatic hydrocarbons (PAHs) in only 7 mins with good reproducibility. Distribution coefficients of 40 compounds (organic acids and bases, and neutral compounds, antioxidants, amino acids, etc.) in IL/water and IL/heptane systems were also reported.<sup>214</sup> The partitioning of ionizable compounds in IL/water is greatly affected by pH. Visser and coworkers demonstrated the pH-dependent partitioning of thymol blue and reverse extraction by CO<sub>2</sub> and NH<sub>3</sub>.<sup>215</sup>

In another investigation,<sup>216</sup> several hydrophilic ILs were used for extraction of ethanol from a mixture of ethyl acetate and ethanol. Ethanol cannot be separated from ethyl

acetate by distillation due to the formation of a low-boiling azeotrop. 1-alkyl-3-methylimidazolium chloride was used as a nearly immiscible IL with ethyl acetate with a high extraction efficiency of 99.27% ethanol from ethyl acetate after 2<sup>nd</sup> extraction round. The IL was later recycled by simple distillation.<sup>216</sup> In a related report, imidazolium-based ILs with either PF<sub>6</sub> or BF<sub>4</sub> anions were employed for extraction of anionic dyes from aqueous solutions.<sup>217</sup> The pH of the aqueous solution affected the charge of the dyes and their extraction efficiency accordingly. They also reported on the increase in extraction efficiency by raising the temperature or using longer-alkyl chain imidazolium cations.<sup>217</sup> An effective extractant for undissociated lactic acid was shown to be a phosphonium-based IL with 2,4,4-trimethylpentylphosphinic anion.<sup>218</sup> The extraction of five phenols from aqueous solutions was performed using 1-methyl-3-alkyl imidazolium BF<sub>4</sub> or PF<sub>6</sub> ILs.<sup>219</sup> The ILs extracted these phenols with partition coefficients of 1-2 orders of magnitude larger than the traditional organic solvents, like dichloromethane and benzene. In some cases, ILs could selectively extract one phenol over others.<sup>219</sup>

ILs are also investigated for extraction of different hydrocarbons<sup>211, 220</sup> The Seddon group, conducted explored the first application of mutually immiscible ILs in the separation of aromatic and aliphatic hydrocarbons by solvent extraction.<sup>211</sup> IL, [BMIM][PF<sub>6</sub>], could extract ethylbenzene from octane with 90% efficiency under optimal conditions.<sup>220</sup>

ILs have been widely applied in desulfurization as well. Desulfurization of diesel fuel using ILs was first reported in 2001.<sup>221</sup> They reported exceptional extraction capacity of ILs for dibenzothiophene, which is difficult to be removed using normal

hydrotreating. The removal of aromatic sulfur compounds from fuels using ILs has also been studied.<sup>222-223</sup> Nie *et al.* could successfully extract 3-methylthiophene, benzothiophene, and dibenzothiophene from gasoline using imidazolium-based ILs with alkyl phosphate anions.<sup>222</sup> Since most research on desulfurization involved imidazolium ILs, Holbrey and coworkers<sup>223</sup> examined different type of ILs for extraction of dibenzothiophene from dodecane. Polyaromatic quinolinium-based ILs paired with NTF<sub>2</sub> anions exhibited great extraction potential. Ethanolate and thiocyanate anions paired with 1-butyl-3-methylpyridinium cations also looked very promising for the same purpose<sup>223</sup> [BMIM][Br] was used as the extraction solvent in the microwave-assisted extraction of *trans*-resveratrol from the Chinese herb *Rhizma Polygoni Cuspidati*. The anion of the IL had a significant impact on the extraction capability of the *trans*-resveratrol. The bromide anion showed higher extraction efficiencies than either chloride or BF<sub>4</sub> analogs.<sup>224</sup>

Liu and coworkers<sup>225</sup> provided a liquid-phase microextraction (LPME) method where ILs were used as solvents for extraction of polycyclic aromatic hydrocarbons (PAHs) from water. A drop of [C<sub>8</sub>MIM][PF<sub>6</sub>] suspended on the tip of a microsyringe was immersed in aqueous sample for headspace extraction of analytes, followed by direct injection into the liquid chromatography system for quantification.<sup>225</sup> They reported an improvement in enrichment by about three times compared to 1-octanol. Using a similar protocol, chlorobenzenes,<sup>226</sup> phenols,<sup>227</sup> dichlorodiphenyltrichloroethane (DDT) and its metabolites<sup>228</sup> in a water sample were preconcentrated and analyzed. A later study showed that many organic pollutants, including BTEX (benzene, toluene, ethylbenzene, and xylene), PAHs, phthalates, phenols, aromatic amines, herbicides, organotin compounds, and organomercury compounds can be preconcentrated by this

method.<sup>229</sup> As ILs are thermally stable and nonvolatile liquids, they are suitable for high-temperature headspace single-drop microextraction (HS-SDME) of volatile compounds. This strategy is applied for extraction of anilines from environmental water samples at temperatures as high as 90°C.<sup>230</sup> The high temperature enhanced the volatilization of analytes into the head space and thus improved the enrichment factor. Through upper critical separation temperature (UCST) behavior, a homogeneous phase of IL and water was obtained upon heating to 70°C, whereas cooling of the homogeneous liquid mixture produced phase separation due to the decreased solubility. [C<sub>6</sub>MIM][PF<sub>6</sub>] was added to water sample, and this was then heated to 70 °C, which enabled the IL to completely dissolve in water. After the extraction, the system was cooled down and IL phase separated from water. Some amino-acid based ILs<sup>231</sup> such as [P<sub>4444</sub>][Tf-Leu]<sup>232</sup> that have lower critical solution temperatures (LCSTs), similarly, have the potential to be applied in extraction.

**Extraction of biological compounds.** The application of ILs in liquid-liquid extraction of biological compounds and large biomolecules, like proteins and DNA, is significantly increasing. The studies have been mostly on the extraction of amino acids and antibiotics,<sup>233</sup> DNA,<sup>234</sup> proteins<sup>235</sup> and enzymes<sup>236</sup>. ILs have been employed to extract antibiotics and amino acids from aqueous phases. Matsumoto and others, showed better extraction of penicillin G by the IL trioctyl methyl ammonium chloride (TOMAC) compared to imidazolium-based ILs; however, it was yet difficult to remove the penicillin from the IL. Therefore, they employed a supported liquid-membrane system with TOMAC as the membrane solution and chloride concentration as the driving force.<sup>233</sup> Erythromycin A in the aqueous phase was extracted into [C<sub>4</sub>MIM][PF<sub>6</sub>].<sup>237</sup>

Amino acids are another group of compounds of great biological importance. In the presence of dicyclohexano-18-crown-6, four amino acids (Trp, Gly, Ala, Leu) were extracted into [C<sub>4</sub>MIM][PF<sub>6</sub>].<sup>238</sup> Wang *et al.* reported the selective extraction of L-Tryptophan from fermentation broth by various imidazolium-based ILs with either [PF<sub>6</sub>] or [BF<sub>4</sub>] anions.<sup>239</sup> The same group<sup>240</sup> systematically studied the extraction of diverse amino acids (L-tryptophan, L-phenylalanine, L-tyrosine, L-leucine and Dvaline) with the same imidazolium-based ILs as the previous report. Results showed that adding crown ether to the system or adjusting the hydrophobicity of the amino acids by changing the pH value allowed the target amino acids to be extracted into hydrophobic ILs.<sup>240</sup> Next, in an investigation on protein extraction, they reported the extraction of bovine serum albumin, trypsin, cytochrome C and  $\gamma$ -globulins using imidazolium-based ILs. The authors described the critical role of hydrophobic and electrostatic interactions and salting-out effect on partitioning.<sup>241</sup> Cytochrome c (Cyt-c) was also extracted from the aqueous phase into a series of NTf<sub>2</sub>-based ILs mediated by dicyclohexano-18-crown-6 (DCH18C6)<sup>242</sup> In another study on protein extraction, hemoglobin was extracted into 1-butyl-3-trimethylsilylimidazolium[PF<sub>6</sub>], without the need to add additives, through the coordination between the cation and the ferrous atom in hemoglobin.<sup>235</sup> To back-extract and remove the protein from IL extractant, sodium dodecyl sulfate was used. A two-phase system which allowed for the extraction of two different alcohol dehydrogenase enzymes from the aqueous solution was explored. An IL with oligoethylene glycol units was found to be mostly immiscible with a concentrated aqueous solution of potassium phosphate. The IL stabilized the enzymes and the hydrophobic substrates, leading to achieve a higher conversion rates and yields.<sup>236</sup>

The first report on the extraction of double-stranded DNA (<5 ng/L) using RTILs [BMIM][PF<sub>6</sub>] was by Wang *et al.* The [BMIM]<sup>+</sup> cation could interact with the oxygen molecules of the DNA phosphate group, changing the conformation of the DNA and allowing for further quantification of the DNA through resonance light scattering without the interference of other species (e.g. proteins and metals). This approach is outstanding compared to the existing phenol/chloroform method, as it avoids denaturing the DNA and use of harmful solvents.<sup>234</sup>

In general, the structures of ILs affect their extraction selectivity and efficiency for various types of compounds, including metal ions, sulfur-containing compounds and proteins. The distribution coefficients for metal cations often increase with decreasing the alkyl chain length in 1-alkyl-3-methylimidazolium ILs.<sup>243</sup> Increasing the alkyl chain length of the IL cations was found to improve the extraction efficiency of proteins.<sup>241</sup> The partition ratios of dibenzothiophene from dodecane to ILs were determined using a series of ILs with different cation classes and anions<sup>223</sup> The partition ratios of dibenzothiophene from dodecane to ILs with different types of cations and anions follow this order: dimethylpyridinium > methylpyridinium > pyridinium~imidazolium~pyrrolidinium.

Since the solubility and miscibility of the ILs could be adjusted by careful selection and change in the nature and functionality of cation or anion, custom-designed ILs for extracting target compounds developed.<sup>244</sup>

### 1.5.2.3 Extraction mechanisms

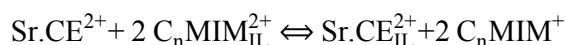
**Partition mechanism:** To understand the separation and enrichment of analytes from the aqueous or organic phase to the IL phase, the partitioning mechanism should be studied. Data on the partition coefficients between ILs and water are very limited in terms of both the analytes and ILs investigated. The Armstrong group examined the partitioning behaviors of 38 compounds in [C<sub>4</sub>MIM][PF<sub>6</sub>]/water and octanol/water systems.<sup>214</sup> It was found that compounds containing acidic functional groups (e.g., carboxyl, phenolic hydroxyl) partitioned less into the IL phase than to octanol, while the reverse was true for amine group-bearing compounds. This could probably be attributed to the lower basicity of ILs compared to octanol. It is noteworthy that the partitioning of ionizable organic compounds (such as PAHs, phenols, BETXs, chlorobenzene, chlorinated anilines, and chlorophenols) between water and ILs is pH dependent. This property enables extraction and back-extraction of the target analytes by adjusting the pH values of different phases.

Rogers *et al.*<sup>165, 245</sup> determined the partition coefficients between IL and water ( $P_{il-w}$ ) of different organic compounds, including six short-chained alcohols, phthalic acid with four derivatives, and benzene with six derivatives. They found that the distribution coefficient was higher for the uncharged form of compounds than for the charged ones. It is generally believed that the transfer of analytes from the aqueous phase to the IL phase by partitioning mechanism is similar to what occurs in traditional organic solvents.

**Ion-exchange mechanisms:** It is often not yet realized that the ionic nature of ILs can result in a variety of extraction mechanisms, including partitioning, solvent ion-pair

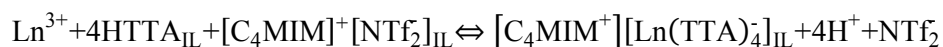


extraction, ion exchange, and simultaneous combinations of these.<sup>246</sup> Although the partitioning mechanism plays a significant role in the extraction of organic compounds from the aqueous to the IL phase, it seems that the transfer of metal ions to IL is based on ion-exchange mechanism. Dietz *et al.*<sup>247</sup> reported the possible extraction mechanism for extraction of metal ion ( $\text{Sr}^{2+}$ ) from aqueous solution containing  $\text{NO}_3^-$  to  $([\text{R}_1\text{R}_2\text{MIM}][\text{NTf}_2])$  and  $([\text{R}_1\text{R}_2\text{MIM}][\text{PF}_6])$  (where  $\text{R}_1$  = ethyl, propyl, or butyl, and  $\text{R}_2$  = H, or methyl) using crown ether (CE) dicyclohexyl-18-crown-6 as the chelating agent which significantly increased the extraction efficiency. They suggested the cation exchange mechanism for this LLE system:



Similar mechanism was proposed to explain the high ability of hydrophobic ILs  $([\text{C}_n\text{MIM}][\text{PF}_6])$  and  $([\text{C}_n\text{MIM}][\text{NTf}_2])$  in extraction of  $\text{UO}_2^{2+}$ . The extraction was assisted by CMPO ligand (carbamoylmethyl phosphine oxide) having the same function as dicyclohexyl-18-crown-6.<sup>248</sup> This mechanism was further supported by Jensen through a coordination environment study.<sup>249</sup>

Sometimes anion exchange anion exchange is the main driving force for the transfer of metal ions into ILs. Jensen *et al.* also proposed the anion exchange rather than cation exchange mechanism for the extraction of lanthanide ( $\text{Ln}^{3+}$ ) into  $([\text{C}_4\text{MIM}][\text{NTf}_2])$  with a chelating agent (1-(2-thienyl)-4,4,4-trifluoro-1,3-butanedione or HTTA). He used several methods such as equilibrium thermodynamics, optical absorption, luminescence spectroscopy, high-energy X-ray scattering, Extended X-Ray Absorption Fine Structure (EXAFS), and molecular dynamics simulations to show the accuracy of the proposed method:<sup>250</sup>



In a related study, the anion exchange mechanism was inferred for the extraction of organic compounds (e.g. dyes) from aqueous phases to ILs, independent of the presence of crown ether.<sup>251</sup> Even though, organic compounds generally tend to be extracted into ILs by partitioning mechanism and metal ions through ion-exchange mechanism, both the partition and ion-exchange mechanisms play important roles in the IL-based extraction processes.

Briefly, separations utilizing ILs as the extracting phase are more complicated than those with simple molecular organic solvents. However, realizing the IL systems and choosing appropriate conditions to design targeted extractions is possible.<sup>246</sup>

### **1.5.3 ILs and Microfluidics**

de Mello and coworkers designed a microfluidic device for precise control of temperature using heat transfer in ILs. [BMIM][PF<sub>6</sub>] and [NTf<sub>2</sub>] were employed as heat transfer liquids where Joule heating supplied by ac current.<sup>252</sup> Since using aqueous potassium chloride was associated with issues like arcing and damage to the chip due to low boiling point, ILs were chosen as the heating liquids. Using this approach, authors could maintain a steady state temperature for long period of time.<sup>252</sup>

In another study, ionic liquid was used to demonstrate a drop-to-drop liquid-liquid microextraction (DTD-LLME) device based on an EWOD (electrowetting on dielectric) digital microfluidic chip. Liquid-liquid microextraction of an acidic dye (solute) from an aqueous droplet (donor) to an IL droplet (extractant) with nanoliter-scale volumes took place at the interface of droplets. The study the extraction kinetics, the device was coupled with image-based concentration monitoring technique and the results suggested the frequency dependency of extraction kinetics on the studied

microextraction device.<sup>253</sup> Loe-Mie *et al.* reported a microdevice for liquid-liquid extraction and sensing of metal ion (mercury) from water into ionic liquid phase. The hydrophobic ionic liquid contained a task-specific IL, which combined fluorogenic and chelating properties to yield fluorescent-sensor ionic liquids (FSILs). They could perform a real-time detection of mercury in water with a high sensitivity with detection limit of 50 ppb.<sup>254</sup>

## 1.6 Thesis Layout and Scope

In this thesis, we leverage the salient features of ionic liquids to illustrate the unique control of microfluidic systems over the formation of fluid interfaces. We demonstrate how droplet microfluidics offers a versatile tool to form complex emulsions with controlled structures. The main focus of this thesis is on the microfluidic formation of compound droplets composed of two (or more) immiscible fluid phases in which IL, with tunable functionality and physicochemical properties, is one of the important components of our proposed system. Such compound droplets have been reported in diverse contexts, from contact heat exchange to cellular phagocytosis and blood oxygenation, and fabrication of highly structured, spatially anisotropic polymeric beads. This thesis also explores the applications of polymerized ionic liquids as matrices for advanced, stimulus-responsive chemical separations and sensing.

In Chapter 2, the formation of partially engulfed IL-aqueous biphasic droplets with tuneable morphologies is described with the aim to introduce a new platform for lab-on-droplets that enables the integration of chemical unit operations on complex droplets. The examined passive methods to completely decouple the two components

of compound droplets, aqueous and IL droplets, and to split such droplets at simple microchannel networks are also elaborated in this chapter. Following this, in Chapter 3, a new and general scheme of droplet microfluidics is demonstrated in which flowing droplets function not only as reaction flasks but are also capable of ‘on-drop’ chemical separation and sensing. Two analytical applications of IL-aqueous compound droplets in selective separation of a binary mixture of organic molecules and dynamic pH sensing are illustrated here. Exploiting the proposed complex microfluidic emulsions with chemically functional fluids, we then demonstrate a reactive sensing scheme for rapid and non-invasive biphasic chemical analyses that are inaccessible at the macroscale. In this demonstration, the chemical tunability of ionic liquids was leveraged in directing analyte (metal ion) transport from the aqueous compartment of a biphasic droplet into an indicator-doped ionic liquid ‘reporter’ compartment and, crucially, in confining a fluorogenic analyte-indicator reaction within the reporter; thus enabling detection of the analyte without the addition of an indicator to the aqueous compartment. In Chapter 4, a simple microfluidics-based method is established for fabrication of highly monodisperse PIL microgel beads with a multitude of functionalities that could be chemically switched in a facile fashion by anion exchange and further enhanced by molecular inclusion. Specifically, exquisite control over bead size and shape enables extremely precise quantitative measurements of anion- and solvent-induced volume transitions in these materials. Later, by exchanging diverse anions into the synthesized microgel beads, stimuli responsiveness and various functionalities are demonstrated including controlled release of chemical payloads, toxic metal removal from water, and robust and *reversible* pH sensing. We finally end with an overview of the contributions made in this thesis, and a discussion of unaddressed questions in Chapter 5.

## 1.7 References

1. <http://www.ted.com/quotes>.
2. Whitesides, G. M., The origins and the future of microfluidics. *Nature* **2006**, 442 (7101), 368-373.
3. Stone, H.; Kim, S., Microfluidics: basic issues, applications, and challenges. *AIChE Journal* **2001**, 47 (6), 1250-1254.
4. Whitesides, G. M.; Stroock, A. D., Flexible methods for microfluidics. *Physics today* **2001**, 54, 42.
5. Voldman, J.; Gray, M. L.; Schmidt, M. A., Microfabrication in biology and medicine. *Annual review of biomedical engineering* **1999**, 1 (1), 401-425.
6. Beebe, D. J.; Mensing, G. A.; Walker, G. M., Physics and applications of microfluidics in biology. *Annual review of biomedical engineering* **2002**, 4 (1), 261-286.
7. Terry, S. C.; Jerman, J. H.; Angell, J. B., A gas chromatographic air analyzer fabricated on a silicon wafer. *Electron Devices, IEEE Transactions on* **1979**, 26 (12), 1880-1886.
8. Shoji, S.; Esashi, M., Microflow devices and systems. *Journal of Micromechanics and Microengineering* **1994**, 4 (4), 157.
9. Gravesen, P.; Branebjerg, J.; Jensen, O. S., Microfluidics-a review. *Journal of Micromechanics and Microengineering* **1993**, 3 (4), 168.
10. Balagaddé, F. K.; You, L.; Hansen, C. L.; Arnold, F. H.; Quake, S. R., Long-term monitoring of bacteria undergoing programmed population control in a microchemostat. *Science* **2005**, 309 (5731), 137-140.
11. Bird, R. B.; Stewart, W. E.; Lightfoot, E. N., *Transport Phenomena* John Wiley & Sons: **1960**.
12. Atencia, J.; Beebe, D. J., Controlled microfluidic interfaces. *Nature* **2005**, 437 (7059), 648-655.
13. Rayleigh, L., On the Capillary Phenomena of Jets. *Proceedings of the Royal Society of London* **1879**, 29, 71-97.
14. Taylor, G., The formation of emulsions in definable fields of flow. *Proceedings of the Royal Society of London. Series A* **1934**, 146 (858), 501-523.
15. Song, H.; Tice, J. D.; Ismagilov, R. F., A microfluidic system for controlling reaction networks in time. *Angewandte Chemie-International Edition* **2003**, 42 (7), 768-772.

16. Jebrail, M. J.; Wheeler, A. R., Let's get digital: digitizing chemical biology with microfluidics. *Current Opinion in Chemical Biology* **2010**, *14* (5), 574-581.
17. Mousa, N. A.; Jebrail, M. J.; Yang, H.; Abdelgawad, M.; Metalnikov, P.; Chen, J.; Wheeler, A. R.; Casper, R. F., Droplet-scale estrogen assays in breast tissue, blood, and serum. *Science Translational Medicine* **2009**, *1* (1), 1ra2-1ra2.
18. Abgrall, P.; Gue, A., Lab-on-chip technologies: making a microfluidic network and coupling it into a complete microsystem—a review. *Journal of Micromechanics and Microengineering* **2007**, *17* (5), R15.
19. Quake, S. R.; Scherer, A., From micro-to nanofabrication with soft materials. *Science* **2000**, *290* (5496), 1536-1540.
20. Sia, S. K.; Whitesides, G. M., Microfluidic devices fabricated in poly (dimethylsiloxane) for biological studies. *Electrophoresis* **2003**, *24* (21), 3563-3576.
21. Xia, Y.; Whitesides, G. M., SOFT LITHOGRAPHY. *Annual Review of Materials Science* **1998**, *28* (1), 153-184.
22. Bohl, B.; Steger, R.; Zengerle, R.; Koltay, P., Multi-layer SU-8 lift-off technology for microfluidic devices. *Journal of Micromechanics and Microengineering* **2005**, *15* (6), 1125-1130.
23. Jia, Y.; Jiang, J.; Ma, X.; Li, Y.; Huang, H.; Cai, K.; Cai, S.; Wu, Y., PDMS microchannel fabrication technique based on microwire-molding. *Chinese Science Bulletin* **2008**, *53* (24), 3928-3936.
24. Abate, A. R.; Krummel, A. T.; Lee, D.; Marquez, M.; Holtze, C.; Weitz, D. A., Photoreactive coating for high-contrast spatial patterning of microfluidic device wettability. *Lab on a Chip* **2008**, *8* (12), 2157-2160.
25. Duffy, D. C.; McDonald, J. C.; Schueller, O. J.; Whitesides, G. M., Rapid prototyping of microfluidic systems in poly (dimethylsiloxane). *Analytical Chemistry* **1998**, *70* (23), 4974-4984.
26. Seemann, R.; Brinkmann, M.; Pfohl, T.; Herminghaus, S., Droplet based microfluidics. *Reports on Progress in Physics* **2012**, *75* (1), 016601.
27. Gunther, A.; Jensen, K. F., Multiphase microfluidics: from flow characteristics to chemical and materials synthesis. *Lab on a Chip* **2006**, *6* (12), 1487-1503.
28. Baroud, C. N.; Gallaire, F.; Dangla, R., Dynamics of microfluidic droplets. *Lab on a Chip* **2010**, *10* (16), 2032-2045.
29. Khan, S. A.; Jensen, K. F., Microfluidic synthesis of titania shells on colloidal silica. *Advanced Materials* **2007**, *19* (18), 2556-2560.
30. Guillot, P.; Colin, A., Stability of parallel flows in a microchannel after a T-junction. *Physical Review E* **2005**, *72*, 066301-4.

31. Tice, J. D.; Song, H.; Lyon, A. D.; Ismagilov, R. F., Formation of Droplets and Mixing in Multiphase Microfluidics at Low Values of the Reynolds and the Capillary Numbers. *Langmuir* **2003**, *19* (22), 9127-9133.
32. Dreyfus, R.; Tabeling, P.; Willaime, H., Ordered and Disordered Patterns in Two-Phase Flows in Microchannels. *Physical Review Letters* **2003**, *90* (14), 144505.
33. Zheng, B.; Roach, L. S.; Ismagilov, R. F., Screening of protein crystallization conditions on a microfluidic chip using nanoliter-size droplets. *Journal of the American Chemical Society* **2003**, *125* (37), 11170-11171.
34. Chan, E. M.; Alivisatos, A. P.; Mathies, R. A., High-temperature microfluidic synthesis of CdSe nanocrystals in nanoliter droplets. *Journal of the American Chemical Society* **2005**, *127* (40), 13854-13861.
35. Khan, S. A.; Duraiswamy, S., Microfluidic emulsions with dynamic compound drops. *Lab on a Chip* **2009**, *9* (13), 1840-1842.
36. Michinao Hashimoto, P. G., George M. Whitesides,, Synthesis of Composite Emulsions and Complex Foams with the use of Microfluidic Flow-Focusing Devices. *Small* **2007**, *3* (10), 1792-1802.
37. Zheng, B.; Ismagilov, R. F., A Microfluidic Approach for Screening Submicroliter Volumes against Multiple Reagents by Using Preformed Arrays of Nanoliter Plugs in a Three-Phase Liquid/Liquid/Gas Flow. *Angewandte Chemie-International Edition* **2005**, *44* (17), 2520-2523.
38. Utada, A. S.; Lorenceau, E.; Link, D. R.; Kaplan, P. D.; Stone, H. A.; Weitz, D. A., Monodisperse double emulsions generated from a microcapillary device. *Science* **2005**, *308* (5721), 537-541.
39. Chokkalingam, V.; Herminghaus, S.; Seemann, R., Self-synchronizing pairwise production of monodisperse droplets by microfluidic step emulsification. *Applied Physics Letters* **2008**, *93* (25), 254101.
40. Holtze, C.; Rowat, A. C.; Agresti, J. J.; Hutchison, J. B.; Angile, F. E.; Schmitz, C. H.; Koster, S.; Duan, H.; Humphry, K. J.; Scanga, R. A.; Johnson, J. S.; Pisignano, D.; Weitz, D. A., Biocompatible surfactants for water-in-fluorocarbon emulsions. *Lab Chip* **2008**, *8* (10), 1632-9.
41. Anna, S. L.; Mayer, H. C., Microscale tipstreaming in a microfluidic flow focusing device. *Physics of Fluids (1994-present)* **2006**, *18* (12), 121512.
42. Yobas, L.; Martens, S.; Ong, W.-L.; Ranganathan, N., High-performance flow-focusing geometry for spontaneous generation of monodispersed droplets. *Lab on a Chip* **2006**, *6* (8), 1073-1079.
43. Christopher, G. F.; Anna, S. L., Microfluidic methods for generating continuous droplet streams. *Journal of Physics D: Applied Physics* **2007**, *40* (19), R319-R336.

44. Thorsen, T.; Roberts, R. W.; Arnold, F. H.; Quake, S. R., Dynamic Pattern Formation in a Vesicle-Generating Microfluidic Device. *Physical Review Letters* **2001**, *86* (18), 4163-4166.
45. Nisisako, T.; Torii, T.; Higuchi, T., Droplet formation in a microchannel network. *Lab on a Chip* **2002**, *2* (1), 24-26.
46. Malsch, D.; Gleichmann, N.; Kielpinski, M.; Mayer, G.; Henkel, T.; Mueller, D.; Steijn, V.; Kleijn, C.; Kreutzer, M., Dynamics of droplet formation at T-shaped nozzles with elastic feed lines. *Microfluidics and Nanofluidics* **2010**, *8* (4), 497-507.
47. Gu, H.; Duits, M. H. G.; Mugele, F., Droplets Formation and Merging in Two-Phase Flow Microfluidics. *International Journal of Molecular Sciences* **2011**, *12* (4), 2572-2597.
48. Collins, J.; Lee, A. P., Control of serial microfluidic droplet size gradient by step-wise ramping of flow rates. *Microfluidics and Nanofluidics* **2007**, *3* (1), 19-25.
49. Lee, W.; Walker, L. M.; Anna, S. L., Role of geometry and fluid properties in droplet and thread formation processes in planar flow focusing. *Physics of Fluids* **2009**, *21* (3), 032103-14.
50. Cubaud, T.; Mason, T. G., Capillary threads and viscous droplets in square microchannels. *Physics of Fluids* **2008**, *20*, 053302.
51. Okushima, S.; Nisisako, T.; Torii, T.; Higuchi, T., Controlled Production of Monodisperse Double Emulsions by Two-Step Droplet Breakup in Microfluidic Devices. *Langmuir* **2004**, *20* (23), 9905-9908.
52. Xu, S.; Nie, Z.; Seo, M.; Lewis, P.; Kumacheva, E.; Stone, H. A.; Garstecki, P.; Weibel, D. B.; Gitlin, I.; Whitesides, G. M., Generation of monodisperse particles by using microfluidics: Control over size, shape, and composition (vol 44, pg 724, 2005). *Angewandte Chemie-International Edition* **2005**, *44* (25), 3799-3799.
53. Tice, J. D.; Lyon, A. D.; Ismagilov, R. F., Effects of viscosity on droplet formation and mixing in microfluidic channels. *Analytica Chimica Acta* **2004**, *507* (1), 73-77.
54. Song, H.; Ismagilov, R. F., Millisecond Kinetics on a Microfluidic Chip Using Nanoliters of Reagents. *Journal of the American Chemical Society* **2003**, *125* (47), 14613-14619.
55. Zeng, S.; Li, B.; Su, X. o.; Qin, J.; Lin, B., Microvalve-actuated precise control of individual droplets in microfluidic devices. *Lab on a Chip* **2009**, *9* (10), 1340-1343.
56. Shestopalov, I.; Tice, J. D.; Ismagilov, R. F., Multi-step synthesis of nanoparticles performed on millisecond time scale in a microfluidic droplet-based system. *Lab Chip* **2004**, *4* (4), 316-321.



57. He, M.; Edgar, J. S.; Jeffries, G. D. M.; Lorenz, R. M.; Shelby, J. P.; Chiu, D. T., Selective Encapsulation of Single Cells and Subcellular Organelles into Picoliter- and Femtoliter-Volume Droplets. *Analytical Chemistry* **2005**, *77* (6), 1539-1544.
58. Song, H.; Bringer, M. R.; Tice, J. D.; Gerdts, C. J.; Ismagilov, R. F., Experimental test of scaling of mixing by chaotic advection in droplets moving through microfluidic channels. *Applied Physics Letters* **2003**, *83* (22), 4664-4666.
59. Bringer, M. R.; Gerdts, C. J.; Song, H.; Tice, J. D.; Ismagilov, R. F., Microfluidic systems for chemical kinetics that rely on chaotic mixing in droplets. *Philosophical Transactions of the Royal Society of London. Series A: Mathematical, Physical and Engineering Sciences* **2004**, *362* (1818), 1087-1104.
60. Günther, A.; Khan, S. A.; Thalmann, M.; Trachsel, F.; Jensen, K. F., Transport and reaction in microscale segmented gas-liquid flow. *Lab on a Chip* **2004**, *4* (4), 278-286.
61. Gunther, A.; Jhunjhunwala, M.; Thalmann, M.; Schmidt, M. A.; Jensen, K. F., Micromixing of Miscible Liquids in Segmented Gas-Liquid Flow. *Langmuir* **2005**, *21* (4), 1547-1555.
62. Garstecki, P.; Fischbach, M. A.; Whitesides, G. M., Design for mixing using bubbles in branched microfluidic channels. *Applied Physics Letters* **2005**, *86* (24), 244108-3.
63. Khan, S. A.; Günther, A.; Schmidt, M. A.; Jensen, K. F., Microfluidic Synthesis of Colloidal Silica. *Langmuir* **2004**, *20* (20), 8604-8611.
64. Martin, K.; Henkel, T.; Baier, V.; Grodrian, A.; Schon, T.; Roth, M.; Michael Kohler, J.; Metzger, J., Generation of larger numbers of separated microbial populations by cultivation in segmented-flow microdevices. *Lab on a Chip* **2003**, *3* (3), 202-207.
65. Ratner, D. M.; Murphy, E. R.; Jhunjhunwala, M.; Snyder, D. A.; Jensen, K. F.; Seeberger, P. H., Microreactor-based reaction optimization in organic chemistry—glycosylation as a challenge. *Chemical Communications* **2005**, (5), 578-580.
66. Watts, P.; Wiles, C., Micro reactors: a new tool for the synthetic chemist. *Organic & Biomolecular Chemistry* **2007**, *5* (5), 727-732.
67. Zheng, B.; Gerdts, C. J.; Ismagilov, R. F., Using nanoliter plugs in microfluidics to facilitate and understand protein crystallization. *Current opinion in structural biology* **2005**, *15* (5), 548-555.
68. Ju, J.; Zeng, C.; Zhang, L.; Xu, N., Continuous synthesis of zeolite NaA in a microchannel reactor. *Chemical Engineering Journal* **2006**, *116* (2), 115-121.
69. Toldy, A. I.; Badruddoza, A. Z. M.; Zheng, L.; Hatton, T. A.; Gunawan, R.; Rajagopalan, R.; Khan, S. A., Spherical Crystallization of Glycine from Monodisperse Microfluidic Emulsions. *Crystal Growth & Design* **2012**, *12* (8), 3977-3982.

70. Song, Y.; Modrow, H.; Henry, L. L.; Saw, C. K.; Doomes, E.; Palshin, V.; Hormes, J.; Kumar, C. S., Microfluidic synthesis of cobalt nanoparticles. *Chemistry of Materials* **2006**, *18* (12), 2817-2827.
71. Takagi, M.; Maki, T.; Miyahara, M.; Mae, K., Production of titania nanoparticles by using a new microreactor assembled with same axle dual pipe. *Chemical Engineering Journal* **2004**, *101* (1), 269-276.
72. Song, Y.; Hormes, J.; Kumar, C. S., Microfluidic synthesis of nanomaterials. *Small* **2008**, *4* (6), 698-711.
73. Duraiswamy, S.; Khan, S. A., Droplet-Based Microfluidic Synthesis of Anisotropic Metal Nanocrystals. *Small* **2009**, *5* (24), 2828-2834.
74. Rahman, M. T.; Krishnamurthy, P. G.; Parthiban, P.; Jain, A.; Park, C. P.; Kim, D.-P.; Khan, S. A., Dynamically tunable nanoparticle engineering enabled by short contact-time microfluidic synthesis with a reactive gas. *RSC Advances* **2013**, *3* (9), 2897-2900.
75. Yen, B. K. H.; Günther, A.; Schmidt, M. A.; Jensen, K. F.; Bawendi, M. G., A Microfabricated Gas-Liquid Segmented Flow Reactor for High-Temperature Synthesis: The Case of CdSe Quantum Dots. *Angewandte Chemie International Edition* **2005**, *44* (34), 5447-5451.
76. Ahmed, B.; Barrow, D.; Wirth, T., Enhancement of reaction rates by segmented fluid flow in capillary scale reactors. *Advanced Synthesis & Catalysis* **2006**, *348* (9), 1043-1048.
77. Burns, J. R.; Ramshaw, C., The intensification of rapid reactions in multiphase systems using slug flow in capillaries. *Lab on a Chip* **2001**, *1* (1), 10-15.
78. Cygan, Z. T.; Cabral, J. T.; Beers, K. L.; Amis, E. J., Microfluidic platform for the generation of organic-phase microreactors. *Langmuir* **2005**, *21* (8), 3629-3634.
79. Carr, R.; Geddes, J.; Wu, F., Oscillations in a Simple Microvascular Network. *Ann Biomed Eng* **2005**, *33* (6), 764-771.
80. Blunt, M. J., Flow in porous media — pore-network models and multiphase flow. *Current Opinion in Colloid & Interface Science* **2001**, *6* (3), 197-207.
81. Yildiz, E.; Keskinler, B.; Pekdemir, T.; Akay, G.; Nuhog˘lu, A., High strength wastewater treatment in a jet loop membrane bioreactor: kinetics and performance evaluation. *Chemical Engineering Science* **2005**, *60* (4), 1103-1116.
82. Thorsen, T.; Maerkl, S. J.; Quake, S. R., Microfluidic Large-Scale Integration. *Science* **2002**, *298* (5593), 580-584.
83. Hong, J. W.; Studer, V.; Hang, G.; Anderson, W. F.; Quake, S. R., A nanoliter-scale nucleic acid processor with parallel architecture. *Nat Biotechnol* **2004**, *22* (4), 435-9.

84. Chien, R.-L.; Parce, W., Multiport flow-control system for lab-on-a-chip microfluidic devices. *Fresenius J Anal Chem* **2001**, *371* (2), 106-111.
85. Willaime, H.; Barbier, V.; Kloul, L.; Maine, S.; Tabeling, P., Arnold Tongues in a Microfluidic Drop Emitter. *Physical Review Letters* **2006**, *96* (5), 054501.
86. Garstecki, P.; Fuerstman, M. J.; Whitesides, G. M., Oscillations with uniquely long periods in a microfluidic bubble generator. *Nature Physics* **2005**, *1*, 168-171.
87. Steinbacher, J. L.; McQuade, D. T., Polymer chemistry in flow: New polymers, beads, capsules, and fibers. *Journal of Polymer Science Part A: Polymer Chemistry* **2006**, *44* (22), 6505-6533.
88. Prakash, M.; Gershenfeld, N., Microfluidic Bubble Logic. *Science* **2007**, *315* (5813), 832-835.
89. Dendukuri, D.; Tsoi, K.; Hatton, T. A.; Doyle, P. S., Controlled Synthesis of Nonspherical Microparticles Using Microfluidics. *Langmuir* **2005**, *21* (6), 2113-2116.
90. Nisisako, T.; Torii, T.; Takahashi, T.; Takizawa, Y., Synthesis of monodisperse bicolored janus particles with electrical anisotropy using a microfluidic co-flow system. *Advanced Materials* **2006**, *18* (9), 1152-1156.
91. Joanicot, M.; Ajdari, A., Droplet Control for Microfluidics. *Science* **2005**, *309* (5736), 887-888.
92. Zeng, J.; Kormeyer, T., Principles of droplet electrohydrodynamics for lab-on-a-chip. *Lab on a Chip* **2004**, *4* (4), 265-277.
93. Schindler, M.; Ajdari, A., Droplet Traffic in Microfluidic Networks: A Simple Model for Understanding and Designing. *Physical Review Letters* **2008**, *100* (4), 044501.
94. Jousse, F.; Farr, R.; Link, D. R.; Fuerstman, M. J.; Garstecki, P., Bifurcation of droplet flows within capillaries. *Physical Review E* **2006**, *74* (3), 036311.
95. Link, D. R.; Anna, S. L.; Weitz, D. A.; Stone, H. A., Geometrically Mediated Breakup of Drops in Microfluidic Devices. *Physical Review Letters* **2004**, *92* (5), 054503.
96. Garstecki, P.; Fuerstman, M. J.; Whitesides, G. M., Nonlinear Dynamics of a Flow-Focusing Bubble Generator: An Inverted Dripping Faucet. *Physical Review Letters* **2005**, *94* (23), 234502.
97. Engl, W.; Roche, M.; Colin, A.; Panizza, P.; Ajdari, A., Droplet Traffic at a Simple Junction at Low Capillary Numbers. *Physical Review Letters* **2005**, *95* (20), 208304.
98. Bretherton, F. P., The motion of long bubbles in tubes. *Journal of Fluid Mechanics* **1961**, *10* (02), 166-188.

99. Wong, H.; Radke, C. J.; Morris, S., The motion of long bubbles in polygonal capillaries. Part 2. Drag, fluid pressure and fluid flow. *Journal of Fluid Mechanics* **1995**, *292*, 95-110.
100. Hodges, S. R.; Jensen, O. E.; Rallison, J. M., The motion of a viscous drop through a cylindrical tube. *Journal of Fluid Mechanics* **2004**, *501*, 279-301.
101. Ahn, K.; Agresti, J.; Chong, H.; Marquez, M.; Weitz, D., Electrocoalescence of drops synchronized by size-dependent flow in microfluidic channels. *Applied Physics Letters* **2006**, *88* (26), 264105-264105-3.
102. Niu, X.; Gulati, S.; Edel, J. B., Pillar-induced droplet merging in microfluidic circuits. *Lab on a Chip* **2008**, *8* (11), 1837-1841.
103. Christopher, G.; Bergstein, J.; End, N.; Poon, M.; Nguyen, C.; Anna, S. L., Coalescence and splitting of confined droplets at microfluidic junctions. *Lab on a Chip* **2009**, *9* (8), 1102-1109.
104. Fidalgo, L. M.; Abell, C.; Huck, W. T. S., Surface-induced droplet fusion in microfluidic devices. *Lab on a Chip* **2007**, *7* (8), 984-986.
105. Bremond, N.; Thiam, A. R.; Bibette, J., Decompressing emulsion droplets favors coalescence. *Physical Review Letters* **2008**, *100* (2), 024501.
106. Jullien, M. C.; Ching, M. J. T. M.; Cohen, C.; Menetrier, L.; Tabeling, P., Droplet breakup in microfluidic T-junctions at small capillary numbers. *Physics of Fluids* **2009**, *21* (7), 072001.
107. Adamson, D. N.; Mustafi, D.; Zhang, J. X. J.; Zheng, B.; Ismagilov, R. F., Production of arrays of chemically distinct nanolitre plugs via repeated splitting in microfluidic devices. *Lab on a Chip* **2006**, *6* (9), 1178-1186.
108. Cristobal, G.; Benoit, J.-P.; Joanicot, M.; Ajdari, A., Microfluidic bypass for efficient passive regulation of droplet traffic at a junction. *Applied physics letters* **2006**, *89* (3), 034104.
109. Link, D. R.; Grasland-Mongrain, E.; Duri, A.; Sarrazin, F.; Cheng, Z. D.; Cristobal, G.; Marquez, M.; Weitz, D. A., Electric control of droplets in microfluidic devices. *Angewandte Chemie-International Edition* **2006**, *45* (16), 2556-2560.
110. Ahn, K.; Kerbage, C.; Hunt, T. P.; Westervelt, R. M.; Link, D. R.; Weitz, D. A., Dielectrophoretic manipulation of drops for high-speed microfluidic sorting devices. *Applied Physics Letters* **2006**, *88* (2), 024104-3.
111. Choi, S.W.; Cheong, I. W.; Kim, J.-H.; Xia, Y., Preparation of Uniform Microspheres Using a Simple Fluidic Device and Their Crystallization into Close-Packed Lattices. *Small* **2009**, *5* (4), 454-459.

112. Lorenceau, E.; Utada, A. S.; Link, D. R.; Cristobal, G.; Joanicot, M.; Weitz, D. A., Generation of polymerosomes from double-emulsions. *Langmuir* **2005**, *21* (20), 9183-9186.
113. De Geest, B. G.; Urbanski, J. P.; Thorsen, T.; Demeester, J.; De Smedt, S. C., Synthesis of monodisperse biodegradable microgels in microfluidic devices. *Langmuir* **2005**, *21* (23), 10275-10279.
114. Ikkai, F.; Iwamoto, S.; Adachi, E.; Nakajima, M., New method of producing mono-sized polymer gel particles using microchannel emulsification and UV irradiation. *Colloid and Polymer Science* **2005**, *283* (10), 1149-1153.
115. Jeong, W. J.; Kim, J. Y.; Choo, J.; Lee, E. K.; Han, C. S.; Beebe, D. J.; Seong, G. H.; Lee, S. H., Continuous Fabrication of Biocatalyst Immobilized Microparticles Using Photopolymerization and Immiscible Liquids in Microfluidic Systems. *Langmuir* **2005**, *21* (9), 3738-3741.
116. Dendukuri, D.; Doyle, P. S., The synthesis and assembly of polymeric microparticles using microfluidics. *Advanced Materials* **2009**, *21* (41), 4071-4086.
117. Seo, M.; Nie, Z. H.; Xu, S. Q.; Mok, M.; Lewis, P. C.; Graham, R.; Kumacheva, E., Continuous microfluidic reactors for polymer particles. *Langmuir* **2005**, *21* (25), 11614-11622.
118. Liu, K.; Ding, H.-J.; Liu, J.; Chen, Y.; Zhao, X.-Z., Shape-controlled production of biodegradable calcium alginate gel microparticles using a novel microfluidic device. *Langmuir* **2006**, *22* (22), 9453-9457.
119. Steinbacher, J. L.; Moy, R. W.; Price, K. E.; Cummings, M. A.; Roychowdhury, C.; Buffy, J. J.; Olbricht, W. L.; Haaf, M.; McQuade, D. T., Rapid self-assembly of core-shell organosilicon microcapsules within a microfluidic device. *Journal of the American Chemical Society* **2006**, *128* (29), 9442-9447.
120. Park, J. I.; Nie, Z.; Kumachev, A.; Abdelrahman, A. I.; Binks, B. R.; Stone, H. A.; Kumacheva, E., A Microfluidic Approach to Chemically Driven Assembly of Colloidal Particles at Gas-Liquid Interfaces. *Angewandte Chemie-International Edition* **2009**, *48* (29), 5300-5304.
121. van der Graaf, S.; Schroen, C.; Boom, R., Preparation of double emulsions by membrane emulsification—a review. *Journal of Membrane Science* **2005**, *251* (1), 7-15.
122. Seo, M.; Paquet, C.; Nie, Z. H.; Xu, S. Q.; Kumacheva, E., Microfluidic consecutive flow-focusing droplet generators. *Soft Matter* **2007**, *3* (8), 986-992.
123. Chu, L. Y.; Utada, A. S.; Shah, R. K.; Kim, J. W.; Weitz, D. A., Controllable monodisperse multiple emulsions. *Angewandte Chemie International Edition* **2007**, *46* (47), 8970-8974.

124. Song, H.; Chen, D. L.; Ismagilov, R. F., Reactions in droplets in microfluidic channels. *Angewandte Chemie-International Edition* **2006**, *45* (44), 7336-7356.
125. Schwarz, M. A.; Hauser, P. C., Recent developments in detection methods for microfabricated analytical devices. *Lab Chip* **2001**, *1* (1), 1-6.
126. Dittrich, P. S.; Tachikawa, K.; Manz, A., Micro Total Analysis Systems. Latest Advancements and Trends. *Analytical Chemistry* **2006**, *78* (12), 3887-3908.
127. Fidalgo, L. M.; Whyte, G.; Bratton, D.; Kaminski, C. F.; Abell, C.; Huck, W. T. S., From microdroplets to microfluidics: Selective emulsion separation in microfluidic devices. *Angewandte Chemie-International Edition* **2008**, *47* (11), 2042-2045.
128. deMello, A. J., Control and detection of chemical reactions in microfluidic systems. *Nature* **2006**, *442* (7101), 394-402.
129. Mazutis, L.; Baret, J.-C.; Griffiths, A. D., A fast and efficient microfluidic system for highly selective one-to-one droplet fusion. *Lab on a Chip* **2009**, *9* (18), 2665-2672.
130. Agresti, J. J.; Antipov, E.; Abate, A. R.; Ahn, K.; Rowat, A. C.; Baret, J.-C.; Marquez, M.; Klibanov, A. M.; Griffiths, A. D.; Weitz, D. A., Ultrahigh-throughput screening in drop-based microfluidics for directed evolution. *Proceedings of the National Academy of Sciences* **2010**, *107* (9), 4004-4009.
131. Klostranec, J. M.; Xiang, Q.; Farcas, G. A.; Lee, J. A.; Rhee, A.; Lafferty, E. I.; Perrault, S. D.; Kain, K. C.; Chan, W. C., Convergence of quantum dot barcodes with microfluidics and signal processing for multiplexed high-throughput infectious disease diagnostics. *Nano Letters* **2007**, *7* (9), 2812-2818.
132. Psaltis, D.; Quake, S. R.; Yang, C., Developing optofluidic technology through the fusion of microfluidics and optics. *Nature* **2006**, *442* (7101), 381-386.
133. Nguyen, N.-T.; Lassemono, S.; Chollet, F. A., Optical detection for droplet size control in microfluidic droplet-based analysis systems. *Sensors and Actuators B: Chemical* **2006**, *117* (2), 431-436.
134. Krüger, J.; Singh, K.; O'Neill, A.; Jackson, C.; Morrison, A.; O'Brien, P., Development of a microfluidic device for fluorescence activated cell sorting. *Journal of Micromechanics and Microengineering* **2002**, *12* (4), 486.
135. Hutzler, S.; Weaire, D.; Elias, F.; Janiaud, E., Juggling with bubbles in cylindrical ferrofluid foams. *Philosophical magazine letters* **2002**, *82* (5), 297-301.
136. Luo, C.; Yang, X.; Fu, Q.; Sun, M.; Ouyang, Q.; Chen, Y.; Ji, H., Picoliter-volume aqueous droplets in oil: Electrochemical detection and yeast cell electroporation. *Electrophoresis* **2006**, *27* (10), 1977-1983.
137. Wang, F.; Burns, M. A., Multiphase bioreaction microsystem with automated on-chip droplet operation. *Lab on a Chip* **2010**, *10* (10), 1308-1315.

138. Rudolph, B.; Wilhelm, T., The electrochemical detection of droplets in microfluidic devices. *Lab on a Chip* **2008**, *8* (11), 1937-1942.
139. Srivastava, N.; Burns, M. A., Electronic drop sensing in microfluidic devices: automated operation of a nanoliter viscometer. *Lab on a Chip* **2006**, *6* (6), 744-751.
140. Xiao, Z.; Niu, M.; Zhang, B., Droplet microfluidics based microseparation systems. *Journal of Separation Science* **2012**, *35* (10-11), 1284-1293.
141. Hatakeyama, T.; Chen, D. L.; Ismagilov, R. F., Microgram-scale testing of reaction conditions in solution using nanoliter plugs in microfluidics with detection by MALDI-MS. *Journal of the American Chemical Society* **2006**, *128* (8), 2518-2519.
142. Nisisako, T., Microstructured devices for preparing controlled multiple emulsions. *Chemical Engineering & Technology* **2008**, *31* (8), 1091-1098.
143. Nie, Z. H.; Xu, S. Q.; Seo, M.; Lewis, P. C.; Kumacheva, E., Polymer particles with various shapes and morphologies produced in continuous microfluidic reactors. *Journal of the American Chemical Society* **2005**, *127* (22), 8058-8063.
144. Nisisako, T.; Okushima, S.; Torii, T., Controlled formulation of monodisperse double emulsions in a multiple-phase microfluidic system. *Soft Matter* **2005**, *1* (1), 23-27.
145. Nisisako, T.; Torii, T., Microfluidic large-scale integration on a chip for mass production of monodisperse droplets and particles. *Lab on a Chip* **2008**, *8* (2), 287-293.
146. Soukup-Hein, R. J.; Warnke, M. M.; Armstrong, D. W., Ionic liquids in analytical chemistry. *Annual Review of Analytical Chemistry* **2009**, *2* (1), 145-168.
147. Wilkes, J. S.; Zaworotko, M. J., Air and Water Stable 1-Ethyl-3-methylimidazolium based ionic liquids. *J. Chem. Soc.-Chem. Commun.* **1992**, (13), 965-967.
148. Hallett, J. P.; Welton, T., Room-temperature ionic liquids: solvents for synthesis and catalysis. 2. *Chemical Reviews* **2011**, *111* (5), 3508-3576.
149. van Rantwijk, F.; Sheldon, R. A., Biocatalysis in Ionic Liquids. *Chemical Reviews* **2007**, *107* (6), 2757-2785.
150. Dupont, J.; de Souza, R. F.; Suarez, P. A. Z., ionic liquid (molten salt) phase organometallic catalysis. *Chemical Reviews* **2002**, *102* (10), 3667-3692.
151. Ohno, H., Functional design of ionic liquids. *Bulletin of the Chemical Society of Japan* **2006**, *79* (11), 1665-1680.
152. Hardacre, C.; Holbrey, J. D.; Nieuwenhuyzen, M.; Youngs, T. G. A., Structure and solvation in ionic liquids. *Accounts Chem. Res.* **2007**, *40* (11), 1146-1155.

153. Chiappe, C.; Pieraccini, D., Ionic liquids: solvent properties and organic reactivity. *Journal of Physical Organic Chemistry* **2005**, *18* (4), 275-297.
154. Freemantle, M., Designer solvents. *Chemical & Engineering News Archive* **1998**, *76* (13), 32-37.
155. Carmichael, A. J.; Seddon, K. R., Polarity study of some 1-alkyl-3-methylimidazolium ambient-temperature ionic liquids with the solvatochromic dye, Nile Red. *Journal of Physical Organic Chemistry* **2000**, *13* (10), 591-595.
156. Olivier-Bourbigou, H.; Magna, L.; Morvan, D., Ionic liquids and catalysis: Recent progress from knowledge to applications. *Applied Catalysis A: General* **2010**, *373* (1), 1-56.
157. Armstrong, D. W.; He, L.; Liu, Y.-S., Examination of ionic liquids and their interaction with molecules, when used as stationary phases in gas chromatography. *Analytical Chemistry* **1999**, *71* (17), 3873-3876.
158. Anderson, J. L.; Armstrong, D. W., High-stability ionic liquids. A new class of stationary phases for gas chromatography. *Analytical Chemistry* **2003**, *75* (18), 4851-4858.
159. Yanes, E. G.; Gratz, S. R.; Baldwin, M. J.; Robison, S. E.; Stalcup, A. M., Capillary electrophoretic application of 1-alkyl-3-methylimidazolium-based ionic liquids. *Analytical Chemistry* **2001**, *73* (16), 3838-3844.
160. Mwongela, S. M.; Numan, A.; Gill, N. L.; Agbaria, R. A.; Warner, I. M., Separation of achiral and chiral analytes using polymeric surfactants with ionic liquids as modifiers in micellar electrokinetic chromatography. *Analytical Chemistry* **2003**, *75* (22), 6089-6096.
161. Vaher, M.; Koel, M.; Kaljurand, M., Ionic liquids as electrolytes for nonaqueous capillary electrophoresis. *Electrophoresis* **2002**, *23* (3), 426-430.
162. Armstrong, D. W.; Zhang, L.-K.; He, L.; Gross, M. L., Ionic liquids as matrixes for matrix-assisted laser desorption/ionization mass spectrometry. *Analytical Chemistry* **2001**, *73* (15), 3679-3686.
163. Carda-Broch, S.; Berthod, A.; Armstrong, D. W., Ionic matrices for matrix-assisted laser desorption/ionization time-of-flight detection of DNA oligomers. *Rapid communications in mass spectrometry* **2003**, *17* (6), 553-560.
164. Suarez, P. A. Z.; Einloft, S.; Dullius, J. E. L.; de Souza, R. F.; Dupont, J., Synthesis and physical-chemical properties of ionic liquids based on 1-n-butyl-3-methylimidazolium cation. *J. Chim. Phys.-Chim. Biol.* **1998**, *95* (7), 1626-1639.
165. Huddleston, J. G.; Visser, A. E.; Reichert, W. M.; Willauer, H. D.; Broker, G. A.; Rogers, R. D., Characterization and comparison of hydrophilic and hydrophobic room temperature ionic liquids incorporating the imidazolium cation. *Green Chemistry* **2001**, *3* (4), 156-164.



166. T., W., Room-temperature ionic liquids. solvents for synthesis and catalysis. *Chemical Reviews* **1999**, *99*, 2071-2084.
167. Gabriel, S.; Weiner, J., On some derivatives of propylamine. *Berichte der deutschen chemischen Gesellschaft* **1888**, *21*, 2669-2679.
168. Walden, P., Molecular weights and electrical conductivity of several fused salts. *Bulletin of the Russian Academy of Sciences* **1914**, 405–422.
169. Chum, H. L.; Koch, V. R.; Miller, L. L.; Osteryoung, R. A., Electrochemical scrutiny of organometallic iron complexes and hexamethylbenzene in a room temperature molten salt. *Journal of the American Chemical Society* **1975**, *97* (11), 3264-3265.
170. Wilkes, J. S.; Levisky, J. A.; Wilson, R. A.; Hussey, C. L., Dialkylimidazolium chloroaluminate melts: a new class of room-temperature ionic liquids for electrochemistry, spectroscopy and synthesis. *Inorganic Chemistry* **1982**, *21* (3), 1263-1264.
171. Fuller, J.; Breda, A.; Carlin, R., Ionic liquid-polymer gel electrolytes. *Journal of the Electrochemical Society* **1997**, *144* (4), L67-L70.
172. Fuller, J.; Breda, A. C.; Carlin, R. T., Ionic liquid-polymer gel electrolytes from hydrophilic and hydrophobic ionic liquids. *Journal of Electroanalytical Chemistry* **1998**, *459* (1), 29-34.
173. Suarez, P. A.; Dullius, J. E.; Einloft, S.; De Souza, R. F.; Dupont, J., The use of new ionic liquids in two-phase catalytic hydrogenation reaction by rhodium complexes. *Polyhedron* **1996**, *15* (7), 1217-1219.
174. Dullius, J. E.; Suarez, P. A.; Einloft, S.; de Souza, R. F.; Dupont, J.; Fischer, J.; De Cian, A., Selective catalytic hydrodimerization of 1, 3-butadiene by palladium compounds dissolved in ionic liquids. *Organometallics* **1998**, *17* (5), 815-819.
175. Silva, S. M.; Suarez, P. A. Z.; de Souza, R. F.; Dupont, J., Selective linear dimerization of 1,3-butadiene by palladium compounds immobilized into 1-n-butyl-3-methyl imidazolium ionic liquids. *Polymer Bulletin* **1998**, *40* (4-5), 401-405.
176. Boxwell, C. J.; Dyson, P. J.; Ellis, D. J.; Welton, T., A highly selective arene hydrogenation catalyst that operates in ionic liquid. *Journal of the American Chemical Society* **2002**, *124* (32), 9334-9335.
177. Ellis, D. J.; Dyson, P. J.; Parker, D. G.; Welton, T., Hydrogenation of non-activated alkenes catalysed by water-soluble ruthenium carbonyl clusters using a biphasic protocol. *Journal of Molecular Catalysis A: Chemical* **1999**, *150* (1), 71-75.
178. Cull, S.; Holbrey, J.; Vargas-Mora, V.; Seddon, K.; Lye, G., Room-temperature ionic liquids as replacements for organic solvents in multiphase bioprocess operations. *Biotechnology and Bioengineering* **2000**, *69* (2), 227-233.

179. Davis, J. H.; Forrester, K. J., Thiazolium-ion based organic ionic liquids (OILs). Novel OILs which promote the benzoin condensation. *Tetrahedron Letters* **1999**, *40* (9), 1621-1622.
180. Huddleston, J.; Rogers, R., Room temperature ionic liquids as novel media for 'clean' liquid-liquid extraction. *Chemical Communications* **1998**, (16), 1765-1766.
181. Dai, S.; Ju, Y.; Barnes, C., Solvent extraction of strontium nitrate by a crown ether using room-temperature ionic liquids. *J. Chem. Soc., Dalton Trans.* **1999**, (8), 1201-1202.
182. Visser, A. E.; Swatloski, R. P.; Griffin, S. T.; Hartman, D. H.; Rogers, R. D., Liquid/liquid extraction of metal ions in room temperature ionic liquids. *Separation Science and Technology* **2001**, *36* (5-6), 785-804.
183. Anderson, J. L.; Ding, J.; Welton, T.; Armstrong, D. W., Characterizing ionic liquids on the basis of multiple solvation interactions. *Journal of the American Chemical Society* **2002**, *124* (47), 14247-14254.
184. Liang, C.; Yuan, C.-Y.; Warmack, R. J.; Barnes, C. E.; Dai, S., Ionic liquids: a new class of sensing materials for detection of organic vapors based on the use of a quartz crystal microbalance. *Analytical Chemistry* **2002**, *74* (9), 2172-2176.
185. Goubaidoulline, I.; Vidrich, G.; Johannsmann, D., Organic vapor sensing with ionic liquids entrapped in alumina nanopores on quartz crystal resonators. *Analytical Chemistry* **2005**, *77* (2), 615-619.
186. Seyama, M.; Iwasaki, Y.; Tate, A.; Sugimoto, I., Room-temperature ionic-liquid-incorporated plasma-deposited thin films for discriminative alcohol-vapor sensing. *Chemistry of Materials* **2006**, *18* (11), 2656-2662.
187. Jin, X.; Yu, L.; Garcia, D.; Ren, R. X.; Zeng, X., Ionic liquid high-temperature gas sensor array. *Analytical Chemistry* **2006**, *78* (19), 6980-6989.
188. Buzzeo, M. C.; Hardacre, C.; Compton, R. G., Use of room temperature ionic liquids in gas sensor design. *Analytical Chemistry* **2004**, *76* (15), 4583-4588.
189. Giovanelli, D.; Buzzeo, M. C.; Lawrence, N. S.; Hardacre, C.; Seddon, K. R.; Compton, R. G., Determination of ammonia based on the electro-oxidation of hydroquinone in dimethylformamide or in the room temperature ionic liquid, 1-ethyl-3-methylimidazolium bis(trifluoromethylsulfonyl)imide. *Talanta* **2004**, *62* (5), 904-911.
190. Wang, R.; Hoyano, S.; Ohsaka, T., O<sub>2</sub> Gas Sensor Using Supported Hydrophobic Room-temperature Ionic Liquid Membrane-coated electrode. *Chemistry Letters* **2004**, *33* (1), 6-7.
191. Wang, R.; Okajima, T.; Kitamura, F.; Ohsaka, T., A Novel Amperometric O<sub>2</sub> Gas Sensor Based on Supported Room-Temperature Ionic Liquid Porous Polyethylene Membrane-Coated Electrodes. *Electroanalysis* **2004**, *16* (1-2), 66-72.

192. Oter, O.; Ertekin, K.; Topkaya, D.; Alp, S., Emission-based optical carbon dioxide sensing with HPTS in green chemistry reagents: room-temperature ionic liquids. *Analytical and Bioanalytical Chemistry* **2006**, *386* (5), 1225-1234.
193. Oter, O.; Ertekin, K.; Derinkuyu, S., Ratiometric sensing of CO<sub>2</sub> in ionic liquid modified ethyl cellulose matrix. *Talanta* **2008**, *76* (3), 557-563.
194. Forzani, E. S.; Lu, D.; Leright, M. J.; Aguilar, A. D.; Tsow, F.; Iglesias, R. A.; Zhang, Q.; Lu, J.; Li, J.; Tao, N., A hybrid electrochemical– colorimetric sensing platform for detection of explosives. *Journal of the American Chemical Society* **2009**, *131* (4), 1390-1391.
195. Poplin, J. H.; Swatloski, R. P.; Holbrey, J. D.; Spear, S. K.; Metlen, A.; Grätzel, M.; Nazeeruddin, M. K.; Rogers, R. D., Sensor technologies based on a cellulose supported platform. *Chemical Communications* **2007**, (20), 2025-2027.
196. Topal, S. Z.; Ertekin, K.; Topkaya, D.; Alp, S.; Yenigul, B., Emission based oxygen sensing approach with tris (2, 2'-bipyridyl) ruthenium (II) chloride in green chemistry reagents: room temperature ionic liquids. *Microchimica Acta* **2008**, *161* (1-2), 209-216.
197. Chen, Y.; Guo, Z.; Wang, X.; Qiu, C., Sample preparation. *Journal of Chromatography A* **2008**, *1184* (1), 191-219.
198. Zaijun, L.; Qiping, P.; Haixia, S., Use of a Novel Medium, the Ionic Liquid 1-Butyl-3-Trimethylsilylimidazolium Hexafluorophosphate, for Liquid-Liquid Extraction of Lead in Water and Its Determination by Graphite Furnace Atomic Absorption Spectrometry. *Journal of AOAC International* **2007**, *90* (4), 1191-1196.
199. Hirayama, N.; Okamura, H.; Kidani, K.; Imura, H., Ionic liquid synergistic cation-exchange system for the selective extraction of lanthanum (III) using 2-thenoyltrifluoroacetone and 18-crown-6. *Analytical Sciences* **2008**, *24* (6), 697-699.
200. Kidani, K.; Hirayama, N.; Imura, H., Extraction behavior of divalent metal cations in ionic liquid chelate extraction systems using 1-alkyl-3-methylimidazolium bis (trifluoromethanesulfonyl) imides and thenoyltrifluoroacetone. *Analytical Sciences* **2008**, *24* (10), 1251-1254.
201. Sun, X.; Wu, D.; Chen, J.; Li, D., Separation of scandium (III) from lanthanides (III) with room temperature ionic liquid based extraction containing Cyanex 925. *Journal of Chemical Technology and Biotechnology* **2007**, *82* (3), 267-272.
202. Zuo, Y.; Liu, Y.; Chen, J.; Li, D. Q., The separation of cerium (IV) from nitric acid solutions containing thorium (IV) and lanthanides (III) using pure [C8mim] PF<sub>6</sub> as extracting phase. *Industrial & Engineering Chemistry Research* **2008**, *47* (7), 2349-2355.

203. Li, M.; Wang, T.; Pham, P. J.; Pittman Jr, C. U.; Li, T., Liquid phase extraction and separation of noble organometallic catalysts by functionalized ionic liquids. *Separation Science and Technology* **2008**, *43* (4), 828-841.
204. De Jong, W. H.; Hagens, W. I.; Krystek, P.; Burger, M. C.; Sips, A. J.; Geertsma, R. E., Particle size-dependent organ distribution of gold nanoparticles after intravenous administration. *Biomaterials* **2008**, *29* (12), 1912-1919.
205. Yang, R. S.; Chang, L. W.; Wu, J.-P.; Tsai, M.-H.; Wang, H.J.; Kuo, Y.-C.; Yeh, T.-K.; Yang, C. S.; Lin, P., Persistent tissue kinetics and redistribution of nanoparticles, quantum dot 705, in mice: ICP-MS quantitative assessment. *Environmental Health Perspectives* **2007**, *115* (9), 1339.
206. Ryan, J. A.; Overton, K. W.; Speight, M. E.; Oldenburg, C. N.; Loo, L.; Robarge, W.; Franzen, S.; Feldheim, D. L., Cellular uptake of gold nanoparticles passivated with BSA-SV40 large T antigen conjugates. *Analytical Chemistry* **2007**, *79* (23), 9150-9159.
207. Wei, G.T.; Yang, Z.; Lee, C.Y.; Yang, H.Y.; Wang, C. R. C., Aqueous-organic phase transfer of gold nanoparticles and gold nanorods using an ionic liquid. *Journal of the American Chemical Society* **2004**, *126* (16), 5036-5037.
208. Huang, H.L.; Wang, H. P.; Wei, G.-T.; Sun, I. W.; Huang, J.-F.; Yang, Y. W., Extraction of Nanosize Copper Pollutants with an Ionic Liquid. *Environmental Science & Technology* **2006**, *40* (15), 4761-4764.
209. Nakashima, T.; Kawai, T., Quantum dots-ionic liquid hybrids: efficient extraction of cationic CdTe nanocrystals into an ionic liquid. *Chemical Communications* **2005**, (12), 1643-1645.
210. Guerra-Abreu, L.; Pino, V.; Anderson, J. L.; Afonso, A. M., Coupling the extraction efficiency of imidazolium-based ionic liquid aggregates with solid-phase microextraction-gas chromatography-mass spectrometry: Application to polycyclic aromatic hydrocarbons in a certified reference sediment. *Journal of Chromatography A* **2008**, *1214* (1), 23-29.
211. Arce, A.; Earle, M. J.; Katdare, S. P.; Rodríguez, H.; Seddon, K. R., Application of mutually immiscible ionic liquids to the separation of aromatic and aliphatic hydrocarbons by liquid extraction: a preliminary approach. *Physical Chemistry Chemical Physics* **2008**, *10* (18), 2538-2542.
212. Absalan, G.; Akhond, M.; Sheikhan, L., Partitioning of acidic, basic and neutral amino acids into imidazolium-based ionic liquids. *Amino acids* **2010**, *39* (1), 167-174.
213. Egorov, V. M.; Smirnova, S. V.; Pletnev, I. V., Highly efficient extraction of phenols and aromatic amines into novel ionic liquids incorporating quaternary ammonium cation. *Separation and Purification Technology* **2008**, *63* (3), 710-715.

214. Carda-Broch, S.; Berthod, A.; Armstrong, D. W., Solvent properties of the 1-butyl-3-methylimidazolium hexafluorophosphate ionic liquid. *Analytical and Bioanalytical Chemistry* **2003**, *375* (2), 191-199.
215. Visser, A. E.; Swatloski, R. P.; Rogers, R. D., pH-dependent partitioning in room temperature ionic liquids provides a link to traditional solvent extraction behavior. *Green Chemistry* **2000**, *2* (1), 1-4.
216. Zhang, D. L.; Deng, Y. F.; Li, C. B.; Chen, J., Separation of ethyl acetate-ethanol azeotropic mixture using hydrophilic ionic liquids. *Industrial & Engineering Chemistry Research* **2008**, *47* (6), 1995-2001.
217. Pei, Y. C.; Wang, J. J.; Xuan, X. P.; Fan, J.; Fan, M., Factors affecting ionic liquids based removal of anionic dyes from water. *Environmental Science & Technology* **2007**, *41* (14), 5090-5095.
218. Marták, J.; Schlosser, Š., Extraction of lactic acid by phosphonium ionic liquids. *Separation and Purification Technology* **2007**, *57* (3), 483-494.
219. Fan, J.; Fan, Y.; Pei, Y.; Wu, K.; Wang, J.; Fan, M., Solvent extraction of selected endocrine-disrupting phenols using ionic liquids. *Separation and Purification Technology* **2008**, *61* (3), 324-331.
220. Zhu, J.Q.; Chen, J.; Li, C.Y.; Fei, W.Y., Centrifugal extraction for separation of ethylbenzene and octane using 1-butyl-3-methylimidazolium hexafluorophosphate ionic liquid as extractant. *Separation and Purification Technology* **2007**, *56* (2), 237-240.
221. Bosmann, A.; Datsevich, L.; Jess, A.; Lauter, A.; Schmitz, C.; Wasserscheid, P., Deep desulfurization of diesel fuel by extraction with ionic liquids. *Chemical Communications* **2001**, (23), 2494-2495.
222. Nie, Y.; Li, C.; Sun, A.; Meng, H.; Wang, Z., Extractive desulfurization of gasoline using imidazolium-based phosphoric ionic liquids. *Energy & Fuels* **2006**, *20* (5), 2083-2087.
223. Holbrey, J. D.; López-Martin, I.; Rothenberg, G.; Seddon, K. R.; Silvero, G.; Zheng, X., Desulfurisation of oils using ionic liquids: selection of cationic and anionic components to enhance extraction efficiency. *Green Chemistry* **2008**, *10* (1), 87-92.
224. Du, F.Y.; Xiao, X.H.; Li, G.K., Application of ionic liquids in the microwave-assisted extraction of *trans*-resveratrol from *Rhizma Polygoni Cuspidati*. *Journal of Chromatography A* **2007**, *1140* (1), 56-62.
225. Liu, J. f.; Jiang, G. b.; Chi, Y. g.; Cai, Y. q.; Zhou, Q. x.; Hu, J. T., Use of Ionic Liquids for Liquid-Phase Microextraction of Polycyclic Aromatic Hydrocarbons. *Analytical Chemistry* **2003**, *75* (21), 5870-5876.
226. Vidal, L.; Psillakis, E.; Domini, C. E.; Grané, N.; Marken, F.; Canals, A., An ionic liquid as a solvent for headspace single drop microextraction of chlorobenzenes from water samples. *Analytica Chimica Acta* **2007**, *584* (1), 189-195.

227. Liu, J.-f.; Chi, Y.g.; Jiang, G.b.; Tai, C.; Peng, J.-f.; Hu, J.-T., Ionic liquid-based liquid-phase microextraction, a new sample enrichment procedure for liquid chromatography. *Journal of Chromatography A* **2004**, *1026* (1–2), 143-147.
228. Ye, C.L.; Zhou, Q.X.; Wang, X.M., Headspace liquid-phase microextraction using ionic liquid as extractant for the preconcentration of dichlorodiphenyltrichloroethane and its metabolites at trace levels in water samples. *Analytica Chimica Acta* **2006**, *572* (2), 165-171.
229. Liu, J. f.; Chi, Y. g.; Jiang, G. b., Screening the extractability of some typical environmental pollutants by ionic liquids in liquid-phase microextraction. *Journal of Separation Science* **2005**, *28* (1), 87-91.
230. Peng, J.f.; Liu, J.f.; Jiang, G.b.; Tai, C.; Huang, M.j., Ionic liquid for high temperature headspace liquid-phase microextraction of chlorinated anilines in environmental water samples. *Journal of Chromatography A* **2005**, *1072* (1), 3-6.
231. Ohno, H.; Fukumoto, K., Amino acid ionic liquids. *Accounts Chem. Res.* **2007**, *40* (11), 1122-1129.
232. Fukumoto, K.; Ohno, H., LCST-type phase changes of a mixture of water and ionic liquids derived from amino acids. *Angewandte Chemie International Edition* **2007**, *46* (11), 1852-1855.
233. Matsumoto, M.; Ohtani, T.; Kondo, K., Comparison of solvent extraction and supported liquid membrane permeation using an ionic liquid for concentrating penicillin G. *Journal of Membrane Science* **2007**, *289* (1), 92-96.
234. Wang, J.H.; Cheng, D.H.; Chen, X.-W.; Du, Z.; Fang, Z.L., Direct extraction of double-stranded DNA into ionic liquid 1-butyl-3-methylimidazolium hexafluorophosphate and its quantification. *Analytical Chemistry* **2007**, *79* (2), 620-625.
235. Cheng, D.H.; Chen, X.W.; Shu, Y.; Wang, J.H., Selective extraction/isolation of hemoglobin with ionic liquid 1-butyl-3-trimethylsilylimidazolium hexafluorophosphate (Btmsim PF<sub>6</sub>). *Talanta* **2008**, *75* (5), 1270-1278.
236. Dreyer, S.; Kragl, U., Ionic liquids for aqueous two-phase extraction and stabilization of enzymes. *Biotechnology and Bioengineering* **2008**, *99* (6), 1416-1424.
237. Cull, S. G.; Holbrey, J. D.; Vargas-Mora, V.; Seddon, K. R.; Lye, G. J., Room-temperature ionic liquids as replacements for organic solvents in multiphase bioprocess operations. *Biotechnology and Bioengineering* **2000**, *69* (2), 227-233.
238. Smirnova, S. V.; Torocheshnikova, I. I.; Formanovsky, A. A.; Pletnev, I. V., Solvent extraction of amino acids into a room temperature ionic liquid with dicyclohexano-18-crown-6. *Analytical and Bioanalytical Chemistry* **2004**, *378* (5), 1369-1375.

239. Jian-Ji, W.; Yuan-Chao, P.; Yang, Z.; Suo-Jiang, Z., Selective extraction of bioproducts by ionic liquids. *Chinese Journal of Chemistry* **2005**, *23* (6), 662-664.
240. Wang, J.; Pei, Y.; Zhao, Y.; Hu, Z., Recovery of amino acids by imidazolium based ionic liquids from aqueous media. *Green Chemistry* **2005**, *7* (4), 196-202.
241. Pei, Y.; Wang, J.; Wu, K.; Xuan, X.; Lu, X., Ionic liquid-based aqueous two-phase extraction of selected proteins. *Separation and Purification Technology* **2009**, *64* (3), 288-295.
242. Shimojo, K.; Kamiya, N.; Tani, F.; Naganawa, H.; Naruta, Y.; Goto, M., Extractive solubilization, structural change, and functional conversion of cytochrome c in ionic liquids via crown ether complexation. *Analytical Chemistry* **2006**, *78* (22), 7735-7742.
243. Luo, H. M.; Dai, S.; Bonnesen, P. V., Solvent extraction of  $\text{Sr}^{2+}$  and  $\text{Cs}^{+}$  based on room-temperature ionic liquids containing monoaza-substituted crown ethers. *Analytical Chemistry* **2004**, *76* (10), 2773-2779.
244. Visser, A. E.; Swatloski, R. P.; Reichert, W. M.; Mayton, R.; Sheff, S.; Wierzbicki, A.; Davis, J. H.; Rogers, R. D., Task-specific ionic liquids for the extraction of metal ions from aqueous solutions. *Chemical Communications* **2001**, (01), 135-136.
245. Huddleston, J. G.; Willauer, H. D.; Swatloski, R. P.; Visser, A. E.; Rogers, R. D., Room temperature ionic liquids as novel media for 'clean' liquid-liquid extraction. *Chemical Communications* **1998**, (16), 1765-1766.
246. Cocalia, V. A.; Holbrey, J. D.; Gutowski, K. E.; Bridges, N. J.; Rogers, R. D., Separations of metal ions using ionic liquids: the challenges of multiple mechanisms. *Tsinghua Science & Technology* **2006**, *11* (2), 188-193.
247. Dietz, M. L.; Dzielawa, J. A., Ion-exchange as a mode of cation transfer into room-temperature ionic liquids containing crown ethers: implications for the 'greenness' of ionic liquids as diluents in liquid-liquid extraction. *Chemical Communications* **2001**, (20), 2124-2125.
248. Visser, A. E.; Jensen, M. P.; Laszak, I.; Nash, K. L.; Choppin, G. R.; Rogers, R. D., Uranyl coordination environment in hydrophobic ionic liquids: An in situ investigation. *Inorganic chemistry* **2003**, *42* (7), 2197-2199.
249. Jensen, M. P.; Dzielawa, J. A.; Rickert, P.; Dietz, M. L., EXAFS investigations of the mechanism of facilitated ion transfer into a room-temperature ionic liquid. *Journal of the American Chemical Society* **2002**, *124* (36), 10664-10665.
250. Jensen, M. P.; Neufeind, J.; Beitz, J. V.; Skanthakumar, S.; Soderholm, L., Mechanisms of metal ion transfer into room-temperature ionic liquids: The role of anion exchange. *Journal of the American Chemical Society* **2003**, *125* (50), 15466-15473.

251. Li, C.; Xin, B.; Xu, W.; Zhang, Q., Study on the extraction of dyes into a room-temperature ionic liquid and their mechanisms. *Journal of Chemical Technology and Biotechnology* **2007**, *82* (2), 196-204.
252. de Mello, A. J.; Habgood, M.; Lancaster, N. L.; Welton, T.; Wootton, R. C., Precise temperature control in microfluidic devices using Joule heating of ionic liquids. *Lab on a Chip* **2004**, *4* (5), 417-419.
253. Wijethunga, P. A.; Nanayakkara, Y. S.; Kunchala, P.; Armstrong, D. W.; Moon, H., On-chip drop-to-drop liquid microextraction coupled with real-time concentration monitoring technique. *Analytical Chemistry* **2011**, *83* (5), 1658-1664.
254. Loe-Mie, F.; Marchand, G.; Berthier, J.; Sarrut, N.; Pucheault, M.; Blanchard-Desce, M.; Vinet, F.; Vaultier, M., Towards an Efficient Microsystem for the Real-Time Detection and Quantification of Mercury in Water Based on a Specifically Designed Fluorogenic Binary Task-Specific Ionic Liquid. *Angewandte Chemie International Edition* **2010**, *49* (2), 424-427.



# Chapter 2

## Microfluidic Compound Droplets:

### Formation and Routing

#### 2.1 Compound Droplets Formation

The formation and dynamics of droplets in microchannels are typically dominated by wettability and fluid-fluid interfacial phenomena. Bubble or drop formation in a variety of geometries has been extensively studied in recent years as a means of producing highly controlled monodisperse emulsions or foams, and the relevant fluid physics is reasonably well understood.<sup>1</sup> At the low Capillary and Reynolds numbers typical to such systems, the dynamic bubble and drop shapes obtained in confined geometries closely resemble their static counterparts.<sup>2</sup> There has also been significant interest in generating double or triple emulsions of two or more fluid phases in an immiscible carrier fluid for the fabrication of precisely structured core-shell beads. Multiple emulsions have found a number of applications in medicine and industry. Encapsulation of active substances in monodisperse particles improves the control over the release profile. It has also been reported that encapsulation of cells from the host tissue enhances their viability. The viability of encapsulated cells may depend on diffusion of media, stimuli and waste products, and on the geometry of the encapsulant. Further, the rate of release of encapsulated molecules can be controlled by tuning the architecture of multiple emulsions (i.e. number of shells, number, composition and size of inner droplets). When two immiscible fluids are dispensed into a third fluid in a microchannel, the dispensed droplets assemble into biphasic

‘compound droplets’ whose interfacial morphologies can be predicted by purely static considerations.

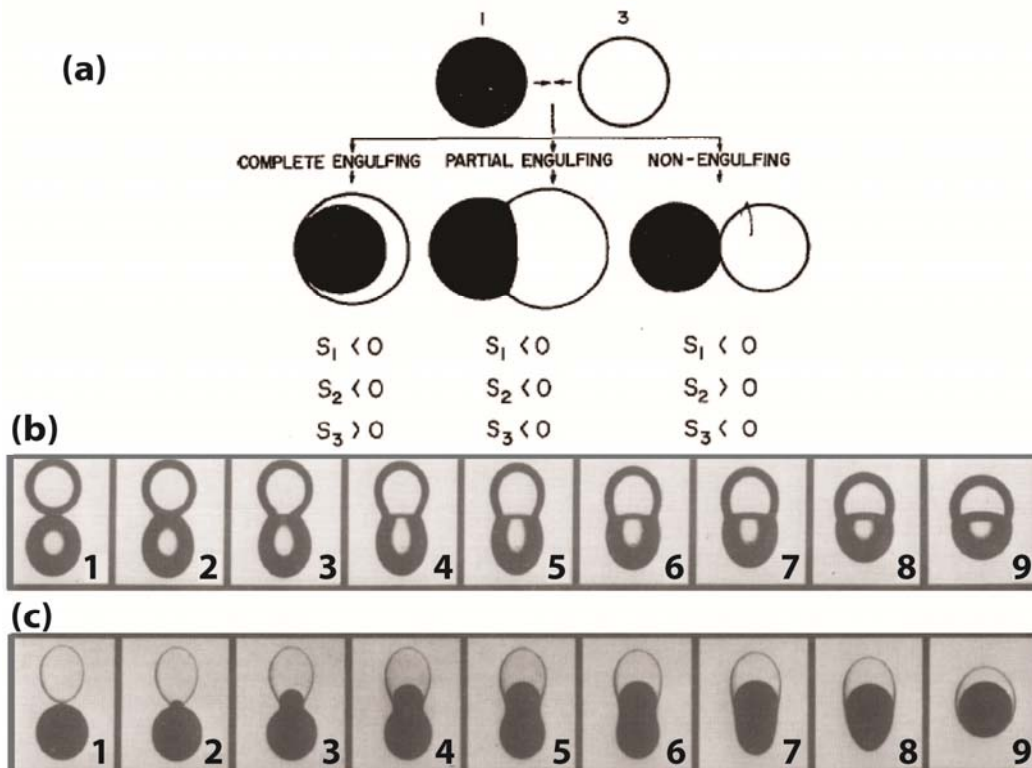


**Figure 2.1.** a) Possible equilibrium configurations corresponding to three sets of spreading parameters,  $S_i$ . Photographs of the stages of b) partial engulfing and c) complete engulfing.<sup>4</sup> (Reprinted from [4], Copyright 1970, with permission from Elsevier.)

Depending on the surface tensions between the three liquid phases, three possible equilibrium interfacial morphologies are predicted by the theory developed by Torza and Mason<sup>3-4</sup>: (1) *completely engulfed* drop-in-drop structures (Figure 2.1), which have been extensively reported in the microfluidics literature, (2) *partially engulfed* structures (dumbbell-like doublet), where a three-fluid contact line is formed (Figure 2.1), and (3) *non-engulfed* droplet pairs where the two dispersed liquids remain unattached and isolated from each other by the continuous liquid phase. In the next section we describe the stability diagram of all the morphologies and the sign of

the curvature of the interface between these two phases as a function of the contact angle and the ratio of volumes. The latter can be controlled by using a microfluidic device, in which the pairs of droplets of desired volumes can be manufactured in a reproducible manner by adjusting the relative flow speeds of the different species.

### 2.1.1 Double Emulsion Structures

By considering two immiscible liquids A and B of volumes  $V_A$  and  $V_B$ , respectively, that are in contact with each other and both immersed in the third liquid O, three interfaces can form. The resultant interfaces are characterized by three different surface tensions as follows:  $\sigma_A$ ,  $\sigma_B$ , and  $\sigma_{AB}$ . At mechanical equilibrium, each of the interfaces is a section of a sphere and the equilibrium shape of the droplet is fully defined by contact angles  $\theta_A$  and  $\theta_B$  between the interfaces at the three-phase contact line and the ratio of the volumes  $V_B/V_A$ . Also, contact angles are related to the three surface tensions  $\sigma_{0A}$ ,  $\sigma_{0B}$  and  $\sigma_{AB}$  via the set of equations 2.1, 2.2, 2.3.<sup>5</sup>

$$\sigma_{AB} + \sigma_{0B} \cos \theta_B + \sigma_{0A} \cos \theta_A = 0 \quad (2.1)$$

$$\sigma_{AB} \cos \theta_B + \sigma_{0B} + \sigma_{0A} \cos \theta_O = 0 \quad (2.2)$$

$$\sigma_{AB} \cos \theta_A + \sigma_{0B} \cos \theta_O + \sigma_{0A} = 0 \quad (2.3)$$

whose geometrical interpretation is known as the Neumann's triangle (see Fig. 1).

Therefore, only  $\theta_A$  and  $\theta_B$  are independent whereas  $\theta_O = 2\pi - \theta_A - \theta_B$ .

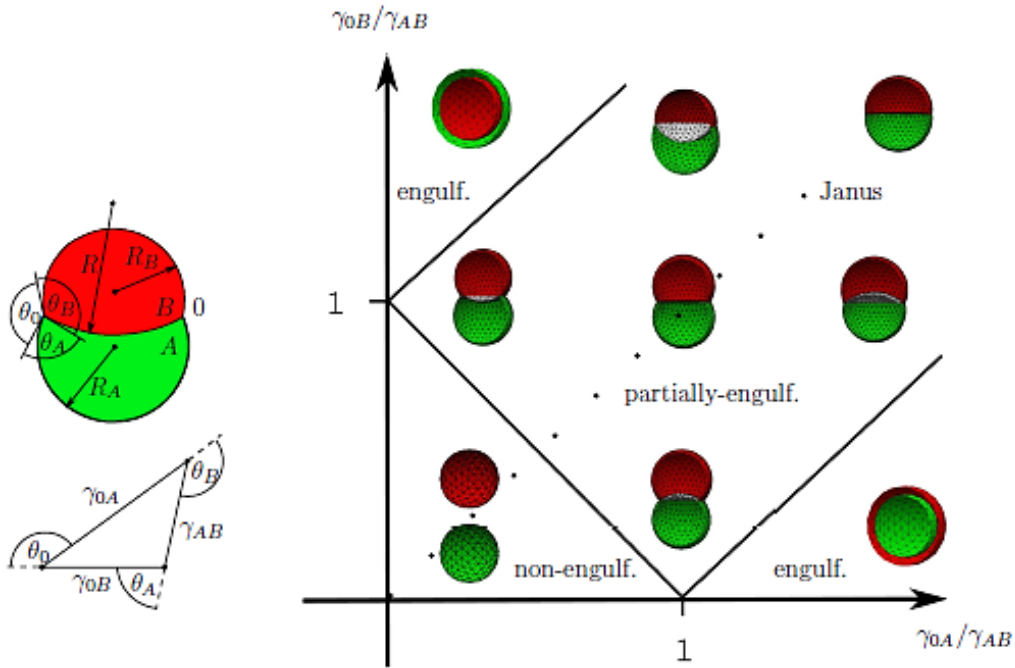


**Figure 2.2.** Left: sketch of the partially engulfing configuration with the phases A and B surrounded by the phase 0 and the Neumann's triangle whose sides have lengths proportional to the surface tensions. Right: the diagram representing possible morphologies formed by the phases A (green) and B (red) in the case of equal droplet volumes  $V_A = V_B$ . The dotted line corresponds to the condition  $\theta_B = \theta_A$ .<sup>5</sup> (Adapted from [5] with permission of The Royal Society of Chemistry.)

Briefly, assuming that the continuous oil-phase completely wets the microchannel walls, the criteria for the various possible topologies can be determined through three spreading parameters  $S_i = \sigma_{jk} - (\sigma_{ij} + \sigma_{ik})$  ( $i \neq j \neq k = O, A, B$ ) for the ternary liquid system using values of equilibrium binary interfacial tensions  $\sigma_{ij}$  and adopting the convention that phase O is that for which  $\sigma_{OA} > \sigma_{AB}$ . The spreading coefficient reflects the tendency of a liquid to spread on a solid surface. In the present case, the solid surface is replaced by an interface between two other liquids. When  $S_i > 0$ , the liquid  $i$  spreads on  $jk$ -interface into a thin film. When  $S_i < 0$ , it rather forms a liquid lens characterized by a finite angle between  $ik$  and  $ij$ -interfaces. Depending on the values of the spreading parameters three possible morphologies can be distinguished.

- *Completely engulfed* droplets are obtained when  $S_O < 0$ ,  $S_A < 0$ ,  $S_B > 0$  (phase B completely engulfs phase A) or vice versa ( $S_O < 0$ ,  $S_B < 0$ ,  $S_A > 0$ ), while
- *Partially engulfed* compound droplets are obtained when  $S_O < 0$ ,  $S_A < 0$ ,  $S_B < 0$ . In this morphology droplets of phases A and B touch each other and are both exposed to the host phase 0
- *Non-engulfed* droplets where droplets of phases A and B are separated by the host phase 0 are obtained when ( $S_O > 0$ ,  $S_B < 0$ ,  $S_A < 0$ ).

In the partially engulfed case, one can solve Eqs. (2.1)-(2.3) with respect to  $\cos \theta_A$  and  $\cos \theta_B$  to get the following expressions:

$$\cos \theta_A = \frac{\sigma_{OB}^2 - \sigma_{AB}^2 - \sigma_{OA}^2}{2\gamma_{AB}\gamma_{OB}} \quad (2.4)$$

$$\cos \theta_B = \frac{\sigma_{OA}^2 - \sigma_{AB}^2 - \sigma_{OB}^2}{2\sigma_{AB}\sigma_{OB}} \quad (2.5)$$

The mathematical bounds  $-1 < \cos \theta_A < 1$  and  $-1 < \cos \theta_B < 1$  translate into  $S_A < 0$ ,  $S_B < 0$ , and  $S_0 < 0$ .

### 2.1.2 Partially Engulfed Structure or Compound Droplets

By considering Eqs. (2.4) and (2.5), one can obtain two limiting characteristic cases:

- *Solid-like phase A*: If  $\sigma_{AB} \rightarrow \sigma_{OA}$  and  $\sigma_{OB}/\sigma_{AB} \rightarrow 0$ , the equations 2.4 and 2.5 lead to:

$$\cos \theta_A = -1 \quad (2.6)$$

$$\cos \theta_B = \frac{\sigma_{OA} - \sigma_{AB}}{\sigma_{OB}} = -\cos \theta_O \quad (2.7)$$

Eq. (2.6) shows that  $\theta_A = \pi$ , meaning that droplet of phase A forms a perfect sphere which behaves like a solid particle at the OB-interface and it does not deform upon surface tension changes but only is partially absorbed by droplet phase B (Figure 2.3). Also, Eq. (2.7) expresses a Young's law<sup>6</sup> for the contact angle at a solid particle.

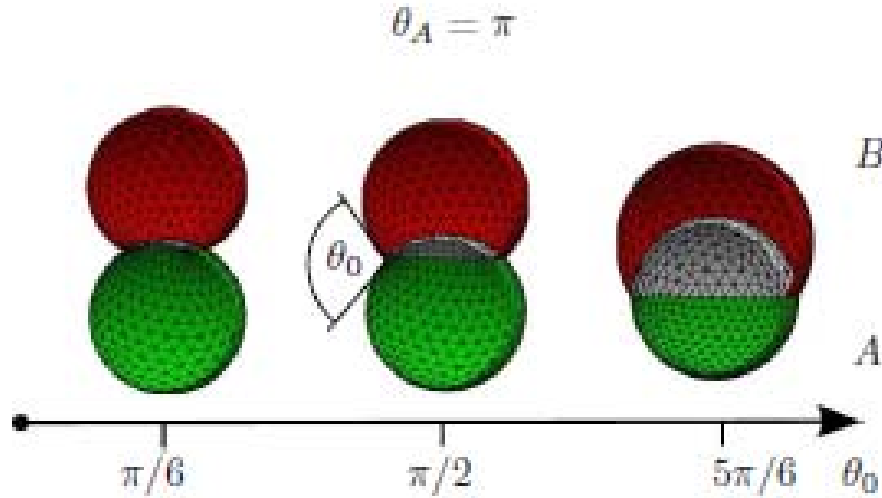


**Figure 2.3.** Configurations of partially engulfed droplets for various  $\theta_0$  in the limiting case  $\sigma_{AB} \rightarrow \sigma_{OA}$  and  $\sigma_{OB}/\sigma_{AB} \rightarrow 0$ , which corresponds to  $\theta_A = \pi$  (Solid-like phase A).<sup>5</sup> (Adapted from [5] with permission of The Royal Society of Chemistry.)

- *Solid-like phase B:* Full analogy to the previous case by interchanging A and B, with the conditions as follows  $\sigma_{AB} \rightarrow \sigma_{OB}$  and  $\sigma_{OA}/\sigma_{AB} \rightarrow 0$ , because the species A and B are equivalent.

- *Janus-like doublet:* With the limits of  $\sigma_{OB} \rightarrow \sigma_{OA}$  and  $\sigma_{OA}/\sigma_{AB} \rightarrow \infty$ , one can obtain the following,

$$\cos \theta_B = \frac{\sigma_{OA} - \sigma_{OB}}{\sigma_{AB}} = -\cos \theta_A \quad (2.8)$$

This can be used to find  $\theta_O = \pi$  since  $\theta_A + \theta_B = \pi = 2\pi - \theta_O$ . This is physically related to the Janus-like droplets in which doublet forms a perfect sphere (Figure 2.4).

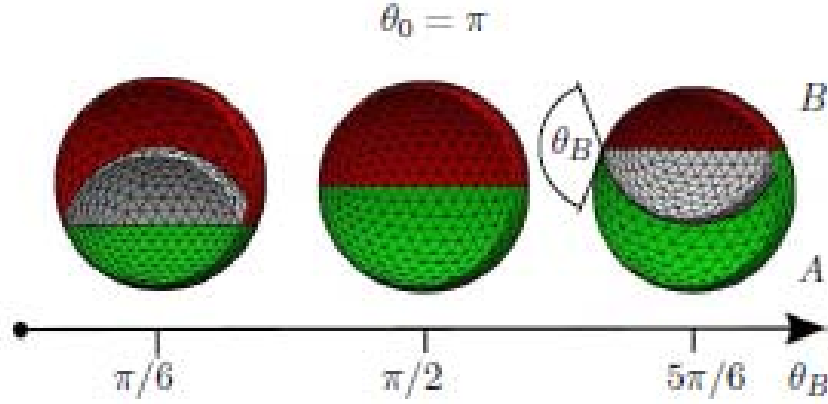


**Figure 2.4.** Configurations of partially engulfed droplets for various  $\theta_B$  in the limiting case  $\sigma_{OB} \rightarrow \sigma_{OA}$  and  $\sigma_{OA}/\sigma_{AB} \rightarrow \infty$ , which corresponds to  $\theta_0 = \pi$  (Janus-like doublet).<sup>5</sup> (Adapted from [5] with permission of The Royal Society of Chemistry.)

It is also noteworthy that, in the partial engulfed scenario, the curvature  $R^{-1}$  of the AB-interface can be formed as negative or positive depending on the contact angles  $\theta_A$ ,  $\theta_B$  and the volume ratio of droplets A and B ( $V_B/V_A$ ). We consider the geometry depicted in Figure 2.2 and the pressure balance in the case of arbitrary  $\theta_A$  and  $\theta_B$ . In addition, the Laplace pressure inside droplet A due to the curvature  $R_A^{-1}$  and the Laplace pressure inside droplet B due to the curvature  $R_B^{-1}$  differ by the Laplace pressure due to the curvature  $R^{-1}$  at the AB-interface (the sign of the curvature is according to Figure 2.2). This relation can be quantified as,

$$\frac{\sigma_{OB}}{R_B} - \frac{\sigma_{OA}}{R_A} = \frac{\sigma_{AB}}{R} \quad (2.9)$$

The surface tensions  $\gamma_{0A}$  and  $\gamma_{0B}$  can be expressed by the contact angles  $\theta_A$  and  $\theta_B$  using the law of sines for the Neumann's triangle (Figure 2.2), which is  $\sigma_{OB}/\sin \theta_B = \sigma_{OA}/\sin \theta_A = \sigma_{AB}/\sin(\pi - \theta_A - \theta_B)$ . This expression and equation (2.9) result in:

$$R = \sin(\theta_A + \theta_B) \left( \frac{\sin \theta_B}{R_B} - \frac{\sin \theta_A}{R_A} \right)^{-1} \quad (2.10)$$

The expression in bracket is a difference of two positive terms since  $R_A > 0$ ,  $R_B > 0$ ,  $0 < \theta_A < \pi$  and  $0 < \theta_B < \pi$ . Therefore, one of the droplet volumes can be chosen big enough such that  $R_A \rightarrow \infty$  or  $R_B \rightarrow \infty$  and makes  $R$  either positive or negative, respectively (Figure 2.5).<sup>5</sup>

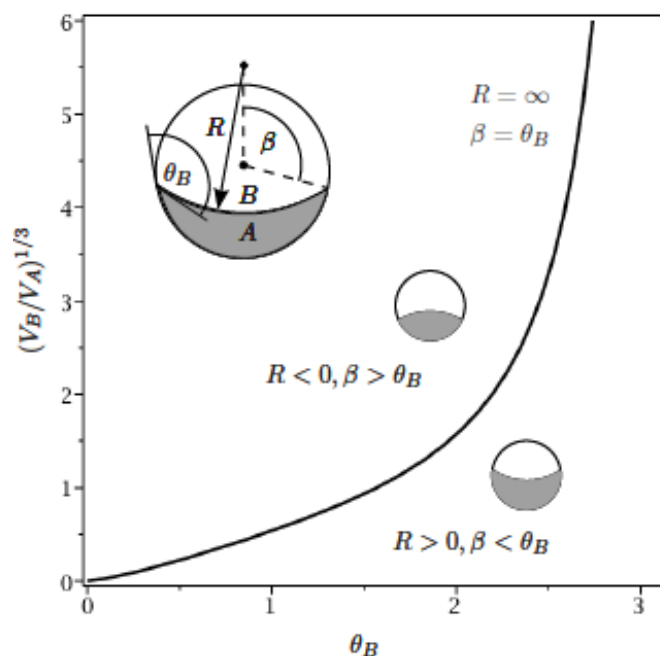


**Figure 2.5.** Diagram represents the regions of positive and negative curvature  $R^{-1}$  of the AB-interface in Janus-like droplets. The solid line corresponds to  $V_B/V_A = (V_B/V_A)_{\text{crit}}$ .<sup>5</sup> (Adapted from [5] with permission from The Royal Society of Chemistry.)

In this thesis, the particular focus is on partially engulfed compound droplets. In the following sections, we first investigate the flow conditions to form various configurations of IL-aq compound droplets. We then demonstrate passive methods to decouple the two compartments of IL-aq biphasic droplets. To fulfill this, hydrodynamic constrictions and bifurcated junctions are used and flow conditions to obtain complete decoupling are examined. Moreover, bifurcated junctions are also employed to split or double compound droplets and the results are described in the last section of this chapter.



## 2.2 Compound Droplets Routing

Flows at the small length scales (10 to 100  $\mu\text{m}$ ) that are characteristic of microfluidic systems typically occur at low Re and thus are dominated by viscosity and inertia plays only a marginal role.<sup>7</sup> Viscosity-dominated flows are governed by equations of motion that are linear in the velocity of the fluid. Classic experiments by Taylor<sup>8</sup> demonstrated how low-Re flows can be reversed. On the other hand, the interfacial stresses present in the multiphase systems introduce nonlinearities into the equations of flow, even at low Re. These nonlinearities are weak compared with the linear contribution to the dynamics,<sup>9</sup> and therefore do not affect the reversibility of the movement of droplets or bubbles through a microchannel. This reversibility makes it possible to encode and decode with droplet trains. Demands of parallelization and integration of multiple functionalities into a single platform, has resulted in an increasing number of devices for multiphase microfluidics consist of interconnected fluidic networks of a high degree of complexity.<sup>10-11</sup> The traffic of bubble and droplet train through even simple microfluidic networks displays complex behavior associated with non-linear dynamics of such systems. The feedback between neighboring droplets and their trajectories through the network can display chaotic dynamics.<sup>12-13</sup> Therefore, there is a great need to investigate such complex dynamics and classify regions with controlled regular behavior. This information is essential to design multiphase microfluidic devices with unit operations to merge, split, sort and direct droplets or bubbles as they navigate through microfluidic networks. A power to control such operations in droplet microfluidics is crucial to broaden the applications of multiphase microsystems.

Inclusion of bifurcations and loops in the network of microchannels, significantly alter the behavior of multiphase flows.<sup>10, 14-15</sup> A droplet reaching a bifurcation or a simple T-junction, might break into two daughter droplets or simply be directed into either of the branches with greater inflow or lower hydrodynamic resistance to flow.<sup>10</sup> There are also flow regimes in which the presence of droplets in a bifurcated arm increases the flow resistance in that arm; thereby, affects the choice of the successive droplets.<sup>9, 16-17</sup> The droplets choose a path based on the number of droplets that occupy each branch. This feedback is amplified by slight inherent differences in the resistance of the bifurcation arms due to the fabrication and makes the flow dynamics complicated for selection of right/left pathways. The nonlinearity in the operation of the system derives from the fluidic resistances of the two arms of the loop and the nonlinear transformation of the intervals between droplets entering the loop and leaving it.

Earlier, the unification of two chemically distinct fluid components into one compound droplet was demonstrated. Since the ultimate application of such compound droplets would be on-drop chemical analyses and separations where one compartment acts as a chemical probe or extractor, an intriguing extension of the idea would involve physical decoupling of the individual fluid compartments after this coupling or splitting into equal size compound droplets. Separation of probe from analyte or extractor from the reaction flask has great potential in controlling the contact time or the extent of interfacial transport where further analysis of the detached aqueous droplet by attaching a different probe compartment is also possible. Compound droplet routing (decoupling, splitting and sorting) can be passively

manipulated by externally driven flows that are varied locally by geometry of the channel in a continuous stream.

Although there have been much interest and research in digital microfluidic techniques, theoretical understanding of droplet breakup in a T junction is limited. Link *et al.*<sup>10</sup> developed a scaling theory based on their experimental studies of droplet breakup in a symmetric (i.e., having daughter channels of equal lengths) T junction of a square cross section. For a strongly confined geometry, at small or moderate capillary numbers, the breakup is more likely to be caused by an increased upstream pressure due to lubrication flow in a thin film between the drop and the channel wall. This mechanism is applicable to a two-dimensional (2D) system where the capillary (Rayleigh–Plateau) instability of a cylindrical liquid thread<sup>10</sup> is not operative, but it is likely to be responsible for the breakup in three dimensions (3D).<sup>18</sup>

Although there are published studies on the behavior of single droplets at microfluidic T-junctions or bifurcated junctions, there has been no report on routing of compound droplets. In-depth understanding of the routing logic of such complex three phase flow requires more careful studies than our proposed preliminary schemes of routing in this thesis. Here, we present a few preliminary demonstrations of passive decoupling processes of IL-aqueous compound droplets using hydrodynamic constriction and bifurcated junctions in addition to splitting compound droplets into identical sized daughter compound drops.

## 2.3 Experimental Details

### 2.3.1 Materials

Octadecafluorodecahydronaphthalene (Perfluorodecalin or FO, Fluka, mixture of cis and trans, 95%), 1*H*,1*H*,2*H*,2*H*-perfluorooctanol (Sigma-Aldrich, 97%), 1-methylimidazole (Sigma-Aldrich, 99%), bromoethane (Sigma-Aldrich), chloroform (BDH AnalaR), Lithium bis(trifluoromethylsulfonyl) imide (TCI, 98%), silicone oil (10 cst, Dow Corning Singapore) were used as obtained. Phosphonium-based ionic liquid ([C<sub>12</sub>(C<sub>4</sub>)<sub>3</sub>P][NTf<sub>2</sub>]) and 1-Methyl-3-methylimidazolium bis(trifluoromethylsulfonyl)imide (synthesized, [MMIM][NTf<sub>2</sub>]) were synthesized according to synthesis protocol of ILs (2.3.2). Ultra-pure water (18 MΩ-cm, ELGA, Singapore) was used for all experiments.

### 2.3.2 Synthesis of IL ([EMIM][NTf<sub>2</sub>])

#### 1-ethyl-3-methylimidazolium bis(trifluoromethylsulfonyl)imide

1-methylimidazole (12.9 g, 157 mmol) and bromoethane (17.2 g, 1.0 equiv) were mixed with 100 mL of toluene (Fisher scientific) in a round-bottomed flask fitted with a reflux condenser. This mixture was heated and stirred at 110°C for 12 h. A biphasic mixture was obtained and the bottom phase solidified upon cooling at room temperature. After decanting the upper toluene phase, the solid (1-ethyl-3-methylimidazolium bromide) was washed with 30 mL of toluene three times, to remove any unreacted material. This solid was then transferred to another flask (300 mL) and dissolved in 50 mL of deionized water. To this solution, 50 mL aqueous solution of Lithium bis(trifluoromethylsulfonyl)imide (50.00 g, 1.1 equiv) was added. Ionic liquid was formed immediately and settled down from the aqueous phase at the

bottom. The upper aqueous phase was decanted and the ionic liquid part was dissolved in chloroform (50 mL). This chloroform solution was washed with deionized water (3x100 mL) to remove any unreacted material and lithium bromide. After separating the organic extract, it was dried over magnesium sulphate and filtered. The filtrate was concentrated by evaporating chloroform (rotary evaporator). The resulting ionic liquid 1-ethyl-3-methylimidazolium bis(trifluoromethylsulfonyl)imide ([EMIM][NTf<sub>2</sub>]), a transparent and almost colorless liquid, 39 ml) was dried under vacuum at 70°C for 5h and then stored at room temperature and characterized by <sup>1</sup>H NMR (see Appendix B- Figure B 1).<sup>19</sup> The diagnostic peaks are 7.55 ppm and 7.63 ppm, corresponding to two asymmetric aromatic protons in the imidazolium ring. The synthesis protocol is summarized in Figure 2.6.

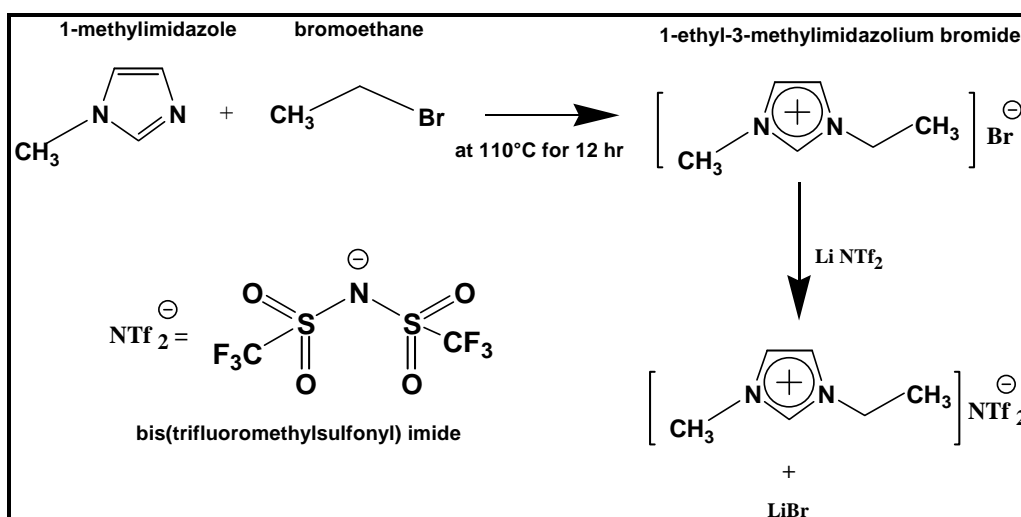


**Figure 2.6** Synthesis protocol of ionic liquid [EMIM][NTf<sub>2</sub>]

### 2.3.3 Physical Properties of IL [EMIM][NTf<sub>2</sub>]

To characterize the physical properties of synthesized [EMIM][NTf<sub>2</sub>], density (Analytical Balance GR-200, 0.1mg resolution), viscosity (Rheometer AR-G2, shear

rate 1-500 s<sup>-1</sup>), and interfacial forces (Contact angle and surface tension analyzer, KSV CAM 200) were measured and compared to data available in the literatures. The results are tabulated in the Table 2.1.

Interfacial tensions were measured between the different fluids using the pendant drop technique (KSV Cam 200). The measured values of interfacial tension between fluorinated oil (PFD:PFO), silicon oil (SO), IL ([EMIM][NTf<sub>2</sub>]) and aqueous phase (water) were as follows: fluorinated oil and water,  $\sigma_{FO-W} = 5.4 \pm 0.6$  mN/m, fluorinated oil and IL,  $\sigma_{FO-IL} = 16.6 \pm 0.5$  mN/m, water and IL,  $\sigma_{W-IL} = 12.1 \pm 0.5$  mN/m, silicone oil and water,  $\sigma_{SO-W} = 48.7 \pm 3$  mN/m, silicone oil and IL,  $\sigma_{SO-IL} = 12.5 \pm 0.5$  mN/m.

[EMIM][NTf <sub>2</sub> ] at 25°C	Measured value	Literature value <sup>20</sup>
Density ( $\rho$ ) g/cm <sup>3</sup>	1.509	1.518
Viscosity (Pa.s)	0.031	0.032
Interfacial Forces (mN.m <sup>-1</sup> )		
<i>IL in air</i>	34.986	35.1
<i>IL and pure water</i>	8.393	----
<i>IL and aqueous solution*</i>	8.531	----

**Table 2.1.** Density, viscosity and interfacial tension of [EMIM][NTf<sub>2</sub>] (\* denotes aqueous solution containing Rhodamine B)

### 2.3.4 Microfabrication

Microfluidic device patterns were fabricated onto silicon wafers by standard photolithography using the negative photoresist SU-8 (2050). Devices were molded in poly(dimethyl siloxane) (PDMS) using the soft lithography technique.<sup>21</sup> Briefly, PDMS was molded onto the SU-8 masters at 70°C for 2.5 hrs, peeled, cut and

cleaned. The inlet and outlet holes (1/16-in. O.D.) were punched into the device which was then sealed to a glass slide pre-coated with a thin layer of PDMS after 35 seconds air plasma treatment. The bounded device was kept in oven 100 °C for 24 hrs. The microchannels had a rectangular cross-section.

#### **2.3.4.1 Formation of complex emulsions of different configurations**

In this work, [EMIM][NTf<sub>2</sub>] is used as the IL phase. We deliver aqueous solutions and an ionic liquid ([EMIM][NTf<sub>2</sub>]) at a microfabricated junction into an immiscible oil to form either completely engulfed drop-in-drop structures with a silicone-based continuous oil phase (Figure 2.14a) or partially engulfed droplets with a fluorinated continuous oil phase (Figure 2.7). We used two different strategies for formation and breakup of complex emulsions, mainly partially engulfed compound droplets. We utilized a hybrid droplet dispensing strategy combining features of both co-axial and cross-flow geometries (Brkup I, Figure 2.7) as the first method of formation of complex emulsions, and were able to access a variety of IL-Aq compound droplet structures by simply varying the volumetric flow rate of oil delivered to the device. This microfluidic device was consisted of microchannels of 300 μm width, ~155 μm depth and 0.45 m length was. To disintegrate the formation of individual compartments of compound droplets, a second formation method contained two separate T-junction for independent formation of IL and aqueous droplets were used in which the two droplets were coupled later in downstream. Considering the challenge of synchronizing the meeting time of individual IL and Aq droplets, high viscous IL break up as a dispersed phase and setup complexity in terms of number of syringe pumps used we engineered the design (Brkup II, Figure) in a way to regularly form compound droplets with uniform shape and size. In Brkup II scheme aqueous

droplets were formed separately in the microchannel and they digitized a stream of IL to form compound droplets (Figure 2.8). Compound droplets were well-separated from each other, did not coalesce and maintained their original geometric configuration throughout the channel network. This microchannel was 300  $\mu\text{m}$  wide and 118  $\mu\text{m}$  deep.

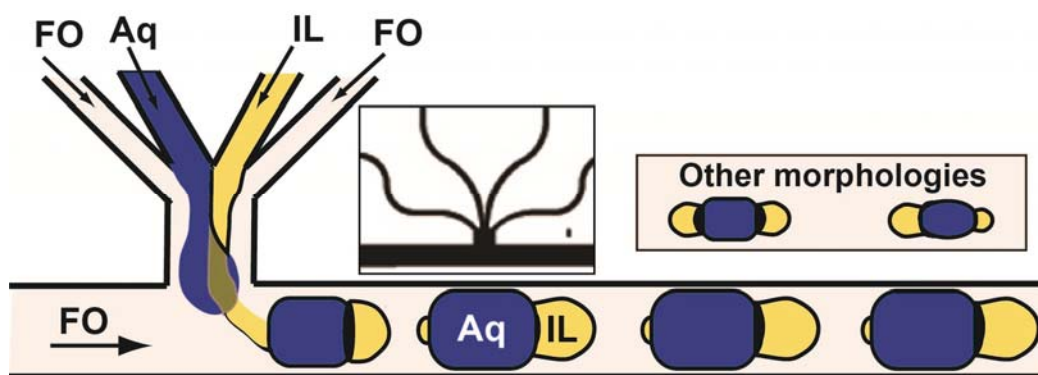


**Figure 2.7.** A schematic illustrating formation and breakup of IL-Aq compound droplets in fluorinated oil (FO) at Brkup I droplet generator. Left inset is the AutoCAD design of the breakup point and the right inset shows schematics of some configurations of compound droplets generated in this work.

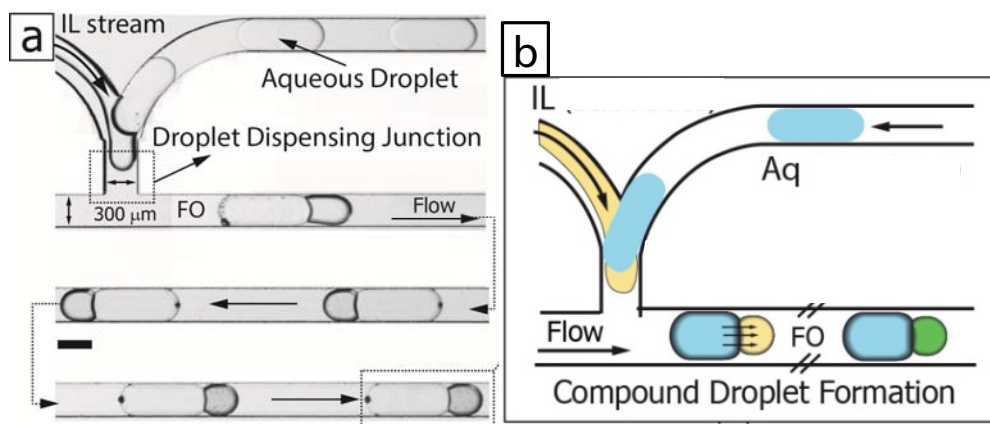


**Figure 2.8.** (a) Stereomicroscopic image, and (b) schematic of compound droplets generation at the Brkup II drop dispensing junction of a PDMS microfluidic device, respectively: merger of preformed aqueous droplet (Aq) with a thin stream of ionic liquid (IL), producing ionic liquid-aqueous (IL-Aq) bi-compartmental compound droplets flowing in continuous phase (fluorinated oil, FO).



### 2.3.4.2 Compound droplets routing

To study the routing (decoupling and splitting) of compound droplets microfluidic devices were designed with two different loop structures combined with the as-mentioned two droplet generators.

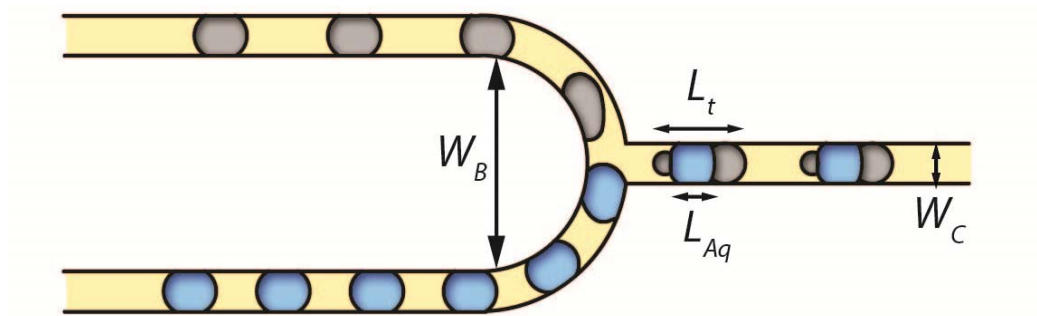


**Figure 2.9.** A schematic of a typical bifurcated junction used in this thesis. Characteristic lengths for both microchannel and compound droplets are also highlighted.

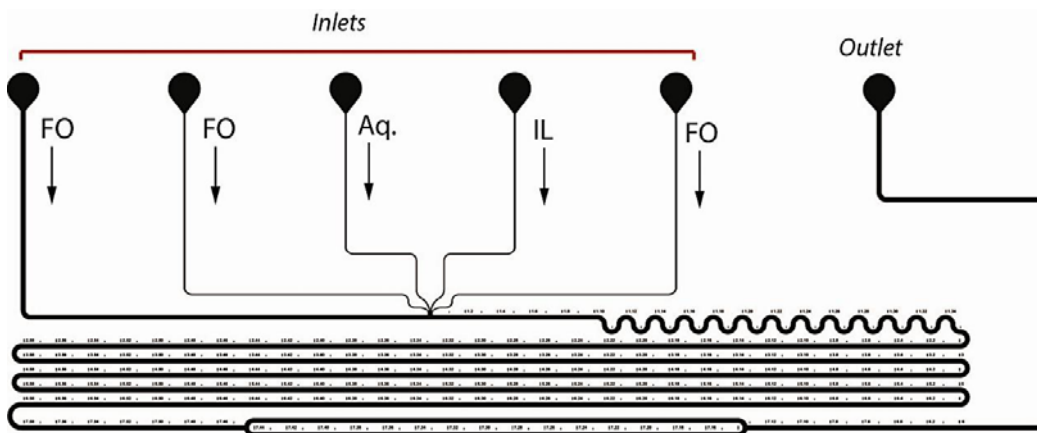


**Figure 2.10.** AutoCAD design of the device containing Brkup I design for compound droplet generation and BIF I bifurcation in downstream of the microdevice. This design was used to study the decoupling of the two compartments of compound droplets versus non-decoupling behavior. Different devices with two different dimensions of bifurcated channels (BIF I and BIF II) were using Brkup I droplet generator.

Figure 2.9 shows typical bifurcation geometry embedded in the downstream of the microdevice. The dimensions of the two bifurcated microchannels are as follows:

Bifurcation I (BIF I) has inner width of 500  $\mu\text{m}$  and length of 31 mm while bifurcation II (BIF II) has inner width of 1800  $\mu\text{m}$  and length of 7 mm. Therefore, combining the two different schemes of bifurcated junctions and compound droplet generators result in the design and fabrication of three different devices used in this thesis: Brkup I-BIF I (Figure 2.10), Brkup I-BIF II, Brkup II-BIF II (Figure 2.11).

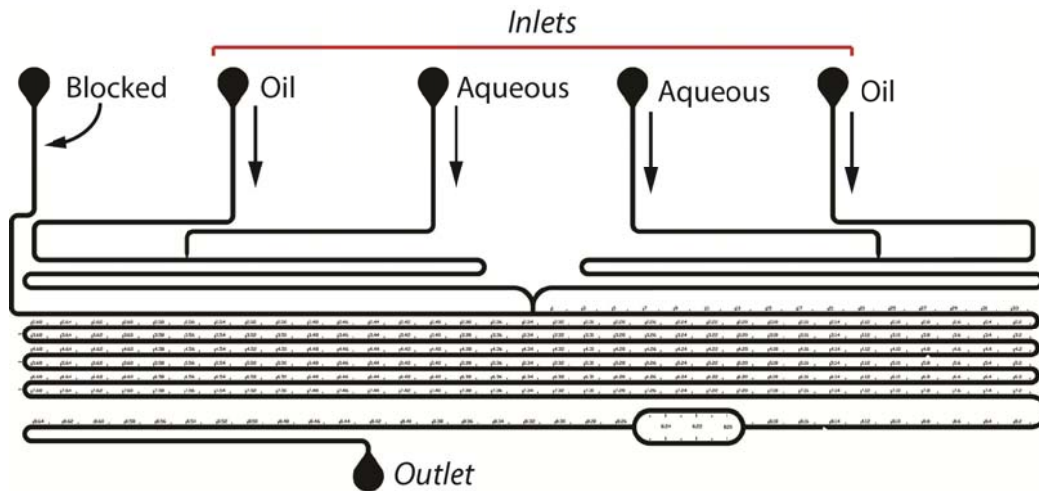


**Figure 2.11.** AutoCAD design of the Brkup II - BIF II device used to study the splitting of IL-aqueous biphasic droplets.

We also used hydrodynamic constrictions as an alternative simple technique to bifurcated microchannel network for passive decoupling of the two compartments of partially engulfed compound droplets. By placing a physical obstacle (a triangular constriction) in the path of a flowing compound droplet, we hydrodynamically perturbed the IL-aqueous interface that ultimately led to complete decoupling of the two segments into individual droplets.



**Figure 2.12.** Constriction geometry at  $l=17.34$  cm of the Brkup II microfluidic device to study the decoupling of IL-Aq compound droplets

### 2.3.5 Device Setup and Operation

Individual syringe pumps (Harvard, PHD 2000) were used to deliver carrier fluid, IL and aqueous solutions to the microfluidic device. A 10:1 (v/v) mixture of perfluorodecalin (PFD) and perfluorooctanol (PFO) was used as the carrier fluid, which will be referred to as fluorinated oil (FO) hereafter, to form partially engulfed compound droplets. To form completely engulfed emulsions the FO was replaced by silicone oil (SO).

#### 2.3.5.1 Formation of complex emulsions of different configurations

The microfluidic device with break up scheme of Brkup I was used to study the flow conditions for the formation of different configurations of IL-Aq compound droplets. Water was used as the aqueous stream. To investigate the flow conditions for generation of different configurations of compound droplets, there are at least three different flow possibilities considering three different immiscible fluids used in experiments. In a simplest strategy, we kept the flow rates of two of the three fluids constant while varying the third one using Brkup I microdevice. Therefore, we first varied the flow rate of FO while IL and water flow rates were constant. To do this, the individual volumetric flow rates of the FO ( $Q_{FO}$ ) streams were varied from 3 to 10  $\mu\text{L}\cdot\text{min}^{-1}$  and that of IL ( $Q_{IL}$ ) and Aq ( $Q_{Aq}$ ) was kept at 3  $\mu\text{L}\cdot\text{min}^{-1}$  (varying carrier fluid FO, Figure 2.17). Next IL volumetric flow rate was varied while the other two were constant. Individual volumetric flow rate of FO was kept constant at 3  $\mu\text{L}\cdot\text{min}^{-1}$  (or total  $Q_{FO}$  of 9  $\mu\text{L}\cdot\text{min}^{-1}$ ) for the next two sets of experiments (varying IL and varying aqueous phase). Aqueous flow rate was kept invariable at either of 1, 2, 3, 5  $\mu\text{L}\cdot\text{min}^{-1}$  flow rate while  $Q_{IL}$  was varied from 0.5 to 15  $\mu\text{L}\cdot\text{min}^{-1}$  for each constant condition (varying IL phase, Figure 2.18). Finally, aqueous (water) flow was changed

keeping the others invariable.  $Q_{IL}$  was remained constant at 0.5, 1, 2 and 3  $\mu\text{L}\cdot\text{min}^{-1}$  and aqueous phase was varied from 1 to 30  $\mu\text{L}\cdot\text{min}^{-1}$  (varying aqueous phase, Figure 2.19). A high speed camera (Basler pi640) mounted on a stereo microscope (Leica MZ 16) was used to capture break up and flow overview snapshots at 100 frames per second.

### **2.3.5.2 Compound droplets decoupling**

***Bifurcation-*** Based on the flow map for various compound droplet configurations, the simplest morphology consisted of one IL compartment and one aqueous compartment was defined for further studies on possibilities for their decoupling. Both bifurcated junctions and hydrodynamic constrictions were used to decouple IL and aqueous compartments of compound droplets. Microfluidic devices with bifurcations (Brkup I- BIF I and Brkup I-BIF II) and with hydrodynamic constriction (Brkup II- constriction) were used to study flow conditions for passive decoupling of compound droplets. Either of FO, IL and aqueous flow rates were varied to access bi-compartmental compound droplets with various size of IL and aqueous droplets ( $L_{Aq}/L_t$  from 0.3 to 0.8, where  $L_{Aq}$  is the length of aqueous droplet and  $L_t$  is the total length of compound droplet) flowing with flow speeds ranging from 3.5 to 18 mm/s. The generated library of compound droplets was then monitored for their behaviour towards decoupling or non-decoupling at bifurcations. A high speed camera (Basler pi640) mounted on a stereo microscope (Leica MZ 16) was used to record formation and decoupling snapshots at 100 frames per second.

***Hydrodynamic Constriction-***Effect of flow speed on compound droplets decoupling at hydrodynamic constrictions was studied using Brkup II- constriction microfluidic

device. To achieve this, defined structure and size compound droplets ( $L_{IL} \sim 300\mu\text{m}$ ,  $L_{Aq} \sim 900\mu\text{m}$ ) were generated and flown through a microfluidic constriction with flow speeds ranging from  $\sim 0.5$  to  $14$  mm/s. A high speed camera (Phantom-Micro eX2) mounted on stereo microscope (Leica MZ 16) was used to capture breakup snapshots at  $1000$  frames per second.

### **2.3.5.3 Compound droplets splitting**

Microfluidic device Brkup II-BIF II was employed to study the splitting of compound droplets at bifurcated junction into two identical-sized daughter compound droplets. Various sizes of compound droplets composed of two compartments of IL and aqueous ( $L_{Aq}/L_t$  from  $0.3$  to  $0.8$ ) were formed and passed through BIFII bifurcation with flow speeds ranging from  $\sim 5.5$  to  $12.7$  mm/s.

## **2.4 Results and Discussion**

### **2.4.1 Formation of Compound Droplet of Different Configurations**

In the work presented in the current and next chapter,  $[\text{EMIM}][\text{NTf}_2]$  is used as the IL phase. We deliver aqueous solutions and an ionic liquid ( $[\text{EMIM}][\text{NTf}_2]$ ) at a microfabricated junction into an immiscible oil to form either completely engulfed drop-in-drop structures (Figure 2.13a and Figure 2.14) with a silicone-based continuous oil phase or partially engulfed droplets (Figure 2.13b-d) with a fluorinated continuous oil phase.

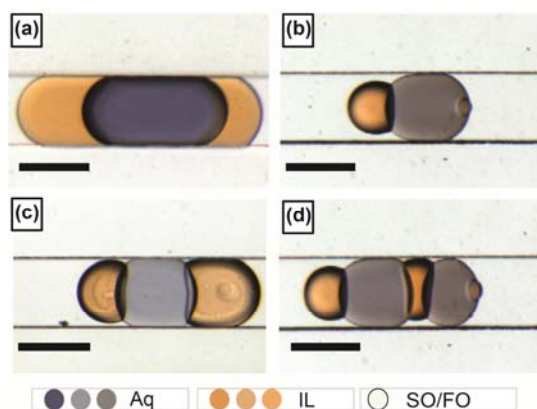


**Figure 2.13.** Stereomicroscope images of compound droplet structures: (a) fully engulfed aqueous-in-ionic liquid compound droplets, formed in a continuous phase of silicone oil, and (b)–(d) partially engulfed aqueous-ionic liquid droplets formed in a fluorinated oil continuous phase. Abbreviations: Aq: aqueous (containing Methyl Blue), IL: ionic liquid (containing Orange II), SO: silicone oil, and FO: fluorinated oil (perfluorodecalin: perfluorooctanol, 10:1 (v/v)).

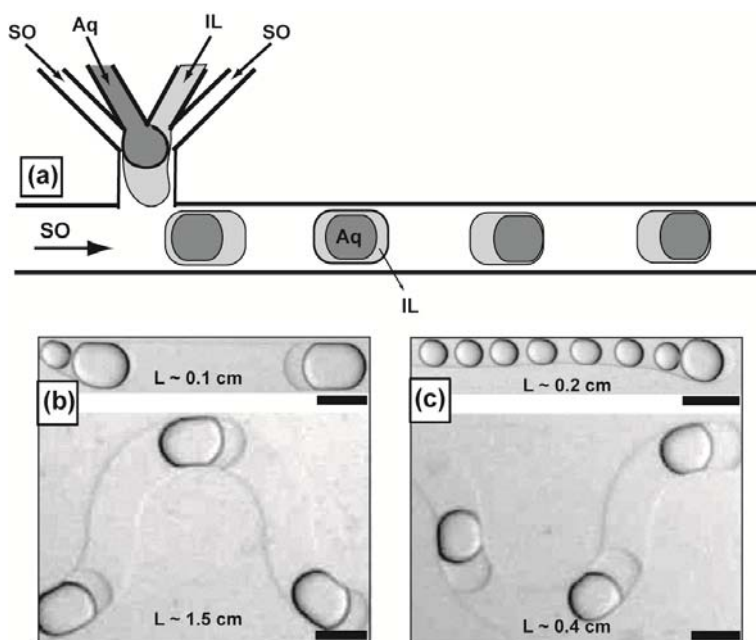


**Figure 2.14.** (a) Schematic illustrating the our method and other droplet morphologies obtained with silicone oil as continuous phase (b) - (c) Stereomicroscopic images of different morphologies of the compound droplets obtained with  $Q_{IL}$  (b)  $2 \mu\text{L}\cdot\text{min}^{-1}$  (c)  $5 \mu\text{L}\cdot\text{min}^{-1}$  at constant  $Q_{Aq}$  ( $5 \mu\text{L}\cdot\text{min}^{-1}$ ) and  $Q_{SO}$  ( $15 \mu\text{L}\cdot\text{min}^{-1}$ ). Scale bars represent  $300 \mu\text{m}$ .

As shown in Figure 2.14, different configurations of aqueous in IL complex emulsions are formed by varying the IL flow rate and keeping the aqueous and silicone oil flow rates constant. There have been several studies on completely engulfed multiple emulsions.<sup>22-23</sup> In this thesis, the particular focus is on partially engulfed compound droplets. Similar water-[BMIM][PF<sub>6</sub>] droplet structures in soybean oil were recently reported by Feng *et al.*,<sup>24</sup> who conducted a parametric study on this three-phase system, and our results are in qualitative agreement.

Two imidazolium and one phosphonium-based ionic liquids were tested for their ability to controllably form IL-aqueous compound droplets. The use of either imidazolium ionic liquid resulted in formation of well-ordered monodisperse IL-aqueous compound droplets (Figure 2.15) while the IL with phosphonium-based cation was disabled to form controlled-shape droplets due to the wettability issues. Compound droplets are not formed in this case as the ionic liquid does not satisfy a key criterion for compound droplet formation and competes with the fluorinated oil in wetting the PDMS microchannel surface.

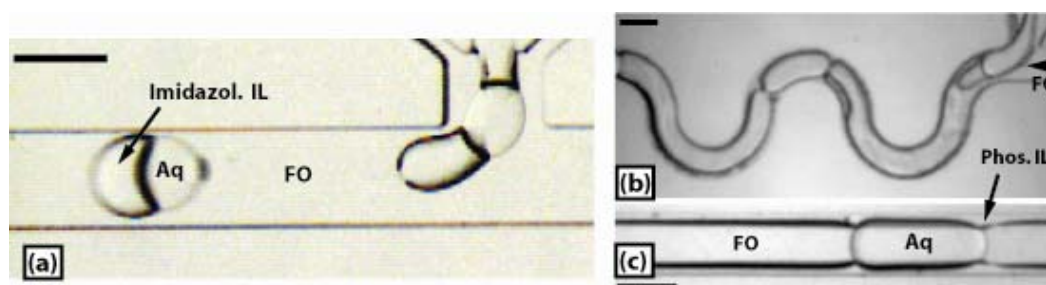


**Figure 2.15.** (a) Aqueous- [MMIM][NTf<sub>2</sub>] (structure provided in Fig. S2) compound droplet generation in fluorinated oil (b, c) Three-phase flow with phosphonium ionic liquid [C<sub>12</sub>(C<sub>4</sub>)<sub>3</sub>P] [NTf<sub>2</sub>]. Compound droplets are not formed in this case as the ionic liquid does not satisfy a key criterion for compound droplet formation; it competes with the fluorinated oil in wetting the PDMS microchannel surface. Scale bars are 300 μm.

The measured equilibrium binary interfacial tensions agreed with the spreading parameter criteria related to partially engulfed structure (section 2.1.2) and confirmed that the observed interface configurations are well predicted by the static considerations. Equilibrium interfacial tensions dictate which fluid-fluid interfaces are possible in general, but the final compound drop structure is governed by the mechanism of breakup of the aqueous and ionic liquid threads entering the microchannel. Herein, we utilize Brkup I droplet dispensing strategy combining features of both co-axial and cross-flow geometries (Figure 2.16), and are able to access a variety of compound droplet structures by simply varying the volumetric flow rate of either of liquid phases delivered to the device (Figure 2.13b-d, Figure 2.17, Figure 2.18 and Figure 2.19). In our dispensing geometry, the aqueous solution is delivered to the microfluidic junction adjacent to the ionic liquid, and the continuous oil phase is delivered both in co-flow and in cross-flow. An analysis of the physics of droplet formation at such hybrid junctions will involve detailed considerations of local flow fields around and within the evolving liquid threads (Figure 2.16). We note here that a key feature of the breakup process is that the ionic liquid thread breaks up later than the aqueous thread due to its higher viscosity ( $\sim 30\times$  that of water), which dampens hydrodynamic instabilities leading to drop formation. As can be seen in Figure 2.16a-i, both aqueous and ionic liquid streams at the breakup junction flow in parallel where the IL thread flows in advance and it pinches in the neck forming a droplet and a smaller satellite drop by the shear stress exerted by the oil flow and aqueous stream pinch off upon breakup.<sup>25</sup> The bigger IL droplet is attached to the front of aqueous droplet while the satellite IL droplet stays in the tail of the aqueous drop. This breakup geometry combines both flow-focusing (Figure 2.16 a-c) and T-junction schemes (Figure 2.16 d-h). Droplet generation in the



locally flow-focusing section and breakup in flow, are the result of the competition of viscous stresses associated with the imposed flow field, and capillary stresses due to surface tension between the two phases.<sup>26</sup> In the flow-focusing design of two phase flow, the shearing comes from the relative magnitude of the co-flowing streams of immiscible liquids. At a channel T-junction, viscous shear stresses from the continuous stream of one liquid overcome surface tension at the liquid-liquid interface and pull off droplets of a second immiscible stream.<sup>27</sup>

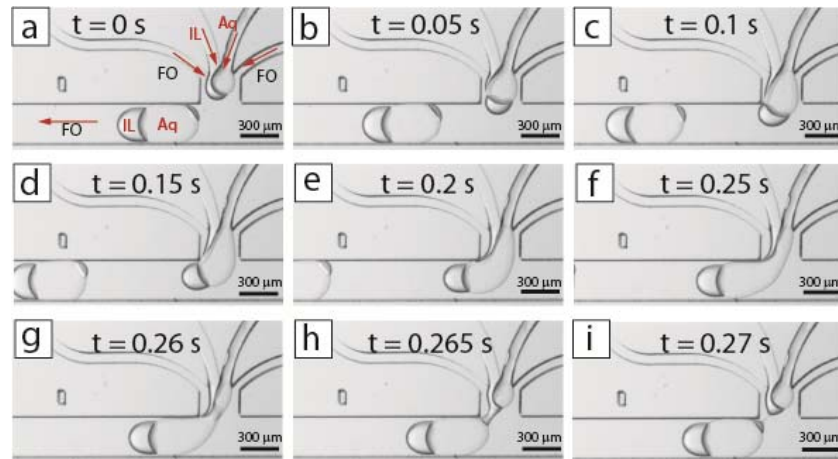


**Figure 2.16.** Stereomicroscopic images of IL-Aq compound droplet break up at Brkup I junction which is operated based on a hybrid of cross-flow and co-axial schemes.

**Varying  $Q_{FO}$**  : By varying the carrier fluid volumetric flow rate ( $Q_{FO}$ ) while  $Q_{Aq}$  and  $Q_{IL}$  are kept invariable different morphologies of compound droplets are formed resulted from different breakup circumstances. As demonstrated in Figure 2.17 a-d, at lower  $Q_{FO}$  the shear forces exerted by the continuous fluid are insufficient to break off the compound droplets right at the T-junction; the breakup point moves downstream leading to the formation of ‘composite’ compound droplets composed of multiple compound droplets connected together (Figure 2.17a). Further increase in  $Q_{FO}$  affects

the position of breakup point and leads to formation of individual compound droplets while the breakup occurs further downstream from the T-junction (Figure 2.17b). In Figure 2.17c,  $Q_{FO}$  is sufficient to generate individual IL-Aq compound droplets right at the T-junction. At higher  $Q_{FO}$ , IL thread is elongated more where it forms single IL droplet in addition to an IL-Aq compound droplet.

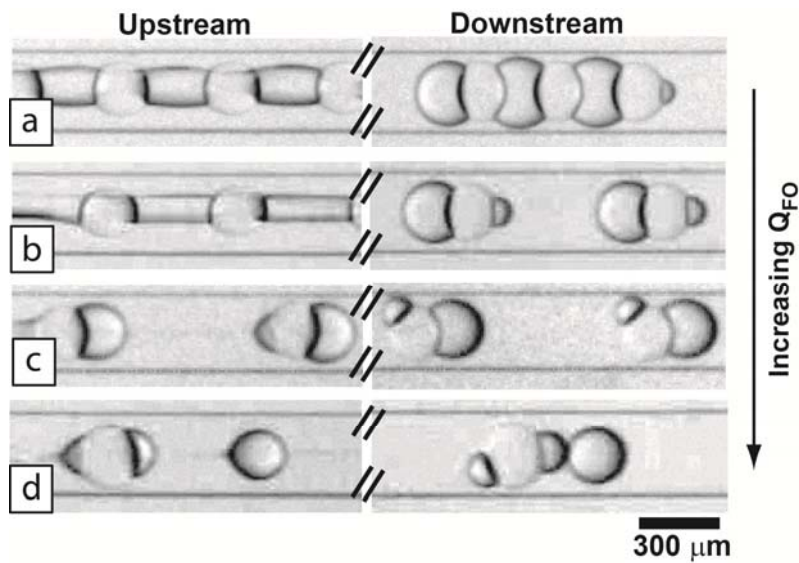


**Figure 2.17.** Stereomicroscopic images of different compound droplet structures obtained with increasing values of  $Q_{FO}$  (a)  $9 \mu\text{L}\cdot\text{min}^{-1}$  (b)  $15 \mu\text{L}\cdot\text{min}^{-1}$  (c)  $21 \mu\text{L}\cdot\text{min}^{-1}$  and (d)  $30 \mu\text{L}\cdot\text{min}^{-1}$  at constant  $Q_{IL}$  and  $Q_{Aq}$  of  $3 \mu\text{L}\cdot\text{min}^{-1}$ .

**Varying  $Q_{IL}$ :** Varying IL volumetric flow rate and keeping  $Q_{FO}$  and  $Q_{Aq}$  constant, lead to the formation of different compound droplet configurations mapped in a graph shown in Figure 2.18. At low  $Q_{IL}$  ( $\leq 2 \mu\text{L}\cdot\text{min}^{-1}$ ), bi-compartmental IL-Aq compound droplets with comparable IL and aqueous compartments are formed with little IL satellite droplet attached to the tail of compound droplet (type A). Increasing  $Q_{IL}$  further ( $3 \mu\text{L}\cdot\text{min}^{-1} \leq Q_{IL} \leq 5 \mu\text{L}\cdot\text{min}^{-1}$ ) causes the breaking off the IL thread into two bigger droplets (instead of a droplet and a satellite drop) at the T-junction and formation of type C compound droplets with two IL attached droplets. At higher

aqueous flow rates while IL flow rate is also sufficiently high, more aqueous droplets are also incorporated in the bigger IL compartment forming train of compound droplets (types B and E). Type E configuration is a chain of partially engulfed aqueous and IL droplets flowing in fluorinated oil along the entire microchannel. Also, at high IL flow rate ( $Q_{IL} > 6 \mu\text{L}\cdot\text{min}^{-1}$ ) and moderate  $Q_{Aq} (\leq 3)$  IL is high enough to form bi-compartmental IL-Aq compound droplets type D in which  $L_{IL} > L_{Aq}$ . At very high IL and aqueous flow rates type F of compound droplets are formed in which IL flows as a continuous stream in the middle of the microchannel while single aqueous droplets are attached to the upper interface of IL stream.

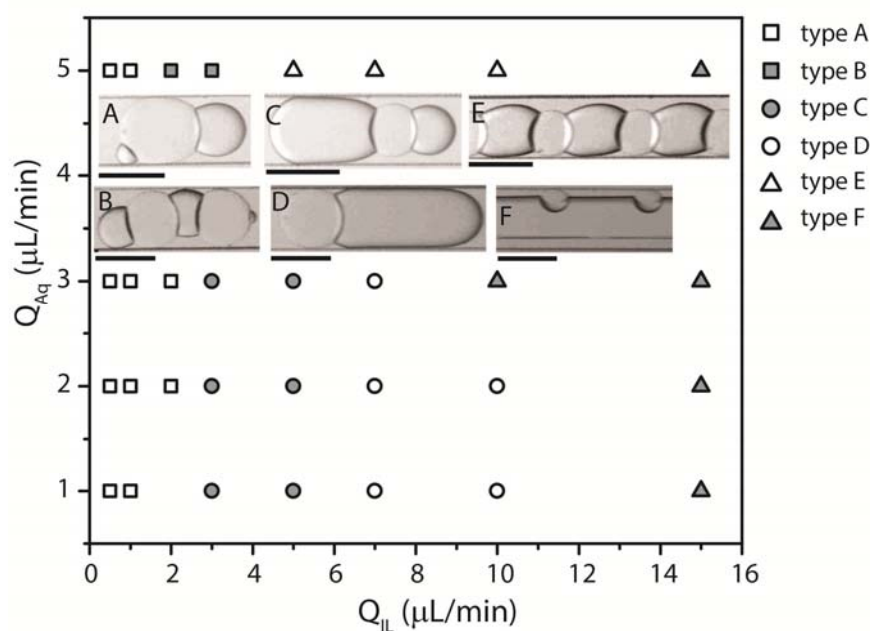


**Figure 2.18.** Flow map of compound droplet configurations when  $Q_{FO}$  remained constant at  $9 \mu\text{L}\cdot\text{min}^{-1}$  and  $Q_{Aq}$  at either of 1, 2, 3 and  $5 \mu\text{L}\cdot\text{min}^{-1}$  while IL flow rate,  $Q_{IL}$ , was varied from 0.5 to  $15 \mu\text{L}\cdot\text{min}^{-1}$ . Scale bars are  $300\mu\text{m}$ .

**Varying  $Q_{Aq}$ :** Various morphologies of IL-Aq compound droplets (Types A, B, C, D) are achieved by manipulating the aqueous flow rate,  $Q_{Aq}$ , and keeping the  $Q_{IL}$  constant (Figure 2.19). At conditions where  $Q_{IL}$  is low ( $\leq 2 \mu\text{L}\cdot\text{min}^{-1}$ ), increasing  $Q_{Aq}$

result in formation of compound droplets of types A and B that transform to type D compound droplets by increasing  $Q_{Aq}$  furthermore. At IL flow rates,  $Q_{IL}$ , higher than  $3 \mu\text{L}\cdot\text{min}^{-1}$ , compound droplets of type C are initially formed which are transformed into type B and later type D configurations by increasing  $Q_{Aq}$ .

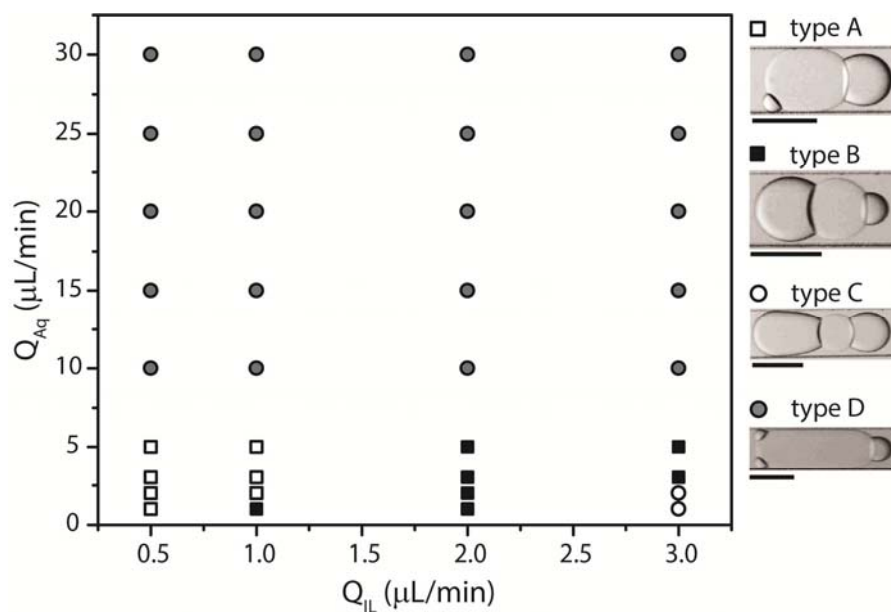


**Figure 2.19.** Flow map of compound droplet configurations when IL phase flow rate,  $Q_{IL}$ , was remained constant at either of 0.5, 1, 2, and  $3 \mu\text{L}\cdot\text{min}^{-1}$  while aqueous flow rate,  $Q_{Aq}$ , is varied from 1 to  $30 \mu\text{L}\cdot\text{min}^{-1}$  ( $Q_{FO}$  was invariable at  $9 \mu\text{L}\cdot\text{min}^{-1}$ ). Scale bars are  $300\mu\text{m}$ .

All the observed IL-Aq compound droplets of various configurations are mapped in the above Figures 2.17 - 2.19 as flow maps and are useful guides for the generation of desired compound droplets.

## 2.4.2 Compound Droplets Decoupling

Microfluidic technology offers capabilities for the precise handling of small fluid volumes dispersed as compound droplets. To fully exploit this potential requires simultaneous decoupling of the constituent compartments. We demonstrate two

methods for passively breaking IL-Aq compound drops into two individual IL and aqueous drops using pressure-driven flow in simple microfluidic configurations: (i) a Hydrodynamic constriction/obstacle and (ii) bifurcated microchannels.

#### **2.4.2.1 Decoupling by hydrodynamic constriction**

After the demonstration of IL-aqueous compound droplet formation, we also present complete and passive detachment of the two compartments at a hydrodynamic obstruction within the microfluidic channel (Brkup II-constriction device). The decoupling of compound droplets paves the way for complex iterative chemical processes. By placing a physical obstacle (a triangular constriction) in the path of a flowing compound droplet, we hydrodynamically perturb the IL-aqueous interface that ultimately leads to complete decoupling of the two segments into individual droplets. The decoupling process occurs in two stages, as seen in the time-stamped stereomicroscope snapshots in Figure 2.20a. The IL segment is squeezed during its passage through the constriction, leading to a rapid decrease in the IL-aqueous interfacial zone, until the IL in the immediate vicinity of the aqueous segment is reduced to a thin, unstable filament that subsequently disengages entirely from the aqueous segment. Further, it is interesting to note that for a given initial size of the compound droplet, this decoupling phenomenon is speed-dependent, and only occurs above a certain critical speed (see Figure 2.20b for an example of a compound droplet that does not decouple).

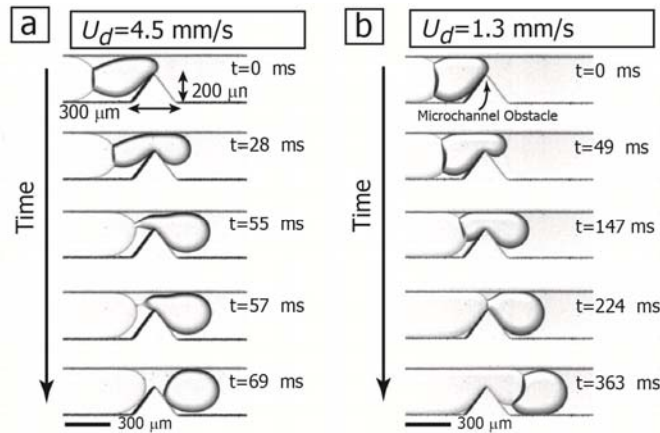


**Figure 2.20.** Stereomicroscope images of: a) compound droplet decoupling at an obstacle in the flow path ( $U = 4.5 \text{ mm/s}$ ), b) compound droplet passing by the obstacle at lower flow speed ( $U = 1.3 \text{ mm/s}$ ), where no decoupling occurs.

For instance, at fixed initial sizes of the two compartments composing the compound droplet ( $L_{IL} \sim 300 \mu\text{m}$ ,  $L_{Aq} \sim 900 \mu\text{m}$ ), the critical flow speed  $U_C$  above which the decoupling of IL segment takes place is  $\sim 2 \text{ mm/s}$  (Figure 2.21). The existence of a critical flow speed for decoupling is not entirely unexpected, and can be understood in terms of the minimal (flow dependent) shear work required to separate the segments of the compound droplet into their individual components.

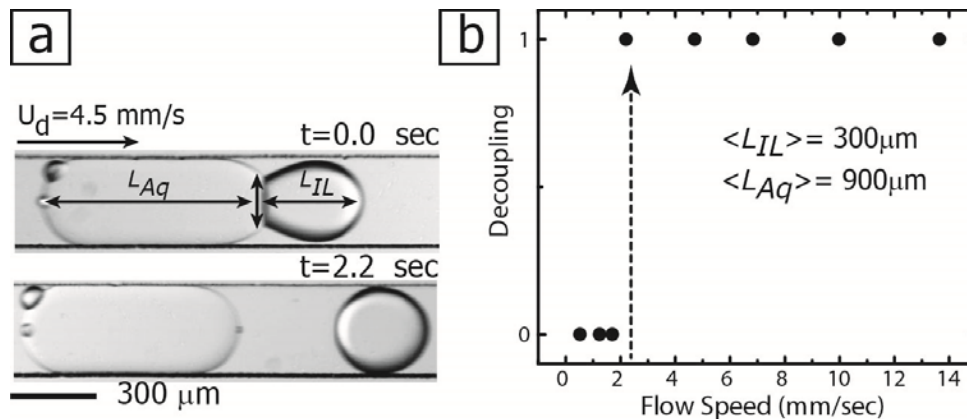


**Figure 2.21.** (a) Morphology of a compound droplet (i) before, and (ii) after the decoupling process. b) Plot of occurrence of decoupling vs the flow speed (for fixed size of compound droplet compartments), i.e., '1' and '0' indicate successful and no decoupling respectively. A critical flow speed ( $\sim 2 \text{ mm/s}$ ) for the decoupling phenomenon is observed.

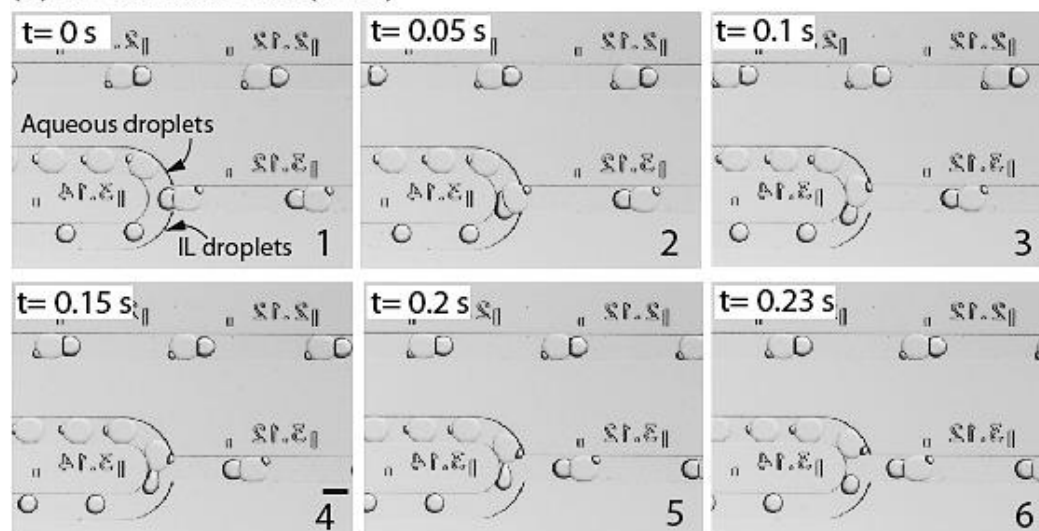
### 2.4.2.2 Decoupling by bifurcated junctions

A compound droplet arriving at a  $T$  intersection, if it does not decouple or split into two daughter compound droplets, flows into the branch characterized by lower resistance to flow. Since the presence of slugs in microchannels increases the resistance to flow, there is a feedback between choices of successive droplets. This feedback combined with the amplification of a slight difference in resistances of the two diverging branches to a left/right choice of the trajectory make for complicated dynamics of compound droplets at bifurcated junctions. In the study presented in this thesis, we focus on flow conditions result in decoupling of compound droplets into the constituent compartments. We utilize Brkup I-BIF I and Brkup I-BIF II geometries (Figure 2.22) to study the decoupling event and categorize the flow behavior into two groups of decoupling (D) and no decoupling (ND) as plotted in Figure 2.23. The latter category (ND) contains both irregular and regular sorting flow behaviors; however, the sorting phenomenon is not the scope of this study and is grouped with conditions that compound droplets do not decouple in a regular basis.

The detachment mechanism of the two partially engulfed droplets can be better understood by the simulation to the well-studied case in which a liquid droplet is adhered to a solid surface and deforms in the presence of shear flow. Similar to the wetting droplet on the solid surface, IL droplet can be assumed to wet the aqueous droplet (as it is appeared from the contact lines, Figure 2.2). When a drop wets an immersed solid surface, it results in the formation of a contact angle the value of which depends on the force balance between the interfacial tensions involved.<sup>28</sup> The adhesion force is related to the dynamic contact angles and the interfacial tension ( $\sigma$ ) between the drop and the surrounding fluid. Similarly, the detachment of a drop from

liquid-liquid interface is not predictable without a complete modeling of the dewetting dynamics, accounting for the dynamic of contact angles and fluid velocity in the vicinity of the droplet entering bifurcated intersection, the formation of a continuous phase between two droplets and the drop-drop interface deformation.<sup>29</sup>

(a) BIFURCATION I (BIF I)



(b) BIFURCATION II (BIF II)

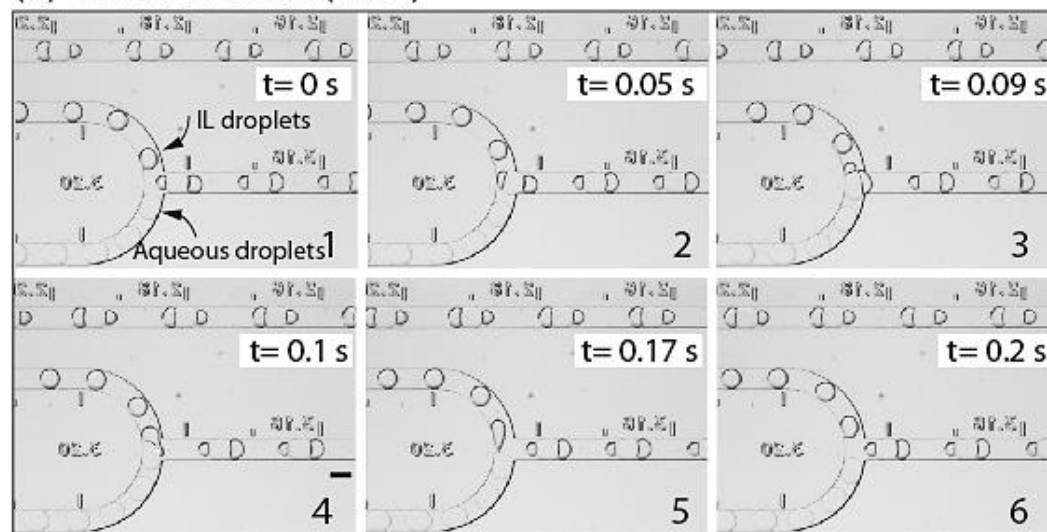


**Figure 2.22.** Time-stamped stereomicroscope images of compound droplet decoupling at two different bifurcations geometries; a) BIF I and b) BIF II. Compound droplets are formed using Brkup I droplet formation scheme. All scale bars are 300  $\mu\text{m}$ .



Herein, we plot our observations in terms of decoupling/non-decoupling events in a way to get insight over the critical fluid conditions to access the decoupling regime. Figure 2.22 illustrates the time-stamped images of compound droplets decouple at bifurcated junction at both BIF I (Figure 2.22a) and BIF II (Figure 2.22b) geometries.

Plots of Figure 2.23 demonstrate  $\text{Log } Ca$  versus dimensionless characteristic length scales which is  $(L_{aq}/L_t)(W_C/W_B)$  in Figure 2.23a and  $(L_{aq}/L_t)$  in Figure 2.23b, where  $L_{aq}$  is the length of aqueous droplet,  $L_t$  is the total length of the compound droplet,  $W_C$  is the width of the microchannel and  $W_B$  is the width of the loop (see Figure 2.9). Capillary number,  $Ca$ , is  $\mu v/\sigma$ , where  $\mu$  is the viscosity of the continuous fluid ( $\mu_{FO}=5.1$  mPa.s),  $v$  is the velocity of compound droplets prior to entering the bifurcation area (m/s),  $\sigma$  is the interfacial tension between the continuous fluid and the dispersed fluid (either of  $\sigma_{FO-IL}$  or  $\sigma_{FO-Aq}$ , mN/m). We used the interfacial tension value between FO and aqueous phase for interfacial tension to get the capillary number. In the plot illustrated in Figure 2.23a, in addition to the characteristic length of compound droplet, the geometry of the bifurcation is taken into consideration while in Figure 2.23b, the characteristic length of compound droplet is merely considered.

Considering the geometry of the bifurcation, results in two separate zones; one belongs to BIF I ( $\circ\bullet$ ) and the other to BIF II ( $\blacksquare$ ) geometry. Decoupling mainly occurs when  $(L_{aq}/L_t)(W_C/W_B) < 0.1$  at BIF I and when this term is  $< 0.4$  for BIF II. Moreover, Figure 2.23b shows that the majority of decoupling phenomena take place at  $L_{aq}/L_t < 0.6$  for both BIF I and BIF II independent of the device geometry. Therefore, when the length of aqueous compartment is less than 0.6 of the total compound droplet compound droplets decouple independent of the flow speed.

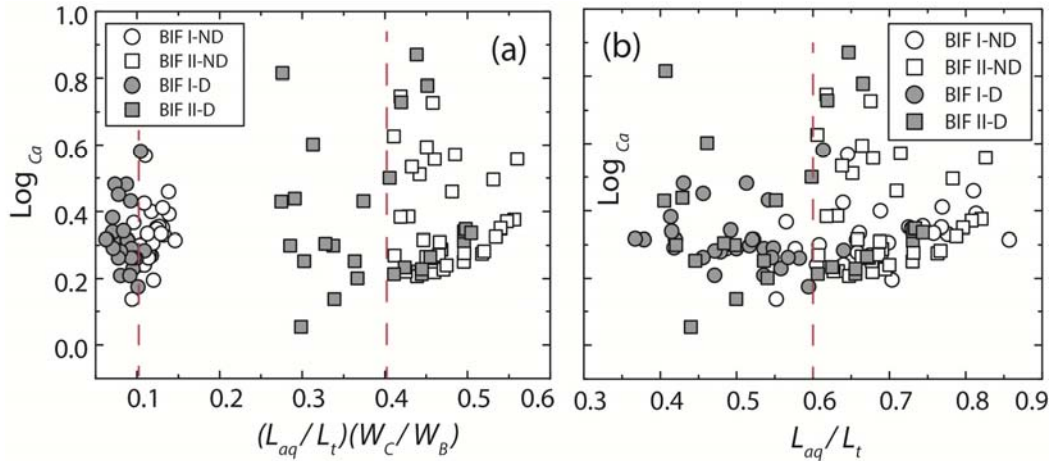


**Figure 2.23.** Graphs of  $Ca$  vs non-dimensional characteristic length scales; a)  $\text{Log } Ca$  vs  $(L_{aq}/L_t)(W_C/W_B)$  b)  $\text{Log } Ca$  vs  $(L_{aq}/L_t)$ . Filled markers are related to complete decoupling marked as D and unfilled markers show non-decoupling designated as ND.

### 2.4.3 Compound Droplet Splitting

Bifurcated junctions are useful means to not only decouple compound droplets but also to facilitate the splitting of compound droplets into precisely controlled size daughter drops (Figure 2.24). The splitting is investigated using Brkup II- BIF II geometry. As can be seen in graph shown in Figure 2.25

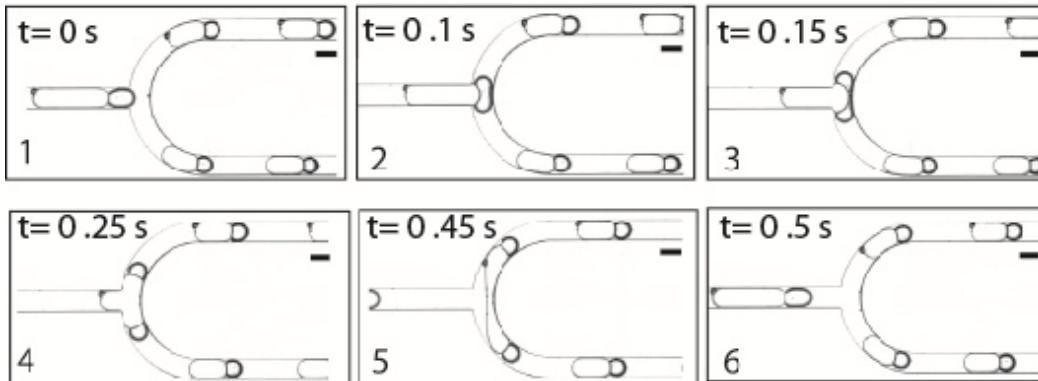


**Figure 2.24.** Time-stamped images of a compound droplet splitting into two equal-sized daughter drops at bifurcated intersection. All scale bars are  $300 \mu\text{m}$ .

Interestingly, as Figure 2.25 demonstrates splitting occurs when  $L_{aq}$  is more than 0.6 of the total length of the compound droplet independent of the droplets speed prior to entering the bifurcation area. Below this limit mainly decoupling of compound droplets take place, which is in agreement with our result for the decoupling studies in Figure 2.23b.

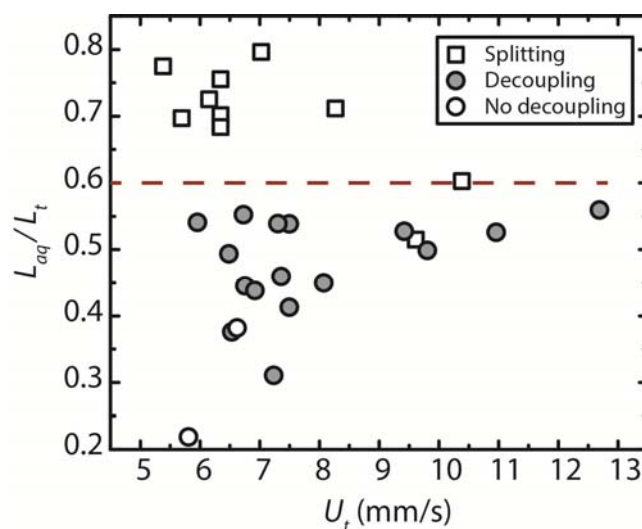


**Figure 2.25.** A graph of  $L_{aq}/L_t$  vs  $U_t$ , illustrating splitting ( $\square$ ), decoupling ( $\bullet$ ) and non-decoupling ( $\circ$ ) domains.

## 2.5 Summary

We presented the formation, decoupling and splitting of IL-aqueous compound droplets. Two different droplet-dispensing schemes, Brkup I and Brkup II were utilized to generate precisely controlled compound droplets. Both geometries were useful in generation of controlled compound droplets; however, Brkup II is limited in manipulating the range of flow rates for formation of various size of compound droplets due to the challenge in synchronizing the droplet formation in both T-junctions and the meeting point. Geometrically mediated decoupling of compound droplets was demonstrated using both hydrodynamic constriction and bifurcated

junctions. Decoupling the two compartments at a hydrodynamic obstacle was shown to be speed dependent while at bifurcated networks this event was observed to be speed independent and relates more on the characteristic length of compound droplets. Bifurcations also assisted the splitting of the compound droplets into equal-size daughter drops and this event was also observed to be drop length dependent rather than speed dependent.

Besides these preliminary observations there is a need, especially in compound drop routing, to conduct modeling and simulation studies for better understanding the dominant forces involved in decoupling and splitting events. Though the dynamics underlying these phenomena are complex, our experimental system may serve as a potential tool to systematically explore the physics of such systems and validate theoretical/computational analyses.

## 2.6 References

1. Anna, S. L.; Mayer, H. C., Microscale tipstreaming in a microfluidic flow focusing device. *Physics of Fluids* **2006**, *18* (12), 121512-13.
2. Ajaev, V. S.; Homsy, G. M., Modeling Shapes and Dynamics of Confined Bubbles. *Annu. Rev. Fluid Mech.* **2006**, *38* (1), 277-307.
3. Torza, S.; Mason, S. G., Coalescence of 2 immiscible liquid drops. *Science* **1969**, *163* (3869), 813-814.
4. Torza, S.; Mason, S. G., Three-phase interactions in shear and electrical fields. *Journal of Colloid and Interface Science* **1970**, *33* (1), 67-83.
5. Guzowski, J.; Korczyk, P. M.; Jakiela, S.; Garstecki, P., The structure and stability of multiple micro-droplets. *Soft Matter* **2012**, *8* (27), 7269-7278.
6. Young, T., An essay on the cohesion of fluids. *Philosophical Transactions of the Royal Society of London* **1805**, *95*, 65-87.

7. Stone, H. A.; Stroock, A. D.; Ajdari, A., ENGINEERING FLOWS IN SMALL DEVICES. *Annu. Rev. Fluid Mech.* **2004**, *36* (1), 381-411.
8. Taylor, G. I., Low Reynolds Number Flows. *National Committee for Fluid Mechanics Films (Education Development Center)* 1966.
9. Bretherton, F. P., The motion of long bubbles in tubes. *Journal of Fluid Mechanics* **1961**, *10* (02), 166-188.
10. Link, D. R.; Anna, S. L.; Weitz, D. A.; Stone, H. A., Geometrically Mediated Breakup of Drops in Microfluidic Devices. *Physical Review Letters* **2004**, *92* (5), 054503.
11. Shim, J.-u.; Cristobal, G.; Link, D. R.; Thorsen, T.; Jia, Y.; Piattelli, K.; Fraden, S., Control and measurement of the phase behavior of aqueous solutions using microfluidics. *Journal of the American Chemical Society* **2007**, *129* (28), 8825-8835.
12. Jousse, F.; Farr, R.; Link, D. R.; Fuerstman, M. J.; Garstecki, P., Bifurcation of droplet flows within capillaries. *Physical Review E* **2006**, *74* (3), 036311.
13. Fuerstman, M. J.; Garstecki, P.; Whitesides, G. M., Coding/decoding and reversibility of droplet trains in microfluidic networks. *Science* **2007**, *315* (5813), 828-832.
14. Garstecki, P.; Fuerstman, M. J.; Whitesides, G. M., Nonlinear dynamics of a flow-focusing bubble generator: an inverted dripping faucet. *Physical Review Letters* **2005**, *94* (23), 234502.
15. Engl, W.; Roche, M.; Colin, A.; Panizza, P.; Ajdari, A., Droplet traffic at a simple junction at low capillary numbers. *Physical Review Letters* **2005**, *95* (20), 208304.
16. Wong, H.; Radke, C. J.; Morris, S., The motion of long bubbles in polygonal capillaries. Part 2. Drag, fluid pressure and fluid flow. *Journal of Fluid Mechanics* **1995**, *292*, 95-110.
17. Hodges, S. R.; Jensen, O. E.; Rallison, J. M., The motion of a viscous drop through a cylindrical tube. *Journal of Fluid Mechanics* **2004**, *501*, 279-301.
18. Leshansky, A. M.; Pismen, L. M., Breakup of drops in a microfluidic T junction. *Physics of Fluids* **2009**, *21* (2), 023303-6.
19. Bonhote, P.; Dias, A.-P.; Papageorgiou, N.; Kalyanasundaram, K.; Gratzel, M., Hydrophobic, Highly Conductive Ambient-Temperature Molten Salts. *Inorganic Chemistry* **1996**, *35* (5), 1168-1178.
20. Fröba, A. P.; Kremer, H.; Leipertz, A., Density, Refractive Index, Interfacial Tension, and Viscosity of Ionic Liquids [EMIM][EtSO<sub>4</sub>], [EMIM][NTf<sub>2</sub>], [EMIM][N(CN)<sub>2</sub>], and [OMA][NTf<sub>2</sub>] in Dependence on Temperature at Atmospheric Pressure. *The Journal of Physical Chemistry B* **2008**, *112* (39), 12420-12430.

21. Xia, Y.; Whitesides, G. M., Soft lithography. *Annual Review of Materials Science* **1998**, *28* (1), 153-184.
22. Shah, R. K.; Shum, H. C.; Rowat, A. C.; Lee, D.; Agresti, J. J.; Utada, A. S.; Chu, L.-Y.; Kim, J.-W.; Fernandez-Nieves, A.; Martinez, C. J.; Weitz, D. A., Designer emulsions using microfluidics. *Materials Today* **2008**, *11* (4), 18-27.
23. Chu, L. Y.; Utada, A. S.; Shah, R. K.; Kim, J. W.; Weitz, D. A., Controllable monodisperse multiple emulsions. *Angewandte Chemie International Edition* **2007**, *46* (47), 8970-8974.
24. Feng, X.; Yi, Y.; Yu, X.; Pang, D.-W.; Zhang, Z.-L., Generation of water-ionic liquid droplet pairs in soybean oil on microfluidic chip. *Lab on a Chip* **2010**, *10* (3), 313-319.
25. Shi, X.; Brenner, M. P.; Nagel, S. R., A cascade of structure in a drop falling from a faucet. *Science-New York then Washington-* **1994**, 219-219.
26. Cristini, V.; Tan, Y.-C., Theory and numerical simulation of droplet dynamics in complex flows-a review. *Lab on a Chip* **2004**, *4* (4), 257-264.
27. Anna, S. L.; Mayer, H. C., Microscale tipstreaming in a microfluidic flow focusing device. *Physics of Fluids* **2006**, *18* (12), 121512-13.
28. Mate, A.; Masbernat, O.; Gourdon, C., Detachment of a drop from an internal wall in a pulsed liquid - liquid column. **2000**, *55*, 2073-2088.
29. Basu, S.; Nandakumar, K.; Masliyah, J. H., A Model for Detachment of a Partially Wetting Drop from a Solid Surface by Shear Flow. *Journal of Colloid and Interface Science* **1997**, (190), 253-257.

# Chapter 3

## Ionic Liquid-Aqueous Microdroplets for Biphase Chemical Analysis and Separations

Purification of chemical and biochemical components are of major importance as the final product concentration and separation of the undesired materials are very critical, specifically for the ones directly used for health-care applications. Liquid-liquid extraction (LLE) is one of the simplest, most popular and least expensive methods for isolation, separation and purification of organic compounds, and involves the selective partitioning of molecules between two immiscible fluid phases brought in contact with each other.<sup>1</sup> LLE can be applied for the purification of biomolecules such as proteins, amino acids, peptides, and organic molecules.<sup>2</sup> Besides this, other separation methods such as capillary electrophoresis (CE) and chromatographic methods are used, all of which adopt the same operating principles as batch systems. Continuous electrophoresis is least frequently used in large scales due to high amount of heat generated from Joule heating, and low resolution caused by convective and electro-osmotic dispersion. Continuous chromatographic methods are the most commonly used due to their high resolution. However, chromatographic methods suffer from low throughput, diffusion limitations due to pore size limitation of adsorptive beads, high pressure drop due to clogging over long time, and are capital and labour intensive while they are not easily scaled up.<sup>3</sup>

Traditionally, LLE involves an organic solvent and aqueous solution as the two immiscible phases.<sup>4</sup> Volatility, high level of toxicity, flammability of most organic

compounds (VOCs) used in LLE pose environmental and safety concerns, especially in pharmaceutical industry,<sup>2, 5-7</sup> which have in recent years prompted a search for greener alternatives to organic solvents. The manifest need for safe, and environmentally benign separation processes to overcome the aforementioned problems with organic solvents has increasingly led to the development of green separation techniques using ionic liquids and other non-classical solvents. Ionic liquids (ILs), liquid salts of organic cations and organic/inorganic anions, have attracted enormous attention due to their unique physical and chemical characteristics.<sup>8-9</sup> Fluid properties such as viscosity, density, hydrophobicity and even chemical reactivity can be predictably altered and tuned by appropriately selecting the cations and anions.<sup>10-11</sup> They can dissolve inorganics, organics and organometallics alike, thus triggering extensive research in their utilization as reaction media.<sup>12-13</sup> Rogers *et al.* demonstrated for the first time that, apart from serving as green reaction media, ionic liquids could be used as an extracting phase to recover organic acids from aqueous solutions.<sup>14</sup> This work subsequently triggered exploratory research into the potential of ionic liquids as an extracting phase for a wide range of separation targets: double stranded DNA, separation of aromatics from aliphatics, amino acids, metal ions from aqueous mixtures, gold nanoparticles and cationic CdTe quantum dots.<sup>15</sup> ILs can interact with solute molecules through polar, ionic, and  $\pi$ - $\pi$  interactions, dispersion, ionic exchange, and hydrogen bonding; all of these interactions can be manipulated to employ ILs as selective extractors based on differential interactions with solutes in a mixture. For example, selective separation of tocopherol homologues has been demonstrated where hydrogen bonding by the IL was employed as selection guide to preferentially separate one of the homologues.<sup>16</sup> Even slight differences in hydrophobicity and H-bonding ability of closely related



antibiotics have been leveraged for preferential separation/extraction of one from the mixture by exploiting the hydrophobic nature of IL.<sup>17</sup>

Microfluidics allows continuous injection of samples, scaling up through scaling out, integration with upstream and downstream analysis steps and real-time feedback. Therefore, they possess great potential to be applied in micro total analysis systems (microTAS). In a microchannel, separation can be effected simply by passive flow methods, where samples are guided to follow a multiphase droplet-based flow, in which diffusion is accelerated by chaotic advection and internal recirculation motions. In addition, a droplet of water suspended in oil within a microchannel occupies merely nanoliter volume, yet can offer a vast 'sea of applications' encompassing chemical and materials syntheses, high-throughput screening, analytics and biological assays.<sup>18-24</sup> Highly monodisperse aqueous droplets can be reliably generated at up to kilohertz frequencies by injecting an aqueous reagent stream into an immiscible oil within microfluidic T-junction or flow-focusing geometries.<sup>25</sup> Each droplet may be considered to be a self-contained entity flowing in the carrier fluid. All the chemical or biological events are compartmentalized within the boundary of a droplet, which is effectively a nanoliter-sized 'test-tube'. Apart from library synthesis, high-throughput screening is possible by interrogating and analyzing individual droplets using optical or other analytical means. Typical droplet-based compartmentalization of a chemical or biological transformation requires the prevention of (i) droplet coalescence and (ii) any molecular transport (chemical cross-talk) amongst the droplets and between droplets and the carrier oil phase. Generally, use of surfactants inhibits coalescence, while chemical nature of the oil phase (polarity-mismatch) restricts the efflux of reagent or product from a droplet to the surrounding continuous phase. A combination

of surfactant and additive<sup>26</sup> or chemical modification of solutes' hydrophilicity<sup>27</sup> can also improve their confinement within the aqueous droplet.

Although a majority of droplet-based microfluidics applications focus on complete chemical isolation of the droplets from the surroundings, there is growing interest in another regime where a droplet is deliberately made to interact with the continuous phase or a neighboring droplet. This provides more flexibility to manipulate the content and chemistry of the droplet by 'outside' intervention, and is contrary to the typical requirements of compartmentalization noted above. For example, designer surfactants can dictate and control biomolecule adsorption<sup>28-29</sup> at the oil-water interface of an aqueous droplet or can catalyze a chemical reaction<sup>30</sup> inside the aqueous droplets. Mass transfer between continuous phase and droplet or droplet-to-droplet may be employed in on-chip liquid-liquid extraction.<sup>31-33</sup> Huck and co-workers reported mass transport between two static aqueous droplets via a surfactant bilayer to initiate an enzymatic reaction.<sup>34</sup> Ismagilov and co-workers have demonstrated that slow diffusion of water from a droplet of protein solution to another droplet containing brine via a fluorinated oil can controllably create supersaturation and lead to crystallization of the protein.<sup>35</sup> More recently this group showed that a reaction product from one droplet can produce a colorimetric signal in another reporter droplet by similar diffusive migration through the continuous oil phase.<sup>36</sup>

Earlier in Chapter 2, we demonstrated a microfluidic method in which an ionic liquid (IL) is introduced as a third fluid along with aqueous (Aq) and oil phases to generate IL-Aq bicompartamental droplets with the aqueous compartment partially or fully engulfed by the IL compartment. In the partially engulfed droplet configuration, denoted as a 'compound droplet', the ionic liquid segment not only protects nearby

aqueous droplets from coalescence,<sup>37</sup> but can also initiate and control chemical cross-talk with the aqueous compartment. In this configuration more direct and reliable intra-droplet chemical communication, which does not rely on transport through the continuous phase, is possible. This task-specific and tunable nature of ionic liquids prompted us to examine their applicability as chemically interacting fluid-components in our compound droplet system.

In this chapter, we first demonstrate IL-aqueous compound droplets flowing in a third inert fluid for on-drop chemical separations where IL is an active compartment in liquid-liquid extraction. A continuous separation method is developed that, in principle, is capable of being integrated with analysis tools. Herein, the liquid-liquid extraction of representative organic solutes using IL-based compound droplets is presented. The ultimate goal of this section is to exploit ionic liquids as designer solvents in droplet microfluidic systems, thus developing a new tool for the miniaturized separation of chemical and biochemical components from mixtures. We also, demonstrate analytical applications of IL-aqueous compound droplets in particularly pH sensing and biphasic reactive sensing and analysis the next.

## **3.1 Method Development**

### **3.1.1 On-drop Chemical Separations**

In the second part of this chapter, we focus our attention on droplet-based microfluidics where the flowing droplets are composed of two (or more) immiscible fluid phases (Figure 3.1). Such 'compound' droplets have been reported in diverse contexts, from contact heat exchange to cellular phagocytosis<sup>38</sup> and blood oxygenation.<sup>39</sup> More recently, compound droplets have been of significant interest in

the formation of tailored multiple emulsions and also in the fabrication of highly structured, spatially anisotropic polymeric beads.<sup>40-43</sup> Biphasic separations in microdevices can also be improved by digitizing the extracting phase in concert with aqueous droplets. By doing so, the direct contact of the extracted molecules with microchannel walls would be prevented. This minimizes the sedimentation and precipitation of molecules on the PDMS wall as droplets are surrounded by a layer of oil. Herein, we demonstrate the selective and rapid extraction of an organic molecule from a binary aqueous mixture into the ionic liquid compartment of partially engulfed compound droplets in an inert third liquid travelling along the microchannel. Ionic liquids<sup>44</sup> are selected as functional fluids whose chemical and physical properties can be tailored to be task-specific.

This novel proof-of-concept demonstration opens up a way for on-drop separations of various molecules by smart attachment of IL drops containing different extractors. Further development of such system can lead to *on-drop* chemical analysis involving selective chemical separation and detection.



**Figure 3.1.** Selective and rapid extraction of OrII (orange II) into IL compartment from a mixture with MeB (Methyl Blue) as compound droplet translates along the microchannel.

### 3.1.2 Dynamic pH Sensing

Typically, pH measurements in microfluidic devices are carried out either by electrochemical means with electrodes whose fabrication involves complex

lithographic steps<sup>45</sup> or by optical means using dissolved pH-sensitive dyes.<sup>46</sup> The latter method, though simple and effective, is not viable in cases where contamination of target solution by the indicator dye is not desired. Alternative approaches to alleviate this problem have been demonstrated, such as coating the walls of the microchannel with the indicator dye<sup>47</sup> or suspending functionalized beads in the target solution.<sup>48</sup> We demonstrate a simple example of on-drop sensing where the ionic liquid in the compound droplet serves as a chemical sensor attached to the aqueous droplet. An indicator-doped ionic liquid is used to dynamically measure the pH of the aqueous phase (Figure 3.2).

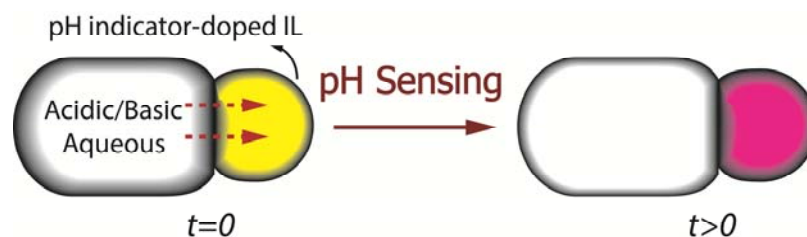


**Figure 3.2.** *On-drop dynamic pH sensing:* pH indicator (thymol blue)-doped IL compartment of the compound droplet changes color from neutral color to acidic/basic color as the IL becomes progressively acidic/basic by mass transfer of acid/base from the aqueous phase.

### 3.1.3 Biphasic Reactive Sensing

We also report a droplet-based chemical analysis method possessing some intriguing features: (i) the unique physical and chemical characteristics of IL enables analyte (metal ion) to partition only between aqueous and ionic liquid compartments and not to the carrier fluorinated oil, (ii) analyte catalyzes the transformation of a substrate into a fluorescence emitting product in the ionic liquid compartment and (iii) both the substrate and fluorescent product remain in the IL compartment due to their preferential solubility in IL, hence any cross-contamination and dilution of fluorescence signal due to leaching out of the substrate/product is minimized.

Contrary to the typical analytical practice of adding indicator to an analyte solution, our method represents a non-invasive version of analysis where transport of analyte from aqueous solution to indicator-rich IL segment (probe) produces a bright fluorescence optical read-out.

To demonstrate the new concept of IL-Aq droplet-based analysis (Figure 3.3a), we selected Au(III) ion (gold salt:  $\text{HAuCl}_4 \cdot 3\text{H}_2\text{O}$ ) as a model aqueous analyte which is soluble in ionic liquids,<sup>49-50</sup> known to catalyze numerous organic reactions<sup>51-53</sup> and a common precursor in nanomaterials synthesis.<sup>54</sup> Real-time investigation of fluorescence evolution in the IL compartment of a compound droplet is easily conducted by tracking the translating compound droplets with an optical stereomicroscope.<sup>55</sup> The generation and confinement of bright fluorescence within a segment of the compound droplet is analogous to magnesium-aided enzymatic bioluminescence<sup>56</sup> localized in the lower abdominal segment of fireflies, and motivated us to call our compound droplets, ‘microfluidic fireflies’ (Figure 3.3c, d). We demonstrate that a simple PDMS-based microfluidic set-up and stereomicroscopic fluorescence imaging enable us to controllably produce compound droplets, perform non-invasive analysis of a metal ion and to gain insights into physico-chemical processes involved.

The chemical principle of Au(III) detection through microfluidic firefly generation is illustrated in Figure 3.3b. Although gold ions are highly soluble in water, they can partition into the polar IL (1-ethyl-3-methylimidazolium bis(trifluoromethylsulfonyl)imide, [EMIM][NTf<sub>2</sub>]) segment which is pre-doped with an aryl alkyne substrate 1. Within the IL segment Au(III), a Lewis acid, first forms a complex with the carbon-carbon triple bond of 1 and subsequently catalyzes a

cyclization reaction producing highly fluorescent coumarin-derivative 2,<sup>57</sup> which is responsible for the firefly-like bright glow in the IL segment under UV irradiation (Figure 3.3b). Ionic liquids are known to accelerate similar Lewis-acid catalyzed intramolecular cyclizations;<sup>58</sup> this facilitates rapid detection in our microfluidic setup.

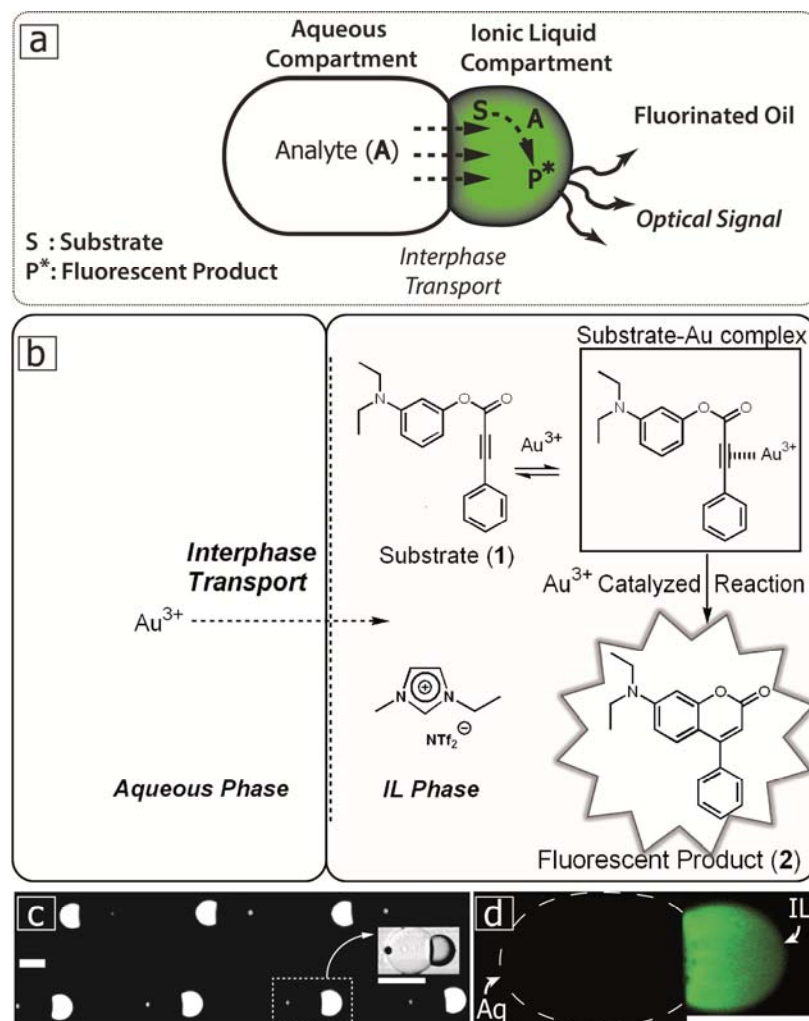


**Figure 3.3.** (a) A schematic of the general concept of 'on-drop' biphasic chemical analysis: Interfacial analyte transport within the ionic liquid compartment of a microfluidic 'firefly'. (b) Metal (analyte)-catalyzed fluorescence generating reaction scheme: gold ions are transferred from the aqueous to ionic liquid compartment, and catalyze the conversion of a substrate into a strongly fluorescing product, triggering bright fluorescence in the IL compartment (excitation: 365nm, emission: 496nm). (c) 'Fireflies-on-a-chip' visualized by mono-chrome camera under UV irradiation, Inset: bright field image of a compound droplet. (d) Stereomicroscope image of a 'firefly-on-a-chip' visualized using color camera under UV irradiation. Scale bars= 300  $\mu$ m.

## 3.2 Experimental Details

### 3.2.1 Materials

Octadecafluorodecahydronaphthalene (perfluorodecalin, Fluka, mixture of *cis* and *trans*, 95%), 1*H*,1*H*,2*H*,2*H*-perfluorooctanol (Sigma-Aldrich, 97%), 1-methylimidazole (Sigma-Aldrich, 99%), orange II (Or II, Sigma), methyl blue (MeB, Sigma), bromoethane (Sigma-Aldrich), chloroform (BDH AnalaR), thymol blue (Th.B, Hayashi Pure Chemicals, Japan), *p*-toluenesulfonic acid monohydrate (P-TSA), lithium bis(trifluoromethylsulfonyl) imide (TCI, 98%), dichloromethane (Aldrich, >99.5%), absolute ethanol (Fisher Scientific), ethyl acetate (Fisher Scientific, analytical grade), n-hexane (Tedia, 95%), lithium bis(trifluoromethylsulfonyl)imide (TCI, 98%), 3-(diethylamino)phenol (Sigma-Aldrich, 98%), phenylpropionic acid (Sigma-Aldrich, 98%), *N,N'*-(dimethylamino)pyridine (Sigma-Aldrich, 99%), hydrogen tetrachloroaurate trihydrate (HAuCl<sub>4</sub>·3H<sub>2</sub>O) (Sigma-Aldrich, 99.999% trace metals basis) were used as obtained. Ultra pure water (18 MU cm, ELGA, Singapore) was used for all experiments.

### 3.2.2 Synthesis of IL [EMIM][NTf<sub>2</sub>]

The synthesis protocol was based on the description in section 2.3.2.

### 3.2.3 Microfabrication

Microfluidic device patterns were fabricated onto silicon wafers by standard photolithography using the negative photoresist SU-8 (2050).<sup>59</sup> Details of the master fabrication are provided in Appendix A and the channel design is shown in Figure 3.4



and Figure 3.5. Devices were molded in poly(dimethyl siloxane) (PDMS) using the soft lithography technique. Briefly, PDMS was molded onto the SU-8 masters at 70°C for 2.5 hours, peeled, cut and cleaned. The inlet and outlet holes (1/16-in. O.D.) were punched into the device which was then sealed to a glass slide pre-coated with a thin layer of PDMS after 35 seconds air plasma treatment (Harrick PDC 32G).

**On drop separations and pH sensing with IL-aqueous compound droplets:** The AutoCAD drawing of the microchannel used for on-drop chemical separation and pH sensing is shown in Figure 3.4. The final microchannels had a rectangular cross section, and were 300  $\mu\text{m}$  wide,  $\sim 155 \mu\text{m}$  on deep and 0.45 m long.

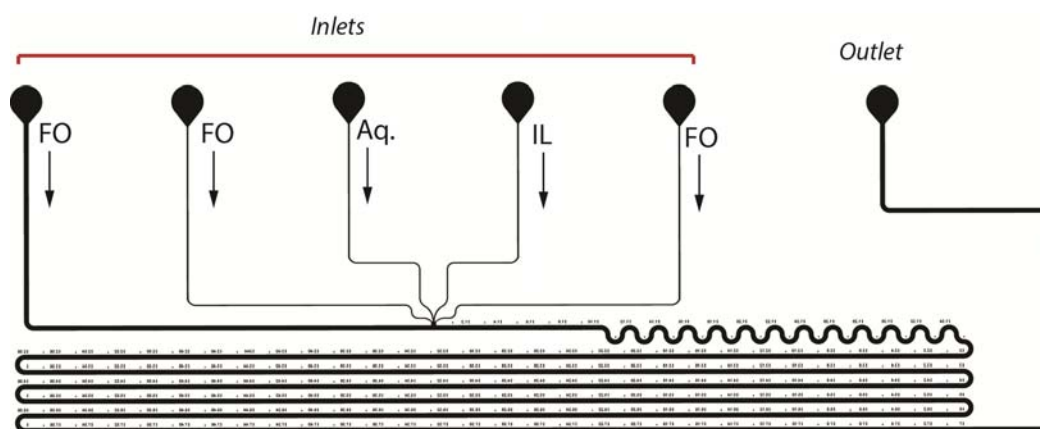


**Figure 3.4.** AutoCAD drawing of the microchannel used for ‘on drop’ separation and pH sensing

**Biphasic reactive sensing with IL-aqueous compound droplets:** The AutoCAD drawing illustrated in Figure 3.5 is used for biphasic reactive sensing. The microchannels had a rectangular cross-section, and were 300  $\mu\text{m}$  wide, 155  $\mu\text{m}$  deep and 0.5 m long.

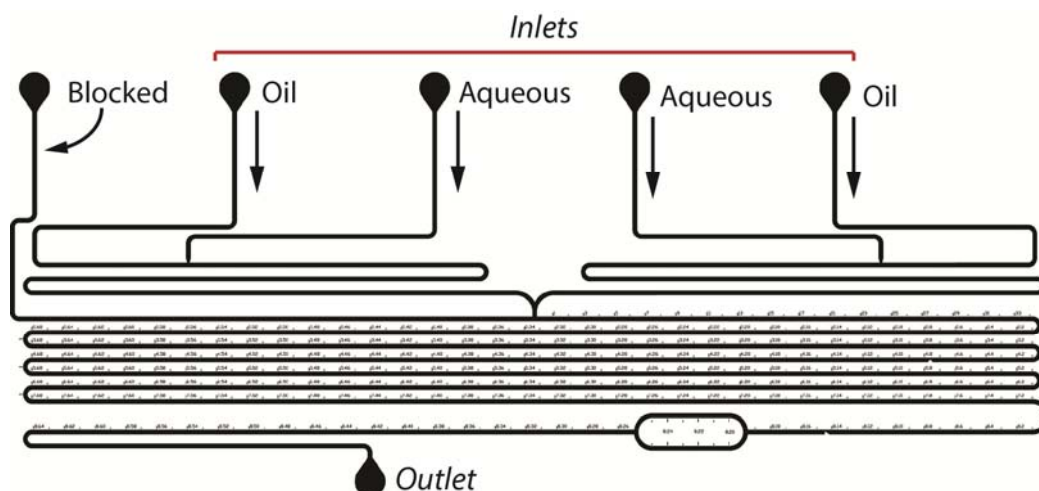


**Figure 3.5.** AutoCAD drawing of the microchannel used for biphasic reactive sensing

## 3.2.4 Device Operation and Setup

### 3.2.4.1 On-drop chemical separations

An aqueous solution containing a binary mixture of 0.75 mM Orange II (OrII) and 1.25 mM Methyl Blue (MeB) was used in the experiments of this section. Individual syringe pumps (Harvard, PHD 2000) were used to deliver carrier fluid, IL and aqueous solutions to the microfluidic device as shown in Figure 3.6. A 10:1 (v/v) mixture of perfluorodecalin (PFD) and perfluorooctanol (PFO) was used as the carrier fluid which will be referred to as fluorinated oil (FO) hereafter. The individual flow rates of each stream,  $Q_{FO}$ ,  $Q_{IL}$  and  $Q_{Aq}$  were  $3 \mu\text{L}\cdot\text{min}^{-1}$ ,  $1 \mu\text{L}\cdot\text{min}^{-1}$  and  $3 \mu\text{L}\cdot\text{min}^{-1}$  respectively.

### 3.2.4.2 Dynamic pH sensing

The device setup is similar to section 3.2.4.1. Aqueous *p*-toluenesulfonic acid (*p*-TSA monohydrate) solutions of varying concentration (5 mM, 10 mM, 100 mM and 1 M) were used while the pH-detector was 1.6mM thymol blue in [EMIM][NTf<sub>2</sub>]. The

individual flow rates of each stream,  $Q_{FO}$ ,  $Q_{IL}$  and  $Q_{Aq}$  were  $3 \mu\text{L}\cdot\text{min}^{-1}$ ,  $1 \mu\text{L}\cdot\text{min}^{-1}$  and  $3 \mu\text{L}\cdot\text{min}^{-1}$  respectively.

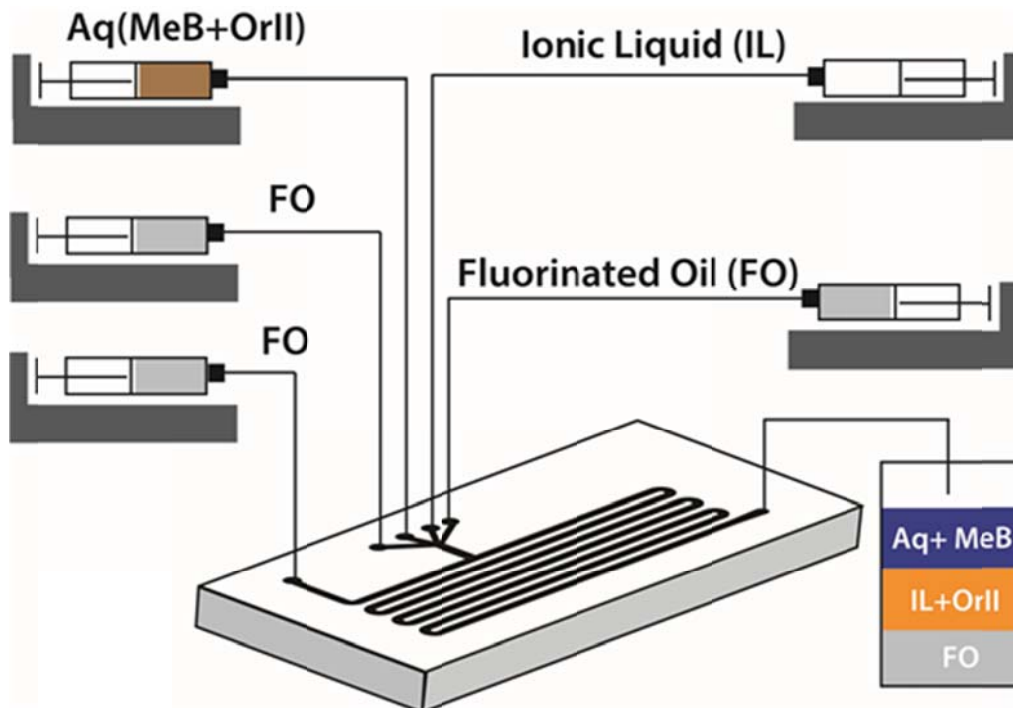


**Figure 3.6.** Schematic view of the experimental set-up

### 3.2.4.3 Biphasic reactive sensing

Aqueous solution (Aq, Aqueous gold ( $\text{HAuCl}_4$ ) solutions of varying concentrations (4.4, 8.8 and 35 mM) in DI water.), Ionic liquid solution (IL, freshly made 0.4 M homogeneous solution of the substrate **1** in ionic liquid [EMIM]  $[\text{NTf}_2]$ ) and fluorinated oil (FO, A 10:1 volumetric mixture of Perfluorodecalin and Perfluorooctanol) were taken in individual Gastight Hamilton syringes. The syringes were then mounted on syringe pumps (Harvard PHD 2000) and connected to the PDMS device via PTFE tubes. Aqueous droplets in FO were generated by flowing Aq (flow rate,  $Q_{Aq} = 3.0 \mu\text{L}\cdot\text{min}^{-1}$ ) and FO ( $Q_{FO} = 3.0 \mu\text{L}\cdot\text{min}^{-1}$ ) at the T-junction. A stream of IL in FO was formed by flowing IL ( $Q_{IL} = 1.0 \mu\text{L}\cdot\text{min}^{-1}$ ) and FO ( $Q_{FO} = 3.0 \mu\text{L}\cdot\text{min}^{-1}$ )

<sup>1</sup>) in the second T-junction. IL stream is digitized by Aq droplets at the droplet dispensing junction to produce compound droplets (Figure 3.7). For studying the effect of the flow speed on fluorescence development, we analyzed fluorescence intensity for three different total flow rates (5, 10 and 15  $\mu\text{Lmin}^{-1}$ ) in microfluidic device while  $\text{HAuCl}_4$  aqueous concentration was 8.8 mM. In these experiments, the flow speed of compound droplets were 2.4, 4.5 and 6.7 mm/s, respectively.

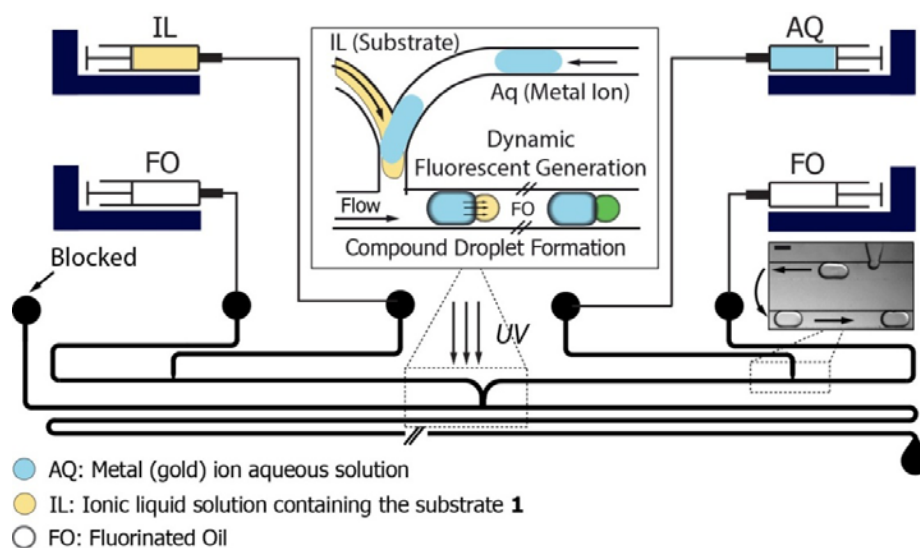


**Figure 3.7.** Microfluidic experimental setup for ‘compound’ droplet generation and fluorescence imaging

### 3.2.5 Data Collection and Image Analysis

#### 3.2.5.1 On-Drop chemical separations and dynamic pH sensing

Quantification of the on-drop separation and pH sensing involved tracking color changes in the functional ionic liquid droplets. Once a steady state operation was achieved the images of the flow were recorded at 23.6 fps by a CCD camera (QImaging, MicroPublisher RTV 5.0) mounted on a stereo microscope (Olympus, SZX7). The images were subsequently analyzed using image processing algorithms implemented in MATLAB. The recorded RGB images were first subtracted from an averaged background intensity. The extraction of orange II into the ionic liquid

droplet, in the case of chemical separation, progressively changes its color to bright orange from an initial colorless state. This color change was best tracked by calculating the average blue intensity of the subtracted image. In dynamic pH sensing analysis, the ionic liquid compartment, as a pH sensor, changed its color from yellow to deep pink and measuring the average green intensity of the subtracted image yielded best results.

### **3.2.5.2 Biphasic reactive sensing**

Quantification of the gold ion detection demonstrated here involved tracking fluorescence changes in the ionic liquid compartment. Once steady state operation was achieved the images of the flowing droplets were recorded at 21 fps and constant gain 5 and exposure time 35.6 ms by a CCD camera (Q-Imaging) mounted on a stereomicroscope (Olympus, SZX7). The fluorescence recording of droplets was performed under UV irradiation from high pressure mercury lamp mounted on the stereomicroscope (filtered through a GFP filter). The images were subsequently analyzed using image processing algorithms implemented in MATLAB.

### **3.2.6 Chemical Synthesis**

For biphasic reactive sensing, the fluorescent probe substrate **1** and the fluorescent product **2** were synthesized according to slightly modified literature methods and later examined with fluorescent spectroscopy.<sup>57</sup>

#### **3.2.6.1 Synthesis of 1**

3-(Diethylamino)phenol (4.9 g, 30 mmol) and phenylpropionic acid (1.27 g, 8.7 mmol) were taken with 15 mL dichloromethane (dried over molecular sieves, 4Å) in a 100 mL three-neck round-bottom flask fitted with a reflux condenser, a dropping

funnel and a nitrogen-filled balloon. This mixture was cooled in an ice water bath. Then, to this cooled reaction mixture was added drop-wise a dichloromethane solution (15 mL) of *N,N'*-Dicyclohexyl carbodiimide (DCC) (9.28 g, 45.0 mmol) and *N,N'*-Dimethylaminopyridine (DMAP) (97 mg, 0.8 mmol). The clear brown-black reaction mixture was stirred at 0°C and allowed to reach room temperature overnight (12 hours). After evaporating all the volatiles under reduced pressure, purification by flash column chromatography on silica gel (EtOAc : n-hexane = 1:4,  $R_f$  = 0.6) afforded the desired product **1** as light brownish oil (1.22 g, yield 48 %, based on phenylpropionic acid used). Structure and purity were confirmed by comparing the  $^1\text{H}$  NMR data to the literature values (Appendix B- Figure B2).<sup>57</sup> Multiplets in the range of 3.43 ppm to 3.36 ppm correspond to the Methylene groups (-CH<sub>2</sub>-) attached to Nitrogen atom of the Diethylamino group, while multiplets at 6.46-7.34 ppm are typical of aromatic rings with *para*-substitutions.

### 3.2.6.2 Synthesis of **2**

To a solution of **1** (528.5 mg, 1.8 mmol) in 5 mL dichloromethane/ethanol (4:1, v/v) was added H<sub>2</sub>AuCl<sub>4</sub>·3H<sub>2</sub>O (71 mg, 0.18 mmol, 10 mol%). The resulting orange-yellow reaction mixture was further stirred overnight for 14 hours. After evaporating all the volatiles under reduced pressure, purification by flash column chromatography on silica gel (EtOAc : n-hexane=1:4,  $R_f$  = 0.22) afforded the desired product **2** as clear bright yellow oil (402 mg, yield 76 %). Structure and purity were confirmed by comparing the  $^1\text{H}$  NMR data to the literature values (Appendix B- Figure B3).<sup>57</sup> Unlike the Substrate **1**, a new peak at 6.05 ppm (-CH- attached to C=C bond) can be attributed to the cyclization of **1** into a Coumarin ring, which is responsible for the fluorescence.

### 3.2.6.3 Fluorescence study

Fluorescence spectra of the substrate **1** and product **2** were measured in Fluorescence Spectroscopy (Photon Technology International). Pure ionic liquid [EMIM][NTf<sub>2</sub>] and a 3.41 mM solution of substrate **1** in the ionic liquid exhibited negligible fluorescence at 365 nm excitation. However, 20 μM solution of the product **2** in ionic liquid exhibited significant fluorescence (Figure 3.8).

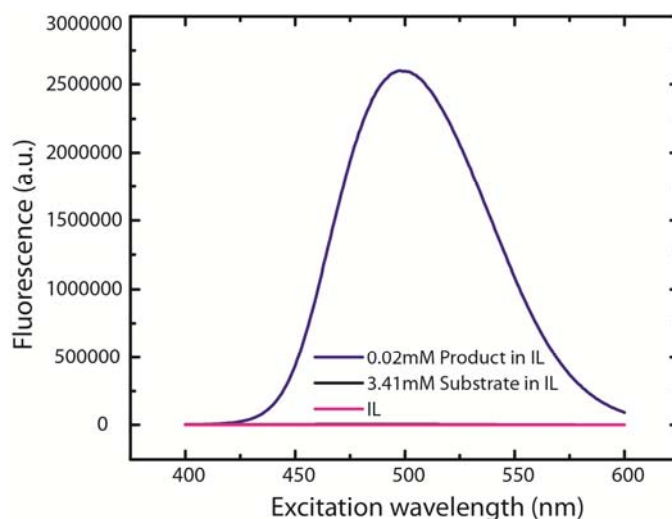


**Figure 3.8.** Fluorescence spectra of ionic liquid, [EMIM][NTf<sub>2</sub>], **1**/ IL solution, and **2**/IL solution ( $\lambda_{\text{ex}}$  365 nm,  $\lambda_{\text{em}}$  496nm).

## 3.2.7 Results and Discussion

### 3.2.7.1 On-drop chemical separations

An aqueous mixture of methyl blue (MeB) and orange II (OrII) dyes that is initially brown in color is prepared (Figure 3.9a) and partially engulfed compound droplets are formed based on the principles described in Chapter 2. OrII is highly soluble in the ionic liquid phase and is rapidly extracted into the ionic liquid compartment, thus coloring it bright orange, while the MeB remains in the aqueous phase (Figure 3.9b, c). This partitioning behavior can be attributed to the mono-anionic nature of Orange II, as compared to with di-anionic MeB which is more hydrophilic in nature (Figure 3.9d, e).



**Figure 3.9.** (a-c) Stereomicroscopic images of selective liquid-liquid extraction of orange II out of an aqueous binary mixture with methyl blue into the ionic liquid compartment along the microchannel. All scale bars represent 300  $\mu\text{m}$ . d, e) Chemical structures of Orange II (OrII) and Methyl blue (MeB), respectively.

As can be seen in Figure 3.10a, the extraction is completed in  $\sim 7$  s. This extraction time is much smaller than the characteristic diffusion time  $t_D \sim w^2/D = 13,846$  s, where  $D = 6.5 \times 10^{-12} \text{ m}^2\text{s}^{-1}$  is a Stokes-Einstein estimate of OrII diffusivity in [EMIM][NTf<sub>2</sub>], and  $w$  is the microchannel width. This dramatically lowered extraction time can be attributed to convection-enhanced diffusive transport, where the characteristic extraction time ( $t_C$ ) is decreased compared to diffusion time ( $t_D$ ) by a flow-dependent factor  $\text{Pe}^{-2/3}$  at short contact times ( $t \ll t_D$ ) (where Peclet number ( $Pe$ )  $\sim Uw/D$  and  $U$  is a flow speed).<sup>31, 60</sup> Taking this convection enhancement into account gives us an estimated convection-enhanced extraction time  $t_C \sim 3$  s for a flow speed of  $5 \times 10^{-3} \text{ m s}^{-1}$ , which is in acceptable agreement with our measurements.

We also set up a 2D finite element method (FEM) model to solve the convection-diffusion problem within compound droplets and successfully confirmed acceleration of mass transport by recirculatory convective motion within each compartment. We implemented an FEM model of compound droplets in COMSOL Multiphysics 3.5a, where we solved the incompressible Navier-Stokes and time-dependent convection-diffusion equations in coupled fashion.



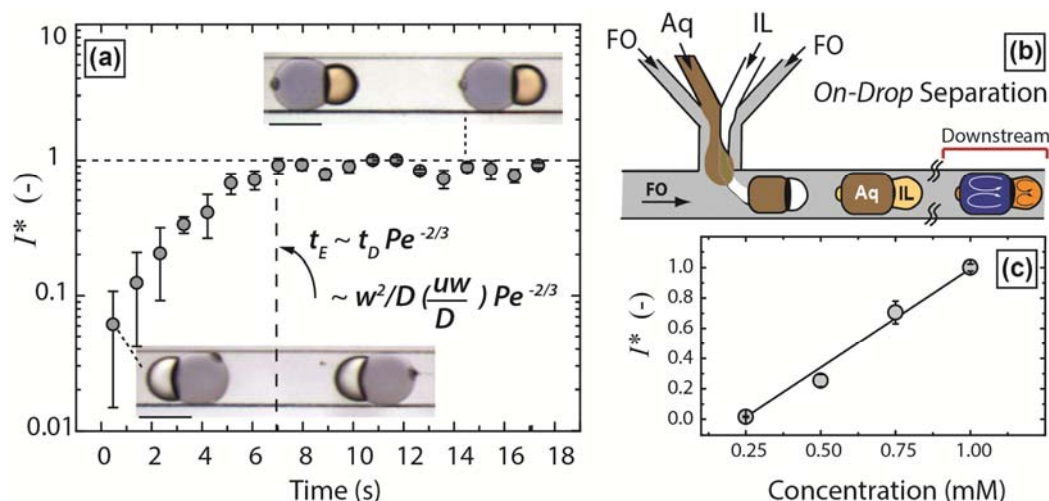


**Figure 3.10.** (a) A plot of the average color intensity (normalized) in the ionic liquid versus time ( $L/v$ , where  $L$  is the distance along the microchannel and  $v$  is the velocity of the compound drops;  $v=0.005 \text{ ms}^{-1}$  obtained using image analysis). Inset stereomicrographs show the compound drops at the initial and final points along the microchannel. (b) Schematic illustration of compound droplets formation in a microchannel and *on-drop* liquid-liquid extraction (c) The plot shows the linear variation of average orange II color intensity (normalized) versus its concentration in ionic liquid. All scale bars represent  $300 \mu\text{m}$ .

We first solved for the outer (continuous fluid) velocity fields assuming fully mobile inner boundaries. We do this in the frame of reference of the compound droplet, and therefore translate the outer walls at a speed  $-U$ . We then use the above outer solution as a boundary condition and solve for the inner (aqueous and IL velocity fields). This method of coupling inner and outer solutions is necessarily an approximation, and over-estimates the velocity, especially in the ionic liquid phase. Besides, it does not account for normal stresses due to interfacial tension. However, the advantage is that this scheme is easy to implement, and will not change the essential physics we wish to examine here - a comparison between purely diffusive mass transport and mass transport in the presence of recirculatory convection within a closed compartment. The inner velocity fields were then used as input to the unsteady convection-diffusion equation to calculate time evolution of area-averaged concentration within both aqueous and ionic liquid compartments.

We used the following parameters in the simulations:  $\mu_{IL} = 30 \times 10^{-3}$  Pa.s,  $\mu_{OIL} = 5.1 \times 10^{-3}$  Pa.s,  $\mu_{H_2O} = 1 \times 10^{-3}$  Pa.s,  $D_{IL} = 6.5 \times 10^{-12}$  m<sup>2</sup>s<sup>-1</sup>,  $D_{H_2O} = 1.69 \times 10^{-10}$  m<sup>2</sup>s<sup>-1</sup>,  $\rho_{OIL} = 1895$  kg m<sup>-3</sup>,  $\rho_{H_2O} = 1000$  kg m<sup>-3</sup>,  $\rho_{IL} = 1509$  kg m<sup>-3</sup>. We simulated the system for an aqueous-phase initial concentration  $C_{AQ} = 0.75$  mM, partition coefficient  $K=1$ , and a wall speed  $U$  of  $5.78 \times 10^{-3}$  m s<sup>-1</sup>. We ran the simulation for 50 s in time steps of 1 s; the aqueous droplet had an initial concentration of 0.75 mM dye, and the ionic liquid contained no dye at the start of the simulation (Figure 3.11).

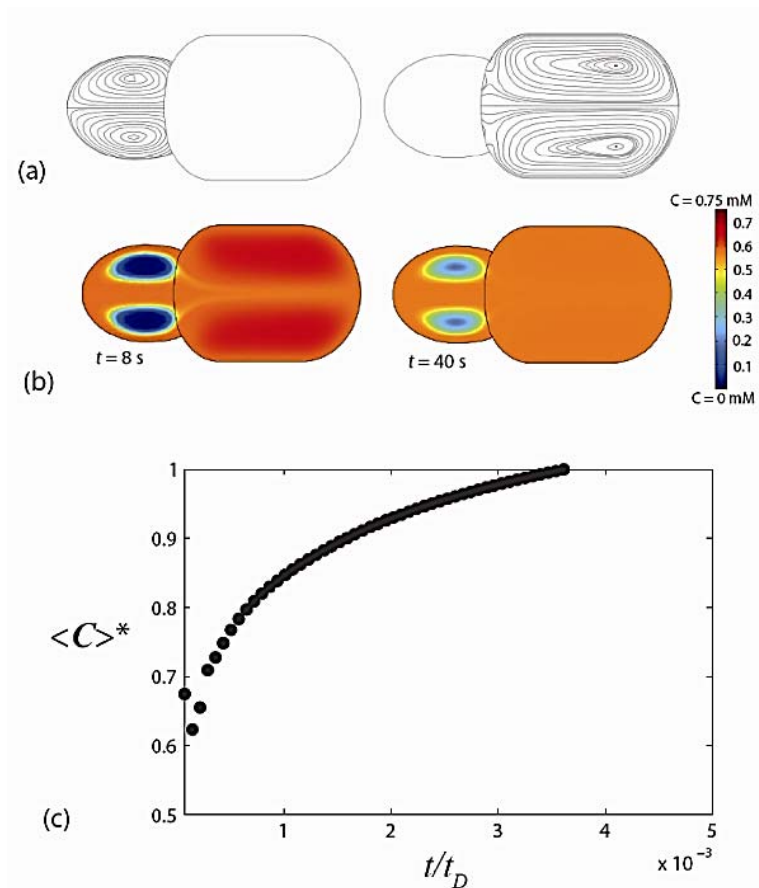


**Figure 3.11.** (a) Calculated streamlines in both aqueous and IL compartments, (b) snapshots of concentration in both compartments at two different times, and (c) normalized area averaged concentration ( $\langle C \rangle^*$ ) in ionic liquid compartment as a function of time (normalized with respect to diffusive time  $t_D = w^2/D$ ). The area-averaged concentration is observed to start leveling at normalized times of  $\sim 2 \times 10^{-3}$ , indicating dramatic acceleration of mass transport by convection.

### 3.2.7.2 Dynamic pH sensing

The aqueous pH is determined by doping the ionic liquid ([EMIM][NTf<sub>2</sub>]) with a pH-responsive dye: thymol blue (ThyB, pK<sub>a</sub> 1.65 and 8.9).<sup>61</sup> At acidic pH, ThyB exists in zwitterionic form, which exhibits pink-red color, quite different from its di-anionic form at neutral pH, which shows light yellow color (Figure 3.12).<sup>62</sup> ThyB is observed to preferentially partition in the ionic liquid, and changes color from yellow to pink as the ionic liquid becomes progressively acidic by mass transfer of the acid from the aqueous phase (Figure 3.13a-c).

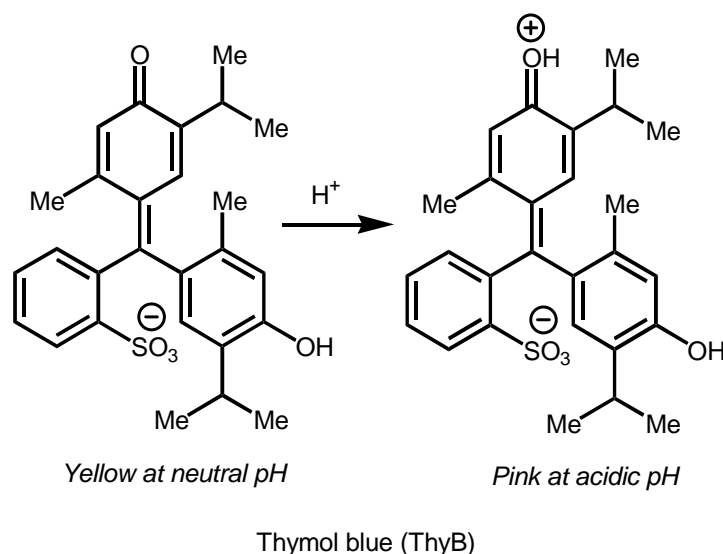


**Figure 3.12.** Molecular structures of thymol blue at neutral and acidic pHs

We carried out a series of experiments wherein the aqueous phase contained different concentrations of *p*-toluene sulphonic acid (*p*-TSA) ranging from 0.005 M to 1 M, the ionic liquid was doped with 0.0016 M of ThyB, and the droplet sizes and speeds were held constant by operating at identical liquid volumetric flow rates. Color images of the flowing compound droplets were digitally captured and analyzed to obtain quantitative information on sensing dynamics. With droplet sizes and speeds held constant the time required for the color in the IL droplet to saturate depends only on

the initial concentration of the acid in the aqueous droplet, with longer times required for lower acid concentrations (higher pH).

Steady-state operation enables us to calibrate pH of the aqueous phase versus dynamic color change of the ionic liquid as the compound droplets translate along the microchannel, as shown in Figure 3.13. The average color intensity within the ionic liquid compartment as a function of aqueous-ionic liquid contact time in the microchannel is plotted (Figure 3.13d), for two different pH values. The color change and saturation are clearly seen to occur more rapidly for the higher acid concentration. Therefore, this is not merely a qualitative end-point measurement where a color change indicates a ‘yes’ or ‘no’ answer, but a quantitative measurement where the color change dynamics can be calibrated against pH (Figure 3.13d, inset). The compound drop pH sensor in its current state has a measurement range of pH 0.2 – 2.7 and is accurate to within 12% with a precision of  $\pm 0.17$  pH units. The measurement range and sensitivity can be further improved by tuning the indicator concentration, relative volumes of the aqueous and IL compartments and their speed of translation. This is a non-invasive reporting technique, does not require sophisticated optical detection, and can be extended to include a multitude of reporters in separate small ionic liquid reporter droplets attached to the aqueous phase (for instance in structures similar to Figure 2.13 c, d).

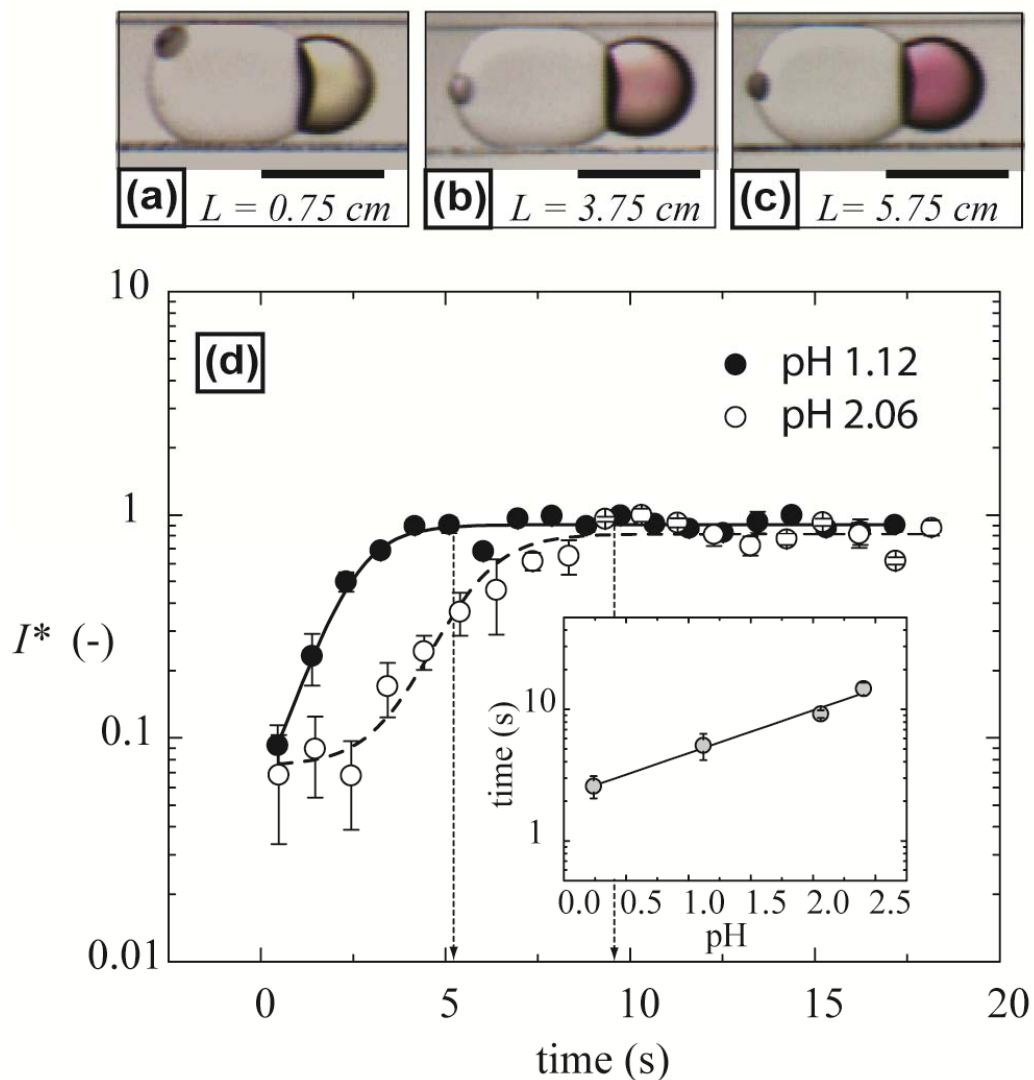


**Figure 3.13.** (a) Stereomicroscopic images illustrating on-drop pH-sensing showing the ionic liquid compartment gradually changing color (from yellow to deep pink) as it translates along the length of the microchannel (b) A plot of average green intensity (normalized) of the ionic liquid droplet against time ( $L/v$ , where  $L$  is the distance along the microchannel and  $v$  is the velocity of the compound drops;  $v=0.005 \text{ ms}^{-1}$  obtained using image analysis) for two different pH values. The inset shows end-point measurements, i.e. the measured time for the saturation of color in the ionic liquid compartment at four different pH values. All scale bars represent  $300 \mu\text{m}$ .

We also confirmed that protonation of Th.B did not appreciably change the original aqueous pH by conducting off-chip pH measurements under comparable conditions of concentration and relative volumes of aqueous and ionic liquid phases. Since the

aqueous to IL droplet volume ratio in microfluidic experiments of this section was 3:1, we conducted batch tests by taking in each case 1 mL of [EMIM][NTf<sub>2</sub>] (containing 0.0016 M thymol blue indicator) solution with 3 mL of aqueous acid solution (*p*-TSA) of varying concentrations in screw-capped glass vials. These biphasic mixtures were vortexed to mix ionic liquid and aqueous phases. Mass transfer of acid from aqueous phase to ionic liquid phase was immediately observed by the intense pink coloration in the latter phase. Then, pH of the aqueous phase (after the partitioning with the IL phase) was measured and compared this with the pH of the original aqueous acid solution (Table 3.1).

Aqueous acid concentration	1.0 M	0.50 M	0.10 M	0.05 M	0.01 M	0.005 M
pH* of aqueous acid solution	0.18	0.46	1.07	1.39	2.03	2.35
pH* of aqueous acid solution after partitioning with IL	0.21	0.48	1.10	1.39	2.17	2.58

**Table 3.1.** Comparison between pH of the aqueous phase (after the partitioning with the IL phase) and pH of the original aqueous acid solution. (\* Measurement uncertainty  $\pm 0.01$ )

### 3.2.7.3 Biphasic reactive sensing

Aqueous droplets were formed separately in the microchannel and they digitized a stream of IL to form compound droplets (Figure 3.7 and Figure 3.14a). Compound droplets were well-separated from each other, did not coalesce and maintained their original geometric configuration throughout the channel network (Figure 3.14a, c). The formation of an interface between ionic liquid and aqueous segments was immediately followed by transport of gold into IL and subsequent catalytic reaction.

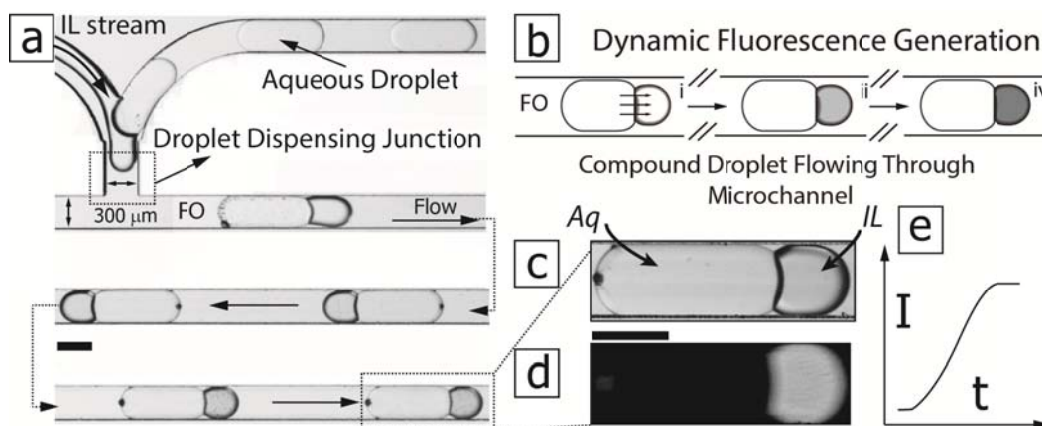


**Figure 3.14.** (a) Stereomicroscopic image of compound droplets generation at the drop dispensing junction of a PDMS microfluidic device: merger of preformed aqueous droplet (Aq) with a thin stream of ionic liquid (IL), producing ionic liquid-aqueous (IL-Aq) bi-compartmental compound droplets flowing in continuous phase (fluorinated oil, FO). (b) A schematic illustrating increase in fluorescence intensity within the ionic liquid compartment of a compound droplet with time as it travels along the microchannel. (c, d) Bright-field and dark-field stereomicroscopic images of an IL-Aq compound droplet flowing in microchannel, respectively. (e) a schematic graph indicating increase in fluorescence intensity of IL compartment with time. Scale bars= 300 μm.

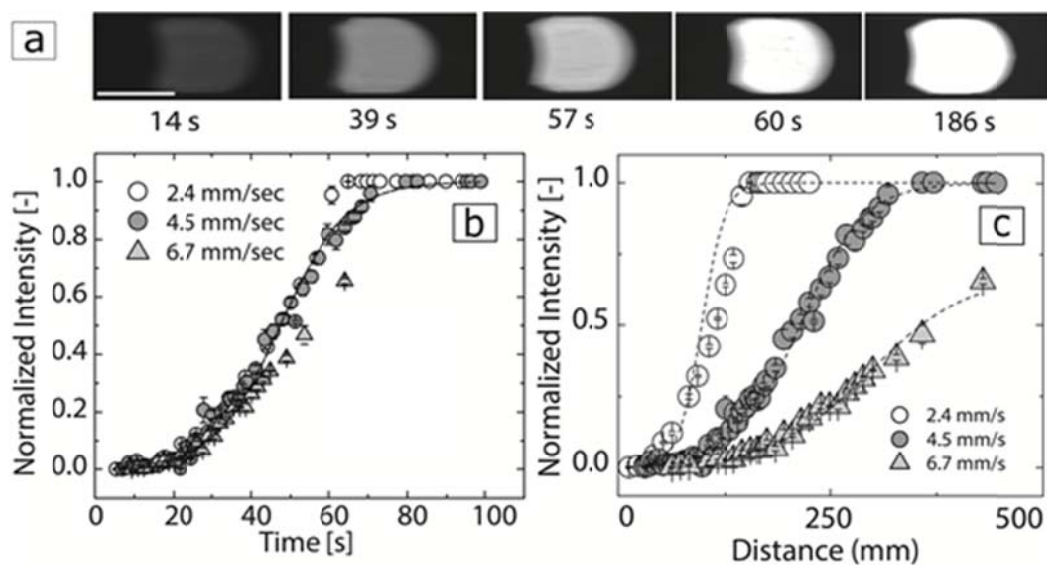


**Figure 3.15.** (a) Stereomicroscope images showing increase in fluorescence intensity within the ionic liquid compartment of a compound droplet with time as it travels along the microchannel. Scale bar=300 μm. (b) Plots of normalized fluorescence intensity of IL compartments flowing at different speeds. (constant concentration of gold in aqueous compartment for all cases, 8.8mM). (c) Plots of normalized fluorescence intensity of IL compartments versus time for two different gold concentrations in the aqueous compartment, flowing at 4.5 mm/s.

The physicochemical aspects of this new analytical method were investigated by measuring and analyzing the kinetics of fluorescence emission. The fluorescence intensity within IL segments gradually increases with time indicating progressive rise in the concentration of the product 2 in IL as a result of the catalytic reaction (Figure 3.14b-e and Figure 3.15a).

The changes in fluorescence intensity in the IL compartment of the translating compound droplet were recorded at various locations (corresponding to various time points), along the length of the microchannel (relative to the drop dispensing junction) for three different droplet speeds (for all cases  $[\text{Au(III)}] = 8.8 \text{ mM}$ ). Interestingly, when the normalized fluorescence intensity for all three droplet speeds is plotted against reaction time, all three curves essentially collapse onto each other (Figure 3.15b, c). To investigate this intriguing observation, we first examined flow-dependent internal convection ('stirring') within droplets, which is a well-studied phenomenon,<sup>63</sup> we previously observed (Chapter 3.2.7.1) that such internal convection could significantly accelerate chemical transport between the compartments of a compound droplet.<sup>33</sup> Internal convection intensifies rapidly with flow speed, and the transport of gold ions from the aqueous to IL segment is faster for higher flow speeds. A convection-enhanced mass transport time for gold to enter and mix within the IL compartment is defined as  $t_C = t_D Pe^{-2/3} = w^2/D (Uw/D)^{-2/3}$ ,<sup>31, 64</sup> where  $w$  is the microchannel width,  $U$  is the flow speed, and  $D$  is the diffusivity of  $\text{Au}^{3+}$  in  $[\text{EMIM}][\text{NTf}_2]$ .  $D$  is estimated using the Stokes Einstein equation to be  $2.4 \times 10^{-11} \text{ m}^2/\text{s}$ .<sup>65-66</sup> Characteristic transport times corresponding to 2.4, 4.5, and 6.7 mm/s flow speeds are calculated as 3.9, 2.6, and 2.0 seconds respectively, which are about 1000



times smaller than the characteristic diffusion time  $t_D = w^2/D = 3750$  s (i.e. the mass transport time in the complete absence of internal convection).

As noted above, the time required for the attainment of saturation fluorescence within the IL segment is speed-independent. In our measurements, fluorescence intensity was used as a surrogate indicator of product concentration. These measurements, like any other kinetic measurements of this kind, involve a finite lag time of the order of  $\sim 10$  seconds in all our experiments, as can be seen in Figure 3.15b (and in Figure 3.15c), before any appreciable intensity is captured in our experimental setup. According to the above estimates of chemical transport times, gold is rapidly transported and homogenized into the ionic liquid compartment within 2-4 seconds; hence gold transport into the IL likely occurs well within the experimental lag time noted above, for all experimental conditions. Therefore, we can state with generality that the measured kinetic traces in our experimental range of gold concentrations are uncoupled from chemical transport, and do shed light (albeit indirect) on the intrinsic kinetics of the process, which are likely nonlinear in catalyst and substrate concentration. In fact, one can envision a much more detailed exploration of the gold-substrate concentration parameter space to infer the full nonlinear chemical rate equation. Next, we describe the results of a partial exploration of this space and its implications on practical applications of our method.

We examined the effect of Au(III) concentrations on the kinetics of fluorescence emission. At a fixed flow speed (4.5 mm/s), the curves of measured fluorescence intensity versus reaction time get steeper with increasing gold concentration in the aqueous segment (Figure 3.16). Therefore, as the dynamic fluorescence response of

the IL compartment is sensitive to the gold concentration in the adjacent compartment, such droplets may be used as semi-quantitative analytical tools for detection of metal ions or other catalytically active species. Advances with regard to detection limit (analyte/probe concentrations) or detection time are certainly possible by judicious selection and optimization of faster and more sensitive probe chemistry.

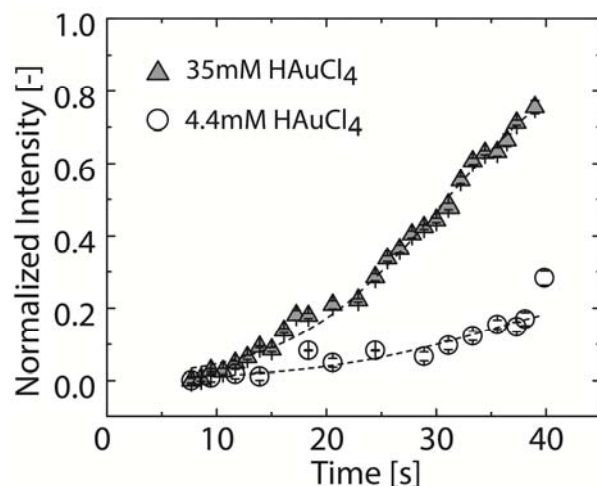


**Figure 3.16.** Plot of normalized fluorescence intensity of IL compartments flowing at different speeds against the distance (location) along the microchannel (constant concentration of gold in aqueous compartment for all cases, 8.8mM).

In order to quantify the partitioning of gold ion into ionic liquid, 300 $\mu$ L ionic liquid [EMIM][NTf<sub>2</sub>] was added to 900  $\mu$ L of 25 ppm Au<sup>3+</sup> aqueous solution (made from HAuCl<sub>4</sub> • 3H<sub>2</sub>O and DI water). This biphasic mixture was vigorously vortexed for 1 min. After both phases completely separated, aliquot of the aqueous part was pipetted out. The same experiment was repeated using ionic liquid [EMIM][NTf<sub>2</sub>] containing substrate (1) (0.4 M). The amount of gold ion present before and after the partitioning processes in the aqueous phase was measured using Inductively Coupled Plasma Mass Spectrometry (Agilent Technologies, ICP-MS, 7500 series). ICP-MS results show that 20% of the initial gold ions partition into ionic liquid phase in both cases

(IL with or without 1). Calibration for concentrations was performed by using commercially available standard gold solution (1000 ppm Au, Hayashi Pure Chemical Industries Ltd., JAPAN).

It is noteworthy that a similar multiphasic analysis in conventional flask-based method would require two counteracting processes: vigorous emulsification of ionic liquid-aqueous phases (for interfacial mass-transfer) and rapid phase separation (for noise-free fluorescence measurements). Hence, finite time lags between any of the processes: mixing, complete phase-separation and fluorescence measurement of IL phase, are likely to obscure the intrinsic kinetics of the coupled physical (transport) and chemical (reaction) processes in this system. On the contrary, the large surface area-to-volume ratio and internal circulation in compound droplets facilitate rapid interfacial mass-transfer, homogenization of analyte and uniform distribution of fluorescence (due to 2) inside IL compartment, while both phases maintain a well-defined and almost constant interfacial area (Figure 3.14a-d and Figure 3.15a). This is why, while all these physical and chemical processes occur in concert within the unperturbed geometric boundary of the compound droplet, optical tracking of the IL compartment at several locations (equivalent to reaction times) in the microfluidic channel enables extraction of a significant amount of kinetic data associated with the cascade of transport, reaction and fluorescence generation phenomena.

### **3.3 Summary**

We demonstrated the selective extraction of an organic molecule from a binary aqueous mixture into the ionic liquid compartment of partially engulfed compound droplets flowing in an inert third liquid in microchannels. Extraction time was

estimated by tracking the color change ( $\sim 7$  s) which is drastically smaller than the characteristic diffusion time ( $\sim 2000$  times smaller). This dramatically lowered extraction time was confirmed to be attributed to convection-enhanced diffusive transport through both experiments and COMSOL simulations. 2D finite element method (FEM) model successfully showed acceleration of mass transport by recirculating convective motion within each compartment of compound droplet.

We also performed rapid and non-invasive *chemical analyses* that are inaccessible at the macroscale. The chemical tunability of ionic liquids was leveraged in directing analyte (proton  $[H^+]$  or metal ion) transport from the aqueous compartment of a biphasic droplet into an indicator-doped ionic liquid ‘reporter’ compartment and, crucially, in confining an analyte-indicator reaction within the reporter; thus enabling detection of the analyte without the addition of an indicator to the aqueous compartment. A simple example of on-drop sensing was demonstrated first, where the ionic liquid in the compound droplet served as a chemical sensor attached to the aqueous droplet. An indicator-doped ionic liquid was used to dynamically measure the pH of the aqueous phase. The time required for the color in the ionic liquid compartment to saturate, as the compound droplets translate along the microchannel, was calibrated for different pHs (various aqueous concentrations of *p*-TSA). Lower the pH (higher the acid concentration), lesser was the time required for the color in the IL compartment to saturate. We envision this technique to eventually enable dynamic sensing of multiple chemical events in the aqueous phase.

Moreover, we presented biphasic microdroplets for non-invasive chemical analysis. Within these bi-compartmental aqueous-ionic liquid droplets metal (gold) ions from

the aqueous compartment partitioned into the adjacent ionic liquid compartment and catalyzed a fluorescence producing reaction. This is a model case where an ionic analyte in one phase could be sensed or detected via a chemical reaction in another compartment through our proposed reactive sensing scheme. We presented detailed measurements of the kinetics of fluorescence emission as a function of metal concentration and droplet flow speed. As ionic liquids can be designed to have preferential affinity for a particular chemical species, the scope of our system can be further extended to where a chemical or biological event in aqueous compartment can be tracked or detected by selectively transporting a product of that event into a task-specific ionic liquid. IL-aqueous compound microdroplets are an exciting addition to the rapidly expanding toolkit of digital microfluidics for unique, non-invasive on-drop measurement, kinetic analysis or reactive sensing

### 3.4 References

1. Schwietzer, P. A., *Handbook of Separations Techniques for Chemical Engineers*. McGraw-Hill: New York, **1996**.
2. Maik W. Jornitz ; Theodore H. Meltzer, *Filtration and Purification in the Biopharmaceutical Industry*, Second Edition. *New York, Informa Healthcare USA* **2008**.
3. Pamme, N., Continuous flow separations in microfluidic devices. *Lab on a Chip* **2007**, 7 (12), 1644-1659.
4. Rydberg, J.; Musikas, C.; Choppin, G., *Principles and Practices of Solvent Extraction*. Marcel Dekker, New York: **1996**.
5. Abraham, M. H.; Zissimos, A. M.; Huddleston, J. G.; Willauer, H. D.; Rogers, R. D.; Acree, W. E., Some Novel Liquid Partitioning Systems: Water-Ionic Liquids and Aqueous Biphasic Systems. *Industrial & Engineering Chemistry Research* **2003**, 42 (3), 413-418.

6. Daintree, L. S.; Kordikowski, A.; York, P., Separation processes for organic molecules using SCF Technologies. *Advanced Drug Delivery Reviews* **2008**, *60* (3), 351-372.
7. Schuberth, J., Volatile Organic Compounds Determined in Pharmaceutical Products by Full Evaporation Technique and Capillary Gas Chromatography/Ion-Trap Detection. *Analytical Chemistry* **1996**, *68* (8), 1317-1320.
8. Fröba, A. P.; Kremer, H.; Leipertz, A., Density, Refractive Index, Interfacial Tension, and Viscosity of Ionic Liquids [EMIM][EtSO<sub>4</sub>], [EMIM][NTf<sub>2</sub>], [EMIM][N(CN)<sub>2</sub>], and [OMA][NTf<sub>2</sub>] in Dependence on Temperature at Atmospheric Pressure. *The Journal of Physical Chemistry B* **2008**, *112* (39), 12420-12430.
9. Castner, J. E. W.; Wishart, J. F., Spotlight on ionic liquids. *The Journal of Chemical Physics* **2010**, *132* (12), 120901-9.
10. Deetlefs, M.; Seddon, K. R.; Shara, M., Predicting physical properties of ionic liquids. *Physical Chemistry Chemical Physics* **2006**, *8* (5), 642-649.
11. Anderson, J. L.; Armstrong, D. W.; Wei, G. T., Ionic liquids in analytical chemistry. *Analytical Chemistry* **2006**, *78* (9), 2892-2902.
12. T., W., Room-temperature ionic liquids. solvents for synthesis and catalysis. *Chemical Reviews* **1999**, *99*, 2071-2084.
13. Fukuyama, T.; Rahman, M. T.; Sato, M.; Ryu, I., Adventures in inner space: Microflow systems for practical organic synthesis. *Synlett* **2008**, (2), 151-163
14. Huddleston, J. G.; Willauer, H. D.; Swatoski, R. P.; Visser, A. E.; Rogers, R. D., Room temperature ionic liquids as novel media for 'clean' liquid-liquid extraction. *Chemical Communications* **1998**, (16), 1765-1766.
15. Han, X.; Armstrong, D. W., Ionic Liquids in Separations. *Accounts Chem. Res.* **2007**, *40* (11), 1079-1086.
16. Yang, Q.; Xing, H.; Cao, Y.; Su, B.; Yang, Y.; Ren, Q., Selective Separation of Tocopherol Homologues by Liquid-Liquid Extraction Using Ionic Liquids. *Industrial & Engineering Chemistry Research* **2009**, *48* (13), 6417-6422.
17. Soto, A.; Arce, A.; Khoshkbarchi, M. K., Partitioning of antibiotics in a two-liquid phase system formed by water and a room temperature ionic liquid. *Separation and Purification Technology* **2005**, *44* (3), 242-246.
18. Huebner, A.; Sharma, S.; Srisa-Art, M.; Hollfelder, F.; Edel, J. B.; deMello, A. J., Microdroplets: A sea of applications *Lab on a Chip* **2008**, *8* (8), 1244-1254.
19. Theberge, A. B.; Courtois, F.; Schaerli, Y.; Fischlechner, M.; Abell, C.; Hollfelder, F.; Huck, W. T. S., Microdroplets in Microfluidics: An Evolving Platform for Discoveries in Chemistry and Biology. *Angewandte Chemie International Edition* **2010**, *49* (34), 5846-5868.

20. Teh, S.-Y.; Lin, R.; Hung, L.-H.; Lee, A. P., Droplet microfluidics. *Lab on a Chip* **2008**, *8* (2), 198-220.
21. Dendukuri, D.; Doyle, P. S., The Synthesis and Assembly of Polymeric Microparticles Using Microfluidics. *Advanced Materials* **2009**, *21* (41), 4071-4086.
22. Song, Y.; Hormes, J.; Kumar, C. S. S. R., Microfluidic Synthesis of Nanomaterials. *Small* **2008**, *4* (6), 698-711.
23. Abou-Hassan, A.; Sandre, O.; Cabuil, V., Microfluidics in Inorganic Chemistry. *Angewandte Chemie International Edition* **2010**, *49* (36), 6268-6286.
24. Vyawahare, S.; Griffiths, A. D.; Merten, C. A., Miniaturization and Parallelization of Biological and Chemical Assays in Microfluidic Devices. *Chemistry & biology* **2010**, *17* (10), 1052-1065.
25. Baroud, C. N.; Gallaire, F.; Dangla, R., Dynamics of microfluidic droplets. *Lab on a Chip* **2010**, *10* (16), 2032-2045.
26. Courtois, F.; Olguin, L. F.; Whyte, G.; Theberge, A. B.; Huck, W. T. S.; Hollfelder, F.; Abell, C., Controlling the Retention of Small Molecules in Emulsion Microdroplets for Use in Cell-Based Assays. *Analytical Chemistry* **2009**, *81* (8), 3008-3016.
27. Woronoff, G.; El Harrak, A.; Mayot, E.; Schicke, O.; Miller, O. J.; Soumillon, P.; Griffiths, A. D.; Ryckelynck, M., New Generation of Amino Coumarin Methyl Sulfonate-Based Fluorogenic Substrates for Amidase Assays in Droplet-Based Microfluidic Applications. *Analytical Chemistry* **2011**, *83* (8), 2852-2857.
28. Holtze, C.; Rowat, A. C.; Agresti, J. J.; Hutchison, J. B.; Angile, F. E.; Schmitz, C. H.; Koster, S.; Duan, H.; Humphry, K. J.; Scanga, R. A.; Johnson, J. S.; Pisignano, D.; Weitz, D. A., Biocompatible surfactants for water-in-fluorocarbon emulsions. *Lab Chip* **2008**, *8* (10), 1632-9.
29. Roach, L. S.; Song, H.; Ismagilov, R. F., Controlling Nonspecific Protein Adsorption in a Plug-Based Microfluidic System by Controlling Interfacial Chemistry Using Fluorous-Phase Surfactants. *Analytical Chemistry* **2004**, *77* (3), 785-796.
30. Theberge, A. B.; Whyte, G.; Frenzel, M.; Fidalgo, L. M.; Wootton, R. C. R.; Huck, W. T. S., Suzuki-Miyaura coupling reactions in aqueous microdroplets with catalytically active fluoruous interfaces. *Chemical Communications* **2009**, (41), 6225-6227.
31. Mary, P.; Studer, V.; Tabeling, P., Microfluidic Droplet-Based Liquid-Liquid Extraction. *Analytical Chemistry* **2008**, *80* (8), 2680-2687.
32. Wijethunga, P. A. L.; Nanayakkara, Y. S.; Kunchala, P.; Armstrong, D. W.; Moon, H., On-Chip Drop-to-Drop Liquid Microextraction Coupled with Real-Time Concentration Monitoring Technique. *Analytical Chemistry* **2011**, *83* (5), 1658-1664.
33. Barikbin, Z.; Rahman, M. T.; Parthiban, P.; Rane, A. S.; Jain, V.; Duraiswamy, S.; Lee, S. H. S.; Khan, S. A., Ionic liquid-based compound droplet

microfluidics for 'on-drop' separations and sensing. *Lab on a Chip* **2010**, *10* (18), 2458-2463.

34. Bai, Y.; He, X.; Liu, D.; Patil, S. N.; Bratton, D.; Huebner, A.; Hollfelder, F.; Abell, C.; Huck, W. T. S., A double droplet trap system for studying mass transport across a droplet-droplet interface. *Lab on a Chip* **2010**, *10* (10), 1281-1285.

35. Zheng, B.; Tice, J. D.; Roach, L. S.; Ismagilov, R. F., A droplet-based, composite PDMS/glass capillary microfluidic system for evaluating protein crystallization conditions by microbatch and vapor-diffusion methods with on-chip X-ray diffraction. *Angewandte Chemie (International ed. in English)* **2004**, *43* (19), 2508-11.

36. Kreutz, J. E.; Shukhaev, A.; Du, W. B.; Druskin, S.; Daugulis, O.; Ismagilov, R. F., Evolution of Catalysts Directed by Genetic Algorithms in a Plug-Based Microfluidic Device Tested with Oxidation of Methane by Oxygen. *Journal of the American Chemical Society* **2010**, *132* (9), 3128-3132.

37. Chen, D. L.; Li, L.; Reyes, S.; Adamson, D. N.; Ismagilov, R. F., Using Three-Phase Flow of Immiscible Liquids To Prevent Coalescence of Droplets in Microfluidic Channels: Criteria To Identify the Third Liquid and Validation with Protein Crystallization. *Langmuir* **2007**, *23* (4), 2255-2260.

38. Kopac, M. J.; Chambers, R., The coalescence of living cells with oil drops. II. Arbacia eggs immersed in acid or alkaline calcium solutions. *Journal of Cellular and Comparative Physiology* **1937**, *9* (3), 345-361.

39. Mori, Y.; Kaminaga, K.; Ando, T., Fluorocarbon-encapsulated oxygen bubbles for blood oxygenation use: An experimental study. *Ann Biomed Eng* **1990**, *18* (3), 285-298.

40. Shum, H. C.; Abate, A. R.; Lee, D.; Studart, A. R.; Wang, B. G.; Chen, C. H.; Thiele, J.; Shah, R. K.; Krummel, A.; Weitz, D. A., Droplet Microfluidics for Fabrication of Non-Spherical Particles. *Macromolecular Rapid Communications* **2010**, *31* (2), 108-118.

41. Chen, C. H.; Shah, R. K.; Abate, A. R.; Weitz, D. A., Janus Particles Templated from Double Emulsion Droplets Generated Using Microfluidics. *Langmuir* **2009**, *25* (8), 4320-4323.

42. Lee, D.; Weitz, D. A., Nonspherical Colloidosomes with Multiple Compartments from Double Emulsions. *Small* **2009**, *5* (17), 1932-1935.

43. Nisisako, T.; Torii, T.; Higuchi, T.; Ieee, Monodisperse anisotropic polymeric particles generated from a micro co-flow system. In *MEMS 2006: 19th IEEE International Conference on Micro Electro Mechanical Systems, Technical Digest*, **2006**; pp 470-473.

44. Wassercheid, P.; Welton, T., *Ionic Liquids in synthesis*. Wiley-VCH Verlags: Weinheim, **2008**.



45. Ges, I. A.; Ivanov, B. L.; Schaffer, D. K.; Lima, E. A.; Werdich, A. A.; Baudenbacher, F. J., Thin-film IrOx pH microelectrode for microfluidic-based microsystems. *Biosensors and Bioelectronics* **2005**, *21* (2), 248-256.
46. Weig, B. H.; Kriebel, J.; Mayes, K. J.; Bui, T.; Yager, P., Whole Blood Diagnostics in Standard Gravity and Microgravity by Use of Microfluidic Structures (T-Sensors). *Mikrochimica Acta* **1999**, *131*, 75-83.
47. Mela, P.; Onclin, S.; Goedbloed, M. H.; Levi, S.; Garcia-Parajo, M. F.; van Hulst, N. F.; Ravoo, B. J.; Reinhoudt, D. N.; van den Berg, A., Monolayer-functionalized microfluidics devices for optical sensing of acidity. *Lab on a Chip* **2005**, *5* (2), 163-170.
48. Maruyama, H.; Arai, F.; Fukuda, T., On-chip pH measurement using functionalized gel-microbeads positioned by optical tweezers. *Lab on a Chip* **2008**, *8* (2), 346-351.
49. Ryu, H. J.; Sanchez, L.; Keul, H. A.; Raj, A.; Bockstaller, M. R., Imidazolium-Based Ionic Liquids as Efficient Shape-Regulating Solvents for the Synthesis of Gold Nanorods. *Angewandte Chemie International Edition* **2008**, *47* (40), 7639-7643.
50. Dash, P.; Scott, R. W. J., 1-Methylimidazole stabilization of gold nanoparticles in imidazolium ionic liquids. *Chemical Communications* **2009**, (7), 812-814.
51. Dyson, P. J.; Geldbach, T. J., *Metal Catalysed Reactions in Ionic Liquids*. Springer: **2005**.
52. Li, Z.; Brouwer, C.; He, C., Gold-Catalyzed Organic Transformations. *Chemical Reviews* **2008**, *108* (8), 3239-3265.
53. Fürstner, A.; Davies, P. W., Catalytic Carbophilic Activation: Catalysis by Platinum and Gold  $\pi$  Acids. *Angewandte Chemie International Edition* **2007**, *46* (19), 3410-3449.
54. Daniel, M. C.; Astruc, D., Gold nanoparticles: assembly, supramolecular chemistry, quantum-size-related properties, and applications toward biology, catalysis, and nanotechnology. *Chem. Rev.* **2004**, *104* (1), 293-346.
55. Marchand, G.; Dubois, P.; Delattre, C.; Vinet, F.; Blanchard-Desce, M.; Vaultier, M., Organic synthesis in soft wall-free microreactors: Real-time monitoring of fluorogenic reactions. *Analytical Chemistry* **2008**, *80* (15), 6051-6055.
56. McElroy, W. D.; Hastings, J. W.; Coulombre, J.; Sonnenfeld, V., the mechanism of action of pyrophosphate in firefly luminescence. *Archives of Biochemistry and Biophysics* **1953**, *46* (2), 399-416.
57. Do, J. H.; Kim, H. N.; Yoon, J.; Kim, J. S.; Kim, H.J., A Rationally Designed Fluorescence Turn-On Probe for the Gold(III) Ion. *Organic Letters* **2010**, *12* (5), 932-934.

58. Song, C. E.; Jung, D.u.; Choung, S. Y.; Roh, E. J.; Lee, S.g., Dramatic Enhancement of Catalytic Activity in an Ionic Liquid: Highly Practical Friedel–Crafts Alkenylation of Arenes with Alkynes Catalyzed by Metal Triflates. *Angewandte Chemie International Edition* **2004**, *43* (45), 6183-6185.
59. Xia, Y.; Whitesides, G. M., Soft lithography. *Annual Review of Materials Science* **1998**, *28* (1), 153-184.
60. Young, W.; Pumir, A.; Pomeau, Y., ANOMALOUS DIFFUSION OF TRACER IN CONVECTION-ROLLS. *Physics of Fluids a-Fluid Dynamics* **1989**, *1* (3), 462-469.
61. Visser, A. E.; Swatloski, R. P.; Rogers, R. D., pH-dependent partitioning in room temperature ionic liquids provides a link to traditional solvent extraction behavior. *Green Chemistry* **2000**, *2* (1), 1-4.
62. Fei, Z. F.; Geldbach, T. J.; Zhao, D. B.; Dyson, P. J., From dysfunction to bis-function: On the design and applications of functionalised ionic liquids. *Chemistry-a European Journal* **2006**, *12* (8), 2123-2130.
63. Song, H.; Tice, J. D.; Ismagilov, R. F., A microfluidic system for controlling reaction networks in time. *Angewandte Chemie-International Edition* **2003**, *42* (7), 768-772.
64. Young, W.; Pumir, A.; Pomeau, Y., Anamalous diffusion of tracer in convection-rolls *Physics of Fluids a-Fluid Dynamics* **1989**, *1* (3), 462-469.
65. Vorotyntsev, M. A.; Zinovyeva, V. A.; Picquet, M., Diffusional transport in ionic liquids: Stokes–Einstein relation or “sliding sphere” model Ferrocene (Fc) in imidazolium liquids. *Electrochimica Acta* **2010**, *55* (18), 5063-5070.
66. Brookes, R.; Davies, A.; Ketwaroo, G.; Madden, P. A., Diffusion Coefficients in Ionic Liquids: Relationship to the Viscosity. *The Journal of Physical Chemistry B* **2004**, *109* (14), 6485-6490.

# Chapter 4

## Microfluidic Synthesis of Polymeric Ionic Liquids with Tunable Functionalities

### 4.1 Monodisperse Polymeric Ionic Liquid Microgels

Ionic liquids are salts of an organic cation (e.g., ammonium, imidazolium or phosphonium) and a counter-anion (organic or inorganic), and unlike mineral salts, are most often liquid at or near room temperature. This unique class of materials has been a topic of much research in the chemical sciences due to a range of remarkable properties including high electrical conductivity, excellent thermal stability, very low volatility and good solvation capability for a broad range of organic, inorganic and biological molecules. Such properties have motivated their use as alternative ‘green’ reaction media for organic and enzymatic reactions.<sup>1-2</sup> Apart from their use in chemical synthesis, ionic liquids (ILs) are of much interest as functional materials in electrochemical devices and batteries due to high electrical/ionic conductivity and wide voltage window.<sup>3-6</sup> A key feature of molecular ionic liquids is that judicious selection of the anion and/or cation enables facile and predictive tailoring of properties such as viscosity, density, hydrophilicity/hydrophobicity, ionic conductivity and chemical reactivity.<sup>7-9</sup>

Such intriguing and tunable features of ILs have been introduced into solid materials either by physically doping ILs into bulk solids or in-situ polymerization of monomers in ionic liquids to form ‘ionogels’,<sup>10-16</sup> or by chemically linking ionic

liquid molecules into polymeric matrices to yield ‘poly(ionic liquid)s’ or PILs.<sup>17-19</sup> In both cases most of the salient features of the ILs are retained and even coupled with the intrinsic properties of the original supporting materials. Furthermore, polymerization of ionic liquid monomers enables expanded functionality, increased chemical stability and physical rigidity<sup>20</sup> and also minimizes any material loss due to leaching.<sup>21</sup> A number of recent studies have demonstrated applications of such novel hybrid materials in carbon dioxide capture, enzyme immobilization and encapsulation for bio-catalytic reactions and sensing,<sup>22-23</sup> controlled drug delivery,<sup>24</sup> lithium batteries and electrochemical devices.<sup>25</sup> The exquisite physico-chemical tunability of these polymeric materials also makes them excellent candidates for the fabrication of smart stimuli-responsive gels for a broad range of potential applications.<sup>26-28</sup> Of particular interest are anion-sensitive PILs, where the chemical nature of constituent anions dictates response of PILs to several features of their chemical environment.<sup>29-32</sup> PILs are typically produced as bulk polymeric materials<sup>33</sup> and often lack regularity in size or shape.<sup>34-36</sup> However, to realize their full potential, especially in applications involving portable, miniaturized environmental sensing and separations, it would be highly desirable to fabricate such materials with regular and tailored sizes and morphologies.

In this chapter, we demonstrate simple, inexpensive microfluidics-based fabrication of highly monodisperse PIL microgels in particulate (bead) form with a multitude of functionalities that can be chemically switched in a facile fashion by anion exchange and further enhanced by molecular inclusion. We show how the exquisite control over bead size and shape enables extremely precise, quantitative measurements of anion- and solvent-induced volume transitions in these materials – a crucial feature driving

several important applications. Next, by exchanging diverse anions into the synthesized microgel beads, we demonstrate stimuli responsiveness and a multitude of functionalities including controlled release of chemical payloads, toxic metal removal from water and robust, reversible pH sensing.

## 4.2 Method Development

We employed a simple, robust droplet-based microfluidic method<sup>26, 37</sup> to fabricate highly monodisperse spherical PIL beads of varying average diameters in the sub-millimeter size range (200-1000  $\mu\text{m}$ ) for facile visual interrogation of their responses to various environmental stimuli (Figure 4.1).<sup>38</sup> We synthesized a doubly-alkenylated imidazolium bromide ionic liquid as the IL-monomer (Figure 4.1b). This IL monomer has two symmetrical polymerizable groups, with the C-2 position of the imidazolium ring blocked with a methyl group to avoid any C-2 deprotonation in the processed polymer (Appendix B- Figure B 4 and Figure B 5).<sup>39</sup> Additional advantages of this monomer included ease of preparation (see SI for experimental details) and solubility in water. We selected poly(ethyleneglycol) diacrylate (PEGDA) as a water-miscible cross-linker, which has been extensively used in polymeric microgels synthesis.<sup>26</sup> We optimized the compositions of the IL monomer, PEGDA, water and photoinitiator (Darocur 1173) (65, 18, 10 and 7% w/w, respectively) in the pre-polymer blend, such that the IL constituted the major component in the blend, sufficient PEGDA was present to promote rapid polymerization within typical microfluidic processing times ( $\sim 2$  mins) and phase separation of the water-immiscible photoinitiator was suppressed. Both carrier and dispersed fluids were continuously delivered into a PEEK cross-junction, using individual syringe pumps. We thereby controllably generated aqueous drops of polymer precursors in the immiscible carrier fluid

(silicone oil) within a transparent microfluidic capillary reactor, which were subsequently polymerized by UV irradiation (Figure 4.1a).

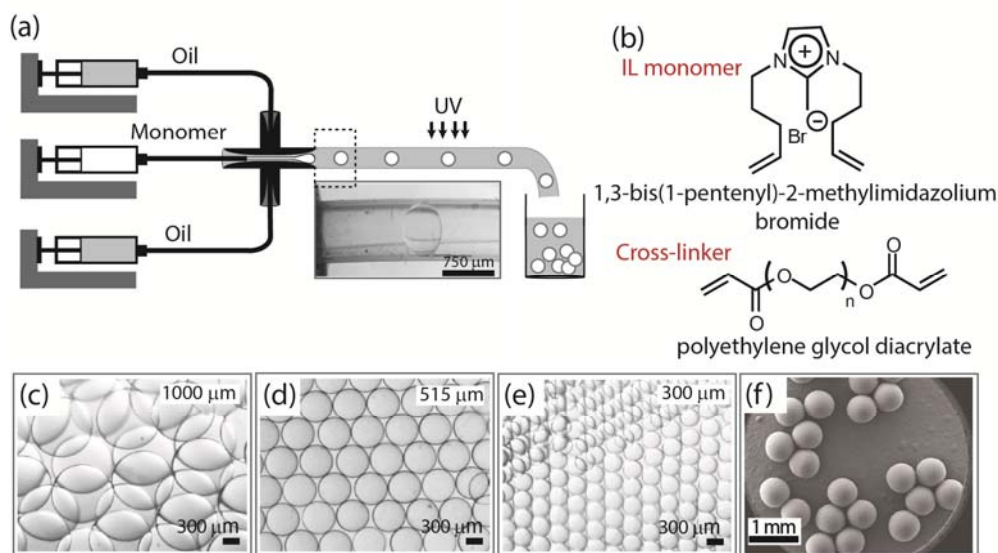


**Figure 4.1.** a) Schematics illustrating capillary-based microfluidic method to generate poly (ionic liquid) microgels; inset shows a stereomicroscope image of a pre-polymer droplet flowing in the transparent capillary tube. (b) Chemical structures of IL monomer and PEGDA crosslinker. (c-e) Stereomicroscope images of PIL microgels showing their monodispersity and transparency (average diameters of 1000 $\mu\text{m}$ , 515 $\mu\text{m}$ , 300 $\mu\text{m}$ , respectively). All scale bars are 300 $\mu\text{m}$ . (f) FESEM image of synthesized PIL[Br]. Scale bar is 1mm.

We obtained highly monodisperse PIL microgels at the exit of the reactor. The sizes of the resultant microgel beads could be tuned by choosing the appropriate monomer and external fluid flow rates and the internal diameters of the capillary tube (Figure 4.1c-e).<sup>26, 40-41</sup> The as-synthesized microbeads were sequentially washed with hexane, ethanol and water to remove any residual silicone oil or unreacted reagents. Microgel beads were of the same size in silicone oil, hexane and in the dried state while they swelled in ethanol and water; swollen PIL microbeads could revert back to the sizes of the first step when exposed to hexane or dried. The microbeads were sequentially and reversibly exposed to different solvents with a vacuum drying step between successive exposures, and it was found that the microbeads retained their

respective sizes in that solvent or at dried state. Hence, there was no discernible material loss due to washing.

## 4.3 Experimental Details

### 4.3.1 Materials

*IL monomer synthesis.* 5-bromo-1-pentene (Sigma-Aldrich, 95%), 2-methylimidazole (Fluka), potassium carbonate (Merck, 99%), acetonitrile (Fischer Scientific), diethyl ether (Merck), Magnesium sulfate (Sigma-Aldrich, 99%) *Microfluidic formation of PIL[Br] and PEGDA microgels.* Silicone oil (Dow Corning, 10cst), polyethylene glycol diacrylate or PEGDA (average Mn 700, Sigma-Aldrich), 2-hydroxy-2-methylpropiophenone (Darocur 1173, Sigma-Aldrich), absolute ethanol (Fisher Scientific, >99.8%), hexane (Fisher Scientific), MiliQ Water, PEEK microcross (P-891, IDEX health and science), PTFE tubing (0.3mm, 0.5mm, 1mm ID, 1/16" OD, Dibafit), UV irradiation source: Black light (Toshiba, Japan, 15 watt bulb, maxima at 365 nm). *Anion-dependent volume transitions.* PIL[Br] microgels, lithium bis(trifluoromethanesulfonyl)imide salt (Li[NTf<sub>2</sub>], Sigma-Aldrich), sodium chloride (NaCl, Sigma-Aldrich, ≥99.5%), sodium iodide (NaI, Sigma-Aldrich, ≥99.5%), ammonium perchlorate monohydrate (NH<sub>4</sub>ClO<sub>4</sub>, Sigma-Aldrich, ≥99.0%), ammonium persulfate ((NH<sub>4</sub>)<sub>2</sub>S<sub>2</sub>O<sub>8</sub>, Sigma-Aldrich, ≥98.0%), ammonium hexafluorophosphate (NH<sub>4</sub>PF<sub>6</sub>, Sigma-Aldrich, ≥98.0%), methyl orange (MO, Sigma-Aldrich, dye content 85%), lithium trifluoromethane sulfonate (LiTfO, Sigma-Aldrich, 96%), silver nitrate (AgNO<sub>3</sub>, Sigma-Aldrich, ≥ 99.0%). *Solvent-dependent volume transitions.* PEGDA microgels, absolute ethanol (Fisher Scientific, >99.8%), ethyl acetate (sigma Aldrich), acetonitrile (Fischer Scientific), hexane (Fisher

Scientific). *Stimulus (pH)- responsive chemical release*. Hydrochloric acid (37%, Merck). *Chemical separations- heavy metal removal*. Potassium dichromate ( $K_2Cr_2O_7$ , Sigma-Aldrich), disodium phosphate ( $Na_2HPO_4$ , Alfa Aesar), PILBr microgels. *Chemical sensing – pH*. PIL[Br] microgels, bromophenol blue (B.Ph.B., Sigma-Aldrich), thymol blue (Th.B., Sigma-Aldrich), bromothymol blue (B.Th.B., Sigma-Aldrich, Dye content 95%), bromocresol green (B.Cr.G., Sigma-Aldrich, Dye content 95%), bromocresol purple (B.Cr.P., Sigma-Aldrich, Dye content 90 %) and phenolphthalein (Ph., Sigma-Aldrich). In all cases MiliQ Water (18 MU cm, ELGA, Singapore) was used.

### **4.3.2 Ionic Liquid Monomer Synthesis**

In a 500 mL round bottom flask were taken 13.5 g (164 mmoles) of 2-methylimidazole, 50.0 g (336 mmoles, 2.0 equiv) of 5-bromo-1-pentene and 55 g (400 mmoles, 2.4 equiv) of potassium carbonate in 300 mL of acetonitrile. The mixture was vigorously stirred at 80 °C for 24 hours. After cooling to room temperature, the mixture was filtered to remove all inorganic salts (excess potassium carbonate and by-product potassium bromide). Then the filtrate was dried over magnesium sulfate to remove water and filtered again. This filtrate was dried in a rotary evaporator to remove all acetonitrile. A light yellow viscous ionic liquid is obtained which was washed with diethyl ether (each time 50 mL) to remove any unreacted starting materials. Finally this ionic liquid monomer was dried in vacuum for extended time (24 hours) to remove any trace of solvents. Yield of 1,3-bis(1-pentenyl)-2-methylimidazolium bromide ionic liquid monomer was 85%, based on 2-methylimidazole used.



### 4.3.3 Microfluidic Formation of PIL Microgels

We blended 1,3-bis(1-pentenyl)-2-methylimidazolium bromide ionic liquid monomer with aqueous PEGDA cross-linker and a photoinitiator (Darocur1173) in a ratio of IL monomer (65% w/w), PEGDA cross-linker (18% w/w), Darocur 1173 (7% w/w) and MilliQ Water (10% w/w) to formulate the monomer fluid. We controllably generated aqueous drops of monomer liquid in an immiscible carrier fluid (silicone oil, 10cst) inside a transparent microfluidic capillary reactor (Figure 4.1a), which were subsequently polymerized by UV irradiation (365 nm, 15 Watt bulb). The tubing was wrapped around the UV lamp to accommodate longer residence time at high flow rates and to provide homogenous UV exposure to the monomer droplets. We also used a small fan for cooling the UV-lamp to prevent any possible deformation of the tube due to heating. Individual syringe pumps (Harvard, PHD 2000) were used to deliver the carrier (Silicone oil) and dispersed (monomer blend) liquids to a PEEK cross-junction. The sizes of the resultant polymeric microgel beads could be tuned by choosing the appropriate monomer and carrier fluid flow rates and the internal diameters of the capillary tube (size range: 200-1000  $\mu\text{m}$ ). In all the applications presented in this paper, PIL microgels with average size of  $517 \pm 15 \mu\text{m}$  (in hydrated state) were utilized. Silicone oil with total flow rate of  $50 \mu\text{L}/\text{min}$  and monomer flow rate of  $0.5 \mu\text{L}/\text{min}$  were introduced to the PEEK cross-junction in order to achieve this size of microgels. The residence time for droplets of monomer blend in the UV-exposed environment was  $\sim 120 \text{ s}$  (flow speed  $\sim 0.003 \text{ ms}^{-1}$ ). During the continuous fabrication of PILs, the microbeads along with silicone oil were collected in a bottle. The as-synthesized microbeads were sequentially washed with hexane, ethanol and water, for 3 times with each solvent assisted by  $\sim 30 \text{ s}$  of vortex and 1 minute of sonication at each step, to remove any residual silicone oil and starting reagents.

#### **4.3.4 Microfluidic Formation of PEGDA Microgels**

The procedures to synthesize and wash the PEGDA microgels are same as the ones for PIL microgels, as described above, with only difference in the monomer composition. For fabrication of PEGDA microgels a solution of PEGDA (83% w/w), Darocur 1173 (7% w/w) as photo-initiator and MiliQ Water (10% w/w) is used as the dispersed phase.

#### **4.3.5 Characterization**

Structural characterization of synthesized IL monomer was carried out by <sup>1</sup>H and <sup>13</sup>C NMR (BRUKER, Model: AVANCE III 400). Synthesized PIL[Br] microgel beads were examined using CCD cameras (QImaging, MicroPublisher RTV 5.0 and Olympus, CAM-XC30) and stereomicroscopes (Olympus, SZX7 and 16SZ). Field emission scanning electron microscope (FESEM, JEOL 2011F) was used to determine the size and morphology of PIL materials. The complete polymerization and the presence of bromide and imidazolium group on the surface of PIL[Br] is supported by XPS, FTIR, elemental analysis and EDX analyses. X-ray Photoelectron Spectroscopy (XPS) analysis was carried out on an Axis Ultra DLD (Kratos) spectrometer with Al mono K $\alpha$  X-ray source (1486.71 eV photons) to determine the elements. All binding energies (BEs) were referenced to the C 1s neutral carbon peak at 284.6 eV. In XPS measurements, C-C, C-O, C-N bonds are identified along with the presence of bromide, suggesting the integration of imidazolium group and the counter anion into the polymeric material (Figure 4.11). Fourier Transform Infrared spectroscopy (FTIR) measurements were performed using a Perkin Elmer spectrometer (Model: Spectrum Two) with KBr as background over the range of 4000-400 cm<sup>-1</sup>. Elemental analyses were performed on a Perkin-Elmer PE 2400

CHNS Elemental Analyzer. Energy-Dispersive X-ray spectroscopy (EDX) analyses were carried out in Oxford Instruments INCA system (15 kV) coupled with a JEOL 6500F Field Emission Scanning Electron Microscope. The thermogravimetric analysis (TGA) was conducted on a TA instrument (Model: TA2050) to monitor the weight loss of dried PIL microgels and IL monomer under N<sub>2</sub> at temperatures from room temperature to 800 °C at a rate of 5 °C/min (Figure 4.11). FTIR, elemental analysis and EDX were also used to support the presence of exchanged anions in PIL[X] microbeads (Figure 4.12, Figure 4.13). Figure 4.13 also shows the presence of bromide in EDX analysis. The concentration of chromium in water was quantified by Inductively Coupled Plasma Mass Spectrometry (ICP-MS, Agilent Technologies, ICP-MS, 7500 series). XPS analysis was also used to support the exchange of bromide with Cr(VI) in heavy metal removal experiment (Figure 4.6).

#### **4.3.6 Anion-Dependent Microbead Sizes**

For chloride (Cl), iodide (I), trifluoromethane sulfonate (TfO), hexafluorophosphate (PF<sub>6</sub>), perchlorate (ClO<sub>4</sub>), and bis(trifluoromethane)sulfonamide (NTf<sub>2</sub>) anions: Approximately 200 PIL[Br] microbeads were taken with 2 mL of 2M aqueous solution of the corresponding salt (for example, NaCl for exchanging Br with Cl) and shaken for 12 hours. Supernatant solution was decanted. Ion exchanged beads were washed five times with water until the supernatant become chloride free (silver nitrate test). Then the PIL[X] beads were stored in 2 mL water.

For persulfate anion (S<sub>2</sub>O<sub>8</sub>): Approximately 200 PIL[Cl] (prepared from PIL[Br], by anion exchange with chloride as described above) microbeads were taken with 2 mL

of 2M aqueous solution of ammonium persulfate and shaken for 12 hours. The remaining procedures are the same as described above.

*For methyl orange (MO):* First a saturated solution of methyl orange in water was prepared by excess amount of solid methyl orange (1.0 g) in 25 mL of water. Supernatant was filtered out using a syringe filter (0.45  $\mu\text{m}$  pore size). To 100 PIL[Br] microbeads, 20 mL of saturated MO solution was added. The remaining procedures were same as described above, except washing with water required prolonged dialysis time to remove any MO that is physically entrapped (not ion exchanged) in the beads.

FTIR, Elemental analysis and EDX were used to support the presence of exchanged anions in PIL[X] microgels.

#### **4.3.7 Optical Microscopic Image Analysis of PIL Microgel Beads**

*Hydrated or solvated PIL microgels:* Circular PDMS Microwells (70 mm diameter and 3 mm depth) were made on glass slides by cutting circular holes on a PDMS slab and plasma bonded (Harrick Plasma) onto a clean glass slide. In each well were taken approximately 50 PIL beads with water or relevant solvents (ethanol, acetonitrile, ethyl acetate, hexane). After the beads attained equilibrium size (which requires only 1 min time) images were captured by a CCD camera (Olympus, CAM-XC30) mounted on Olympus 16SZX stereomicroscope and particles size determined by CellSense software. *Dry PIL microbeads:* water or other solvent was carefully removed from the well using a micropipette without taking the microbeads out. Microgel beads were then dried in vacuum and images recorded afterwards.

#### **4.3.8 Stimulus (pH)-Responsive Chemical Release**

In a microwell was taken single PIL[MO] bead with 100  $\mu$ L MiliQ water, the microbead was fully immersed in water. To it was added slowly 50  $\mu$ L of 1 M HCl solution in such a way not to displace or perturb the bead (final concentration of HCl = 0.33M, pH $\sim$ 0.5). Images were taken at regular intervals to profile the release of dye under acidic condition.

#### **4.3.9 Chemical Separations – Heavy Metal Removal**

Cr(VI) adsorption experiments were carried out using batch equilibrium technique in aqueous solution of potassium dichromate at pH 3 (adjusted by addition of HCl) and at room temperature. Briefly, 10 mL of Cr(VI) solution of different concentrations (i.e., 10 ppm to 250 ppm) were added to 15 mg of dried PIL[Br] beads and shaken in a thermostatic water-bath shaker at 200 rpm. The supernatant was analyzed by Inductive Coupled Plasma Mass Spectrometry (ICP-MS) to measure the concentration of Cr(VI) ions. For desorption studies, Cr(VI) was first adsorbed into the PIL[Br] microgels using 15 mg of dried PIL[Br] beads and 10 mL of 25 ppm Cr(VI) solution at pH 3. Desorption was then examined by adding 5 mL of either desorption eluents of 0.01 M NaOH or 0.2 M Na<sub>2</sub>HPO<sub>4</sub> to the metal-sorbed PIL beads. After shaking at 200 rpm for 4 hours, PIL microbeads were separated and the concentration of Cr(VI) ions in the supernatant was measured by ICP-MS. PIL microgels with dark yellow color after adsorption of Cr(VI), reverted to original colorless state after Cr(VI) desorption.

### 4.3.10 Chemical Sensing – pH

We used different types of pH indicator solutions (thymol blue, Th.B., 0.04% w/w; bromothymol blue, B.Th.B., 0.04% w/w; bromophenol blue, B.Ph.B., 0.04% w/w; bromocresol green, B.Cr.G., 0.04% w/w, bromocresol purple, B.Cr.P., 0.04% w/w, phenolphthalein, Ph., 0.1% in ethanol: water (1:1)). Six different sets of PIL[Br] microbeads separately doped with pH indicators were used and exposed to solutions of different pH (on a 24-well cell culture plate). A collection of all these bead types has a unique *collective* color signature between pH 1 to pH 11 (Figure 4.8a and Figure 4.9), very much akin to conventional pH-strips.

## 4.4 Results and Discussion

### 4.4.1 Anion-Dependent Volume Transitions

In the as-synthesized PILs, the imidazolium cations are fixed within the polymeric backbone while the bromide anions are labile. There is currently much interest in designing, understanding and exploiting the hydrogel volume transition in materials and biological applications.<sup>42</sup> In most studies, hydrogel volume transition in a particular environment is controlled by elaborate chemical optimizations - fine tuning of composition (monomers and cross-linker), extent of cross-linking, electrolyte dopants, surfactants etc. Clearly, the chemically and operationally simple procedure of labile anion exchange is a compelling alternative to tune hydrogel swelling or shrinkage. To accomplish this, we generated a diverse library of functional PIL beads by exchanging bromide with nine structurally and chemically diverse anions (chemical analyses validating anion exchange are provided in section title “Characterization”, Figure 4.12 and Figure 4.13), and examined how each anion

modified the size of parent PIL[Br] microgels under varying environments. Interestingly, for all anions tested the dried beads had very similar sizes ( $\sim 307 \pm 8$   $\mu\text{m}$ ) while large size variations (up to 38%) were observed in the hydrated state for different anions (Figure 4.2a,b). The microgel beads were highly monodisperse in all cases ( $\text{CV} < 3\%$ , Figure 4.3). The trends in Figure 4.2 can be rationalized by analyzing the relative hydrophilicity/phobicity of the PILs in terms of their free IL counterparts. Though cations play a significant role in determining the physico-chemical properties of ionic liquids, water content and relative hydrophilicity/phobicity are both principally dictated by the chemical nature of the anions.<sup>43-45</sup> Anionic radii, charge density (partial charge), polarizability and hydrogen-bond formation ability play significant roles in determining the extent of interaction and sorption of water in ILs. Differences in water sorption in molecular ionic liquids of up to 15% have been reported by varying the anions.<sup>43</sup> Halides are smaller than other polyatomic anions, possessing highly localized charge and hydrogen bonding capability; these features render PILs with halide anions most accommodating to water. In our case, the largest hydrogel diameter of PIL[Cl] microbeads can be attributed to the smallest size, high charge density and greater hydration enthalpy of Cl among all halides used.<sup>44</sup> Interestingly, identity of the constituent anion not only dictates the equilibrium diameter in the hydrated state, it also influences the time required for the attainment of swelling equilibrium. The hydration or swelling time for PIL microbeads presented in Figure 3b are 90 s for [Cl], 120 s for [Br], 135 s for [I], 150 s for [PF<sub>6</sub>], 180 s [ClO<sub>4</sub>] and [NTf<sub>2</sub>], and 225 s for [MO], indicating that different anion-water interactions can regulate both the kinetic and thermodynamic outcome of swelling.

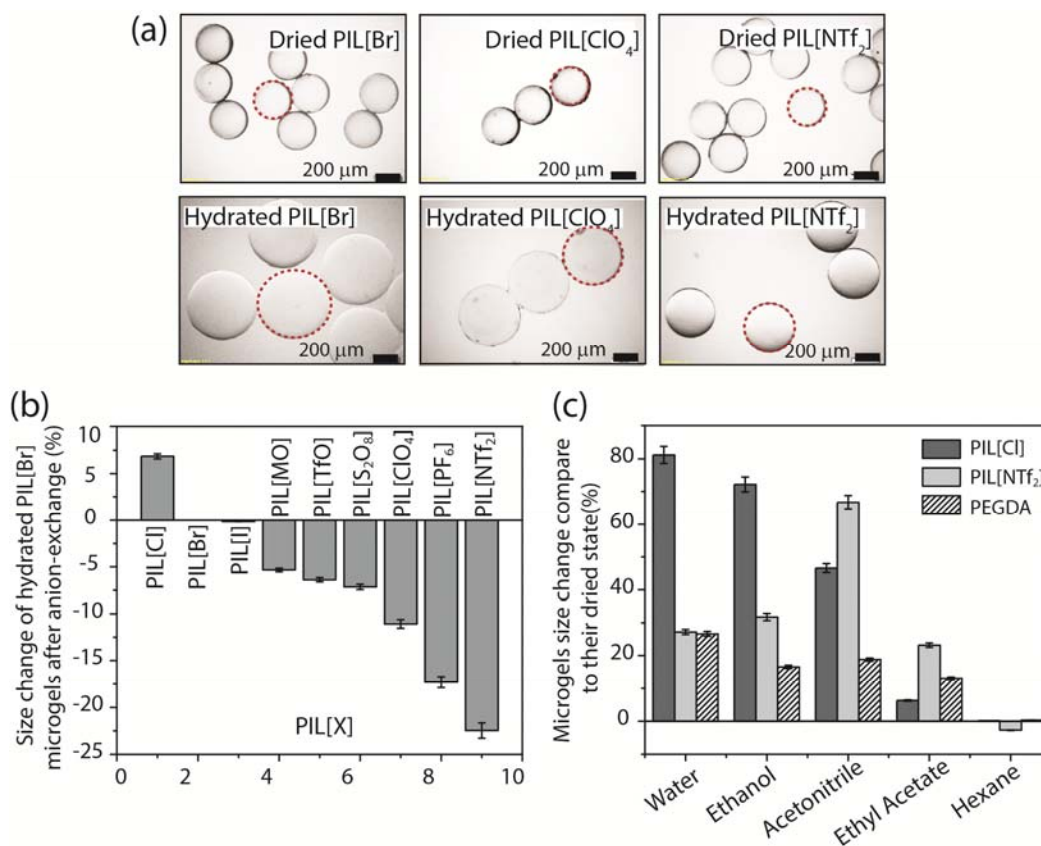


**Figure 4.2.** (a) Stereomicroscope images of samples of PIL[Br], PIL[ClO<sub>4</sub>] and PIL[NTf<sub>2</sub>] microgels with visibly similar sizes in the dried state and with distinct sizes in the hydrated state. All scale bars are 200 μm. (b) Plot of percentage size change (shrinkage/swelling) of hydrated PIL[Br] microgels after anion exchange with Cl<sup>-</sup>, I<sup>-</sup>, MO<sup>-</sup>, TfO<sup>-</sup>, (NH<sub>4</sub>)S<sub>2</sub>O<sub>8</sub><sup>-</sup>, ClO<sub>4</sub><sup>-</sup>, PF<sub>6</sub><sup>-</sup>, NTf<sub>2</sub><sup>-</sup>. (c) Plot of percentage size change of PIL[Cl], PIL[NTf<sub>2</sub>] and PEGDA microgels (compared to the dried state) in various solvents. 50 microbeads were used for each measurement.

We further investigated the influence of anions in solvent-induced volume transitions, taking presumably the most hydrophilic (PIL[Cl]) and most hydrophobic (PIL[NTf<sub>2</sub>]) microgel beads as model cases (Figure 4.2c). Both PIL[Cl] and PIL[NTf<sub>2</sub>] assume similar sizes in solvent free conditions (dried state) or in highly non-polar solvents such as hexane, while significant size differences (up to ~ 80%) are observed in weakly and strongly polar (both protic and aprotic) solvents (Figure 4.2c). The diffuse nature of negative charge, lack of strong H-bonding and lower hydration energy of PIL[NTf<sub>2</sub>] imply comparatively less swelling in water and ethanol compared to



PIL[Cl], in which the chloride anion can strongly interact via hydrogen bonding and dipole-dipole interactions.<sup>46</sup> Conversely, the non-polar nature of ethyl acetate, a low dielectric solvent (dielectric constant  $\sim 6.02$ ), implies that PIL[NTf<sub>2</sub>] swells more than PIL[Cl].<sup>47</sup> Interestingly, although acetonitrile is highly polar (dielectric constant  $\sim 37.5$ ), this aprotic solvent can interact with both the polar and non-polar parts of ionic liquids which makes acetonitrile highly soluble particularly in NTf<sub>2</sub>-based ILs.<sup>48</sup> Therefore PIL[NTf<sub>2</sub>] swells most in acetonitrile in our experiments, while the strong ion-pairing between imidazolium and chloride in PIL[Cl] cannot be significantly perturbed by acetonitrile, which has no hydrogen-bonding ability, thus resulting in less swelling compared to PIL[NTf<sub>2</sub>]. It is noteworthy, when homopolymerized PEGDA microgels are exposed to various solvents (as above), swelling varies only between  $\sim 10$ -30 % attesting to the fact that the constituent ionic liquid (and associated anion) plays the major role in dictating the volume transition of PIL beads. In summary, the above results highlight how our monodisperse microgel beads enable precise measurements on anion-dependent volume transitions, which can be subsequently employed in a number of application scenarios.

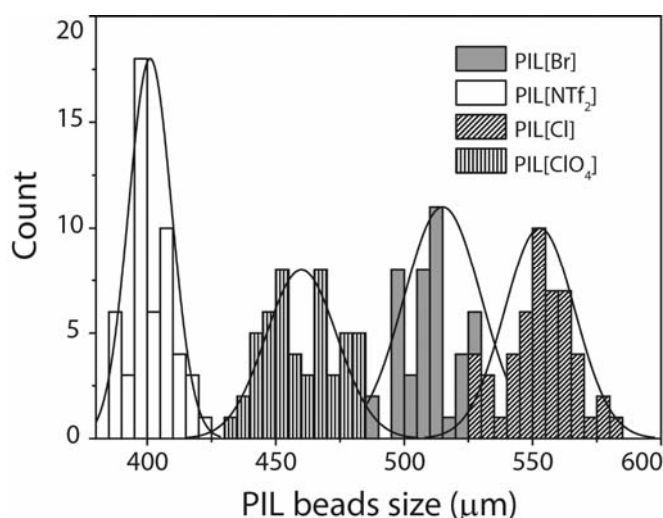


**Figure 4.3.** Histograms showing the monodispersity in the size of anion exchanged PIL microgels for the smallest PIL[NTf<sub>2</sub>], mid-size PIL[ClO<sub>4</sub>] and largest PIL[Cl] along with the parent PIL microgels PIL[Br].

#### 4.4.2 Stimulus (pH)-Responsive Chemical Release

To demonstrate pH-responsive chemical release, we incorporated methyl orange (MO) by anion exchange of Br with MO (validation of anion exchange by elemental analysis, FTIR and EDX of PIL[MO], Figure 4.12 and Figure 4.13). We chose MO as a highly colored dye for facile visual inspection. When PIL[MO] beads were exposed to ultrapure water, no visible leaching of MO was observed, attesting the fact that MO was bound within the PIL via ion-pairing. However, when the pH of the surrounding aqueous medium was lowered (pH  $\sim$  0.5) by adding HCl (pKa of methyl orange is 3.47), slow sustained release of MO into water was observed (Figure 4.4). After prolonged exposure ( $\sim$ 24 hrs) of the microbeads in HCl solution, they attained the original light yellow and transparent appearance, indicating complete release of the MO payload to the surrounding. EDX and Elemental Analysis of the obtained microgels showed complete absence of any residual sulphur (from MO or derivative). Prominent chloride peaks in EDX suggest that protonation of MO by HCl causes the slow release, where ion exchange between MO ion and chloride occurs to generate PIL[Cl]. The regular, symmetric bead shape enables quantitative measurement of MO diffusion kinetics into the surrounding medium - a valuable guide to understand the release profile for reactive molecules from such responsive materials. Figure 4.4b depicts measured diffusion profiles of MO from a PIL microgel bead to the surrounding environment at various times; such profiles naturally suggest the possibility of measuring and understanding transport within and from the gel. For example, one can fit the release kinetics to simple diffusive transport models. However, we note that the profiles in Figure 4.4b are not amenable to a simple, analytical transport analysis, due to its non-ideal geometry (sphere resting on a flat slab). A more 'ideal' geometry would be to cast the gel as a flat slab and make similar

measurements, as is common in hydrogel-based drug delivery. This system can be explored for similar pH-induced release of anionic drugs from the PIL matrix.<sup>24</sup>

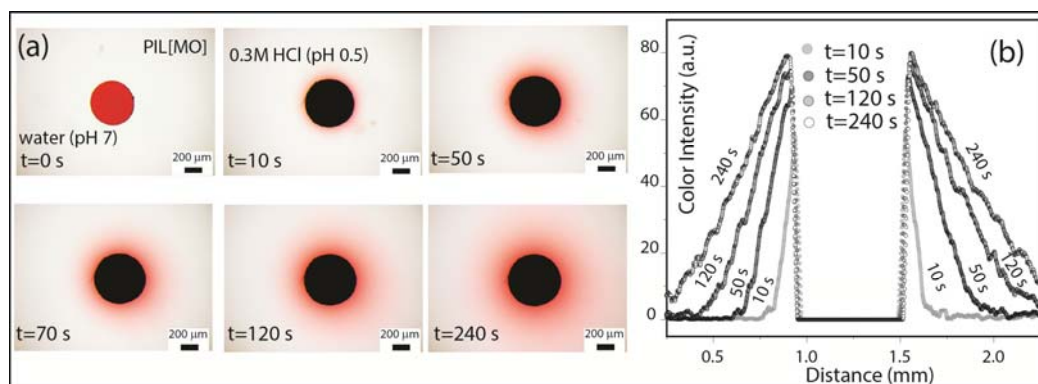


**Figure 4.4.** (a) Stereomicroscope images of PIL[MO] microbead at pH 7 and during controlled release of methyl orange from microbead to the surrounding medium at pH 0.5 (b) Measured diffusion profiles of MO from the PIL[MO] microbead to the surrounding environment. All scale bars are 200μm.

#### 4.4.3 Chemical Separations – Heavy Metal Removal

Removal of chromium in the form of hexavalent chromium has been a major focus of wastewater purification techniques<sup>49-50</sup> and ion exchange based adsorbents are widely used for this purpose.<sup>51-53</sup> The ability to rapidly exchange the parent bromide of as-synthesized PIL[Br] microgel beads with other anions, like toxic metal anions, can expand the application of these materials in separation and purification processes of toxic contaminants from water. In an appropriate pH-range (~ pH 3) chromium (VI) remain as negatively charged anions,  $\text{HCrO}_4^-$  and  $\text{Cr}_2\text{O}_7^{2-}$ , that can be easily exchanged with bromide ions and hence the toxic metal components can be removed from the aquatic system by ‘ion-entrapment’ (Figure 4.5 and Figure 4.6). The as-synthesized PIL microgels are capable of reaching 74 mg/g adsorption capacity in chromium (VI) removal from wastewater, and the adsorption isotherm shows excellent agreement with the theoretical Langmuir isotherm (Figure 4.5). Equilibrium

for chromium adsorption is reached within ~2 hrs. We briefly studied possible desorption routes to recover the adsorbed toxic metal ions from the PIL microbeads, which is essential for any potential regeneration of the adsorbent PIL microbeads. We found that dialysis of chromate-doped beads with 0.01 M NaOH or 0.2 M phosphate buffer ( $\text{Na}_2\text{HPO}_4$ ) enabled us to desorb 70% and 75% of the adsorbed chromate, respectively.

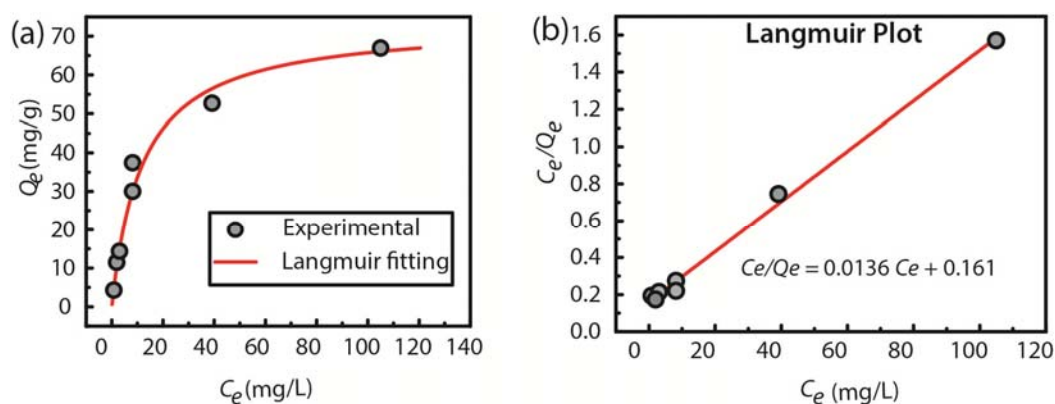


**Figure 4.5.** (a) Plot of chromium (VI) adsorption capacity ( $Q_e$ , Weight of adsorbed component, mg/ weight of adsorbent, g) versus  $C_e$ , concentration of potassium dichromate solution for both experimental data and Langmuir fitted curve, (b) Plot of  $C_e/Q_e$  at different concentrations of potassium dichromate solution.

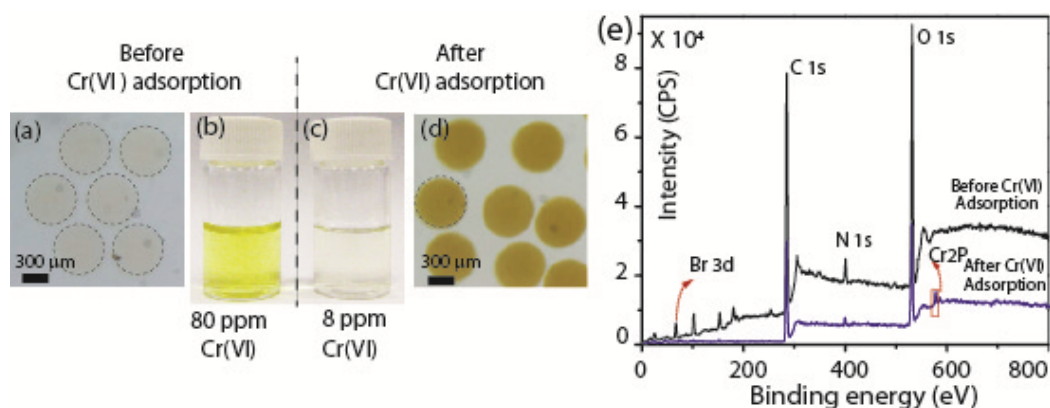


**Figure 4.6.** Adsorption of Cr(VI): (a) Colorless PIL[Br] microgels before any adsorption, (b) yellow color solution of 80 ppm Cr(VI) before the adsorption. (c) disappearance of yellow color of original Cr(IV) solution due to adsorption (d) dark yellow colored PIL microgels after adsorption of Cr(VI). (e) Br 3d peak is suppressed and Cr 2P peak is appeared in XPS spectra of PIL microgels after Cr(VI) adsorption.

#### 4.4.4 Chemical Sensing – pH

Finally, we demonstrate that PIL microgel beads can be used as solid-phase probes for robust and reversible pH sensing. Solid-phase immobilization of pH indicators is an active research area, particularly for pH measurements in biological systems. Such probes can non-invasively detect pH without chemical interference, thus being promising candidates for detection of, for example, extracellular pH gradients that are characteristics of tumor and wound environments and for investigation of the effect of pH on cellular migration.<sup>54</sup> Incorporation of pH indicator molecules into solid matrices typically requires chemical modification of both pH indicator and polymeric backbone<sup>55-58</sup> or physical doping into a polymeric gel.

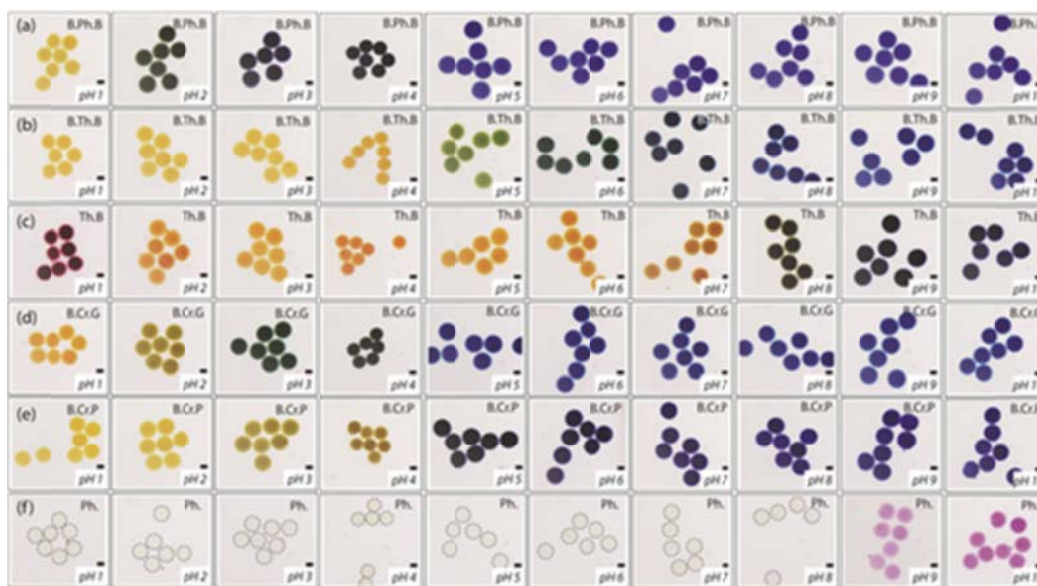


**Figure 4.7.** Six different sets of PIL[Br] microgels doped with their individual pH indicators, exposed to successive increments in pH. All scale bars are 300  $\mu\text{m}$ .

As ionic liquids are known to accommodate several polar and non-polar solute molecules, we opted to design PIL microgel-based pH sensors by stably doping small quantities of several commercially available pH indicators into the microbeads for

reversibly probing a wide range of pHs, with minimum or no leaching of the indicator into aqueous analyte solution. We separately doped PIL[Br] microbeads with six different pH indicators to cover a wide range of pHs. Doping required less than 10 s and no leaching was observed after several washing steps. When each category of PIL-indicator beads was exposed to solutions with varying pH, distinct colors were observed within the beads with negligible indicator leaching (A matrix of images for individual indicators, Figure 4.7).

We constructed a simple bead-based pH-strip with an assortment of six pairs of different indicator-doped microgel beads (Figure 4.8). Upon exposure to different pH environments these beads assumed a distinct, uniquely pH-dependent band of colors, very much analogous to commercial pH-strips (Figure 4.8a).

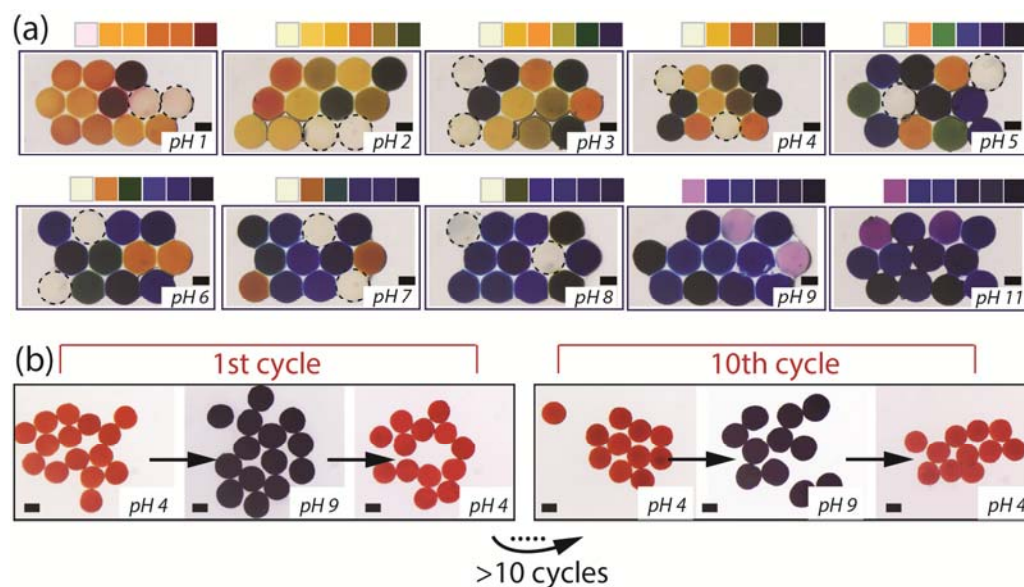


**Figure 4.8.** Reversible and recyclable pH-Strip with PIL microgels. (a) *3D pH Strip*: an assortment of six pairs of different pH indicator-doped PIL microgels (two beads each contain the same pH indicator) are exposed to different pH solutions iteratively. (b) *Reversible pH sensing*: pH indicator (Thymol blue)-doped PIL microgels colorimetrically respond to the pH of the surrounding medium in a reversible fashion. The reversibility has been successfully tested for at least 10 cycles without any performance lost. All scale bars are 300 $\mu$ m.

An elegant and unique feature of these pH-indicator microgel beads is that they respond reversibly to the switching of pH environments. As shown in Figure 4.8b, Thymol blue-doped PIL microgels can be switched between pHs 4 and 9 ten times without any leaching or compromised performance (in terms of color intensity and response time). Such reversible, reusable and non-invasive pH sensing, unlike the conventional method of doping soluble pH indicator into the analyte solution, may pave the way for monitoring biological or other sensitive samples where cross-contamination by the indicator itself could be detrimental. Stable confinement of the indicator dye molecules within the PIL matrix can be attributed to electrostatic interactions between the ionizable indicator molecules and imidazolium groups, as well as to the hydrophobic interaction of alkyl (-CH<sub>2</sub>- groups) side chains of the ionic liquid segments with the non-polar moieties (alkyl and aromatic) of the indicators.<sup>60</sup> Such interactions are not present within PEGDA microbeads, thus explaining the differences in indicator retention from the PIL[Br] beads. During indicator doping, PIL microgel beads show visible, nearly instantaneous (~ seconds) color change when exposed to indicator solutions, and the indicator is retained stably (at pH 7) within the beads over several months. In contrast, PEGDA microbeads do not show a distinct color change even after hours of exposure to indicator solution, and the indicators leach out while stored in neutral water (within ~24 hrs). Moreover, upon exposing indicator-doped PIL microbeads to a solution of controlled pH in a small microwell, mild pipette tip-aided stirring results in rapid response of PILs to the surrounding pH (seconds to minutes), while PEGDA beads respond to pH change on a time scale of minutes to hours under similar conditions. Specific response times vary within these ranges, depending on the indicator used and pH level. Response time for such sensing can be very crucial should these beads be used in flow-cell based sensing devices.

Thus, we believe the ionic liquid motif is essential for the stable doping and quick and reversible sensing of the pH. Further along similar lines, we also demonstrate a capillary-based 3D pH-strip for iterative pH analyses, where PIL microgels are embedded inside a glass-capillary and are exposed to flowing solutions with varying pH (Figure 4.9).

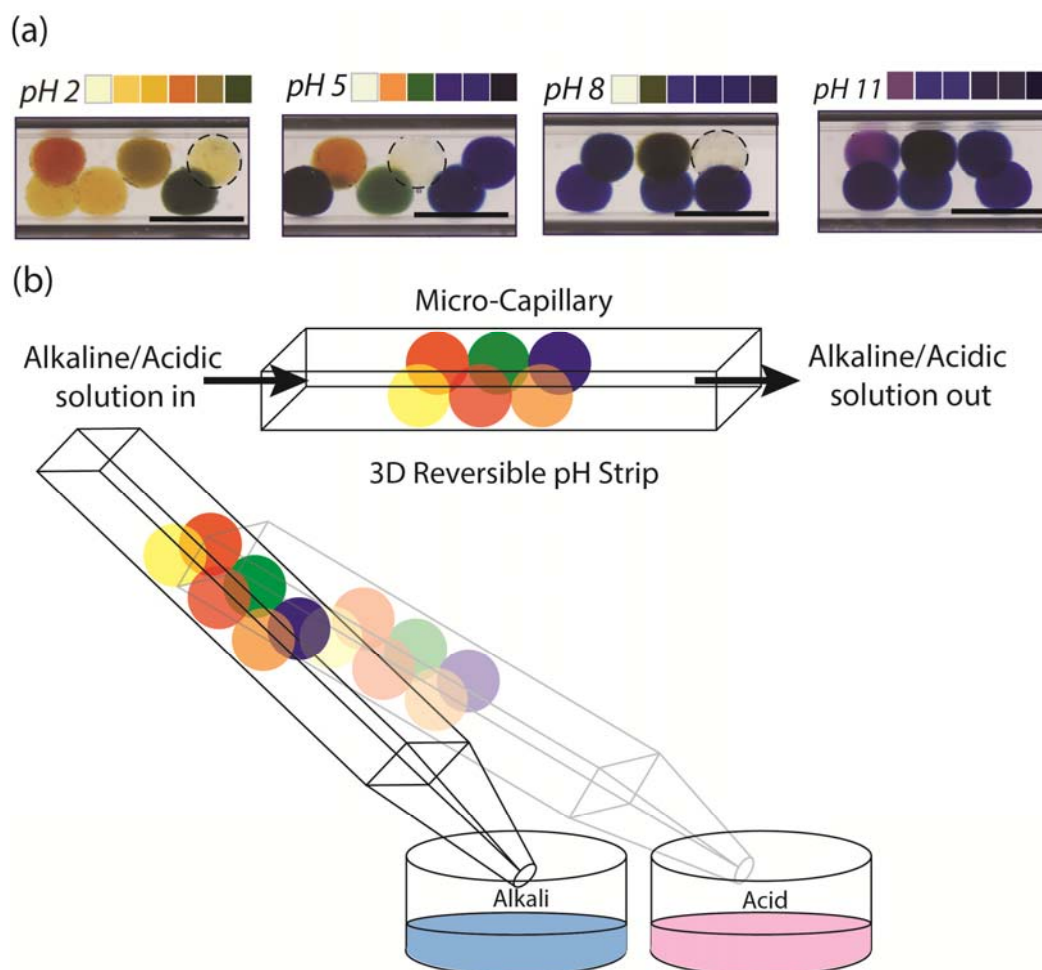


**Figure 4.9.** Capillary-based reversible pH sensing using 3D-structured PIL microgels. (a) Stereomicroscope images of 6 microgel beads containing individual pH indicators, embedded in a glass capillary with square cross-section, which is successively exposed to flowing solutions of different pH. (b) Concept of a capillary-based 3D pH-strip for reversible pH analysis. All scale bars are 1mm.



#### 4.4.5 Characterization

Structural characterization of synthesized IL monomer was carried out by  $^1\text{H}$  and  $^{13}\text{C}$  NMR (Appendix B, Figure B 4 and Figure B 5) and chemical composition was confirmed by elemental analysis:  $^1\text{H}$  NMR (400 MHz, DMSO- $d_6$ ,  $\delta$ ): 7.74 (s, 2H, Ar H), 8.25 (m, 2H, 2x -HC=CH<sub>2</sub>), 5.04 (m, 4H, 2x -HC=CH<sub>2</sub>), 4.12 (m, 4H, 2x -CH<sub>2</sub>-), 2.63 (s, 3H, CH<sub>3</sub>), 2.06 (m, 4H, 2x -CH<sub>2</sub>-), 1.84 (m, 4H, 2x -CH<sub>2</sub>-),  $^{13}\text{C}$  NMR (100 MHz, DMSO- $d_6$ ,  $\delta$ ): 143.8 (Ar C), 137.1 (-HC=CH<sub>2</sub>), 121.3 (Ar C), 115.6 (-HC=CH<sub>2</sub>), 47.0 (-CH<sub>2</sub>-), 29.7 (-CH<sub>2</sub>-), 28.0 (-CH<sub>2</sub>-), 0.4 (-CH<sub>3</sub>), elemental analysis (Anal. Calcd.) for C<sub>14</sub>H<sub>23</sub>N<sub>2</sub>Br: C 56.00, H 7.75, N 9.36, Br 26.72; found: C 55.54, H 7.97, N 9.39, Br 29.68.  $^1\text{H}$  NMR clearly shows the diagnostic peaks for unsaturation (-CH=CH<sub>2</sub>) at 8.25 and 5.04 ppm, whereas singlet at 7.74 ppm corresponds to imidazolium protons from the ionic liquid structure. This assertion about structure is further corroborated by  $^{13}\text{C}$  NMR showing peaks at 143.8 and 121.3 ppm for imidazolium group where signals at 137.1 ppm and 115.6 ppm correspond to the carbon-carbon unsaturation (-HC=CH<sub>2</sub>).

Chemical and physical characterization of PIL microbeads was carried out via several complementary techniques SEM (Figure 4.1f), EDX, XPS (Figure 4.11b and Figure 4.13), and FTIR (Figure 4.10). FTIR measurements indicated nearly complete attenuation of characteristic peaks due to monomer units (both from ionic liquid and PEGDA) in the polymer matrix (Figure 4.10), from which we inferred successful copolymerization of ionic liquid monomer with PEGDA. In XPS measurements, C-C, C-O, C-N bonds were identified along with the presence of bromide, suggesting the integration of imidazolium group and the counter anion into the polymeric material. Elemental analysis of the hydrogel beads showed that the IL motif constitutes ~60%

of the total mass of the bulk material, with ~10% of entrapped water and other volatiles as measured by thermogravimetric analysis (TGA, Figure 4.11a). Presence of the constituent anion of PIL, in this case bromide, on the particle surface was validated via energy dispersive X-ray spectroscopy (EDX) analysis. The as-synthesized PIL microgels also showed high thermal stability of up to 230 °C which is comparable to the parent ionic liquid monomer (Figure 4.11a).

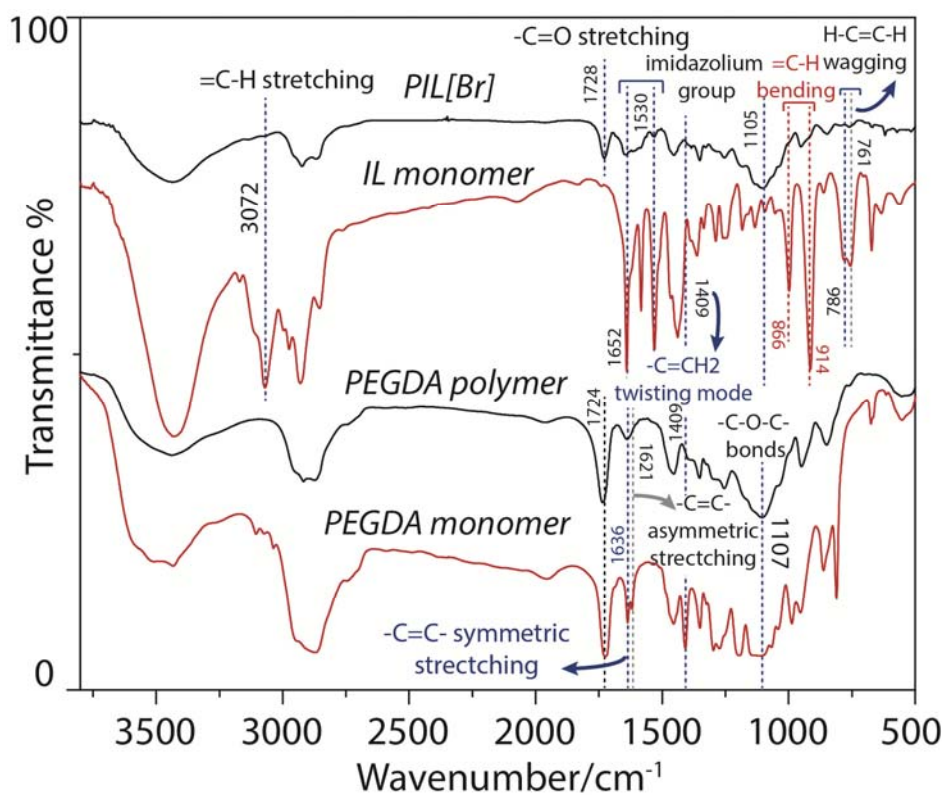


**Figure 4.10.** FTIR spectra of PEGDA monomer, PEGDA polymer, IL monomer and poly(ionic liquid) PIL[Br].

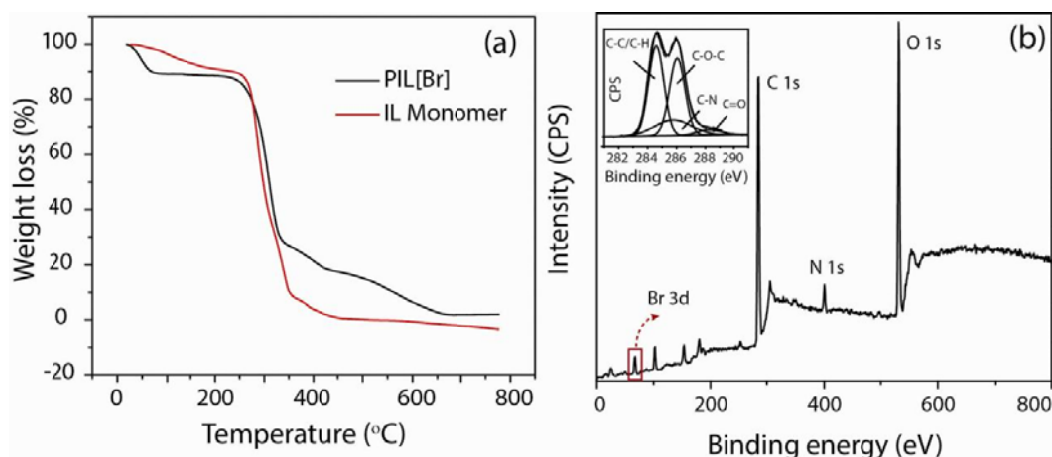


**Figure 4.11.** a) TGA curves for both PIL[Br] and IL monomer show similar primary decomposition temperatures ( $\sim 230^\circ\text{C}$ ). The secondary decomposition temperature of PIL[Br] at  $\sim 330^\circ\text{C}$  indicates improvement of thermal stability presumably due to crosslinking. b) XPS spectra show the presence of C-C, C-O, C-N bonds; thereby, integration of imidazolium group into the polymeric material, and the presence of counter anion, bromide, in the synthesized polymer PIL[Br].

FTIR, Elemental analysis and EDX were used to support the presence of exchanged anions in PIL[X] microgels.

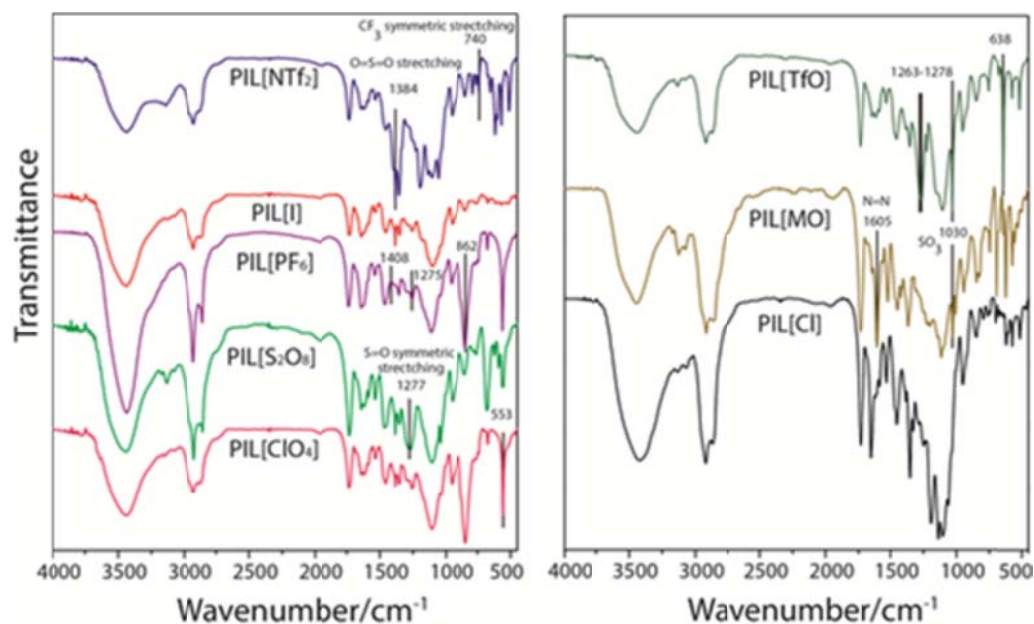


**Figure 4.12.** FTIR spectra and the corresponding signature peaks for PIL[NTf<sub>2</sub>], PIL[I], PIL[PF<sub>6</sub>], PIL[S<sub>2</sub>O<sub>8</sub>], PIL[ClO<sub>4</sub>], PIL[TfO], PIL[MO] and PIL[Cl].

Monomers	Polymeric material PILBr
<p><u>Ionic Liquid :</u></p> <p><i>Polymerizable alkene (C=C) bond:</i>  3072 cm<sup>-1</sup> (=C-H stretching)  998 cm<sup>-1</sup> and 914 cm<sup>-1</sup> (Out-of-plane =C-H bending)  786 cm<sup>-1</sup> and 761 cm<sup>-1</sup> doublet (H-C=C-H wagging)</p> <p><i>Imidazolium group:</i>  1652 cm<sup>-1</sup> and 1530 cm<sup>-1</sup></p>	<p>Almost completely attenuated; indicating significant participation of alkene groups in polymerization</p> <p>present in the polymer, indicating imidazolium group incorporation into the polymer matrix</p>
<p><u>Polyethyleneglycol diacrylate (PEGDA):</u></p> <p><i>Polymerizable alkene (C=C) bond:</i>  1636 cm<sup>-1</sup> (C=C symmetric stretching)  1621 cm<sup>-1</sup> (asymmetric stretching )  1409 cm<sup>-1</sup> (-C=CH<sub>2</sub> twisting)</p> <p><i>Carbonyl group (C=O) and C-O-C groups:</i>  1728 cm<sup>-1</sup> (C=O stretching)  1107 cm<sup>-1</sup> (C-O-C stretching)</p>	<p>significantly diminished or disappeared</p> <p>present as prominent peaks, suggesting incorporation of PEGDA</p>

**Table 4.1.** Comparison between the monomers and the polymerized product.

FTIR traces for other halides such as PIL[Cl] and PIL[I] exhibited almost identical peaks as of PIL[Br] as expected. However, when the bromide of PIL[Br] was exchanged with other functional anions, several new characteristic peaks appeared corresponding to the anion used (Table 4.2).

The amount of bromide present in the bulk PIL microbeads, before and after anion exchange, was investigated by elemental analysis. (PIL[Br] microgels: Bromide (Br) content was measured as 16.65% of the total mass. PIL[MO]: Br content reduced to 0.36% due to ion exchange.

Anion	Characteristic peaks
NTf <sub>2</sub>	1384 cm <sup>-1</sup> (SO <sub>2</sub> stretching ), 848 cm <sup>-1</sup> , 740 cm <sup>-1</sup> (CF <sub>3</sub> stretching)
PF <sub>6</sub>	862 cm <sup>-1</sup> (PF <sub>6</sub> assym stretching)
S <sub>2</sub> O <sub>8</sub>	1277 cm <sup>-1</sup> ( S=O symmetric stretching)
TfO	1263-1278 cm <sup>-1</sup> (S=O symmetric stretching), 1030 cm <sup>-1</sup> (SO <sub>3</sub> symmetric stretching), 638 cm <sup>-1</sup> (SO <sub>3</sub> asymmetric stretching).
ClO <sub>4</sub>	553 cm <sup>-1</sup>
MO	1605 cm <sup>-1</sup> (N=N stretching)), 1030 cm <sup>-1</sup> (SO <sub>3</sub> symmetric stretching)

**Table 4.2.** Characteristic peaks for the corresponding anions in ion-exchanged PIL microbeads.

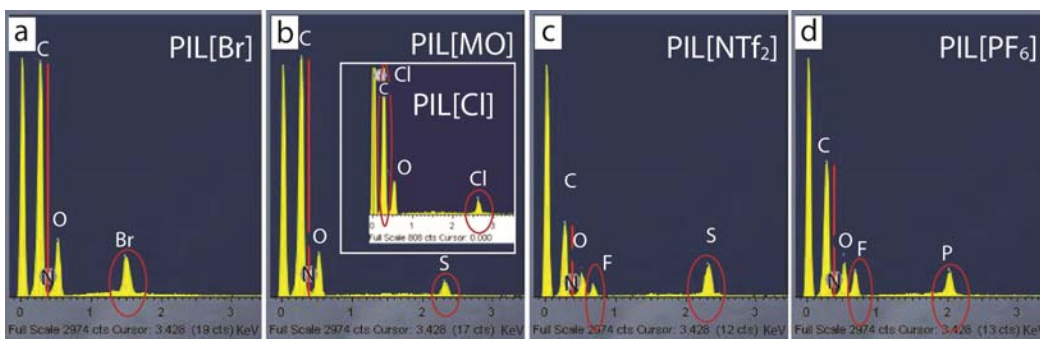


**Figure 4.13.** EDX analysis confirm the exchange of parent anion, [Br], with anions such as [MO]<sup>-</sup>, [NTf<sub>2</sub>]<sup>-</sup> and [PF<sub>6</sub>]<sup>-</sup>. The EDX spectra show the presence of characteristic element(s) on the respective beads (a) Bromide 'Br' on the surface of PIL[Br] (b) Sulfur 'S' on PIL[MO] (inset: EDX spectra of PIL microbead after HCl induced slow release of MO; absence of the sulfur peak and prominent 'Cl' peaks indicate the ion exchange of MO with Cl) (c) Sulfur 'S' and Fluorine 'F' for PIL[NTf<sub>2</sub>] (d) Fluorine 'F' and Phosphorus 'P' on the surface of PIL[PF<sub>6</sub>].

#### 4.4.6 Summary

In conclusion, we employ a simple and inexpensive microfluidic method to fabricate monodisperse spherical polymeric ionic liquid microgel beads. We demonstrate how simple anion exchange can enable fine-tuning of size and swellability of these beads. By incorporating diverse anions, we are able to impart a multitude of functionalities to these beads, ranging from controlled-release of payload, toxic metal removal and robust, reversible pH sensing. We envision that these chemically switchable stimulus-responsive beads will open up a vast array of potential applications in portable and preparative chemical analysis, separations and spatially addressed sensing. They can, for example, be geometrically arrayed as 1D or 2D matrices to perform cascades of chemical reactions, separation and sensing in integrated, flow-through fashion by judiciously choosing the anions for each operation.

## 4.5 References

1. Hallett, J. P.; Welton, T., Room-temperature ionic liquids: solvents for synthesis and catalysis. 2. *Chemical Reviews* **2011**, *111* (5), 3508-3576.
2. van Rantwijk, F.; Sheldon, R. A., Biocatalysis in ionic liquids. *Chemical Reviews* **2007**, *107* (6), 2757-2785.
3. Chum, H. L.; Koch, V. R.; Miller, L. L.; Osteryoung, R. A., Electrochemical scrutiny of organometallic iron complexes and hexamethylbenzene in a room temperature molten salt. *Journal of the American Chemical Society* **1975**, *97* (11), 3264-3265.
4. Armand, M.; Endres, F.; MacFarlane, D. R.; Ohno, H.; Scrosati, B., Ionic-liquid materials for the electrochemical challenges of the future. *Nat Mater* **2009**, *8* (8), 621-629.
5. MacFarlane, D. R.; Forsyth, M.; Howlett, P. C.; Pringle, J. M.; Sun, J.; Annat, G.; Neil, W.; Izgorodina, E. I., Ionic liquids in electrochemical devices and processes: managing interfacial electrochemistry. *Accounts Chem. Res.* **2007**, *40* (11), 1165-1173.
6. Hapiot, P.; Lagrost, C., Electrochemical Reactivity in Room-Temperature Ionic Liquids. *Chemical Reviews* **2008**, *108* (7), 2238-2264.
7. Ohno, H., Functional design of ionic liquids. *Bulletin of the Chemical Society of Japan* **2006**, *79* (11), 1665-1680.
8. Hardacre, C.; Holbrey, J. D.; Nieuwenhuyzen, M.; Youngs, T. G. A., Structure and Solvation in Ionic Liquids. *Accounts Chem. Res.* **2007**, *40* (11), 1146-1155.
9. Chiappe, C.; Pieraccini, D., Ionic liquids: solvent properties and organic reactivity. *Journal of Physical Organic Chemistry* **2005**, *18* (4), 275-297.
10. Le Bideau, J.; Viau, L.; Vioux, A., Ionogels, ionic liquid based hybrid materials. *Chemical Society Reviews* **2011**, *40* (2), 907-925.
11. Klingshirn, M. A.; Spear, S. K.; Subramanian, R.; Holbrey, J. D.; Huddleston, J. G.; Rogers, R. D., Gelation of Ionic Liquids Using a Cross-Linked Poly(Ethylene Glycol) Gel Matrix. *Chemistry of Materials* **2004**, *16* (16), 3091-3097.
12. Visentin, A. F.; Panzer, M. J., Poly(Ethylene Glycol) Diacrylate-Supported Ionogels with Consistent Capacitive Behavior and Tunable Elastic Response. *ACS Applied Materials & Interfaces* **2012**.
13. Néouze, M.-A.; Bideau, J. L.; Gaveau, P.; Bellayer, S.; Vioux, A., Ionogels, New Materials Arising from the Confinement of Ionic Liquids within Silica-Derived Networks. *Chemistry of Materials* **2006**, *18* (17), 3931-3936.

14. Vioux, A.; Viau, L.; Volland, S.; Le Bideau, J., Use of ionic liquids in sol-gel; ionogels and applications. *Comptes Rendus Chimie* **2010**, *13* (1–2), 242-255.
15. Kavanagh, A.; Byrne, R.; Diamond, D.; Fraser, K. J., Stimuli Responsive Ionogels for Sensing Applications—An Overview. *Membranes* **2012**, *2* (1), 16-39.
16. He, Y.; Lodge, T. P., A thermoreversible ion gel by triblock copolymer self-assembly in an ionic liquid. *Chemical Communications* **2007**, (26), 2732-2734.
17. Lu, J.; Yan, F.; Texter, J., Advanced applications of ionic liquids in polymer science. *Progress in Polymer Science* **2009**, *34* (5), 431-448.
18. Mecerreyes, D., Polymeric ionic liquids: Broadening the properties and applications of polyelectrolytes. *Progress in Polymer Science* **2011**, *36* (12), 1629-1648.
19. Yuan, J. Y.; Antonietti, M., Poly(ionic liquid)s: Polymers expanding classical property profiles. *Polymer* **2011**, *52* (7), 1469-1482.
20. Green, O.; Grubjesic, S.; Lee, S.; Firestone, M. A., The Design of Polymeric Ionic Liquids for the Preparation of Functional Materials. *Polymer Reviews* **2009**, *49* (4), 339-360.
21. Chen, H.; Elabd, Y. A., Polymerized Ionic Liquids: Solution Properties and Electrospinning. *Macromolecules* **2009**, *42* (9), 3368-3373.
22. Nakashima, K.; Kamiya, N.; Koda, D.; Maruyama, T.; Goto, M., Enzyme encapsulation in microparticles composed of polymerized ionic liquids for highly active and reusable biocatalysts. *Organic & Biomolecular Chemistry* **2009**, *7* (11), 2353-2358.
23. López, M.; Mecerreyes, D.; López-Cabarcos, E.; López-Ruiz, B., Amperometric glucose biosensor based on polymerized ionic liquid microparticles. *Biosensors & bioelectronics* **2006**, *21* (12), 2320-2328.
24. Cui, W.; Lu, X.; Cui, K.; Niu, L.; Wei, Y.; Lu, Q., Dual-Responsive Controlled Drug Delivery Based on Ionically Assembled Nanoparticles. *Langmuir* **2012**, *28* (25), 9413-9420.
25. Xiong, Y.-B.; Wang, H.; Wang, Y.-J.; Wang, R.-M., Novel imidazolium-based poly(ionic liquid)s: preparation, characterization, and absorption of CO<sub>2</sub>. *Polymers for Advanced Technologies* **2012**, *23* (5), 835-840.
26. Dendukuri, D.; Doyle, P. S., The Synthesis and Assembly of Polymeric Microparticles Using Microfluidics. *Advanced Materials* **2009**, *21* (41), 4071-4086.
27. Hwang, D. K.; Oakey, J.; Toner, M.; Arthur, J. A.; Anseth, K. S.; Lee, S.; Zeiger, A.; Van Vliet, K. J.; Doyle, P. S., Stop-Flow Lithography for the Production of Shape-Evolving Degradable Microgel Particles. *Journal of the American Chemical Society* **2009**, *131* (12), 4499-4504.



28. Seiffert, S.; Weitz, D. A., Microfluidic fabrication of smart microgels from macromolecular precursors. *Polymer* **2010**, *51* (25), 5883-5889.
29. Batra, D.; Hay; Firestone, M. A., Formation of a Biomimetic, Liquid-Crystalline Hydrogel by Self-Assembly and Polymerization of an Ionic Liquid. *Chemistry of Materials* **2007**, *19* (18), 4423-4431.
30. Suarez, I. J.; Sierra-Martin, B.; Fernandez-Barbero, A., Swelling of ionic and non-ionic minigels. *Colloids and Surfaces A: Physicochemical and Engineering Aspects* **2009**, *343* (1-3), 30-33.
31. Texter, J., Anion Responsive Imidazolium-Based Polymers. *Macromolecular Rapid Communications* **2012**, *33* (23), 1996-2014.
32. Suárez, I. n. J.; Rubio-Retama, J.; Sierra-Martín, B. n.; Javier de las Nieves, F.; Mecerreyes, D.; López-Cabarcos, E.; Márquez, M.; Fernández-Barbero, A., Ion-Specific and Reversible Wetting of Imidazolium-Based Minigels. *The Journal of Physical Chemistry B* **2008**, *112* (35), 10815-10820.
33. Tokuda, M.; Minami, H.; Mizuta, Y.; Yamagami, T., Preparation of Micron-Sized Monodisperse Poly(ionic liquid) Particles. *Macromolecular Rapid Communications* **2012**, *33* (13), 1130-1134.
34. Muldoon, M. J.; Gordon, C. M., Synthesis of gel-type polymer beads from ionic liquid monomers. *Journal of Polymer Science Part A: Polymer Chemistry* **2004**, *42* (15), 3865-3869.
35. Yuan, J.; Antonietti, M., Poly(ionic liquid) Latexes Prepared by Dispersion Polymerization of Ionic Liquid Monomers. *Macromolecules* **2011**, *44* (4), 744-750.
36. Marcilla, R.; Sanchez-Paniagua, M.; Lopez-Ruiz, B.; Lopez-Cabarcos, E.; Ochoteco, E.; Grande, H.; Mecerreyes, D., Synthesis and characterization of new polymeric ionic liquid microgels. *Journal of Polymer Science Part A: Polymer Chemistry* **2006**, *44* (13), 3958-3965.
37. Tumarkin, E.; Kumacheva, E., Microfluidic generation of microgels from synthetic and natural polymers. *Chemical Society Reviews* **2009**, *38* (8), 2161-2168.
38. Barikbin, Z.; Rahman, M. T.; Jardeh, D.; Badruddoza, M. A. Z.; Doyle, S. P.; Khan, S. A., Microfluidic fabrication of polymerized ionic liquid microgels. *Proceedings of MicroTAS 2012, Okinawa* (Japan), 1786-1788.
39. Sowmiah, S.; Srinivasadesikan, V.; Tseng, M.-C.; Chu, Y.-H., On the chemical stabilities of ionic liquids. *Molecules* **2009**, *14* (9), 3780-3813.
40. Kumacheva, E.; Garstecki, P., Microfluidic reactors for polymer particles. *John Wiley & Sons, Ltd*, **2011**, *Chichester* (UK), Ch. 8.
41. Wang, J.T.; Wang, J.; Han, J.J., Fabrication of advanced particles and particle-based materials assisted by droplet-based microfluidics. *Small* **2011**, *7* (13), 1728-1754.

42. Wu, S.; Li, H.; Chen, J. P.; Lam, K. Y., Modeling Investigation of Hydrogel Volume Transition. *Macromolecular Theory and Simulations* **2004**, *13* (1), 13-29.
43. Cao, Y.; Chen, Y.; Sun, X.; Zhang, Z.; Mu, T., Water sorption in ionic liquids: kinetics, mechanisms and hydrophilicity. *Physical Chemistry Chemical Physics* **2012**, *14* (35), 12252-12262.
44. Klähn, M.; Stüber, C.; Seduraman, A.; Wu, P., What Determines the Miscibility of Ionic Liquids with Water? Identification of the Underlying Factors to Enable a Straightforward Prediction. *The Journal of Physical Chemistry B* **2010**, *114* (8), 2856-2868.
45. Cammarata, L.; Kazarian, S. G.; Salter, P. A.; Welton, T., Molecular states of water in room temperature ionic liquids. *Physical Chemistry Chemical Physics* **2001**, *3* (23), 5192-5200.
46. Chiappe, C.; Malvaldi, M.; Pomelli, C. S., Ionic liquids: Solvation ability and polarity. *Pure and Applied Chemistry* **2009**, *81* (4), 767-776.
47. Bonhote, P.; Dias, A.-P.; Papageorgiou, N.; Kalyanasundaram, K.; Gratzel, M., Hydrophobic, Highly Conductive Ambient-Temperature Molten Salts. *Inorganic Chemistry* **1996**, *35* (5), 1168-1178.
48. Bardak, F.; Xiao, D.; Hines, L. G.; Son, P.; Bartsch, R. A.; Quitevis, E. L.; Yang, P.; Voth, G. A., Nanostructural Organization in Acetonitrile/Ionic Liquid Mixtures: Molecular Dynamics Simulations and Optical Kerr Effect Spectroscopy. *Chemphyschem* **2012**, *13* (7), 1687-1700.
49. Mohan, D.; Singh, K. P.; Singh, V. K., Removal of Hexavalent Chromium from Aqueous Solution Using Low-Cost Activated Carbons Derived from Agricultural Waste Materials and Activated Carbon Fabric Cloth. *Industrial & Engineering Chemistry Research* **2005**, *44* (4), 1027-1042.
50. Hu, J.; Chen, G.; Lo, I. M. C., Removal and recovery of Cr(VI) from wastewater by maghemite nanoparticles. *Water Research* **2005**, *39* (18), 4528-4536.
51. Cao, C.-Y.; Qu, J.; Yan, W.S.; Zhu, J.F.; Wu, Z.Y.; Song, W.G., Low-Cost Synthesis of Flowerlike  $\alpha$ -Fe<sub>2</sub>O<sub>3</sub> Nanostructures for Heavy Metal Ion Removal: Adsorption Property and Mechanism. *Langmuir* **2012**, *28* (9), 4573-4579.
52. Abou El-Reash, Y. G.; Otto, M.; Kenawy, I. M.; Ouf, A. M., Adsorption of Cr(VI) and As(V) ions by modified magnetic chitosan chelating resin. *International Journal of Biological Macromolecules* **2011**, *49* (4), 513-522.
53. Deng, Y.; Long, T.; Zhao, H.; Zhu, L.; Chen, J., Application of Porous N-Methylimidazolium Strongly Basic Anion Exchange Resins on Cr(VI) Adsorption from Electroplating Wastewater. *Separation Science and Technology* **2011**, *47* (2), 256-263.
54. Paradise, R. K.; Whitfield, M. J.; Lauffenburger, D. A.; Van Vliet, K. J., Directional cell migration in an extracellular pH gradient: A model study with an

engineered cell line and primary microvascular endothelial cells. *Experimental Cell Research* **2013**, *319* (4), 487-497.

55. Li, G.; Xiao, J.; Zhang, W., A novel dual colorimetric fiber based on two acid-base indicators. *Dyes Pigm* **2012**, *92* (3), 9-9.

56. Liu, Z.; Liu, J.; Chen, T., Facile synthesis, characterization, and potential applications of two kinds of polymeric pH indicators: Phenolphthalein formaldehyde and o-cresolphthalein formaldehyde. *Journal of Polymer Science Part A: Polymer Chemistry* **2005**, *43* (5), 1019-1027.

57. Cho, J. K.; Wong, L. S.; Dean, T. W.; Ichihara, O.; Muller, C.; Bradley, M., pH Indicating resins. *Chemical Communications* **2004**, *0* (13), 1470-1471.

58. Uchiyama, S.; Makino, Y., Digital fluorescent pH sensors. *Chemical Communications* **2009**, (19), 2646-2648.

# Chapter 5

## Conclusions and Future Directions

Ionic liquids (ILs), entirely composed of ions, belong to a new class of materials often considered as ‘green’ alternatives to molecular solvents due to their unique attributes such as low volatility, high thermal stability, electrical conductivity, dissolvability for wide range of solutes, recyclability, and accommodating wide range of chemical reactions.<sup>1-2</sup> In addition, simple engineering of the ILs’ structures in cation-anion combinations can make dramatic changes in physical and chemical characteristics of ILs.<sup>3</sup> Hence, ILs are called ‘designer’ solvents and have recently been a viable choice as a reaction medium for conducting chemical<sup>4</sup> and biochemical reactions<sup>5</sup>. Droplet or digital microfluidics is a rapid growing field in microfluidics-based chemical sciences. Using this approach, a fluid is emulsified in the form of nano to picoliter size droplets in a second carrier fluid within a microchannel network with a precise control over individual droplet formation.<sup>6-7</sup> Excellent mass and heat transfer in microchannels together with internal recirculating motions within each droplet ensures efficient mixing of different chemical reagents and explicit manipulation of chemical and biological events occurring within droplet boundaries. Each droplet, therefore, acts as an isolated chemical reactor that enables high-throughput screening and optimization of reaction conditions, chemical analyses, biological assays, nano and microparticle production.<sup>8-10</sup> Compartmentalization of reacting fluid into individual droplets not only improves mixing within its boundary; it can also benefit from interaction with their surroundings to promote interfacial chemical interactions,<sup>11</sup> catalysis,<sup>12</sup> extraction,<sup>13</sup> and catalyst screening<sup>14</sup>. In this context,

dynamic drop-to-drop chemical cross-talk, i.e. chemical interaction of individual reaction flasks with each other while flowing in a microchannel, for chemical analysis and separations has remained a challenge with very limited studies on this topic<sup>14</sup>. By exploiting striking features of ionic liquids as designer liquids, this thesis in overall aimed for presenting new droplet-based scheme for dynamic drop-to-drop chemical communications in microchips and applications in chemical analysis and separations, followed by microfluidic formation of controlled-size and shape functional materials.

## 5.1 Conclusions

The primary contribution of this thesis was formation of new and general droplet microfluidic scheme with ionic liquid-aqueous compound droplets in which droplet components functioned not only as isolated reaction flasks, but were also capable of on-drop chemical analysis. The formation of these biphasic partially engulfed droplets based on spreading parameters in microchannels with rectangular cross section and later in rounded capillaries together with their routing in simple microfluidic networks were studied (Chapter 2). In the line of later case, sorting and splitting (doubling) of compound droplets were observed in microfluidic bifurcated junctions. In addition to bifurcated junctions, decoupling of two droplets was performed by other techniques such as channel constrictions.

In Chapter 3, IL-aqueous compound droplets for selective separation of a binary mixture of molecules were presented as new separation or purification technique for flowing droplets. These complex microfluidic emulsions with chemically functional fluids were used to perform rapid and non-invasive chemical analyses that are inaccessible at the macroscale. The chemical tunability of ionic liquids was leveraged

in directing analyte (metal ion or proton [H<sup>+</sup>]) transport from the aqueous compartment of a biphasic droplet into an indicator-doped ionic liquid ‘reporter’ compartment and, crucially, in confining an analyte-indicator reaction within the reporter; thus enabling detection of the analyte without the addition of an indicator to the aqueous compartment. In this regard, dynamic pH-sensing of the aqueous compartment and chemical analysis (metal ion) were successfully presented in this chapter. This work paves the way for applications where a myriad of reactive and analytical processes occur concurrently within flowing microscale droplets, thus greatly expanding the realm of possibilities for droplet-based microfluidics.

Finally, in Chapter 4, a simple microfluidic method based on microcapillaries was established for fabrication of highly monodisperse PIL microgel beads with a multitude of functionalities that could be chemically switched in a facile fashion by anion exchange and further enhanced by molecular inclusion. Specifically, exquisite control over bead size and shape enabled extremely precise, quantitative measurements of anion- and solvent-induced volume transitions in these materials. In addition, by exchanging diverse anions into the synthesized microgel beads, stimuli responsiveness and various functionalities were demonstrated including controlled release of chemical payloads, toxic metal removal from water and robust, *reversible* pH sensing.

## **5.2 Future Directions**

This thesis exploited salient features of ionic liquids as designer liquids and developed droplet-based microfluidic methods for biphasic chemical separations and analysis by controlled formation and routing of complex emulsions in Chapters 2 and 3. It also

explored the controlled microfluidic formation and applications of polymerized ionic liquids as matrices for advanced, stimulus-responsive chemical separations and sensing in Chapter 4. To further improve the methods and build new research areas based on the conceptual ideas described in these chapters, we propose the following experimental and theoretical investigations:

1- *Biphasic biochemical reaction screenings*: An important extension of our non-invasive biphasic chemical analyses technique using microfluidic compound droplets (Chapter 3), can be in wide range of biochemical screening and kinetic assays. The cells are always involved in exchanging chemicals and biochemicals from the media through the cell walls. These biological activities can be monitored on-line in a non-invasive manner using an attached droplet that is capable of accommodating the further analysis steps. For instance, enzymatic assays (e.g. determining  $\beta$ -galactosidase activity using X-Gal which yields in formation of insoluble blue precipitant<sup>15</sup>), can be simply performed in a way that enzyme which is in aqueous droplet takes part in an *intra*-droplets reaction with the substrate hosted by the attached droplet and form a product with optical readout that can retain in the non-aqueous droplet.<sup>16</sup> Since ionic liquids can be designed to have preferential affinity for a particular chemical species, the scope of our presented microfluidic system can be further extended to cases where a chemical or biological event in aqueous compartment can be tracked or detected by selectively transporting a product of that event into a task-specific ionic liquid.

2- *Bioanalytics*: IL-aqueous compound droplets can be employed for bioanalysis of enzymatic reactions. A chemical species that is produced by an enzymatic reaction accommodated in the aqueous droplet can be transported into the IL compartment

containing a probe molecule. Upon interaction of the chemical species with the probe molecule a product with an optical readout would be formed; hence, inferring the enzymatic activity. For instance, Glucose in the presence of Glucose Oxidase (GOD) forms  $I^-$  (Iodide) and  $H_2O_2$  (Hydrogen peroxide).  $I^-$  and  $H_2O_2$  undergo a very slow reaction to produce  $I_3^-$ . Upon addition of catalyst HRP (Horse Raddish Peroxidase), the reaction can be enhanced greatly. The HRP is combined with  $H_2O_2$  to form a compound HRP I that oxidizes excess  $I^-$  to produce HRP II and  $I_3^-$ , and the HRP II is reduced to HRP and more  $I_3^-$  is produced. This reaction can take place in the aqueous phase while produced  $I_3^-$  can transport into IL droplet. Since Rhodamine B, a probe molecule, preferentially retain in ionic liquid environment, the presence of  $I_3^-$  can be detected easily. As soon as it transports into IL compartment, it will react with Rhodamine B and quench the fluorescence. Therefore, two enzymatic reactions can be monitored through a simple optical readout.<sup>17-18</sup>

3- *Preparative Chemistry*: There are some enzymatic reactions that require quick removal of the product from aqueous system as the product may decompose or revert back to the starting materials. Our proposed IL-aqueous compound droplet system can potentially be an ideal case for such scenarios where a chemical product can be removed from the reaction media. For example, dipeptide derivatives which are synthesized by  $\alpha$ -chymotrypsin-catalyzed coupling reactions in aqueous systems undergo a reversible reaction and transform into original amino acid substrates. The attached IL compartment in our poroposed system can help in preferential transportation of dipeptide derivates into IL compartment; thereby increasing the reaction yield.<sup>19</sup>

4- *Investigation on hydrodynamics of compound droplets with different morphologies and their behavior at bifurcated junctions*: IL-aqueous compound



droplets with different sizes and flow speed in bifurcated junctions were carefully observed for regular decoupling and splitting into two equally-sized daughter compound drops. Besides, random behavior of such droplets at microchannel network at certain flow conditions has been also noticed. More detailed understanding of compound droplet dynamics at bifurcated junctions is a crucial extension of our preliminary studies and observations, should our proposed compound droplet method be used to integrate upstreams and downstreams for full lab-on-drops chemical processes. Therefore, the governing physics behind all the observed phenomena should be studied meticulously to obtain precise control over decoupling, sorting and splitting of compound droplets at bifurcations. Such power of flow control enhances the flexibility in manipulating compound droplets for chemical processes and makes large scale extension of chemical analyses of multiple analytes possible through addition of chemically tailored IL sensing compartments to the pre-decoupled aqueous sample compartment. Moreover, further studies on formation and break up of more structurally-complex compound droplets at microfluidic junctions may open up opportunities for simultaneous on-drop chemical separation, sensing and purification.

*5- Exploiting the interface of IL-aqueous compound droplets with different morphologies for interfacial polymerization to form remarkable polymeric structures and colloidal self-assembly:* Since compound droplet system has three distinct phases and interfaces where different chemical events can occur, there are various possible approaches for interfacial polymerization.<sup>20</sup> Therefore, selection of monomers and photoinitiators based on their mutual solubility/insolubility in a particular phase can lead to interesting and different structures and chemistries. For example, by doping aqueous phase with functional monomers, formation of polymeric brushes can occur at IL-aqueous interface while, on the other side, hydrophobic IL monomer can be

used to form a cup shape microparticle. These polymeric brushes can give particular functionalities like thermo-sensitivity and hydrophilicity to the hydrophobic anisotropic IL-microparticle which has electric field-response property. The combination of polymeric brushes<sup>21</sup> and cup-shape microparticles can create microfluidic functional microstructures with hydrophobic body and hydrophilic brushes which resembles functional 'jellyfishes'. Ionic liquid-water interface can also perform as scaffold for colloidal self-assembly.<sup>22</sup> Further studies can also focus on capability of colloidal self-assembly at IL-water interface to produce functional polymeric materials.

6- *Extension of capillary-based formation of IL-aqueous compound droplets:* Due to extreme ease in preparation, assembly and scaling up of our microcapillary setup demonstrated in Chapter 4 to produce monodisperse single emulsions and multiple emulsions like compound droplets, we suggest further development of this setup for high-throughput screening and material synthesis. The advantage of simple scaling and setup preparation of such systems make them hands-on devices for certain experimentations.

7- *Formation of poly(ionic liquid) microgels with simultaneous multifunctionalities:* In Chapter 4 we demonstrated that incorporating diverse anions, could impart a multitude of functionalities to PIL microbeads, ranging from controlled-release of payload, toxic metal removal, and robust and reversible pH sensing. However we performed all these functionalities independently in different beads to prevent unnecessary complications. Here, we suggest the integration of such functionalities in every bead i.e. one bead show multiple functionalities upon the chemical condition of the environments. This can be addressed by spatial modification of PIL microbeads or combining both strategies of molecular inclusion and ion-exchange to explore

multifunctionality of PILs. Microfluidic-assisted spatial modification enables, for instance, creating different pH-indicator doped zones in a single PIL microgel to form micro pH-strips.

8- *Poly(ionic liquid)s as material construction of microdevices*: Microfluidic devices composed of PILs in the body of the device or as parts of the device (e.g. micropillars, walls, wells, etc.)<sup>23</sup> can build a new class of active devices for lab-on-a-chip purposes. These smart and active materials not only can effectively take part in chemical reactions, they can also detect and purify the target sample in-flow.

### 5.3 References

1. Rogers, R. D.; Seddon, K. R., Chemistry: ionic liquids--solvents of the future *Science* **2003**, *302* (5646), 792-793.
2. Wasserscheid, P.; Welton, T., *Ionic liquids in synthesis*. Wiley Online Library: **2008**; Vol. 1.
3. Hardacre, C.; Holbrey, J. D.; Nieuwenhuyzen, M.; Youngs, T. G. A., Structure and Solvation in Ionic Liquids. *Accounts Chem. Res.* **2007**, *40* (11), 1146-1155.
4. Hallett, J. P.; Welton, T., Room-Temperature Ionic Liquids: Solvents for Synthesis and Catalysis. 2. *Chemical Reviews* **2011**, *111* (5), 3508-3576.
5. van Rantwijk, F.; Sheldon, R. A., Biocatalysis in Ionic Liquids. *Chemical Reviews* **2007**, *107* (6), 2757-2785.
6. Baroud, C. N.; Gallaire, F.; Dangla, R., Dynamics of microfluidic droplets. *Lab on a Chip* **2010**, *10* (16), 2032-2045.
7. Teh, S.-Y.; Lin, R.; Hung, L.-H.; Lee, A. P., Droplet microfluidics. *Lab on a Chip* **2008**, *8* (2), 198-220.
8. Theberge, A. B.; Courtois, F.; Schaerli, Y.; Fischlechner, M.; Abell, C.; Hollfelder, F.; Huck, W. T. S., Microdroplets in Microfluidics: An Evolving Platform for Discoveries in Chemistry and Biology. *Angewandte Chemie International Edition* **2010**, *49* (34), 5846-5868.

9. Vyawahare, S.; Griffiths, A. D.; Merten, C. A., Miniaturization and Parallelization of Biological and Chemical Assays in Microfluidic Devices. *Chemistry & biology* **2010**, *17* (10), 1052-1065.
10. Huebner, A.; Sharma, S.; Srisa-Art, M.; Hollfelder, F.; Edel, J. B.; deMello, A. J., Microdroplets: A sea of applications *Lab on a Chip* **2008**, *8* (8), 1244-1254.
11. Mellouli, S.; Bousekkine, L.; Theberge, A. B.; Huck, W. T. S., Investigation of "On Water" Conditions Using a Biphasic Fluidic Platform. *Angewandte Chemie International Edition* **2012**, *51* (32), 7981-7984.
12. Theberge, A. B.; Whyte, G.; Frenzel, M.; Fidalgo, L. M.; Wootton, R. C. R.; Huck, W. T. S., Suzuki-Miyaura coupling reactions in aqueous microdroplets with catalytically active fluorinated interfaces. *Chemical Communications* **2009**, (41), 6225-6227.
13. Mary, P.; Studer, V.; Tabeling, P., Microfluidic Droplet-Based Liquid-Liquid Extraction. *Analytical Chemistry* **2008**, *80* (8), 2680-2687.
14. Kreutz, J. E.; Shukhaev, A.; Du, W. B.; Druskin, S.; Daugulis, O.; Ismagilov, R. F., Evolution of Catalysts Directed by Genetic Algorithms in a Plug-Based Microfluidic Device Tested with Oxidation of Methane by Oxygen. *Journal of the American Chemical Society* **2010**, *132* (9), 3128-3132.
15. Horwitz, J. P.; Chua, J.; Curby, R. J.; Tomson, A. J.; Da Rooge, M. A.; Fisher, B. E.; Mauricio, J.; Klundt, I., Substrates for Cytochemical Demonstration of Enzyme Activity. I. Some Substituted 3-Indolyl- $\beta$ -D-glycopyranosides 1a. *Journal of medicinal chemistry* **1964**, *7* (4), 574-575.
16. Bai, Y.; He, X.; Liu, D.; Patil, S. N.; Bratton, D.; Huebner, A.; Hollfelder, F.; Abell, C.; Huck, W. T. S., A double droplet trap system for studying mass transport across a droplet-droplet interface. *Lab on a Chip* **2010**, *10* (10), 1281-1285.
17. Jiang, Z.; Liang, Y.; Huang, G.; Wei, X.; Liang, A.; Zhong, F., Catalytic resonance scattering spectral determination of ultratrace horseradish peroxidase using rhodamine S. *Luminescence* **2009**, *24* (3), 144-149.
18. Seong, G. H.; Heo, J.; Crooks, R. M., Measurement of enzyme kinetics using a continuous-flow microfluidic system. *Analytical chemistry* **2003**, *75* (13), 3161-3167.
19. Kuhl, P.; Schaaf, R.; Jakubke, H.-D., Studies on enzymatic peptide synthesis in biphasic aqueous-organic systems with product extraction. *Monatshefte für Chemie/Chemical Monthly* **1987**, *118* (11), 1279-1288.
20. Gao, H.; Jiang, T.; Han, B.; Wang, Y.; Du, J.; Liu, Z.; Zhang, J., Aqueous/ionic liquid interfacial polymerization for preparing polyaniline nanoparticles. *Polymer* **2004**, *45* (9), 3017-3019.
21. Enright, T. P.; Hagaman, D.; Kokoruz, M.; Coleman, N.; Sidorenko, A., Gradient and patterned polymer brushes by photoinitiated "grafting through" approach. *Journal of Polymer Science Part B: Polymer Physics* **2010**, *48* (14), 1616-1622.

22. Nakashima, T.; Kimizuka, N., Water/Ionic Liquid Interfaces as Fluid Scaffolds for the Two-Dimensional Self-Assembly of Charged Nanospheres†. *Langmuir* **2011**, 27 (4), 1281-1285.
23. Beebe, D. J.; Moore, J. S.; Yu, Q.; Liu, R. H.; Kraft, M. L.; Jo, B.-H.; Devadoss, C., Microfluidic tectonics: A comprehensive construction platform for microfluidic systems. *Proceedings of the National Academy of Sciences* **2000**, 97 (25),13488-13493.

# Appendix A

## **Protocol for photolithography, soft lithography, bonding and packaging of a microreactor<sup>1</sup>**

Rapid prototyping is the technique of converting a design into a device rapidly which is the first step for any continuous synthesis experiment. Device fabrication is the second and critical step for successful completion of the reaction which is the third step. The time taken to convert a design to a device hence in general is preferred to be short for experimental devices. Rapid prototyping is possible on PDMS device through the technique of soft lithography. PDMS is molded on silicon wafer masters, fabricated using SU-8 2050 (Negative photoresist, Microchem Corporation, MA), using photolithography techniques. The steps involved in rapid prototyping and setting up the reactor for experiments once the device is ready for use is as follows.

### **Photolithography of Master Patterns**

4" silicon wafers (SYST Integration) are used for the fabrication of masters. Photolithography involves designing of mask, spin coating, lithography and development. Design of channels and other required patterns were made using autoCAD. This design was then transferred onto an emulsion transparency in the negative form called the mask. The process of spin coating, photolithography and development are performed in a clean room at the Institute of Materials Research and Engineering (IMRE) and the process involves the following steps:

**a.**Wafers were initially baked for 20 mins at 200 °C on a hot plate (Brewer Science Inc.) to remove the adsorbed moisture.

- b.** The wafer was then transferred onto the spin-coater (CEE 100, Brewer Science Inc.). Small amount (approximately 2mL) of SU-8 was dispensed onto the wafer and the spin coater was turned on. The spin coater was programmed to spin at 500 rotations per minute (rpm) for 15 s and at 1100 rpm for 35 s to get a uniform layer of 80  $\mu\text{m}$  thick SU-8 coating on the wafer. The channel dimension, height in this case depends on the rotation rate and time of spin.
- c.** The wafer with a layer of SU-8 was then transferred onto a hot-plate at 65  $^{\circ}\text{C}$ , for 10 mins which was then ramped to 95  $^{\circ}\text{C}$  for 45 mins, after which it was cooled to room temperature.
- d.** Another layer of SU-8 was spin coated onto the wafer following the same procedure as in steps b and c.
- e.** The wafer was then exposed to UV light. This process is called photolithography, performed in a mask aligner (MA8/BA6 SUSS MicroTec.). The mask aligner is designed to fit the wafer below the mask and the UV light hits the wafer through the mask, passing through the transparent channels of the mask. SU-8 being a negative photoresist crosslinks when exposed to light and the unexposed part of the wafer can be washed off with appropriate reagents.
- f.** The exposure time was 80 s, with multiple exposure (7 times) at 5 s intervals each. This needs to be set depending on the mode (constant intensity or constant current) in which the mask aligner is operated and on the power required.
- g.** The freshly exposed wafer was then placed onto the hot-plate at 65  $^{\circ}\text{C}$ , for 10 mins which was then ramped to 95  $^{\circ}\text{C}$  for 30 mins and cooled to room temperature.
- h.** The wafer was developed using the SU-8 developer (Microchem Corporation), rinsed with isopropyl alcohol and dried with nitrogen gas.

The SU-8 user worksheet is used as a reference for the spin coater rotation rate and time for spin coating, time and temperature of pre and post bake.

### **Prototyping**

**a.** The master wafer was then silanised with trichloro(1H,1H,2H,2H-perfluorooctyl)-silane (97%, Sigma- Aldrich Pte.). The procedure involved: wafer was placed in a petri dish (145/20mm, Greiner Bio-one, GMBH Austria) and approximately 0.1mL of silane was transferred into a centrifuge tube (750  $\mu$ L, Eppendorf type microconical test tube, CE Medical Diagnostic) which was taped to the wall of the petri dish. The dish was then placed inside a vacuum desiccator, left undisturbed for atleast 6 hours. The process essentially leaves a layer of silane on the SU-8 patterns, to prevent irreversible bonding between PDMS and SU-8.

**b.** PDMS (PDMS Dow Corning Sylgard Brand 184 Silicone Elastomer, Essex-Brownell Inc.) prepolymer was cast on the silicon masters. The prepolymer was made by mixing the curing agent and the base in 1:10 ratio. Bubbles introduced in the prepolymer due to mixing have to be removed before casting them onto the master by degassing the mixture in a vacuum desiccator for ~1hr.

**c.** The setup was then cured at 70 °C for 2 hrs in an oven (Mettmert vacuum oven, Singapore).

**d.** The replica was then peeled off the master. The patterns on the master were transferred onto the replica in relief (i.e. the ridges on the master would be valleys on the replica).

**e.** The replica was then cut and cleaned. Inlet and outlet holes (1/16 in. o.d.) were punched.



**f.** For synthesis purposes, the glass slides (50 x 75 mm, 1 mm thick, Corning Inc.) used for closing the channel were coated with a thin layer of PDMS prepolymer, using a spin coater (Laurell Tech. Co.) and cured at 70 °C for 2 hrs in the oven. The spin coater was programmed to spin at 1500 rpm for 30 s, 2000 rpm for 15 s and 3000 rpm for 10 s to get a uniform and thin layer of PDMS on the glass plate.

**g.** The contacting surface of the glass slide (PDMS coated surface) as well as the channel side of the device were exposed to 40 s oxygen plasma (Harrick Co., PDC-32G) prior to sealing, to activate their surface (by introducing silanol groups (Si-OH) replacing the methyl groups (Si-CH<sub>3</sub>)) thus leading to irreversible bonding (Si-O-Si bond).

**h.** PEEK tubings (1/16 in. o.d., 750 μm i.d., Upchurch Scientific.) were introduced into the inlet and outlet holes and glued to the device with 5 min epoxy (Devcon). The outer surface of the bonded device was activated by oxygen plasma for 90 s, to increase the adhesion of epoxy onto the device.

The glass plate is coated with a thin layer of PDMS so that all four walls of the microchannels are made of the same material. Liquids and gases were delivered to the device using syringe pumps from Harvard Apparatus (PHD 2000 Infusion/Withdraw pumps), through PEEK fittings (Upchurch Scientific.) and Teflon tubing (1/16 in. o.d., 750 μm i.d., Upchurch Scientific.). The entire setup was placed under an inverted stereomicroscope (Leica) fitted with a high speed CCD camera (Q imaging Micropublisher 5.0 RTV or Basler). The flow of fluids in the channel was monitored by either as “Q-capture pro” or “Streampix”, imaging softwares.

1. Duraiswamy, S., *Microfluidic Processes for Synthesis of Plasmonic Nanomaterials. PhD Dissertation* **2011**.

# Appendix B

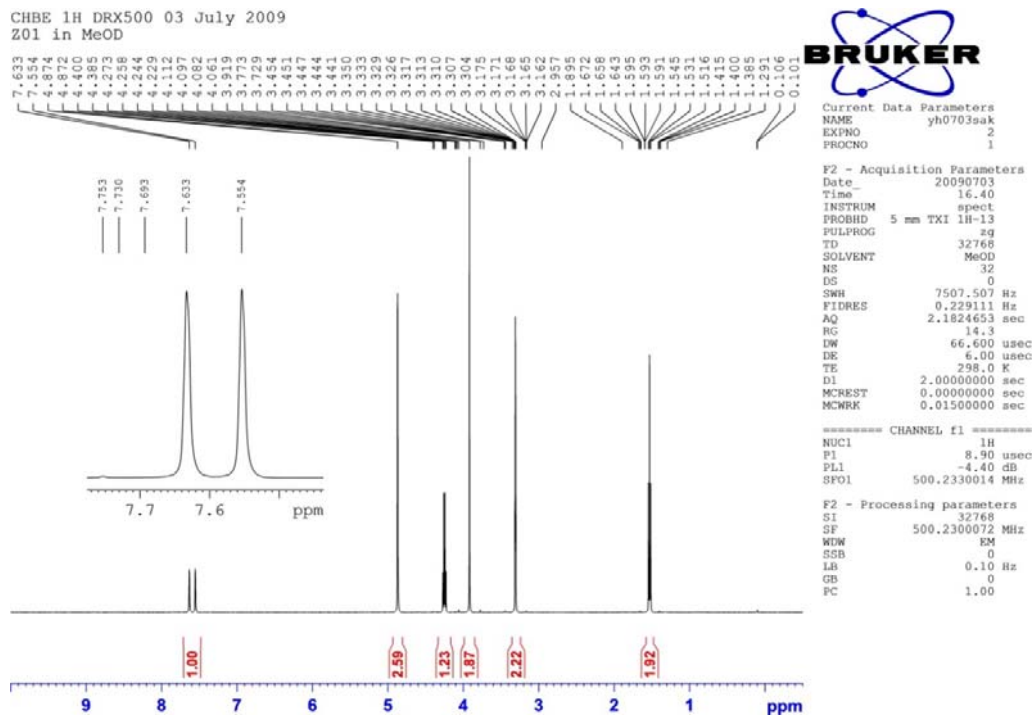


Figure B 1. <sup>1</sup>H-NMR of synthesized ionic liquid [EMIM][NTf<sub>2</sub>]

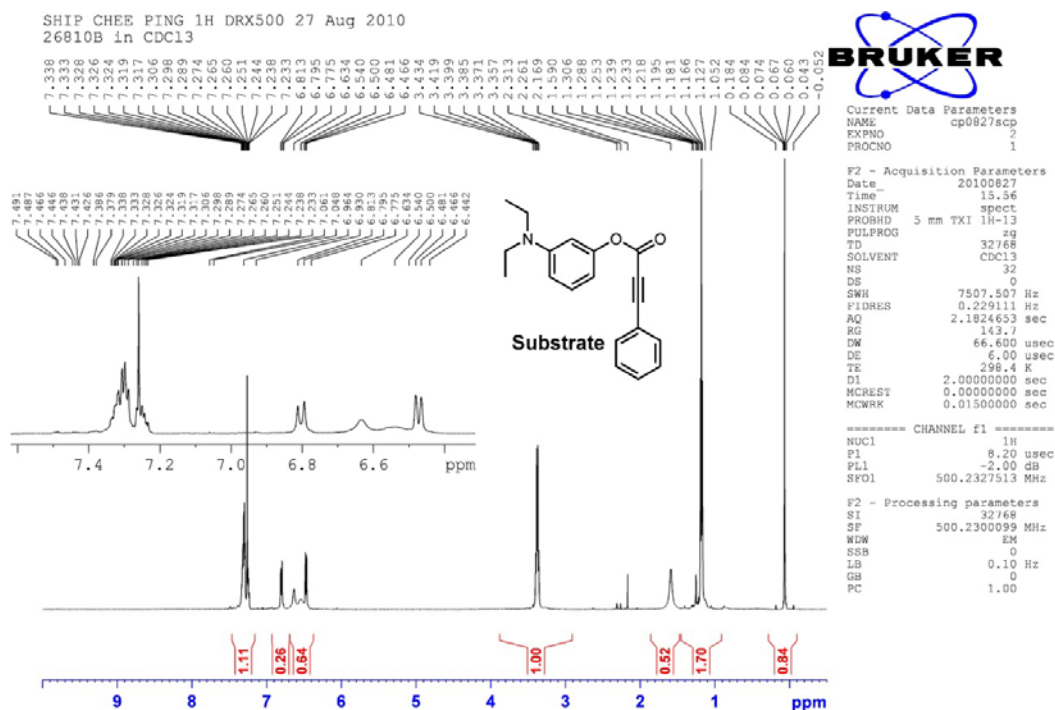
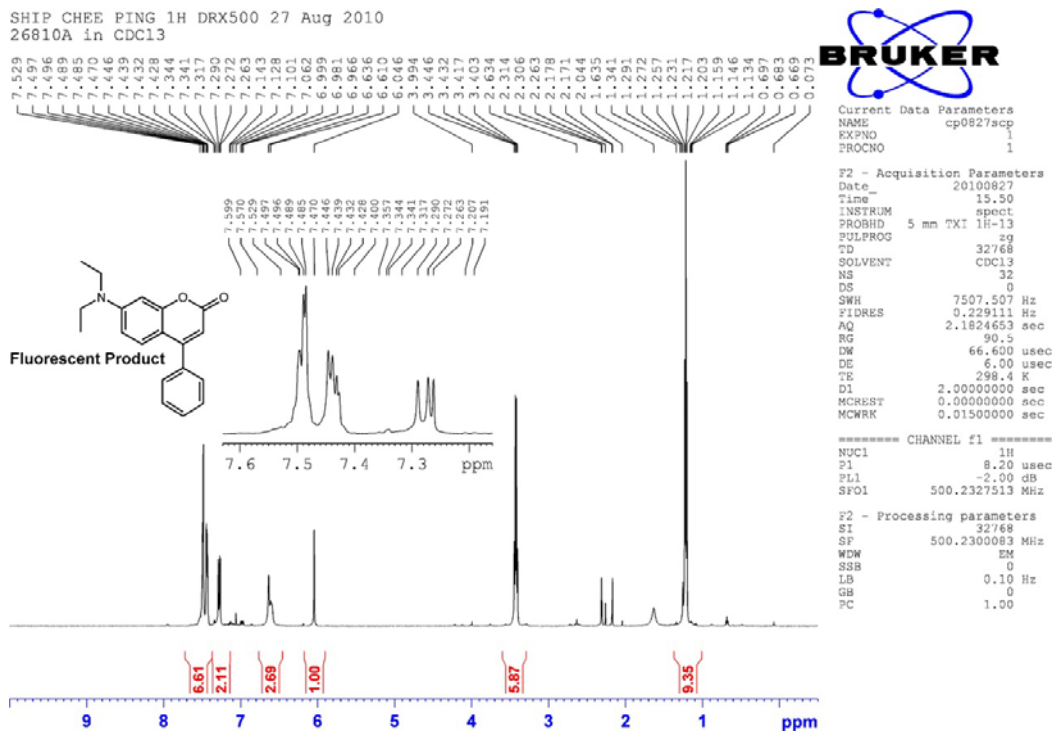
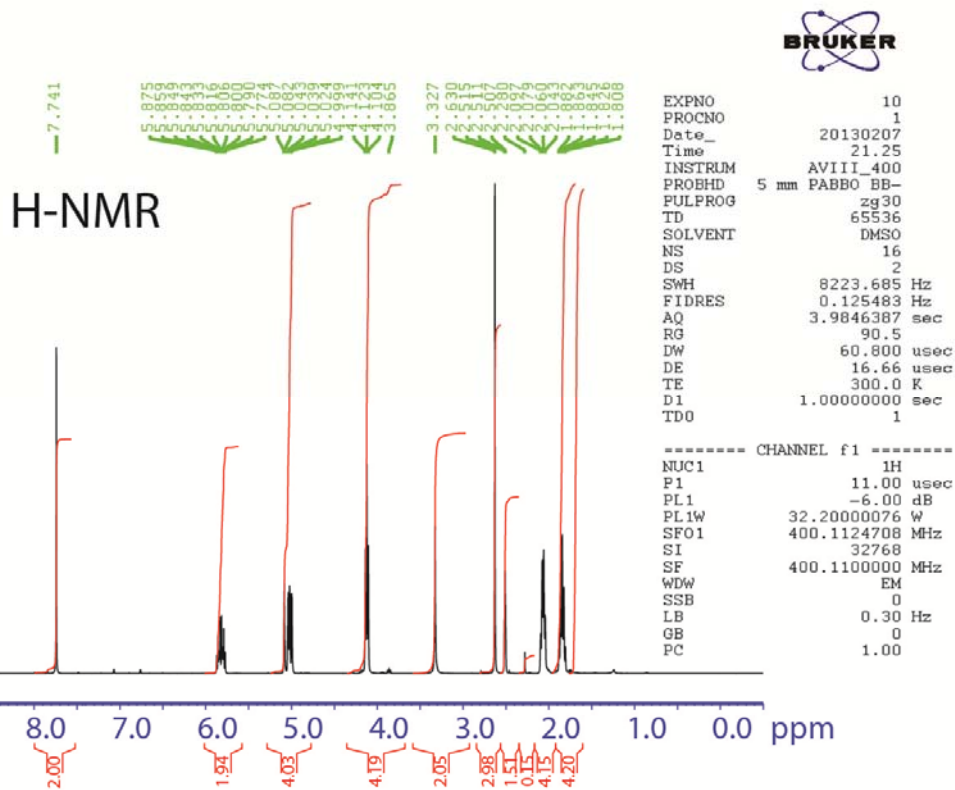


Figure B 2. <sup>1</sup>H NMR of synthesized substrate 1.



**Figure B 3.**  $^1\text{H}$  NMR of synthesized product 2.



**Figure B 4.**  $^1\text{H}$  NMR of synthesized ionic liquid monomer (1,3-bis(1-pentenyl)-2-methylimidazolium bromide)

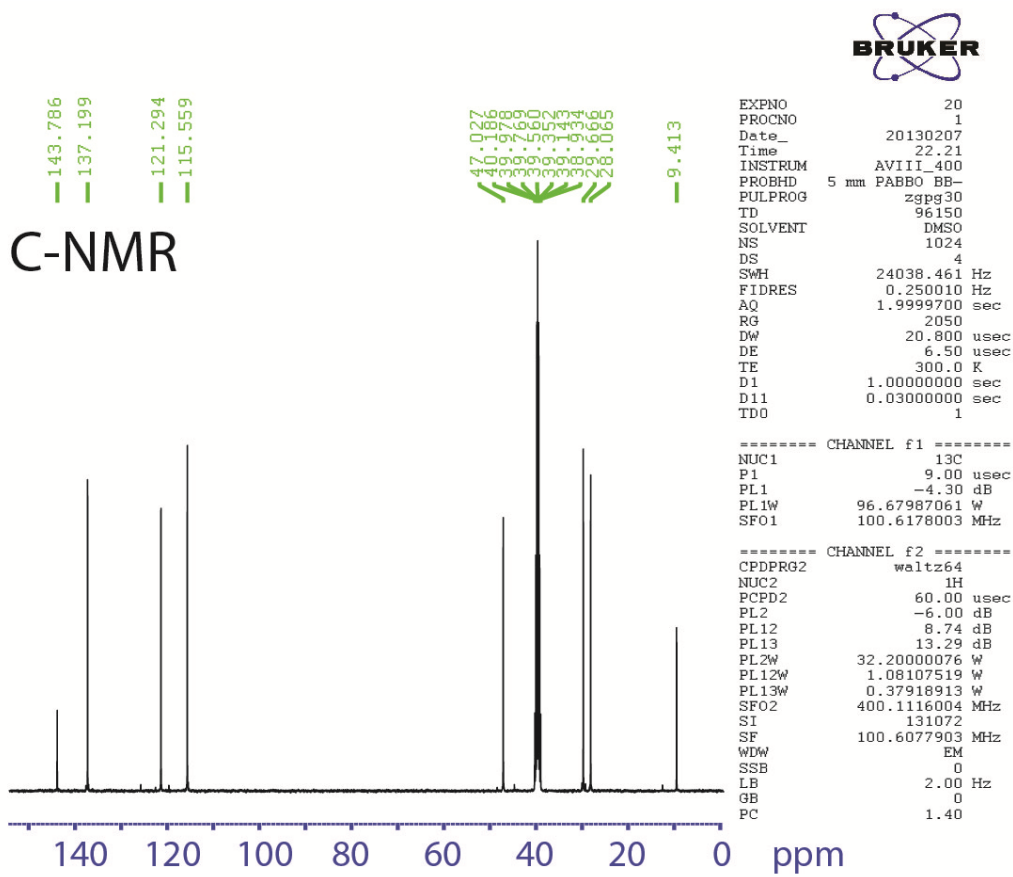


**Figure B 5.**  $^{13}\text{C}$ -NMR of synthesized ionic liquid monomer (1,3-bis(1-pentenyl)-2-methylimidazolium bromide)